Intracellular killing in D. discoideum: role of Vps13F and LrrkA

Bodinier, Romain

UNIVERSITÉ DE GENÈVE FACULTÉ DE MEDECINE
Section LIFE SCIENCES
Département de Physiologie Cellulaire et Métabolisme Professeur P. Cosson

Intracellular killing in *D. discoideum*: role of Vps13F and LrrkA.

THÈSE

présentée aux Facultés de médecine et des sciences de l'Université de Genève
pour obtenir le grade de Docteur ès sciences en sciences de la vie,
mention Sciences biomédicales

par

Romain Bodinier

de

Boulogne-billancourt (France)

Thèse N° 43

GENÈVE
Migros Printshop Plainpalais
2020

LIFE SCIENCES PhD SCHOOL GENEVA

DOCTORAT ÈS SCIENCES EN SCIENCES DE LA VIE DES FACULTÉS DE MÉDECINE ET DES SCIENCES MENTION SCIENCES BIOMÉDICALES

Thèse de Mr Romain BODINIER

intitulée :

«Intracellular killing in D. discoideum : role of Vps13F and LrrkA »

Les Facultés de médecine et des sciences, sur le préavis de Monsieur Pierre COSSON, professeur ordinaire et directeur de thèse (Département de Physiologie Cellulaire et Métabolisme), Monsieur Thierry SOLDATI, Professeur associé (Département de Biochimie) Monsieur François LETOURNEUR, Professeur (Institut National de la Santé et de la Recherche Médicale, Montpellier, France) autorisent l'impression de la présente thèse, sans exprimer d'opinion sur les propositions qui y sont énoncées.

Genève, le 04.05.2020

Thèse - 43 -

Le Doyen
Faculté de médecine

Le Doyen
Faculté des sciences

N.B. - La thèse doit porter la déclaration précédente et remplir les conditions énumérées dans les "Informations relatives aux thèses de doctorat à l'Université de Genève".

Table of Contents

RÉSUMÉ

Contexte : l'élimination intracellulaire est un processus complexe par lequel des cellules phagocytaires éliminent des microorganismes après les avoir absorbés. Chez l'humain, l'élimination intracellulaire est tout aussi vitale pour combattre des agents pathogènes tels que *Klebsiella pneumoniae* que pour maintenir l'homéostasie des tissus. C'est le plus souvent au sein des macrophages et des neutrophiles que s'opère ce processus. *Dictyostelium discoideum* est régulièrement utilisé comme organisme modèle pour les macrophages, ce qui nous a permis de réaliser un criblage mutagénétique aléatoire à grande échelle dans le but d'identifier des gènes impliqués dans l'élimination intracellulaire de *K. pneumoniae*. Deux d'entre eux ont déjà été décrits : *kil*1 et *kil*2. Kil1 est une sulphotransférase et Kil2 est une pompe à magnésium phagosomale. Ces deux gènes ne sont ni dans la même voie métabolique, ni complémentaires. Qui plus est, notre connaissance des régulateurs et des effecteurs de ces voies métaboliques est lacunaire.

But : Identifier de nouveaux gènes potentiellement impliqués dans l'élimination intracellulaire au sein de *D. discoideum.*

Méthode : À l'issue du criblage mutagénétique aléatoire, nous avons caractérisé les mutants présentant un défaut d'élimination intracellulaire de *K. pneumoniae*, ainsi que leurs liens avec *kil*1 et *kil*2. Cette caractérisation repose essentiellement sur des observations de cellules vivantes en microscopie à fluorescence.

Résultats : Nous avons trouvés deux gènes impliqués dans l'élimination intracellulaire : *vps13*F et *lrrk*A. Vps13F est une protéine de la famille des *vacuolar sorting protein* et LrrkA de la famille des *leucine rich repeats kinase*. À la suite du développement de notre nouvelle analyse de l'élimination intracellulaire, nous avons mesuré le temps médian nécessaire pour qu'une cellule de la souche sauvage élimine une bactérie *K. pneumoniae*. Ce temps médian est de 7.5 minutes. En comparaison avec la souche sauvage, les cellules mutantes *vps13*F KO et *lrrk*A KO mettent respectivement 18 minutes et 25 minutes. Néanmoins, elles ne présentent pratiquement aucunes anomalies durant leur croissance, leur développement, ni dans leur voie endocytique.

LrrkA et Vps13F ne sont pas situées dans la même voie métabolique d'élimination intracellulaire. Comparé aux mutants simples, le double mutant Δ*vps13*FΔ*kil*2 présente un défaut additionnel d'élimination intracellulaire. Ceci n'est pas le cas du double mutant Δ*lrrk*AΔ*kil*2, dont le défaut peut, à l'instar du mutant *kil*2, être partiellement corrigé par l'ajout de Mg^{2+}.

Contrairement à nos attentes, nous avons non seulement découvert que l'ajout de folate peut stimuler l'élimination intracellulaire, mais aussi que celle-ci dépend de la voie métabolique affectée par les mutants. L'ajout extracellulaire de folate ne stimule l'élimination intracellulaire, dans le cas des mutants simples *lrrk*A KO et *vps13*F KO, que le mutant *vps13*F. Pour confirmer l'hypothèse que la reconnaissance du folate est critique pour une élimination intracellulaire efficace, nous avons montrés que les mutants insensibles au folate, *far*1 KO and *fsp*A KO, présentent eux aussi un défaut d'élimination intracellulaire.

De surcroît, l'addition de folate ne stimule pas la mobilité du mutant *lrrk*A, ce dernier étant constamment plus mobile que la souche sauvage. Ce phénotype induit par ailleurs une phagocytose plus importance chez le mutant que pour la souche sauvage.

Conclusion : Vps13F est certainement impliqué dans le trafic vers le phagosome des effecteurs de l'élimination intracellulaire. Nos prédictions génétiques supportent plus précisément que ce sont les enzymes lysosomal sulfatées par Kil1 qui sont concernées.

LrrkA, de son côté, est à la convergence de la détection de signal bactérien (i.e. folate) et de l'activation des mécanismes d'élimination intracellulaire. Cette dernière passe par l'activation de la motilité en présence de folate et de la régulation de l'activité de Kil2 durant la maturation du phagosome.

SUMMARY

Background: Intracellular killing is a complex process by which phagocytic cells eliminate microorganisms, once engulfed. In human tissues, intracellular killing is vital to fight off invading pathogens such as *Klebsiella pneumoniae* or for tissue homeostasis. Intracellular killing is mainly carried out within macrophages and neutrophils. Using *Dictyostelium discoideum* as a model organism for macrophages enables us to perform large scale random mutagenesis screen to find genes involved in intracellular killing of *K. pneumoniae*. Two of them have already been described: *kil*1 and *kil*2. Kil1 is a sulphotransferase and Kil2 a phagosomal magnesium pump. Both genes are involved in intracellular killing pathways that do not complement each other's phenotype. Furthermore, our knowledge of regulators and effectors in these pathways is sparse.

Aim : Increase the number of candidate genes implicated in intracellular killing in *D. discoideum*.

Method: Characterize mutants from a random mutagenesis screen for intracellular killing deficient mutants of *K. pneumoniae*, as well as their mutation dependencies on *kil*1 or *kil*2. We focused on fluorescence based live cell imaging techniques.

Results: We found two genes implicated in IC killing: *vps13*F and *lrrk*A. Vps13F is a cytosolic protein from the vacuolar protein sorting family, and LrrkA is a cytosolic kinase from the Leucine Rich Repeats kinase family. Following the development of a new intracellular killing assay, we measured the median time for WT *D. discoideum* cells to kill a single *K. pneumoniae* at 7.5 min. Compared to the WT, *vps13*F KO cells are at 18min and *lrrk*A KO cells at 25min. *vps13*F and *lrrk*A mutants nevertheless display virtually no abnormalities during growth, development, or in their endocytic pathway.

LrrkA and Vps13F work in separate IC killing pathways. Compared to single mutants, the double mutant Δ*vps13*FΔ*kil*2 exhibits an additive IC killing defect, whereas Δ*lrrk*AΔ*kil*2 does not. In addition, *lrrk*A KO cells IC killing defect can be reversed by adding Mg^{2+}, a phenotype observed in *kil*2 KO cells.

Unexpectedly, folate can stimulate IC killing. This stimulation is pathway-dependent, as exogenous addition of folate boosts IC killing in *vps13*F KO but not in *lrrk*A KO. This unexpected folate-dependent IC killing stimulation result is reinforced by both folate-sensing deficient mutants, fspA and far1 KO cells, being IC killing deficient as well.

Additionally, *lrrk*A KO cells are insensitive to the stimulation of motility by folate and are constantly more motile than the WT, resulting in increased phagocytosis compared to WT.

Conclusion: Vps13F is most likely involved in trafficking IC killing effectors to the phagosomes. Genetic prediction suggests more specifically a role in trafficking Kil1-sulfated lysosomal enzymes.

LrrkA is at the convergence between sensing bacterial cue (i.e. folate) and activating intracellular killing mechanisms by respectively enhancing motility when folate is present and regulating Kil2 activity during the phagosome maturation.

ACKNOWLEDGEMENTS

« Ce n'est pas que la vie soit courte, c'est que le temps passe vite... » et sur ces paroles d'Henry Jeanson, je remercie mes parents pour avoir non seulement rempli la première condition nécessaire au travail de thèse, c'est-à-dire l'existence, mais aussi de continuer à accompagner avec amour depuis toujours.

La deuxième condition est d'avoir un directeur de thèse et cette dernière c'est toi, Pierre, qui l'a remplie. Pour cela je ne sais comment te remercier. Le dernier conseil de mon maître de thèse était de choisir un professeur avant de choisir un sujet de thèse, et je le remercie pour ce conseil. Merci pour ton accompagnement et tes encouragements tout au long de ces 5 années.

Il y a peu de mots pour décrire tous les sentiments d'affection et même d'amour que j'ai pour l'équipe du laboratoire. Jade, Ayman, Alex, Jackie, Philippe, Tania, Estelle, Chéryl, Otmane, Cyril et Xénia, vous avez été formidables. Tout comme ce comptoir à l'entrée de nos bureaux, lieu de vie, de rencontres, de fêtes, de débuts de discussions, et de soutien dans les instants de faible glycémie ; ainsi que cette porte, ornée de nos souvenirs, et citations.

L'équipe ne saurait être au complet si je ne remerciais pas Anna, Astrid, c'était un plaisir de travailler dans un laboratoire aussi bien tenu.

Un mot aussi pour Thierry Soldati et François Letourneur qui, je l'espère, trouveront dans mes publications des pistes et réponses pour continuer de faire avancer leur recherche. Merci encore pour votre temps, et pour avoir le courage de lire cette thèse.

La vie au laboratoire ne s'arrêtait pas aux murs de celui de Pierre. Si je remercie les comités qui ont organisé les PhD retreats, c'est surtout Semia et Daniele qui pour moi ont été deux amis en dehors du labo. Je profite de l'occasion aussi pour remercier l'équipe de « ma thèse en 180 secondes » qui m'a aidé à me révéler un goût pour la vulgarisation scientifique.

Merci aussi à Karina, Margaux, Laure, Siroune et Marion pour leur soutien.

Pour finir je souhaite remercier les associations Geneva E-Sport et Swiss Esports Federation. Des heures investies avec le sourire et dont a jailli des amitiés, des projets, des aventures… Je recommande à tous les doctorants d'avoir une passion comme celle-ci qui se concrétise sur le côté. La thèse est un marathon, mais ayant été aussi bien entouré, je suis heureux du chemin que nous avons fait ensemble.

INTRODUCTION

Humans and bacteria peacefully cohabit most of the time (Turnbaugh et al., 2007). Indeed, numerous bacteria in our gut or on our skin are beneficial to human health. Only few bacteria have developed virulent strategies that harm the human body. In addition, the human body is equipped with an immune system preventing undesirable microorganism colonization of tissues (Tosi et al., 2005).

The first line of defense of the immune system is called the innate immune system. It notably comprises a set of cells that exhibit microbicidal activities, allowing them to contain or eradicate invading microorganisms (Silva et al., 2012). Their modus operandi is the following: they track microorganisms, ingest them in a membrane-enclosed organelle called a phagosome, and eventually kill and digest them. Uptake of particles larger than 200nm is called phagocytosis. Immune cells with remarkably high phagocytic activity are referred to as professional phagocytes and include macrophages, neutrophils, dendritic cells, osteoclasts, and eosinophils (Gordon et al., 2016). In contrast cells having a low phagocytic activity are designated as nonprofessional phagocytes and include fibroblasts, epithelial cells, and endothelial cells. Although nonprofessional phagocytes usually do not ingest microorganisms, they play a role in the phagocytic ingestion and elimination of apoptotic bodies (Gordon et al., 2016).

Once a foreign microorganism is sequestered in the lumen of a phagosome, a series of complex phagosomal maturation events occur, allowing intracellular killing and degradation of the microorganism. Within minutes after closure, the phagosome becomes a highly acidic, degradative and oxidative compartment (Pauwels et al., 2017). An extensive literature on human professional phagocytes describes their intracellular microbicidal activities, yet it remains unclear which of these mechanisms are most necessary for intracellular killing and if we have today discovered the whole spectrum of mechanisms. It is also largely unclear whether killing of different microorganisms relies on similar or distinct killing mechanisms.

Phagocytosis of microorganisms plays a second role in the immune system as proper degradation of invading microorganisms is required to efficiently trigger the immune system’s second line of defense: the adaptative immunity. Unlike innate immune cells that use a defined set of receptors to recognize foreign molecules and pathogens, cells of the adaptive immune system respond to foreign antigen fragments displayed by the major histocompatibility complex (MHC) class I and II at the surface of macrophages, dendritic cells, and to a lesser extent neutrophils (Vono et al., 2017). Therefore, efficient digestion of foreign particles in the phagosome is necessary to properly load foreign antigens fragments on the MHCs (Litman et al., 2010).

In summary, studying intracellular killing mechanisms within the phagosome of professional phagocytic cells is essential to understand how the human body protects itself against foreign microorganisms.

I. *Dictyostelium Discoideum* a professional phagocyte model

D. discoideum is classified as an amoeba belonging to the phylum Amoebozoa, infraphylum Mycetozoa. Historically, amoebae were first observed in 1755 by Rösel von Rosenhof and described as small motile protozoon. In 1822 the name Amiba, from the Greek amoibè (ἀμοιβή) meaning "change", was coined by Bory de Saint-Vincent and last changed to Amoeba 10 years later by Ehrenberg. In 1869, Brefeld observed Dictyostelids, a family of amoeba, and Raper in 1935 performed the first characterization of a prominent member of the family: *D. discoideum*.

D. discoideum, originally isolated from decaying leaves from a hardwood forest in North Carolina mountains, can be found in two main states: a vegetative state characterized by motile single cells of approximately 5-10µm diameter capable of feeding on a bacterial lawn ; on the opposite, the developmental stage corresponds to a multicellular development cycle where starving cells aggregate to form a slug, which undergoes morphogenesis into a fruiting body (Raper, 1935) (Fig.1).

The capacity of *D. discoideum* amoebae to undergo a complex multicellular developmental cycle is a remarkable feat. Starving cells release cAMP as a signal to regroup. When 10^5 to 10^6 cells aggregate, a slug is formed. Formation of the slug induces a complete transcriptional change for most of the cells. This change triggers tropism toward light, heat, and humidity enabling the slug to migrate towards favourable grounds. The last step includes differentiation into two distinct subpopulations of cells in the fruiting body: the stalk and the sorus/spores (Katz, 2002). Eventually, the spores germinate and give rise to new vegetative cells. This facultative multicellular process is the reason why *D. discoideum* is often nicknamed a “social amoeba”.

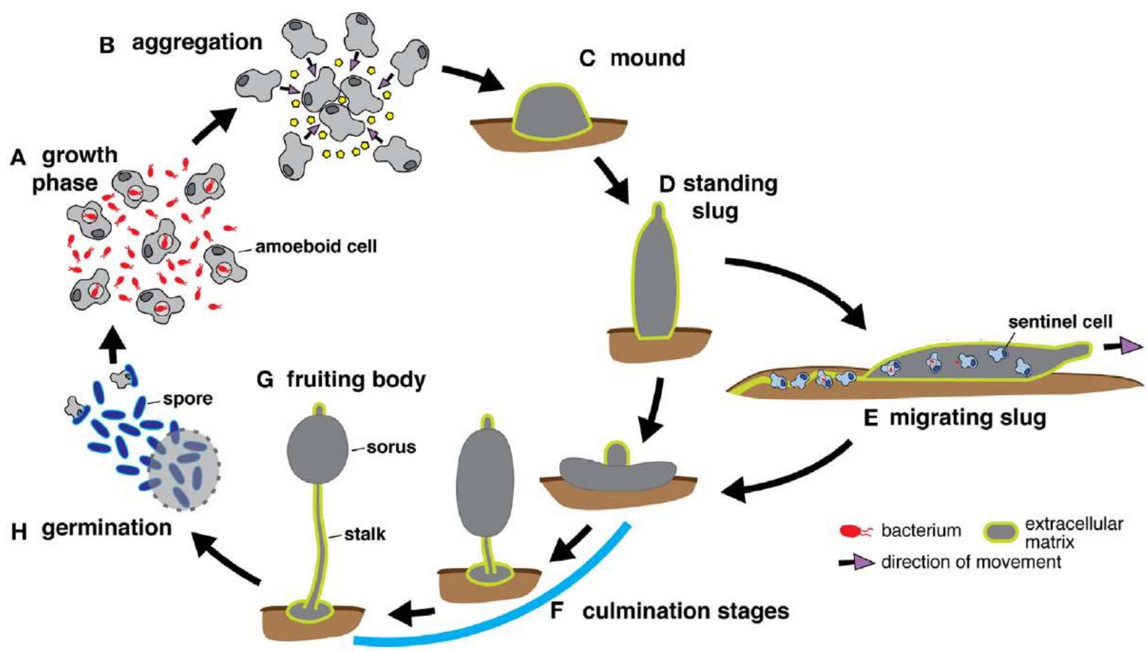

Fig.1 *D. discoideum* life cycle
(A) Amoeboid cells feed on bacteria and replicate by binary fission. (B) The development cycle is initiated upon resource depletion, and aggregation occurs when starving cells secrete cAMP. (C) The aggregating cells organize to form the mound stage, enclosed within an extracellular matrix and (D) continue to develop into the standing slug. (E) Depending on its environment, the standing slug either falls over to become a migrating slug that moves towards heat and light or (F) proceeds directly to the culmination stages that (G) ultimately produce the fruiting body, which consists of a spore-containing structure, the sorus, and a stalk of dead cells. (H) Spores are released from the sorus and germinate into growing cells. Adapted from Dunn et al., 2018.

D. discoideum was used as a model organism for studying phagocytosis and intracellular (IC) killing of bacteria in 1978 by Depraitère (Depraitère and Darmon, 1978), and it was used as a model for studying phagocytosis in the following decades. Hägele opened the path to using *D. discoideum* as a model phagocytic cell exposed to pathogenic bacteria in a study of Legionella in 2000 (Hägele et al., 2000). *D. discoideum* infection by Legionella recapitulates the same pathogenicity as in macrophages, leading the authors to hypothesize that amoebae are probably the original target of Legionella in the environment. In 2005 the sequencing of the full genome of *D. discoideum* was published and made available on dictybase (Eichinger et al., 2005) revealing that most of the genes involved in phagocytosis, phagosome maturation, and IC killing are strikingly conserved from *D. discoideum* to human (Boulais et al., 2010). The conservation of these genes is one of the main reasons to use *D. discoideum* as a model phagocytic cell (Dunn et al., 2018) and allowed *D. discoideum* to be used as a model organism for studying the infection course of a dozen pathogens (Table 1).

Bacterial pathogens	References
Legionella pneumophila	Hägele et al., 2000
Mycobacterium avium, M. marinum, M. tuberculosis	Skriwan et al., 2002, Hagedorn et al., 2007, Solomon et al., 2003
Pseudomonas aeruginosa	Cosson et al., 2002
Vibrio cholerae	Pukatzki et al., 2006
Klebsiella pneumoniae	Benghezal et al., 2006
Neisseria meningitidis	Colucci et al., 2008
Burkholderia cenocepacia	Aubert et al., 2008
Salmonella enterica/typhimurium	Jia et al., 2009
Francisella noatunensis	Lampe et al., 2016

Although the mouse is a standard model organism for studying professional phagocytic cells, and more generally the immune system in mammals, it remains challenging to perform large scale systematic analysis of gene products directly implicated in IC killing. (Swearengen, 2018). Using *D. discoideum* for large random mutagenic screens and subsequent characterization of mutants presents five experimental advantages: it is simple, short, scalable, cheap and robust. Simple, because in optimal growth conditions, *D. discoideum* is in a vegetative state, which is characterized by freely moving single cells. Phenotypes observed are therefore mostly cell-autonomous reducing the complexity of the interpretations. Short, because *D. discoideum* doubling time is 6 hours. It is almost 5 times shorter than a standard macrophage cell line (Van Furth et al., 1987). Scalable, because *D. discoideum* cells grow in less stringent growth conditions to higher concentration. Cells grows at 20-25 C° without the need to control for 0_2 and $C0_2$. Cheap, because cells can be cultivated on a bacterial lawn or even in a cheap nutritive medium for axenic strains and *D. discoideum* cells do not required treated culture plastic to grow. Robust, because *D. discoideum* genetic modifications are better controlled and defined compared to the diploid mouse macrophage genome. *D. discoideum* cells have a haploid genome and strategies to generate libraries of KOs or KIs mutants are readily available. Recent adaptation of the Crisper-Cas9 system to *D. discoideum* facilitates even more the generation of mutants (Sekine et al., 2018).

In numerous laboratories, *D. discoideum* strains used are called axenic, meaning they can grow on liquid media without bacteria. In a rich medium, cells remain in a vegetative state with high phagocytic and macropinocytic rate avoiding entry in the multicellular stage. In 2015, Bloomfield et al. showed that the axenic phenotype is due to the loss of the RasGAP: NF1. Excessive Ras activity, generated by NF1 loss, increases macropinocytic activity enabling the cells to survive in nutrient-rich media (Bloomfield et al., 2015). It does not affect axenic cells capacity to grow on a bacterial lawn and axenic cells are still considered a valid model for macrophages.

II. Phagocytosis: comparative analysis in human and *D. discoideum*

Phagocytosis comes from Ancient Greek phagein (φαγεῖν) and kytos (κύτος) meaning "to eat" and "cell". It is the process allowing cells to engulf particles larger than 200 nm. The term was coined by Carl Friedrich Wilhelm Claus to describe the set of cells capable of absorbing and degrading citrus thorns inserted into starfish larvae observed in 1882 by Élie Mechnikov.

In human cells, phagocytosis role extends beyond immunity, for example it prevents severe anemia by enabling clearance of erythroblast nuclei (Kawane et al., 2001), it prevents toxic iron deposits in the kidney by removing senescent erythrocytes (Theurl et al., 2016), it enables correct synaptogenesis by pruning the synapses that are superfluous or inactive to optimize neuronal communication (Petanjek et al., 2011) and prevents permanent brain damage by clearing cellular debris during brain ischemia (Morizawa et al., 2017), it clears the lumen of seminiferous tubules from apoptotic cells for efficiency spermatogenesis (Shaha et al., 2010), and it even prevents blindness by clearing the shed outer segments of photoreceptor cells in the retina (Nandrot et al., 2000). Underlying this plethora of roles, we still find common cellular mechanisms.

At the cellular level, phagocytosis is a three step process: first, receptors present at the cell surface recognize the foreign particle; second, a local remodeling of the cytoskeleton and plasma membrane is induced by a signaling cascade, and forms the phagocytic cup around the foreign particle; third, the phagocytic cup closes and forms an intracellular compartment called a phagosome (Desjardins et al., 2005) (Fig.2).

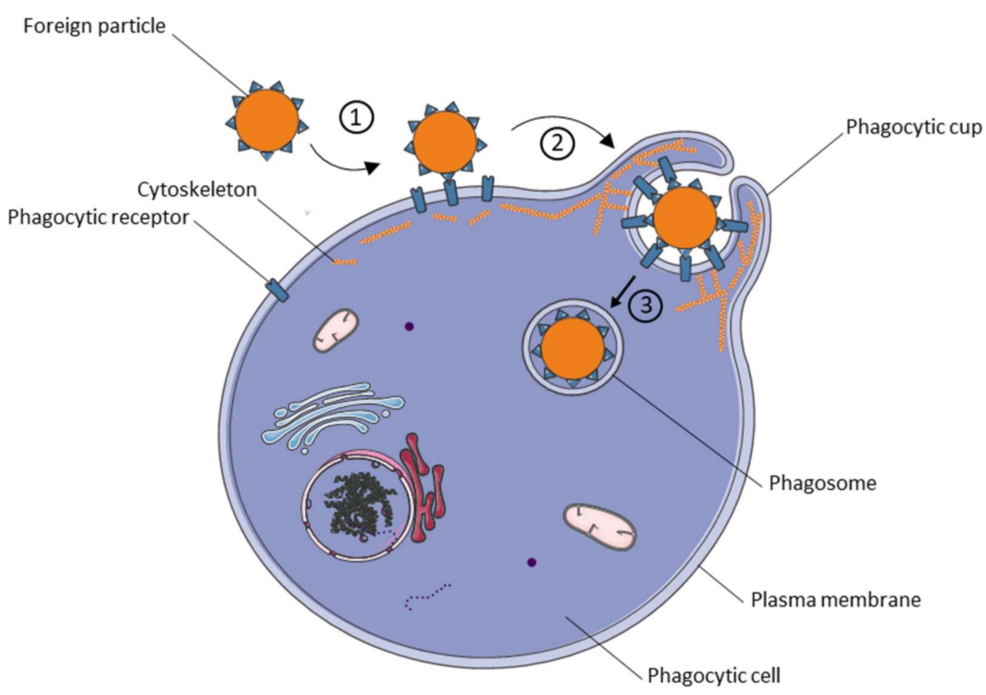

Fig.2 Phagocytosis – General overview

Phagocytosis is a three step process: first, receptors present at the cell surface recognize the foreign particle (in orange); second, a local remodeling of the cytoskeleton and plasma membrane is induced by a signaling cascade, and forms the phagocytic cup around the foreign particle; third, the phagocytic cup closes and forms an intracellular compartment called a phagosome, In *D. discoideum*, phagocytosis, like for numerous unicellular organisms, is mainly used for feeding purposes. *D. discoideum* cells mainly phagocytose bacteria, and the same general steps are conserved. Only internalization of *D. discoideum* lectin (Discoidin I) coated bacteria differs from the typical course of phagocytosis and phagosome maturation. Discoidin-coating of extracellular bacteria protects them from IC killing (Dinh et al., 2018). When fluorescent Discoidin-coated *E. coli* were fed to *D. discoideum*, the fluorescent signal within the cells persisted on average 25 min, whereas it persisted 4 min with fluorescent non-coated *E. coli*. The results indicated that *E. coli* survived longer within the phagosomes when coated by Discoidin I. The authors hypothesized that Lectin-induced modified bacterial internalization can be distinguished from phagocytosis and has a different maturation process. One explanation could be that during starvation, it might be beneficial to store bacteria as food and delay their IC killing, to provide germinating spores with a readily available food source.

1. Binding and recognition of particle

Human phagocytic cells exhibit at the plasma membrane, endosomal membranes and in the cytosol, specific pattern recognition receptors (PRR). These PRRs recognize either damage-associated molecular pattern (DAMP) molecules or microbial-associated molecular pattern (MAMP) molecules (Tang et al., 2012) (Fig.3). More specifically MAMPs ranges from components of the peptidoglycan cell wall to nucleic acids. Four types of PRRs directly bind them: toll-like receptors (TLRs), integrins, scavenger receptors, C-type lectins (Iwasaki et al., 2015). Another set of receptors, called opsonic receptors, recognize host-derived opsonins, from the Greek opsōneîn "to prepare for eating", bound to foreign microorganisms. Opsonic receptors include FcγR (antibodies), CR3 (complement), Integrin alpha-5/beta-1 receptor (fibronectin), and Integrin alpha-v/beta-3 and alpha-v/beta-5 receptors (lactadherin) (Liu et al., 2013, Freeman et al., 2014) (Fig.3). Heterologous expression of lectins, scavenger receptors, integrins and FcγR in non-phagocytic cells is sufficient to trigger phagocytosis; TLRs on the other hand do not (Flannagan et al., 2012). Although TLRs do not directly trigger phagocytosis, they play two important roles. First, they stimulate phagocytosis: incubation of macrophages with the TLRs ligands increases bacterial phagocytosis and conversely presence of TLRs antagonists reduces the phagocytic rate of the macrophages (Doyle et al., 2004). Second, TLRs activation induces a signaling cascade triggering inflammation, another innate immune system mechanism. In short, upon binding to MAMPs, TLRs recruit adaptor molecules possessing a Toll–interleukin 1 receptor (TIR) domains such as MyD88, Mal, TRIF, TRAM, and SARM. In turn, TIR adaptors activation leads to stimulation of mitogen activated protein kinases (MAPKs) and NF-κB, eventually upregulating phagocytosis and inflammation-related genes (Cen et al., 2018). Not all plasma membrane located PRRs are direct phagocytic receptors, but all do trigger a signaling cascade leading directly or indirectly to phagocytosis.

In *D. discoideum* opsonin-independent phagocytosis has been described: five integrin-like protein (Sib family), and three scavenger-like receptors (Lmp family) have been identified and characterized (Cornillon et al., 2006, Sattler et al., 2018) (Fig.4). The Sib family, which comprises 5 members (SibA-E), shows similarity with integrin β. Among them, SibA and SibC are involved directly in adhesion to substrate, beads and bacteria. Moreover, all Sib proteins interact directly, via their membrane-proximal NPxY motif, with TalinA, an actin-binding protein (Cornillon et al., 2006, Cornillon et al., 2008). Both features make SibA and SibC good phagocytic receptors candidates. However, we should take into consideration that TalinA is mostly found at the posterior cortex during migration, whereas a recent study would suggest that TalinB, the second homolog of Talin in *D. discoideum*, is restricted to the leading edge of migrating cells. Compared to TalinA, TalinB contains a I/LWEQ domain and a villin headpiece domain in its C-terminal actin-binding region which seem to play a role in both TalinA and B segregation (Tsujioka et al., 2019). Phagocytic receptors binding TalinB could be better phagocytic receptor candidates as phagocytosis compares to a directed migration over a surface. SibA and C binding affinity to TalinB have not been measured yet. Concerning the Lmp family, which comprises 3 members (LmpA-C), they are homologs of LIMP-2/CD36 scavenger receptors. LmpA and C are found in endosomes and lysosomes similar to LIMP-2, and LmpB is present at the cell surface like CD36 (Sattler et al., 2018). LmpA genetic inactivation induces a severe defect in phagocytosis for beads as well as Gram+ and Gram- bacteria, whereas LmpB inactivation specifically inhibits uptake of mycobacteria and *B. subtilis*. Most likely LmpA affects actin dynamic as *lmp*A KO cells have a massive decrease of motility, and LmpB regulates phagocytosis triggering as binding to bacteria is not affected (Sattler et al., 2018). LmpB is an interesting PRR candidate, specific for Gram+ bacteria, and LmpA play a more global role in phagocytosis, motility and even phagosome maturation, which is heavily perturbed in *lmp*A KO cells.

1) Opsonin-dependent phagocytosis

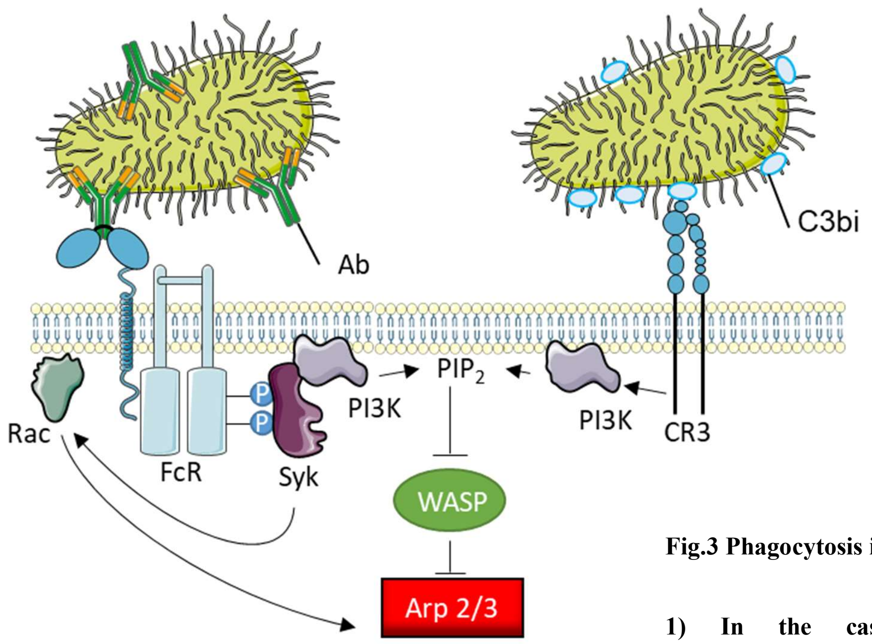

2) Opsonin-independent phagocytosis

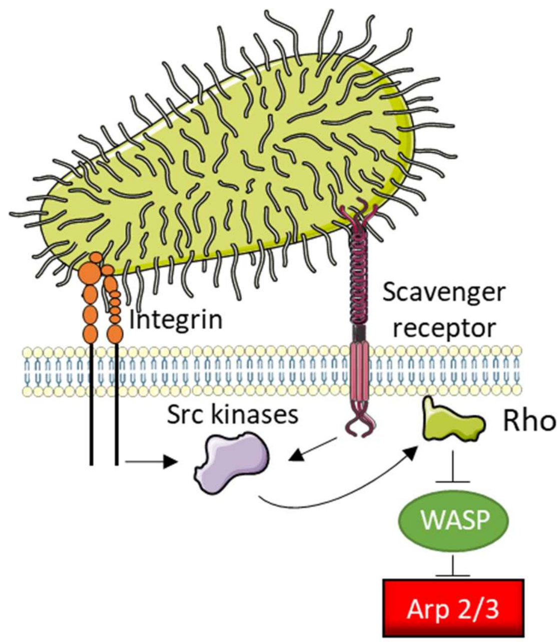

Fig.3 Phagocytosis initiation in macrophages

1) In the case of opsonin-dependent phagocytosis: antibodies (Ab) and C3bi, opsonizing the bacteria, are bound respectively by FcR and CR3. In Ab bound-state, the FcR is quickly phosphorylated, Syk recognizes the phosphorylated immunoreceptor tyrosine-based activation motifs. Activation of Syk, further stimulates RAC, which in turn activates the actin-branching Arp 2/3 complex. In the case of C3bi binding to CR3, activation of CR3 stimulates PI3K activity, leading to PIP_2 formation with binds WASP relieving inhibition of Arp 2/3.

2) In the case of opsonin-independent phagocytosis: the MAMPs are directly recognized by the receptors. Both integrins and scavenger receptors stimulate Src kinases after binding. Src kinases activates Rho, which will release the WASP inhibition on Arp2/3 to allow actin-branching. The represented scavenger is class A member MARCO which binds bacterial CpG DNA.

Interestingly in *D. discoideum* no C-type lectins, nor TLR enchased in the plasma membrane have been characterized so far (Fig.4). Concerning TLRs, two cytosolic proteins in *D. discoideum* contain toll/interleukin 1 receptor (TIR) domains: TirA and TirB. TIR domains are a hallmark of TLRs, but neither TirA nor TirB contain both TLR canonical domains: leucine-rich repeats (LRR) and transmembrane domains. Despite not displaying all the features of a TLR, TirA still plays a role in efficient IC killing: *tir*A mutant cells exposed to an avirulent strain of Legionella exhibit a growth defect (Chen et al., 2007).

D. discoideum cells, unlike in human cells, use a single G-protein coupled receptor (GPCR), fAR1, to induce phagocytosis following binding to folate and lipopolysaccharide (LPS) (Pan et al., 2016, Pan et al., 2018) (Fig.4). Folate and LPS are two classical MAMPS: Folate is secreted by many bacterial species such as *K. pneumoniae* and is a strong chemoattractant for *D. discoideum* and LPS are a component on the bacterial outer membrane. In human cells, LPS binds TLR4 and folate binds folate receptors, which are cell surface glycosylphosphatidylinositol-anchored glycoproteins. In contrast, *D. discoideum* cells use a single receptor for the two MAMPS. In addition, fAR1 is also different from other chemoattractant GPCRs: it belongs to the class C GPCR family and exhibits a VFT extracellular domain for sensing multiple ligands (Pan et al., 2018). The main features of fAR1 is that it binds folate and LPS and also mediates engulfment of *K. pneumoniae*, as *far1* KO cells exhibit a specific phagocytosis defect (Pan et al., 2016). fAR1 is the only known GPCR bridging chemotaxis and phagocytosis.

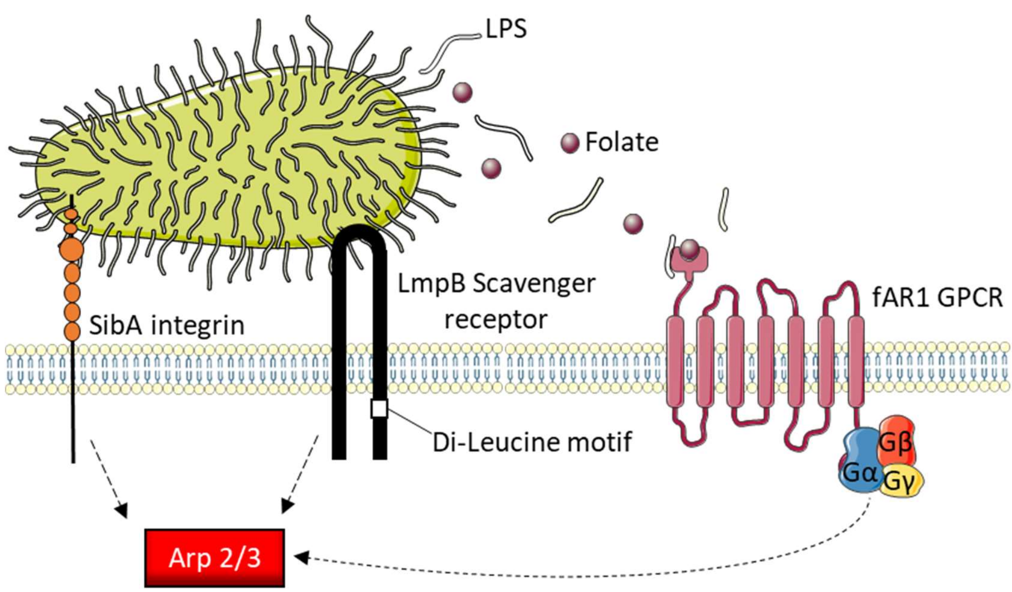

Fig.4 Phagocytosis initiation in *Dictyostelium discoideum*

Like in macrophages, MAMPs are directly recognized by their cognate receptors eventually triggering phagocytosis. SibA shares similarities with mammalian β integrin: notably an extracellular Von Willebrandt A domain, a glycine-rich transmembrane domain and a highly conserved cytosolic domain interacting with TalinA. LmpB is a scavenger receptor similar to the mammalian CD36 scavenger receptor. fAR1 is a GPCR, binding folate and LPS directly inducing phagocytosis.

2. Phagocytic cup: formation

The membrane cytoskeleton of human phagocytes is very dynamic, even in its "resting" state before induction of phagocytosis. In FRAP experiments, locally photobleached GFP-tagged cytoskeleton components (actin, α-actinin, ezrin and myosins) are replaced by their fluorescent counterparts within seconds. Cytoskeleton core components have a turn-over of a few seconds (Fritzsche et al., 2013). The dynamic remodeling activity of the cytoskeleton relies on a competition between two polymerizing F-actin networks: an actin branching system relying on Arp2/3, and a mesh system relying on Rho/formin/myosin (Lomakin et al., 2015). For phagocytosis to happen, the balance needs to tilt towards Arp2/3 branched structures, as formin-polymerized actin immobilizes transmembrane proteins obstructing membrane ruffling and the diffusion of non-tethered membrane proteins and even lipids (Ostrowski et al., 2016).

Tilting the balance begins by activation of the Src-Family Kinase (SFK), after the binding of the microorganism to PRRs. Activation of the SFKs recruits locally Syk, which in turn phosphorylates adaptors, kinases, and lipases. The unstimulated Arp2/3 complex is weakly active and requires stimulation by nucleation promoting factors (NPFs) to branch a novel actin filament at a 70° angle from an existing one (Goley and Welch, 2006). Members of the Wiskott-Aldrich syndrome protein (WASP) family are known to be major enhancers of the Arp2/3 complex activity (Politt and Insall, 2009). The WASP family contains two principal classes of proteins : WASPs and SCAR/WAVEs. Conformation change of WASPs proteins from inactive to active is triggered by binding to PIP_2, a phospholipid, whereas the Scar/WAVE complex is activated by the Rho GTPase Rac. Once activated both classes of proteins enhance Arp2/3 branching activity (Fig.5).

Remodeling the cytoskeleton contributes to an increased diffusion of non-engaged PRRs, thus favoring the formation of novel focal points of adhesion to the target. Moreover, further activation of integrins via Rap GTPases, downstream of Syk activation, provides a linkage between the target and the actin cytoskeleton via talin, kindlin, vinculin, and other associated proteins. The integrins engaged and tethered to the actin cytoskeleton are in fact sufficient to form diffusional barriers for a majority of protein and even lipid rafts (Maxson et al., 2018). The diffusional barrier is necessary to delimits a perimeter for optimal phagocytosis. Furthermore, if the target is too voluminous, presence of the diffusional barrier enables the maturation of the open tubular phagosomes while limiting a potential inflammation through the leakage of its content (Maxson et al., 2018).

In addition to the Integrin-based diffusion barrier, the protrusion is consolidated by Bin-Amphiphysin-Rvs167 (BAR) domain containing proteins. The BAR proteins are involved in stabilizing membrane curvature. Additionally, they bind directly the WASP family proteins, including N-WASP and WAVE, which then activate the Arp2/3 complex (Hanawa-Suetsugu et al., 2019).

Concerning the phagocytosis machinery in *D. discoideum*, overall the protrusion extension mechanism is very similar to that used by mammalian cells. MAMPs binding to PRRs leads to the stimulation of the SCAR/WAVE complex by Rac homologs, notably Rac1. The SCAR/WAVE complex activates Arp2/3 leading to actin branching that drives the formation of the phagocytic cup (Rivero and Xiong, 2016) (Fig.6). Similarly, segregation of membrane proteins is visible in the phagocytic cup by a mechanism restricting lateral diffusion (Mercanti et al., 2006). Additionally, BAR proteins stabilize the phagocytic cup. Among the BAR proteins in *D. discoideum*, only one localizes specifically at the protrusive rim of the cup and regulates both Rac and Ras activity: RGBARG. RGBARG induces protrusion formation by activating RacG, whilst restricting expansion of the cup interior by locally inhibiting Ras activity (Buckley et al., 2019).

3. Phagocytic cup: guiding and closure

In addition to PRRS, membrane lipids are actively involved in phagocytosis (Bohdanowicz et al., 2013). Phosphoinositides (PIs) are phospholipids that can be phosphorylated at different positions (3, 4 or 5) of their inositol head group. PIP_2 and PIP_3 play essential functions in phagocytosis. PIP_2, mostly localized to the inner plasma membrane leaflet and constitutes 1–2% of plasma membrane lipids. PIP_2 recruits and binds actin-binding proteins driving local actin branching (Mu et al., 2018). Conversion of PIP_2 to PIP_3, by the action of the PI3 kinase at the tip of the protrusion recruits myosins which exert contractile activity and function as a purse string to facilitate phagosome closure (Ostrowski et al., 2016). Phagosome closure eventually needs dephosphorylation of PIP_3 and disappearance of PIP_2 mediated by respectively by OCRL and Inpp5B (Bohdanowicz et al., 2012).

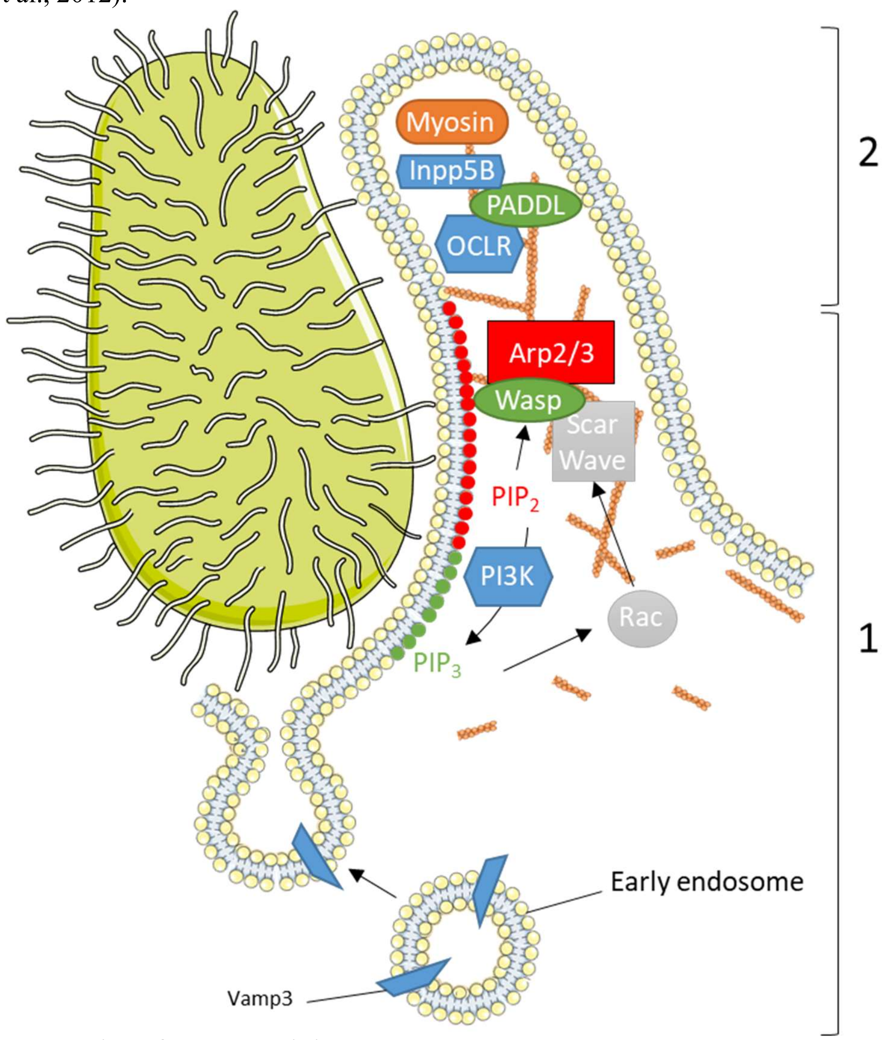

Fig.5 Molecular mechanism of phagocytosis in macrophages

1) Pseudopod extension. The extension is driven by actin polymerization by the Arp 2/3 complex. Activation of the Arp 2/3 complex depends on both relieving WASP inhibition and activating the Scar/Wave complex. WASP inhibition is relieved by binding PIP2. Scar/Wave complex activation is induced by RAC. RAC is notably stimulated after the production of PIP3 which results from the phosphorylation of PIP2 by PI3K. Finally, membrane supply, to support the extension of the phagosome cup, are delivered via fusion in the actin free bottom of the phagocytic cup. **2) Phagosome closure**. PIP3 and PIp2 are depleted at the tip of the pseudopod by OCRL and Inpp5B, reinstating WASP inhibition on Arp 2/3. OCRL is bound to the cytoskeleton by PADDL and the myosin located at the tip of the pseudopod generated the contractile force to close the phagosome.

Additionally, PIP_3 also recruits Rho GAPs that inactivate Rac1, terminating actin polymerization at the base of the phagocytic cup. Concomitant cleavage of PIP_2, to DAG and IP_3, by phospholipase C (PLC), also releases actin-binding proteins such as cofilin, WASp, and ezrin at the base of the phagocytic cup. The joint action of Rho GAPs and PLC, leading to the loss of actin at the base of the phagocytic cup, allows for fusion of vesicles with the plasma membrane (Niedergang and Chavrier, 2004). In a nutshell, PIP regulation is crucial to the protrusion formation, phagosome sealing and membrane fusion at the nascent phagosome base (Fig.5).

Interestingly PIP_2 is sensitive to the membrane curvature. New evidence suggests that it could autonomously induce receptor-independent phagocytosis. Binding of a solid particle curves the membrane, which induces a local sorting of PIP_2. PIP_2 recruits and activate moesin in turn binding Syk and leading to receptor-independent phagocytosis (Mu et al., 2018). The authors hypothesized that this mechanism it may explain how phagocytes recognizes almost all variations of solid.

In *D. discoideum*, the role of phosphoinositides is also established. PIP_2 accumulates near engaged PRRs and recruits NPFs and actin-binding proteins involved in membrane deformation in a similar fashion. PIP_2 is also phosphorylated by PI3K and cleaved by PLC. The PIP_2 decrease allows actin disassembly at the base of the phagocytic cup for vesicle fusion. Regarding phagosome closure, Dd5P4, the *Dictyostelium* homolog of human OCRL, dephosphorylates PIP_3 into PIP_2 which is an important step for the phagosome closure (Loovers et al., 2007). In conclusion, similar to mammalian phagocytic cells, PIP_2 decrease allows actin disassembly and PIP_3 dephosphorylation is also necessary for phagosome closure (Fig.6).

Phosphoinositides also plays a role in phagosome maturation in both human phagocytes and *D. discoideum* cells and will be subsequently described (Buckley et al., 2019, Luscher et al., 2019).

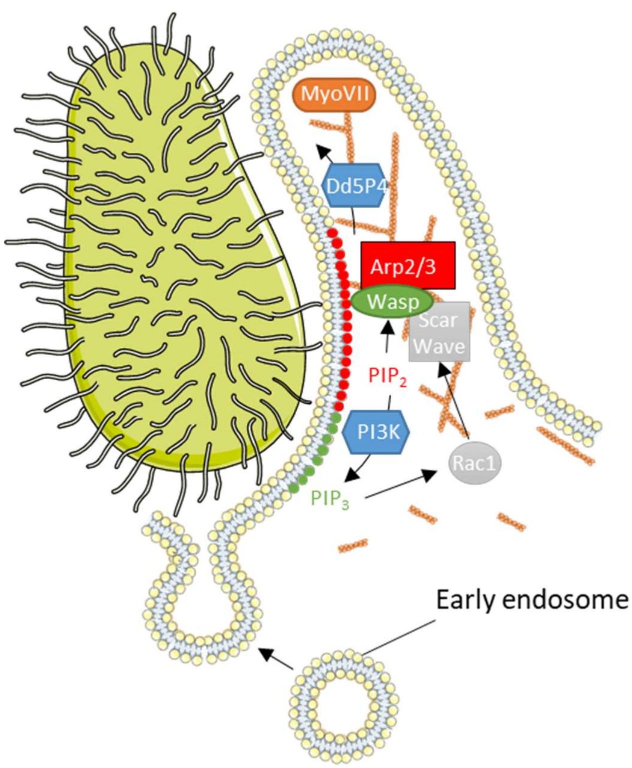

Fig.6 Molecular mechanism of phagocytosis in *Dictyostelium discoideum*

The phagocytic cup extension is, like in macrophages, driven by actin polymerization catalyzed by the Arp 2/3 complex. In a similar fashion activation of the Arp 2/3 complex requires to relieve WASP inhibition and promote the Scar/Wave complex activation. WASP inhibition is relieved by PIP_2 binding. Scar/Wave complex activation is done by RAC1. RAC1 is stimulated after production of PIP_3. PIP_3 production is catalyzed by PI3K from PIP_2. Membrane supply to support the extension are delivered via fusion in the actin free bottom of the phagocytic cup. At the tip of the pseudopod Dd5P4, the OCRL ortholog participates in reinstating WASP inhibition on Arp 2/3. Myosin located at the tip of the pseudopod generates the contractile for to close the phagosome. MyoVII is probably the main driving force.

III. Phagosomal maturation: comparative analysis in human and *D. discoideum*

The nascent phagosome quickly undergoes maturation. Within minutes after closure the phagosome becomes a highly acidic, degradative and oxidative compartment (Pauwels et al., 2017) (Fig.7). The maturation of the phagosome, both in human cells and in *D. discoideum*, is divided in three parts: fusion with the early endosomes, followed by fusion with late endosomes and finally with lysosomes. These three steps are a prerequisite for the phagosome to obtain its full microbicidal capacity. Interestingly, new material delivered to the phagosomes does not increase significantly the phagosome size nor decrease the size of the endosomes. This observation led to a model, coined *"kiss and run" (*Duclos et al., 2000), that favors repeated transient fusion events over a full fusion between compartments, although both events occur. The phagosomal maturation is also supported by a recycling machinery for protein sorting and recycling in order to allow several cycles of phagocytosis.

1. Rab GTPases regulates phagosome maturation

In human cells, the sequence of phagosome fusion with compartments of the endocytic pathway, as well as recycling of components from the phagosome, is highly regulated by Rab GTPases (Prashar et al., 2017) (Fig.7). Rabs are small GTPases, that cycle between a GTP-bound active state to a GDP-bound inactive state. Rabs show homology to YPT1/SEC4, which regulates membrane trafficking between internal organelles in yeast. Rabs are present on various organelles along the endocytic pathway and are often used to define the organelle identity (Gutierrez, 2013). Functionally, Rabs in conjunction with Rab adaptors and effectors, allow coordinated and sequential fusion of the phagosomes with vesicles (Gutierrez, 2013).

Over 20 Rabs are associated with phagosomes (Gutierrez, 2013). Among them, Rab5 and Rab7 where the first described and are essential for proper phagosome maturation (Chavrier et al., 1990). The first step of maturation is regulated by Rab5. Rab5 is recruited to phagosomes in a Rabex-5/Rabaptin-5 dependent manner (Horiuchi et al., 1997). Once Rab5 is recruited, it activates the Class III phosphoinositide3-kinase vacuolar protein-sorting 34 (VPS-34) (Kinchen et al., 2008). VPS-34 catalyzes the production of PI(3)P, which recruits proteins with PX or FYVE domains such as EEA1 (early endosomal antigen 1), PIKfyve, p40 (subunit of the NADPH oxidase) Hrs (Hepatocyte growth factor-regulated tyrosine kinase substrate), and the class C core vacuole/endosome tether (CORVET) complex (Vieira et al., 2004, Kinchen et al., 2008, Prashar et al., 2017). At this step the phagosome is able to fuse with early endosomes, in an EEA1 and SNARE dependent manner (Christoforidis et al., 1999), and to transition to the second step. The transition from an early phagosome to a late phagosome is marked by the conversion from Rab5 to Rab7 and the CORVET to HOPS (homotypic fusion and vacuole-sorting) complex switch (Gordon et al., 2016). Both conversions depend on the Mon1–Ccz1 complex activity. Mon1 inactivates RAB-5 by displacing RABX-5 and Ccz1 recruits Rab7 (Nordmann et al., 2010). Following the Rab5-to-Rab7 switch, late phagosomes are devoid of Rab5 and Rab5-bound-CORVET complex, while decorated with active Rab7 and the Rab7-bound-HOPS complex. The HOPS complex activity is necessary for the fusion with late endosomes and Rab7 activity is a prerequisite for the centripetal movement of phagosomes. During maturation, phagosomes migrate from the cell periphery to the vicinity of the microtubule-organizing center (MTOC) where lysosomes are numerous (Harrison et al., 2003). Binding to the microtubule is carried by the Rab7 effector RILP and the cholesterol sensor ORP1L working together to recruit the dynactin complex (Li et al., 2016). The marker for the completion of phagosome to lysosome fusion are LAMP1 and 2 (Huynh et al., 2007). Once acquired the phagosome can fuse efficiently with lysosomes in a SNAREs dependent fashion. A process again partly under the regulation of PIPs, where PI(3)P is required to prime SNAREs for fusion and PI(4)P is required during and after tethering of the HOPS complex to lysosomes (Jeschke and Haas, 2017).

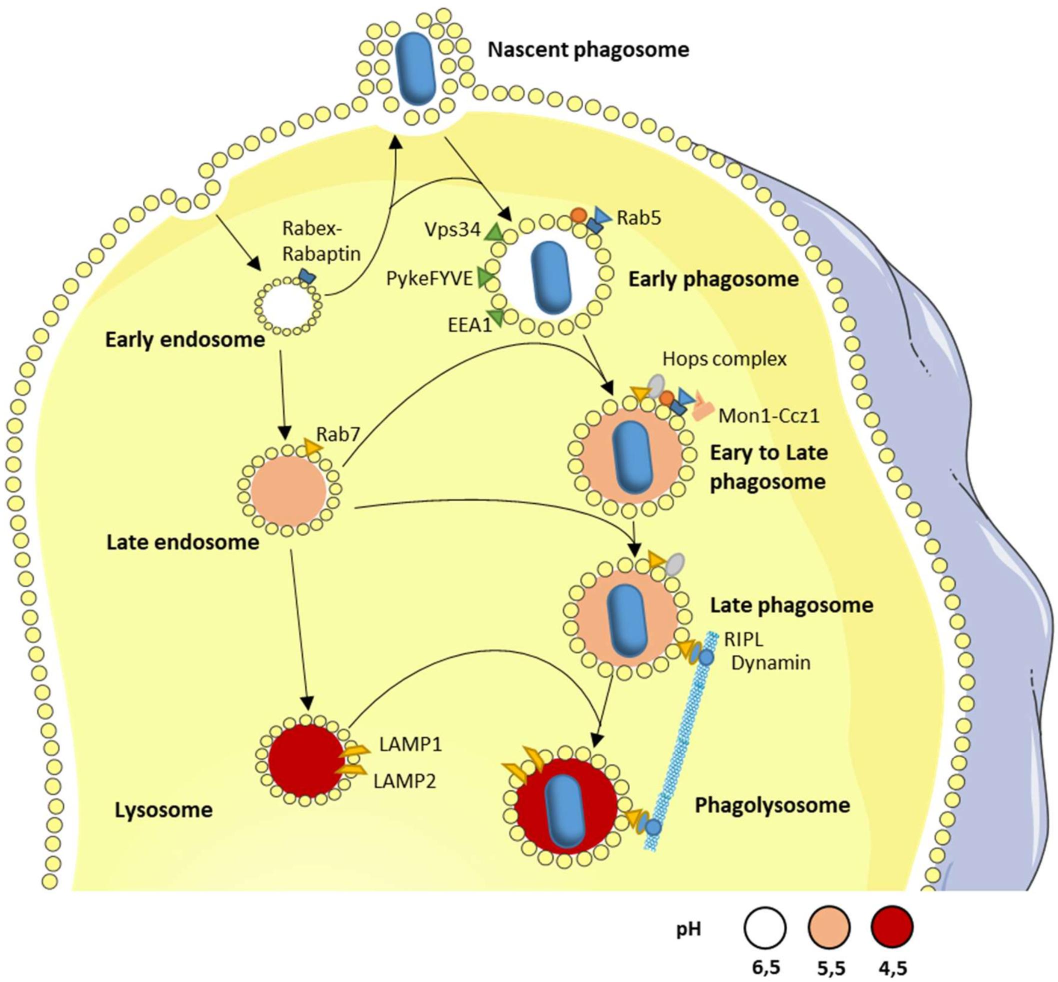

Fig.7 Maturation of the phagosome

Once the phagosome is sealed, the phagosome matures during a successive series of transient fusions with endosomes and lysosomes, leading to the formation of the phagolysosome. The first maturation marker, Rab5, is recruited to the phagosome by the Rabex/Rabaptin complex delivered via fusion with early endosomes. Rab5 activates VPS34 which produces PI(3)P. PI(3)P production serves to dock protein with PIP3-binding FYVE domains (PykeFYVE, EEA1). Rab5 also recruits the CORVET complex, a fusion machinery allowing fusion with endosomes. The phagosome up until the recruitment Rab7 is called the early phagosome. Transition to the late phagosome happens when Rab7 is delivered to the phagosome. Quickly Rab5 will be sorted out of the phagosome membrane by the Mon1–Ccz1 complex. Once only Rab7 is detectable the phagosome is known as the late phagosome. Transition to the phagolysosome occurs when the acidic lysosomes fuse with the late phagosome. RIPL, a Rab7 adaptor, anchors the late phagosomes to microtubules, driving the late phagosomes towards the Microtubule Organizing Center. The lysosomes, also anchored to the microtubules and numerous near the Microtubule Organizing Center, fuse with the phagosome. Fusion is detectable by the presence of LAMP1/2 on the membrane of the phagosome. The phagosome is now an acidic Rab7-LAMP1/2 positive phagolysosome.

In *D. discoideum,* phagosome maturation follows the *"kiss and run"* model but unlike in human phagocytes, fusion events are more rapidly orchestrated by Rab7 (Fig.8). Within 3 minutes after ingestion, Rab7 is localized at the phagosome (Rupper et al., 2001) whereas in macrophages it takes 30min (Seto et al., 2011). Early recruitment of the VPS-34 homolog DdPIK5 is also necessary (Zhou et al., 1995) and production of PI(3)P by VPS-34 recruits proteins with PX or FYVE domains such as PIKfyve (Buckley et al., 2019). Fusion with lysosomes is also important for proper maturation in *D. discoideum*. Similarly to human phagocytes, this fusion is mediated by SNAREs, in this case Vamp7 and syntaxin 7 (Flannagan et al., 2012).The fusion process is at least partially under LvsB control. LvsB inhibits Rab14 which promotes fusion between lysosomes and postlysosomes (Kypri et al., 2013). The main difference between the *D. discoideum* and human late phagocytic pathway is that the *D. discoideum* phago-lysosome typically matures into a postlysosome which is similar to the secretory lysosomes of some specialized mammalian cells (Blott et al., 2002). Vacuolar-ATPase, responsible for acidifying the phagosomes, is removed from the membrane of phagosomes in budding vesicles 30 minutes after ingestion (Carnell et al., 2011). The WASH complex, a regulator of actin polymerization is essential for the sorting out of V-ATPase (Carnell et al., 2011). Interestingly in human, WASH is enriched in the early recycling pathway compared to the late degradative pathway, as seen by its preferential colocalization with Rab5 but far less or not with Rab7 and LAMP (Derivery et al., 2019). The postlysosome, devoid of V-ATPase, exhibiting a near neutral pH, and an actin coat eventually fuses with the plasma membrane (Lima et al., 2012). Fusion of the postlysosome with the plasma membrane is regulated in a Ca^{2+} dependent manner by mucolipin, a member of the transient receptor potential ion channel family.

Other Rab GTPases play important regulating function in the endocytic pathway. In humans, Rab1 and Rab2 mediate the interactions between the phagosome and the ER, post-Golgi and ERGIC compartments (Gutierrez, 2013). Rab14 is involved in Trans-Golgi Network (TGN) to early endosomes and plasma membrane transport. Rab22A regulates the Rab5 to Rab7 switch. Rab32 and Rab34 regulates in conjunction with Rab7 fusion of the phagosome with the late endocytic pathway (Seto et al., 2011). Lastly, Rab4 and Rab11 regulates phagosomal recycling (Gutierrez, 2013). In *D. discoideum*, homologs of Rab1, Rab4, Rab11 and Rab14 have similar functions (Harris and Cardelli, 2002).

2. The recycling machinery

Proteins delivered to the phagosome during maturation, or originating from the plasma membrane, are recycled in order to allow their use in several cycles of phagocytosis (Fig.9). In human cells, cargoes delivered into early sorting endosomes that are destined to be degraded are segregated from cargoes destined to be recycled. Cargoes destined for degradation are ubiquitinated and recognized by the ESCRT complexes, which induce the formation of multivesicular bodies (MVBs). MVB formation results from the invagination of a portion of the limiting membrane of an endosome into its own lumen (Piper and Katzmann, 2007). The early endosome then matures into late endosome/lysosome, where its content is degraded when the MVBs fuse with lysosomes. On the other hand, cargoes that need to be recycled are spatially segregated into tubular structures of the sorting endosome (Piper and Katzmann, 2007). There, they are transported back to the surface or to the TGN by a "fast" recycling dependent on the retromer or retriever complexes, or via a "slow" recycling through the endosomal recycling compartment (ERC) (Maxfield and McGraw, 2004; Simonetti and Cullen, 2018). Both recycling pathways relies on Rab GTPases activity and a family of proteins involved in sorting cargoes: the sorting nexin family (SNXs). SNXs bind PI(3)P, via their PX domain. A subset of SNXs also contains BAR domains and induces membrane bending and tubulation (Worby and Dixon, 2002).

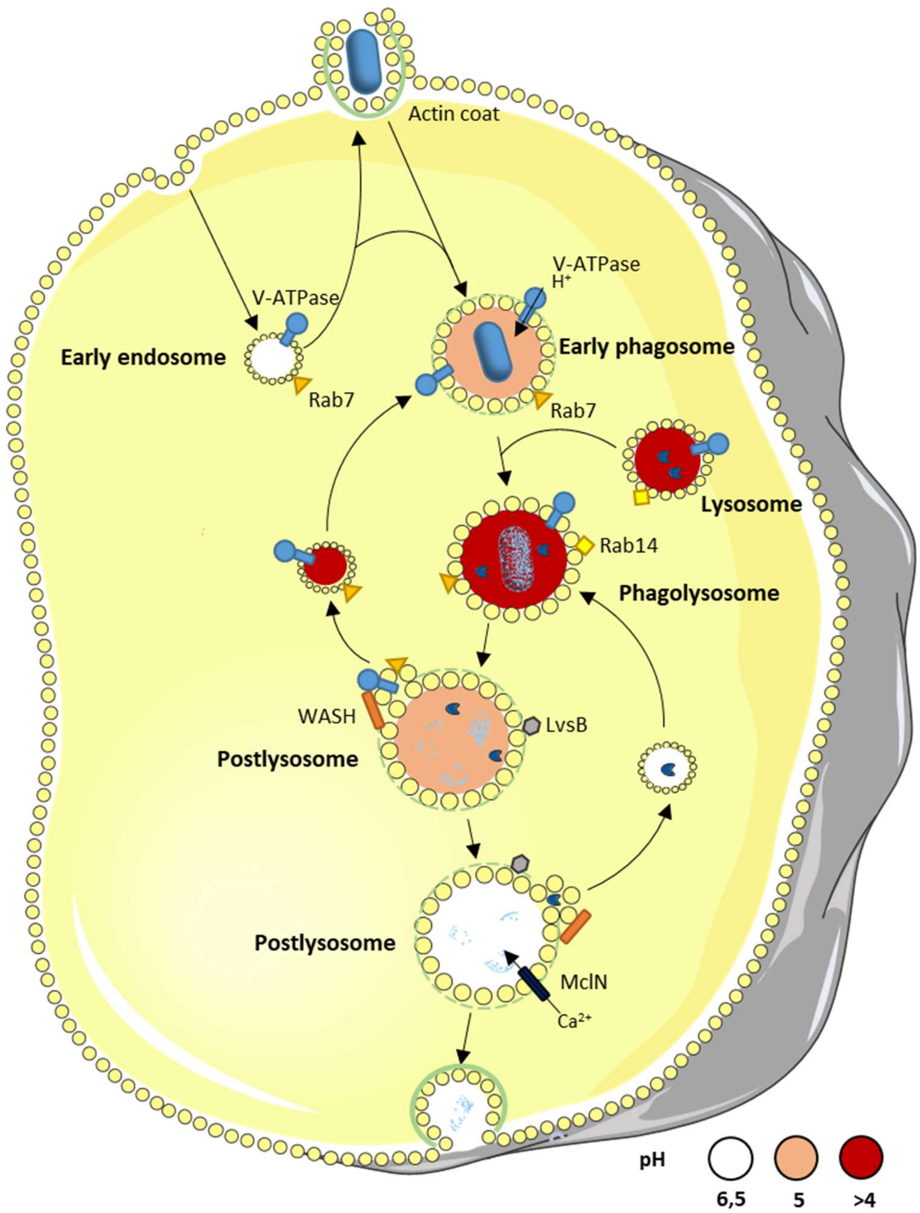

Fig.8 Phagosome maturation in *Dictyostelium discoideum*

Once closed, the phagosome containing bacteria sheds its actin coat, and rapidly acquires the V-ATPase and Rab7. The Rab7 positive phagosome fuses rapidly with lysosomes. Rapid acidification of the phagosome luminal pH is necessary for the lysosomal enzymes function. Fusion between phagolysosomes and lysosome is stimulated by Rab14. The phagolysosomes stay at peak acidity during approximately 20-30 min. Quickly after the V-ATPase and lysosomal enzymes are recycled by the WASH complex and the phagosome acquires LvsB, preventing fusion with acidic compartments. The phagolysosomes mature in a pH neutral large vacuolar named postlysosome. 40 to 60 min after, non-digested bacterial components are exocytosed by fusion of the postlysosome with the plasma membrane. Exocytosis speed is partially under the control of McIN, which store calcium in the postlysosome lumen, slowing down fusion with the plasma membrane.

Regarding the "fast" recycling, the retromer and retriever complexes are both heterotrimers composed respectively of: Vps35, Vps29, Vps26 and DSCR3, C16orf62, Vps29 (McNally et al., 2017, Gallon and Cullen, 2015). Regulation of how Vps29 interacts with the retromer or the retriever complex is unknown. However, both complexes interact with SNXs. The Retromer complex is known to interact with SNX-BAR heterodimers and ensures the recycling of membrane proteins from early endosomes to the TGN (Gallon and Cullen, 2015). The retromer complex can also interact with SNX27, for the recycling of certain plasma membrane proteins (Seaman, 2012; Burd and Cullen, 2014; Gallon and Cullen, 2015). Regarding the retriever complex, it was proposed to interact with other SNXs, such as SNX17, which binds NPx(Y/F)/Nxx(Y/F) motifs present on certain plasma membrane proteins, for example β1-integrin (McNally et al., 2017; McNally and Cullen, 2018).

An important partner of both the retromer and retriever is the WASH complex, an NPF responsible for activating the Arp2/3 complex, and thus driving actin polymerization (Carnell et al., 2011). The WASH complex localizes at retromer-enriched membranes on the membrane of early endosomes. Interaction with the retromer is carried out by the binding of the WASH complex subunit FAM21 with Vps35 (McGough et al., 2014). The WASH/Retromer complex creates an emerging tubule from the endosome, further pulled by dynein bound to SNXs. A scission mediated by EHD1 and dynamin separates the vesicle from the endosome (Lucas et al., 2016). EHD1 is one of the four members of the C-terminal Eps15 homology domain family of proteins which are ATPases that bind endocytic membranes and induce tubulation or vesiculation (Naslavsky and Caplan, 2011). WASH activity in early endosomes allows fast recycling of surface proteins back to the plasma membrane and retrograde transport of phagosome content to the TGN (Derivery et al., 2009; Gomez and Billadeau, 2009).

Regarding the "slow" recycling, the ERC, found at the juxtanuclear region, is enriched in Rab11 which is necessary for transport of proteins to the plasma membrane (Maxfield and McGraw, 2004). The ERC function is also regulated by SNX4 and members of the EHD family (Traer et al., 2007, Grant and Donaldson, 2009; Naslavsky and Caplan, 2011). SNX4 plays an important role in sorting the transferrin receptor (TfR) from the sorting endosome to the ERC (Traer et al., 2007) and EHD1 and EHD4 are involved in vesiculating tubular structures of the ER allowing transport of cargoes to the plasma membrane (Cai et al., 2013).

In *D. discoideum*, like in human phagocytes, plasma membrane components are efficiently recycled from an early endocytic compartment (Neuhaus and Soldati, 2000, Vines and King, 2019). Two phases can be distinguished. A fast phase, mediated by the WASH and retromer complexes, in an myoB-independent manner. A slow phase, relying on a juxtanuclear recycling compartment regulated by Rab11b, vacuolin and potentially MyoB activity (Neuhaus and Soldati, 2000, Bosmani et al., 2018). WASH participates in recycling of certain plasma membrane proteins, including SibA, presumably through its interaction with the retromer complex (Buckley et al., 2016). WASH induces F-actin polymerization providing forces to pull tubules from the sorting endosome (Simonetti and Cullen, 2018). Unlike in human phagocytes, the interplay between dynamin and EHD for the scission of the tubule is poorly understood. The unique EHD protein in *D. discoideum* induces vesiculation and scission of endosomal tubules, like DymA the dynamin ortholog in *D. discoideum,* but is delivered to the phagosome independently from DymA (Gueho et al., 2016). Moreover in *D. discoideum*, WASH, EHD and DymA overlaps only for a few minutes on phagosomes in the early stages and association between the WASH complex and EHD/DymA has not been demonstrated yet (Gueho et al., 2016).

While WASH promotes actin polymerization on the phagosome and retrieval of cargoes, the actin network coating the phagosome also prevents efficient delivery (Dieckmann et al., 2012). Abp1, a major F-actin binding protein on phagosomes, play a critical role: in *abp1* KO cells lysosomal fusion to phagosomes is increased, likely due to a disorganized actin network on the phagosome (Dieckmann et al., 2012). Abp1 regulation is important for the function of DymA in the early maturation step and MyoB in the late stage (Gopaldass et al., 2012). Proper delivery and retrieval of material back and forth from the phagosome require a tight regulation of the phagosome actin coating.

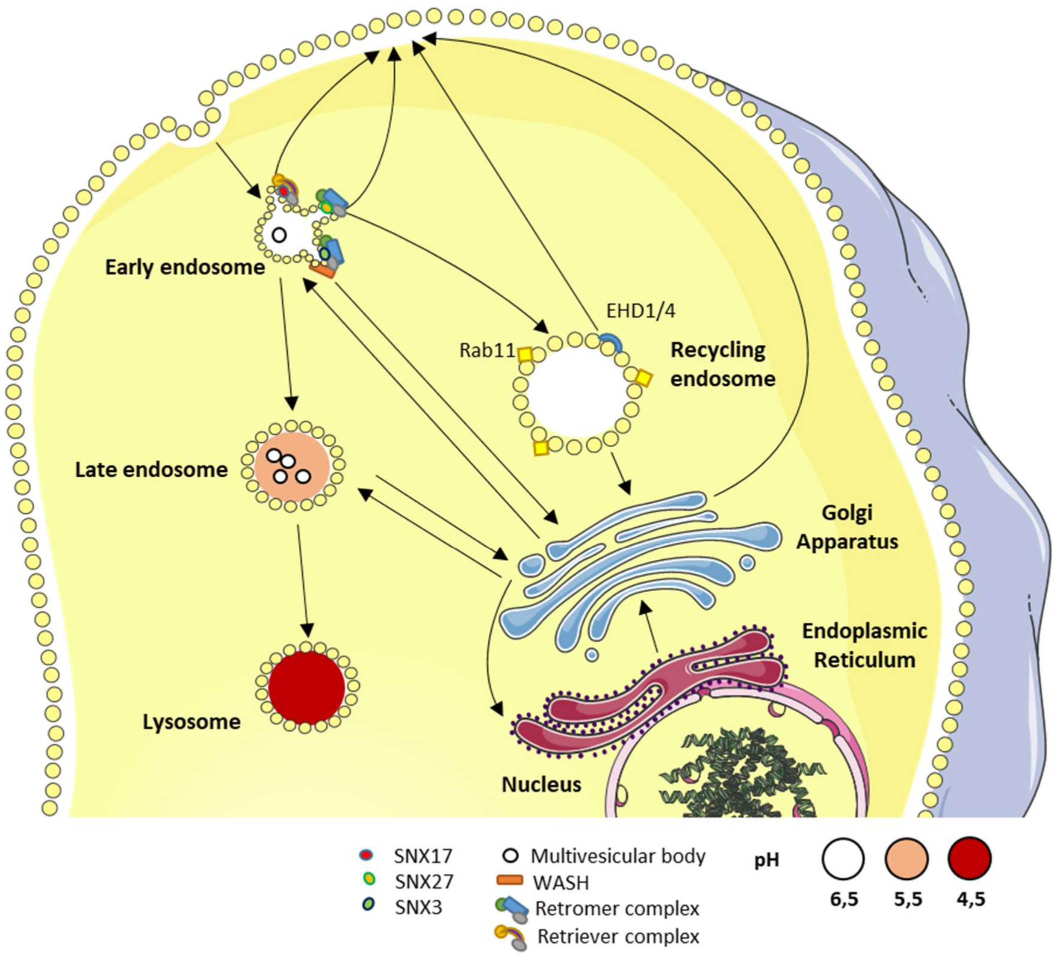

Fig.9 The recycling machinery

In mammalian cells, cargoes delivered for degradation into the early endosome are segregated from cargoes destined for recycling. Cargoes for degradation will be ubiquitinated and recognized by the ESCRT complex. It induces formation of multivesicular bodies (MVBs). Early endosomes then mature into late endosomes, where their content is degraded when the MVBs fuse with lysosomes. On the other hand, cargoes that need to be recycled are spatially segregated into tubular structures of the sorting endosome. They are transported back to the surface or to the TGN by a "fast" recycling dependent on the retromer or retriever complexes, or via a "slow" recycling through the endosomal recycling compartment (ERC). Both recycling pathways relies on Rab GTPases activity and a family of proteins involved in sorting cargoes: the sorting nexin family (SNXs).

IV. Intracellular killing mechanism: comparative analysis in human and *D. discoideum*

While the phagosome matures, a linear sequence of event unfolds starting with the acidification of the lumen of the phagosome, quickly coupled with the production of reactive oxygen species (ROS) and followed by the delivery of lysosomal enzymes. At the same time, metal transporters selectively deplete several metal ions and pump toxic metal ions into the phagosomal lumen (Dunn et al., 2018). All these mechanisms contribute to killing and digesting the phagocytosed bacteria. Role of autophagy will also be discussed in this section.

1. Acidification of the phagosome lumen

Acidification of the phagosome lumen by the H^+ V-type (vacuolar) ATPases minutes after closure was first measured 30 years ago (Lukacs et al., 1990). This proton pump consists of two subcomplexes, the membrane associated V0 and cytosolic V1 complexes. The V1 subcomplex is responsible for hydrolysis of the ATP, which causes a conformational change allowing the V0 complex to pump H^+ protons inside the phagosome lumen (Maxson and Grinstein, 2014). The V-ATPase is delivered by fusion to the phagosome of lysosomal vesicles or tubules (Sun-Wada et al., 2009). The lowest pH reached between 10 and 30 min after phagosome formation in macrophages is 4,5–5 (Sun-Wada et al., 2009). Acidification plays an important role in both intracellular killing and phagosome maturation: knocking down a subunit of the V-ATPase, leads to a pH neutral phagosome. It does not completely prevent maturation of the phagosomes but prevents efficient bacterial killing (Sun-Wada et al., 2009). pH alone can adversely affect bacterial growth, for *E. coli* growth is halted in media at pH 4 (Tsuji et al., 1982) and killed below pH 2.5 (Zhu et al., 2006) but in the phagosomes the pH does not drop below 4.5. It is more likely that acidification is required for several other IC killing mechanisms to take place (Sattler et al., 2013) (Fig.10).

Pathogenicity of several microorganisms relies on hijacking the V-ATPase function: either by preventing its delivery to the phagosome or inhibiting its function. In the case of *M. tuberculosis*, the pathogen produces PtpA, a protein which binds a subunit of the V-ATPase blocking its insertion in the phagosome membrane (Wong et al., 2011). Numerous others bacteria such as, *H. capsulatum, Streptococcus pyogenes, Rhodococcus equi, Yersenia pestis,* and even fungi such as *C. albicans* prevent the insertion of the V-ATPase in the phagosome membrane (Strasser et al., 1999, Nordenfelt et al., 2012, Toyooka et al., 2005, Pujol et al., 2009, Fernández-Arenas et al., 2009). Failure to hijack the V-ATPase function or delivery often results in less pathogenic strains (Uribe-Querol and Rosales, 2017).

Optimizing H^+ accumulation requires also efflux of cations and influx of anions, such as chloride through CFTR and CLC transporters (Di et al., 2006, Soldati and Neyrolles, 2012), to dissipate the development of a restrictive electrical gradient induced by the H+ influx (Di et al., 2017). Furthermore, it appears that chloride transporter plays an additional role in regulating the release of luminal Ca^{2+}, which is essential for phagosome-lysosome fusion in macrophages (Wong et al., 2017). Interestingly, a pH and voltage dependent selective proton channel Hv1 is enchased in the phagosome membrane. Hv1 allows a more pronounced acidification of the phagosome in macrophages at the cost of lower ROS production. On the contrary, it maintains a neutral phagosomal pH to sustain high ROS production in neutrophils (El Chemaly et al., 2014). This dichotomy is due to the ability of Hv1 proton channels to prevent the luminal alkalinisation caused by ROS production, which in neutrophils results in lower accumulation of VATPases that would acidify phagosomes (El Chemaly et al., 2014).

In *D. discoideum*, V-ATPase is rapidly delivered to the phagosomes and they acidify faster (Clarke et al., 2002) (Fig.11). In *D. discoideum* a GFP-tagged subunit of the V-ATPase is delivered to yeast-containing phagosomes 1-2 minutes after their closure and maximum acidification is reached 15 min after ingestion (Clarke et al., 2002). In mouse macrophages, the same delivery takes 6 min and the phagosome reaches its lowest pH 60 min after ingestion (Sun-Wada et al., 2009). This difference is most likely explained by the need for *D. discoideum* to ensure a rapid action of its lysosomal enzyme that requires an acidic pH (Sattler et al., 2013). *D. discoideum* phagosomes are also more acidic than mouse macrophages, with pH 4 or below (Marchetti et al., 2009, Sattler et al., 2013). Achieving a lower pH for *D. discoideum* ensures growth inhibition for a wider range of bacteria. As previously described, in *D. discoideum* the V-ATPase is sorted out of the postlysosome membrane 45-60min after ingestion by the WASH complex. Unfortunately, less studies have identified and characterized the counter-ion channels in *D. discoideum* on the phagosome membrane, the closest homolog to the chloride channel CFTR is ABCC.8 a member of ABC superfamily of transporter (Anjard et al., 2002) but has not been characterized, nor homologs to the cation transporter TRPM2 or even Hv1.

To survive in the highly acidic phagosome of *D. discoideum*, pathogens use similar strategies to those characterized in macrophages. For example, infection by *M. marinum* of *D. discoideum,* is very similarly to *M. avium* infection in macrophages. The mycobacterium initially prevents delivery or promotes extraction of the V-ATPase from the phagosome membrane. In *D. discoideum*, barely 50% of the phagosomes display the presence of a GFP-tagged subunit of the V-ATPase in the *M. marinum* containing phagosomes 20 min post infection; and the number keeps decreasing with time (Hagedorn et al., 2007).

Creating a proton gradient ensures not only regulation of the pH, in both organisms, but also transport of other ions in or out of the phagosome as well as transport and optimal activity of lysosomal enzymes, which will be subsequently described. Thus, association and dissociation of the v-ATPase is highly regulated during phagocytosis (Maxson and Grinstein, 2014).

2. ROS production in the phagosome

Enzymes that scavenge superoxide (O_2^-) and hydrogen peroxide (H_2O_2), such as superoxide dismutase or peroxiredoxins or catalases, are ubiquitously expressed in eukaryotic organisms. This observation drove research in oxidative stress since McCord in 1971 hypothesized that oxygen toxicity is mediated by partially reduced oxygen species, which are by-products of the aerobic metabolism and should be kept in check (McCord et al., 1971). Due to the high reactivity of the partially reduced oxygen species, they were labelled reactive oxygen species (ROS). Since their discovery ROS have been shown to function as antimicrobial effectors (Kovacs et al., 2015), signaling molecules that regulate NF-κB, (Yang et al., 2013), autophagy (Huang et al., 2009), cytokine secretion (Liu et al., 2014), inflammasome activation (Cruz et al., 2007), apoptosis (Miller et al., 2010), cytoskeleton dynamics and chemotaxis (Stanley et al., 2014). Generation of ROS is carried out by members of the NADPH oxidase (NOX) family (Buvelot et al., 2019). More specifically, the production of ROS in the phagosome of neutrophils and macrophages specifically has been linked to the NADPH oxidase: NOX2 (Royer-Pokora et al., 1986). NOX2 generates superoxide by transferring electrons from the cytosolic NADPH to a luminal O_2 molecule. The phagocyte oxidase (phox) complex comprises five subunits: gp91^{phox}/Nox2, p22^{phox}, p40^{phox}, p47^{phox}, and p67^{phox}. The phox complex also requires Rac1 and 2 for complete activation (Abo et al., 1991, Knauss et al., 1991). Two main enzymes subsequently convert superoxide into other ROS: superoxide dismutase and myeloperoxidase. The superoxide dismutase catalyzes superoxide conversion to hydrogen peroxide (H_2O_2). The myeloperoxidase, which catalyzes the production of hypochlorous acid HOCL (Nguyen et al., 2017). Hypochlorous acid (HOCl) is highly bactericidal at neutral or low pH (Levine and Segal, 2016). H_2O_2 oxidizes ferrous iron to generate highly reactive hydroxyl radicals •OH through a mechanism known as the Fenton reaction. Protons and chloride are provided for these reactions respectively by Hv1 and chloride transporters of the CFTR and CLC family (El Chemaly et al., 2014, Dunn et al., 2018) (Fig.10).

ROS targets are DNA, lipids, proteins and Iron-Sulphur (Fe-S) clusters. Interaction of ROS (notably •OH) with DNA can generate double strand DNA breaks. ROS induce other forms of DNA damage by oxidizing nucleoside bases leading to G-T or G-A transversions if unrepaired (Srinivas et al., 2019). ROS also induce mitochondrial DNA lesions, strand breaks and degradation of mitochondrial DNA (Srinivas et al., 2019). Efficient DNA repair is paramount to overcome ROS DNA damage. For example, knocking down endonuclease III and endonuclease VIII (that target DNA damaged by oxidizing agents in *E.coli*) results in a 100-fold growth defect after H_2O_2 treatment (Saito et al., 1997, Jankowski et al., 2002). Concerning lipids, peroxidation of polyunsaturated fatty acids alters the membrane bilayer by causing the formation of lipoperoxyl radicals (LOO•), which, in turn, react with lipids to yield a lipid radical and a lipid hydroperoxide (LOOH). LOOHs are unstable: they generate new peroxyl and alkoxy radicals and decompose to secondary products (Barrera, 2012). Glutathione peroxidase 4 KO mice, which are unable to stop this chain reaction, die prematurely underlying the importance to prevent lipid peroxidation (Muller et al., 2007). For proteins, ROS can cause oxidation of both amino acid side chains and protein backbones, resulting in protein fragmentation or protein-protein cross-linking. Oxidative modifications of proteins can change their physical and chemical properties, including conformation, structure, solubility, susceptibility to proteolysis, and enzymatic activity (Zhang et al., 2013). Additionally, HOCL produced by myeloperoxidase can chlorinate proteins, a process important during intracellular killing (Green et al., 2014). Finally, Iron-Sulphur (Fe-S) clusters are the most diversely used enzymatic cofactor. ROS oxidize ferrous iron to its ferric form, which quickly precipitates and becomes insoluble (Imlay, 2019). Aerobic organisms have evolved strategies to prevent oxidation of ferrous iron to keep using it as enzymatic factor.

Numerous pathogens have evolved an array of defenses against ROS, which is a good indicator of the damage oxidative stress could do. Bacterial defenses against ROS include an array of superoxide dismutases (SODs), catalases, and peroxiredoxins, but also various iron sequestering mechanism and oxidized DNA damage repair mechanisms. Some pathogens can also prevent ROS production in the phagosome lumen (Imlay, 2019). For example, to inhibit the Fenton reaction, *S. aureus* bacteria produces two superoxide dismutases and a catalase: sodA and sodM convert O_2- into H_2O_2 and the catalase KatA breaks down H_2O_2 into oxygen and water. KatA genetic inactivation decreases by 10^4-fold the resistance of *S. aureus* to oxidative stress (Cosgrove et al., 2007). This result suggests that *S. aureus* faces heavy ROS potential damage that are mitigated by the presence of KatA. *M. tuberculosis* has evolved mechanisms to subvert ROS production, by producing the ROS neutralizing protein nuoG, to avoid macrophage apoptosis and maintain a pathogen-friendly niche (Miller et al., 2010). Other pathogens even prevent recruitment of the full phox complex. For example, *H. pylori* prevents the recruitment of $p40^{phox}$ and $p67^{phox}$ (Allen et al., 2005) and *Coxiella burnetti* prevent the recruitment of $p47^{phox}$ and $p67^{phox}$ on the phagosome membrane (Siemsen et al., 2009). Conversely, bacterial strains unable to counter ROS production or its effect are to less pathogenic (Nguyen et al., 2017).

Following the sequencing of the *D. discoideum* genome, three catalytic NOX subunits (NoxA, B and C) were identified by homology with the mammalian NOX family. NoxA and NoxB are homologs of Nox2, and NoxC is a homolog of Nox5. Two other homologs of the phox complex have been identified: CybA and NcfA, respectively homologs to $p22^{phox}$ and $p67^{phox}$ (Lardy et al., 2005, Zhang et al., 2013). Combined RT-PCR and RNAseq experiments indicate that NoxA, CybA and NcfA are expressed during vegetative growth while NoxB and NoxC are mainly expressed during multicellular development (Lardy et al., 2005, Rosengarten et al., 2015). NoxB expression is also upregulated when an axenic strain grows on a lawn of *K. pneumoniae*, but the role of NoxB in this situation remains to be determined (Nasser et al., 2013). Surprisingly, *nox*A KO cells in vegetative state exhibit no detectable killing defect of non-pathogenic strains of *Klebsiella* and *B. subtilis* (Benghezal et al., 2006). Either ROS production is too low to cause a significant oxidative stress for the bacteria, or redundant killing mechanisms compensate for the loss of ROS production. To check if ROS production is sufficient to induce DNA damage, the mutation rate was measured in a *D. discoideum* lacking the Xpf nuclease, a component of the DNA damage repair machinery. When grown in the presence of bacteria (Pontel et al., 2016), The mutant strain accumulated more mutations than in bacteria-free medium, suggesting that ROS production in the presence of bacteria is potent enough to damage even the amoeba's own DNA. The lack of a killing defect in *nox*A KO cells is thus more likely to be a consequence of redundant killing mechanisms. In agreement with the idea that ROS production in *D. discoideum* is high. *D. discoideum* membranes have been shown to be highly resistant to oxidative stress (Katoch and Begum, 2003), and the genome encode for numerous SODs and catalases (Akaza and Yasukawa, 2002).

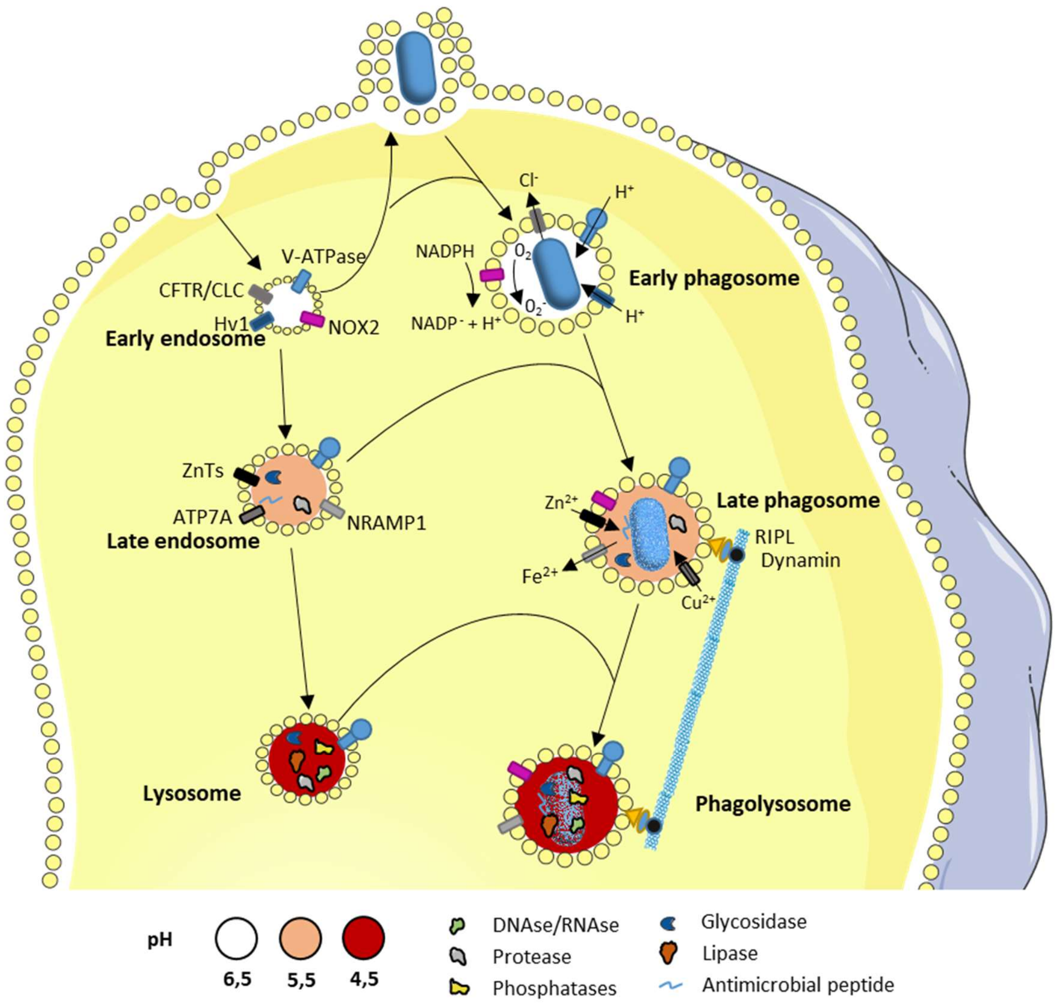

Fig.10 Bacterial Intracellular killing in macrophages

Early during the maturation of the phagosomes both the V-ATPase and the NOX2 complex are delivered to the phagosome containing the bacteria. The V-ATPase pumps protons in the phagosome lumen, while the NOX2 complex generates ROS in the phagosome lumen. The phagosome becomes an acidic and oxidative environment for the bacteria. After fusion with early endosomes, the phagosome fuses with late endosomes delivering the first antimicrobial peptides and degradative enzymes often in their proenzyme state to finish their maturation in the acidic phagosome. Additionally, transporters such as NRAMP1, depleting the phagosome of traces ions, are delivered with late endosomes. Conversely, other metal transporters such as ZnTs an ATP7A pump zinc and copper inside the phagosome lumen to poison the bacteria. The phagosome acquires full intracellular killing efficiency when it fuses with lysosomes. Reaching its peak acidic pH, the bacteria now faces mature lysosomal enzymes, antimicrobial peptides, oxidative stress, nutritional immunity and metal poisoning.

Although in *D. discoideum* the role of ROS in intracellular killing of bacteria remains to be established, ROS play a role in chemotaxis (Castillo et al., 2017), and during the multicellular development (Bloomfield and Pears, 2003, Zhang et al., 2016). During the development cycle, a subpopulation called sentinel cells retains a high phagocytic capacity compared to other cells in the slug. Interestingly, sentinel cells can produce DNA extracellular traps (ETs), a feature initially observed in mammalian immune cells (Brinkmann et al., 2004, Boe et al., 2015). The ETs consist of antimicrobial peptides, proteases, and signalling molecules bound to DNA released from the nucleus or mitochondria. Not only does *D. discoideum* use a similar strategy to mammalian phagocytes but it can also be triggered in a similar fashion: a strong LPS stimulation leads to ETs release in a ROS dependent manner (Zhang et al., 2016). Indeed, a *nox*ABC triple mutant in *D. discoideum* is unable to produce ROS and does not produce ETs. Although NOX-independent ETs have been described in mammalian immune cells as well as other stimuli that trigger ETs release (Arai et al., 2014, Douda et al., 2015), it remains fascinating that *D. discoideum* cells share this mechanism with human phagocytes (Zhang and Soldati, 2016).

3. Lysosomal enzymes

Further along the maturation pathway, phagosomes fuses with lysosomes. Lysosomes act as the digestive system of the cell, although they are also essential in the regulation of numerous other functions such as cells growth, division or differentiation (Lawrence and Zoncu, 2019). Over 50 monogenic human genetic diseases ranging from mild to severe symptoms are associated with lysosomal dysfunctions (Lübke et al., 2009) (Fig.10).

The digestion of the phagocytosed content is performed by an array of enzymes, present in the lysosome lumen, capable of breaking down virtually all types of biological polymers—proteins, nucleic acids, carbohydrates, and lipids (Luzio et al., 2014). Almost all the lysosomal enzymes are acid hydrolase with optimal functional pH around 4.6 (Xu an Ren, 2015) highlighting the importance of acidifying the phagosome. In human cells, transfer of lysosomal enzymes to the lysosomes is carried out by two pathways, a Mannose 6-phosphate-dependent and a Mannose 6-phosphate-independent pathway (Luzio et al., 2014, Blantz et al., 2015). Most luminal lysosomal enzymes are routed to the lysosome by the Mannose 6-phosphate-dependent pathway: after insertion in the lumen of the endoplasmic reticulum, signal sequence cleavage, and core glycosylation, they traffic to the Golgi complex where they are modified with M6P residues. When they reach the trans-Golgi network (TGN), they are recruited by one of two Mannose 6-phosphate receptors and trafficked to endosomes. The acidic pH of the endosome lumen dissociates the enzymes from their receptors allowing the receptors to recycle to the TGN via the retromer machinery. The acid hydrolases then move on to endolysosomes and lysosomes and can be further modified, leading to enzyme activation. On the other hand, Mannose 6-phosphate-independent delivery to lysosomes is more poorly understood (Lawrence and Zoncu, 2019). One of the best described modalities implicates the scavenger receptor LIMP-2, acting as a trafficking receptor for the β-glucocerebrosidase (Blantz et al., 2015).

In most intracellular pathogens described previously, an important defense is to prevent the fusion between lysosomes and phagosomes. A second line of defense is the production of specific lysosomal enzymes inhibitors. For example, *S. aureus* can secrete three related protease inhibitors, Eap EapH1 and EapH2, which specifically target the neutrophil serine proteases (Stapels et al., 2014). They are very potent inhibitors; the enzymatic activity of neutrophil serine proteases is 20 times higher when the neutrophils are mixed with a supernatant of ΔeapΔH1ΔH2 *S. aureus* compared to cells exposed to a supernatant of WT *S. aureus.* The ΔeapΔH1ΔH2 mutant *S. aureus* is also less pathogenic when injected in mice (Stapels et al., 2014). Blocking lysosomal enzymes is a very effective way for pathogens to extend their survival in the degradative phagosome environment.

D. discoideum harbours two main classes of lysosomal enzymes. The first class includes enzymes bearing modified N-linked oligosaccharide chains with mannose-6-phosphomethyldiester and/or mannose-6-sulfate (Freeze et al., 1990) (Fig.11). The second class of enzymes exhibit an N-acetylglucosamine-1-phosphate (GlcNAc-1-P) (Souza et al., 1997). The first class contains enzymes such as α-mannosidase, β-glucosidase, and cathepsins and in the second class cysteine proteases. These two families are present in different vesicles, and delivered to phagosomes in a sequential manner, with first a wave of GlcNAc-1-P modified lysosomal enzymes followed by enzymes bearing the mannose-6-sulfate modification (Gotthardt et al., 2002).

Lysosomal enzymes such as cathepsin D could potentially play a role in intracellular killing, but very little is known about their cellular function. A cathepsin D KO *D. discoideum* grew as efficiently as WT cells in the presence of *K. pneumoniae* bacteria, suggesting that it does not play a critical role in intracellular killing (Journet et al., 1999). On the other hand, some mutants affect transport or activity of several enzymes : WASH, LvsB, AP3, Phg1A/Kil1. Many of these mutant cells feed poorly upon bacteria, suggesting that they may be defective in intracellular killing (King et al., 2013, Kypri et al., 2014, Charette and Cosson, 2008, Le Coadic et al., 2013). This observation suggests that *D. discoideum* is capable of using degradative enzymes to kill ingested bacteria. Among the abovementioned mutants, WASH and Phg1A/Kil1 directly affect IC killing as measured by improved survival of ingested bacteria (King et al., 2013, Le Coadic et al., 2013). Correct recycling and/or correct targeting of lysosomal enzymes are necessary for efficient intracellular killing of bacteria.

4. Lysozyme

The lysozyme remains a specific case of lysosomal enzyme since only one third is stored in lysosome while the rest is secreted. The lysozyme is delivered to the lysosome in a M6P-independent pathway and the optimal pH for the muramidase activity extends from 5 to 7 (Lemansky and Hasilik, 2000). The first observation of the lysozyme microbicidal activity by Alexander Fleming dates back to 1922. Nasal secretion of a patient suffering from acute coryza were shown to inhibit growth of a large spectrum of microorganisms (Fleming, 1922). The microbicidal activity is carried out by a single enzyme coined lysozyme. More specifically the lysozyme has a muramidase activity, it hydrolyzes the β-1,4 glycosidic bond between N-acetylglucosamine (NAG) and N-acetylmuramic acid (NAM). This disaccharide is a major component of the bacterial cell wall. Lysozyme defective for the muramidase activity still retain a microbicidal pore-forming role suggesting that it may participates in bacterial killing both by digesting the bacterial cell wall and by permeabilizing its membrane(s) (Düring et al., 1999, Nash et al., 2006).

To survive in the phagosome when exposed to the lysozyme activity, a bacterium should evolve an anti-lysozyme strategy. One efficient strategy is to modify the bacterial cell wall to prevent recognition by the lysozyme: for example, *S. aureus* acetylates its surface peptidoglycans. The modification is catalyzed by the acetyl-transferase OatA. In an OatA-defective mutant *S. aureus* acetylation of peptidoglycans is no longer detectable by HPLC (Bera et al., 2006). This strain is highly sensitive to lysozyme. Conversely, in a lysozyme-sensitive Staphylococcus strain, expression of OatA was sufficient to restore growth in presence of Lysozyme (Bera et al., 2006). Modification of the peptidoglycan by OatA is thus an efficient strategy to counter the lysozyme activity.

The *D. discoideum* genome encodes 22 putative lysozymes (Lamrabet et al., 2020) of which only AlyA has been characterized (Müller et al., 2005). AlyA account for 50% of *D. discoideum* lysozyme activity, but there is no direct evidence of a role in killing. Maybe this result is due to the fact that *aly*A KO cells progressively compensate the loss in lysozyme activity (Müller et al., 2005). For the other members of the ALY family: AlyB, C, D, and L only RNAseq data has been published (Nasser et al., 2013). The data shows that the expression of AlyA, B, C, and D are upregulated when *D. discoideum* cells are exposed to Gram+ bacteria whereas only AlyL was upregulated in the presence of Gram- bacteria (Nasser et al., 2013). Differential expression of ALYs in the presence of Gram+ or Gram- bacteria suggests non redundant functions of the set of lysozymes. This result favors the hypothesis that *D. discoideum* cells are capable of discriminating bacterial types and adapt accordingly their digestion and/or intracellular killing mechanisms.

5. Antimicrobial peptides

In mammalian phagocytes, antimicrobial peptides (AMPs) are found in granules of neutrophils and secreted by epithelial cells (Mahlapuu et al., 2016). AMPs mostly share three features: a short aa sequence (10-50aa), a global positive charge (+2 to +11) and on average 50% of hydrophobic residues. Most of the AMPs described target the integrity of the membrane, and a subset target metabolic pathways or DNA stability/synthesis (Nguyen et al., 2011). They also activate elements of the human acquired immune system, notably T cells and dendritic cells (Yang et al., 1999; Kosikowska and Lesner, 2016). Bacterial membranes are negatively charged allowing AMPs to bind (Mahlapuu et al., 2016). When bound to a membrane, AMPs form a pore and permeabilize the membrane. Some AMPs exhibit in addition target other key cellular processes including protein synthesis, protein folding, DNA/RNA and enzymatic activity, and cell wall synthesis (Joo et al., 2016).

To resist AMPs, bacteria have evolved resistance mechanisms including sequestration in biofilm, proteolytic degradation, repulsion by cell surface/membrane alteration, and export by efflux pumps (Joo et al., 2016). Once again, the case of *S. aureus* is interesting to decipher resistance mechanisms to AMPs, because lysogenic strains have evolved both (1) a mechanism sequestering α-defensins, and (2) a change of surface charge which limits the effectiveness of AMPs. (1) Lysogenic strains of *S. aureus* produce staphylokinase (SAK) a protein that binds α-defensins, one of the prominent family of AMPs in the neutrophil granules, decreasing its microbicidal effect (Ganz et al., 1985, Jin et al., 2004, Joo et al., 2016). Conversely, *S.aureus* strains like LS-1 that do not express SAK are very sensitive to α-defensins, a phenotype that can be compensated by the expression of *sak* in LS-1 strains. (2) AMPs are cationic and bind predominantly negatively charged membrane lipids (Peschel et al., 2001). Lipid analysis of *S. aureus* shows a high concentration of an unusual Lysyl-phosphatidylglycerol (L-PG) lipid which results from esterification of phosphatidylglycerol (PG) with L-lysine, a positively charged aa (Peschel et al., 2001). The PG to L-PG esterification is catalyzed by MprF, as demonstrated by the observation that a mutant with an inactivated *mprF* lacks L-PG. An *mprF* mutant strain exhibits an increased binding to AMP and a faster kinetic of IC killing by neutrophils (Peschel et al., 2001). Repelling AMPs by positively charging bacterial surface components participates actively in the increased survival of *S. aureus* inside the phagosome.

Only few antimicrobial peptides have been characterized in *D. discoideum*, the last to date is a member of the saposin-like proteins (SAPLIP) called AplD (Dhakshinamoorthy et al., 2018). SAPLIPs interact with membranes and have a pore-forming role, in multiple organism, notably in amoeba (Leippe, 2014). AplD is a member of the amoebapore-like peptides (Apl) family. AplD is not necessary for intracellular killing in vegetative cells, but when undergoing multicellular development *apl*D KO cells forms a slug devoid of protection against *K. pneumoniae* (Dhakshinamoorthy et al., 2018). *apl*D expression increases during the development cycle. The *Dictyostelium discoideum* genomes encodes 17 Apl genes, and it is likely that other Apls play a role in IC killing and/or protection of the slug.

6. Nutritional immunity

In 1975, Weinberg coined the term nutritional immunity to describe how plants and animals try to fight off pathogens by limiting access to iron for the pathogens (Weinberg, 1975). Today it refers to the inhibition of microbial growth in the host through the concerted action of effectors that sequester essential nutrients from invading bacteria notably iron, zinc and manganese (Juttukonda and Skaar, 2017). Although zinc starvation is observed at the organism level to fight off infection, zinc is toxic in excess (Niederweis et al., 2015, Hennigar and McClung, 2016). Immune cells use it to increase the concentration of zinc and other metals such as copper in the phagosome, in a process referred as metal poisoning (Dunn et al., 2018) (Fig.10).

Regarding nutritional immunity, the Natural Resistance-Associated Macrophage Protein (NRAMP) family of divalent-metal transmembrane transporters regulates metal-ion homeostasis and transports a broad range of transition metals (Wessling-Resnick, 2015). In human cells, two NRAMP members have been identified: NRAMP1 and NRAMP2 which are transmembrane proteins with >70% sequences similarities (Wessling-Resnick, 2015). Both protein are not interchangeable cation transporters, NRAMP1 is located in the membrane of late endocytic compartment, lysosomes, and maturing phagosomes in professional phagocyte and preferentially transports Mn^{2+}, Fe^{2+}, and Co^{2+}, NRAMP2 is located at the plasma membrane of virtually all cells and is a less restrictive transporter of Mn^{2+}, Fe^{2+}, and Co^{2+} as well as Zn^{2+}, Cd^{2+}, Cu^{2+}, Ni^{2+}, and Pb^{2+} (Wessling-Resnick, 2015). NRAMP1 contributes to the resistance to intracellular bacterial infection: mice with reduced NRAMP1 activity are more susceptible to infection by several intracellular pathogens such as *Mycobacterium* species, *Leishmania donovani*, and *Salmonella* species (Vidal et al., 1995). Both NRAMPs activity depend on a H^+ gradient to drive metal transport, in the case of NRAMP1 the gradient is generated by the V-ATPase (Garrick et al., 2006, Jabado et al., 2000). NRAMP2 acts as a proton symporter, but it remains to be determined if NRAMP1 is a cotransporter or an exchanger (Wessling-Resnick, 2015). Arguments favoring the latter correlates well with both sequence similarities between NRAMPs and the current hypothesis of nutritional immunity in which pathogen access to metals is restricted (Niederweis et al., 2015).

Iron is the divalent metal of choice for catalysis of a range of redox-based life-supporting reactions, and availability to the microorganism once phagocytosed is vital (Núñez et al., 2018). One strategy to counter iron depletion in the phagosome is to secrete siderophores meaning "iron carrier" in Greek. In hypervirulent *K. pneumoniae*, aerobactin is the main secreted iron siderophore (Russo et al., 2014). A knockdown of *iucA*, a gene involved in the synthesis of aerobactin causes 92% reduction in siderophore activity. In vivo data in the same study showed that mice infected with WT *K. pneumoniae* have a 10% chance of survival 15 days post infection, whereas mice infected with an *iucA* KO *K. pneumoniae* strain have an 80% chance of survival (Russo et al., 2004). Iron capture by siderophores to counter nutritional immunity is of paramount importance for the pathogen and has been demonstrated in numerous pathogens (Núñez et al., 2018)

The *D. discoideum* genome encodes two NRAMP proteins called NRAMP1 and NRAMPB (formerly NRAMP2). NRAMP1 is orthologous to NRAMP1 in mammals, whereas NRAMPB is more closely related to the prototypical NRAMP from bacteria (Buracco et al., 2015). Both transporters are in different subcellular compartments: NRAMP1 localizes to macropinosomes, phagosomes, and to the Golgi region, NRAMPB is exclusively found in the membrane of the contractile vacuole (CV). The two transporters function differently: NRAMP1 transports Fe^{2+} and Mn^{2+} in a proton-dependent manner, whereas NRAMPB transports only Fe^{2+} in a proton-independent manner (Buracco et al., 2015). More specifically, NRAMP1 acts as a symporter using the V-ATPase-generated proton gradient to transport iron out of the phagosome. Although the V-ATPase complex localizes also at the membrane of the CV, it is inactive. Nonetheless, NRAMP2 is able transport Fe^{2+} inside the lumen of the CV (Peracino et al., 2015). During the maturation of phagosomes, iron is progressively exported out of the phagosomes. This efflux is abolished in *nramp*1 KO cells (Buracco et al., 2015). This result indicates that NRAMP1 is the main transporter ensuring efflux of iron out of the phagosome (Buracco et al., 2015) (Fig.11). The exact role of iron efflux in the maturation of the phagosome is not clear but failure to restrict iron access to intracellular pathogen leads to increase replication of the pathogen (Peracino et al., 2005): infection of a *nramp1* KO strain and a nramp1-overexpressing strain by *L. pneumophila* gave diametrically opposed results. The KO strain contained almost 100 times more viable bacteria than the overexpressing strain (Peracino et al., 2005). The *nramp*1 KO strain is thus more permissive for intracellular growth of *L. pneumophila* but also facilitates *Mycobacterium* species escape from the phagosome (Simeone et al., 2015). Both phenotypes could be linked by the ability of *L. pneumophila* and *Mycobacterium* species to inhibit the recruitment of the V-ATPase to the phagosome, which prevent NRAMP1 proton-driven iron transport activity. By doing so the pathogens ensure that iron ions in the phagosomes are not depleted. Thus, nutritional immunity is also a means for *D. discoideum* to limit replication of pathogens in the phagosomes, notably by restricting access to iron.

7. Metal poisoning

After iron, zinc is the second most abundant trace element essential for all living organisms. It exists as a divalent cation (Zn2+) which is not redox active under physiological conditions. (Kambe et al., 2015). Among its numerous roles, zinc is essential for macrophage antimicrobial functions (Vignesh and Deepe, 2016). The macrophage selectively intoxicates or deprives ingested microorganisms, by importing zinc in the phagosome or exporting it out (Vignesh and Deepe, 2016). Both processes are respectively dependent on Zrt-, Irt-related proteins (Zips) that transfer extracellular and intra-organelle Zn into the cytosol, and zinc transporters (ZnTs) that export cytosolic Zn from the cytosol into the extracellular space and into organelles. Both processes occur in conjunctions with Zn binding proteins such as calprotectin and metallothioneins (Vignesh and Deepe, 2016).

Some pathogens have evolved strategies to counter Zn poisoning. For example, during *M. tuberculosis* infection, zinc poisoning is suspected to happen via its release from metallothioneins during the oxidative burst (Botella et al., 2011). To counter this release *M. tuberculosis* uses a battery of heavy metal efflux P-type ATPases (CtpC, CtpG, and CtpV) (Botella et al., 2011). *Ctp*C mutants exhibit impaired intracellular growth, demonstrating the necessity to resist zinc poisoning (Botella et al., 2011).

In *D. discoideum* , eleven putative zinc transporters have been previously identified and categorized into different subgroups by functional analogy to mammalian zinc transporters (Sunaga et al., 2008). The classification in 3 Zips, 4 “LZT-like superfamily” and 4 “Cation efflux subfamily” was challenged in 2018 (Dunn et al., 2018). The updated classification is 7 Zips and 4 ZnT (Dunn et al., 2018). Functional analysis remains to be carried out to confirm if *D. discoideum* cells use Zn poisoning or deprivation to hamper pathogen replication or increase bacterial killing.

Another ion implicated in metal poisoning strategies of macrophages is copper (Hodgkinson and Petris, 2012). Unlike zinc, copper is redox active and cycles between the two oxidative states Cu^{+} and Cu^{2+}. This redox property enables copper to catalyze the production of hydroxyl radicals via the Fenton and Haber Weiss reaction, therefore generating ROS. Alternatively, copper can also bind protein, especially via binding to cysteine, and disrupt their structure. This structural damage is particularly disruptive for iron-sulfur cluster proteins (Hodgkinson and Petris, 2012). To prevent self-damage to the organism, proteins involved in copper uptake, sequestration, and trafficking tightly regulate copper homeostasis in cells. Copper uptake into the cytosol is mediated by the copper permease CTR1. Intracellular copper is taken over by chaperones such as ATOX1, CCS, and COX17. Copper is imported into the TGN by the action of two P-type ATPases: ATP7A and ATP7B. ATP7A is localized at the TGN, at the plasma membrane where it mediates copper efflux from the cytosol to the extracellular space, and at the phagosomal membrane, where it imports copper from the cytosol into the phagosomal lumen; ATP7B is localized a the TGN and only translocates to the membrane and endo-lysosome under copper overload (Besold et al., 2016, Parisi et al., 2018).

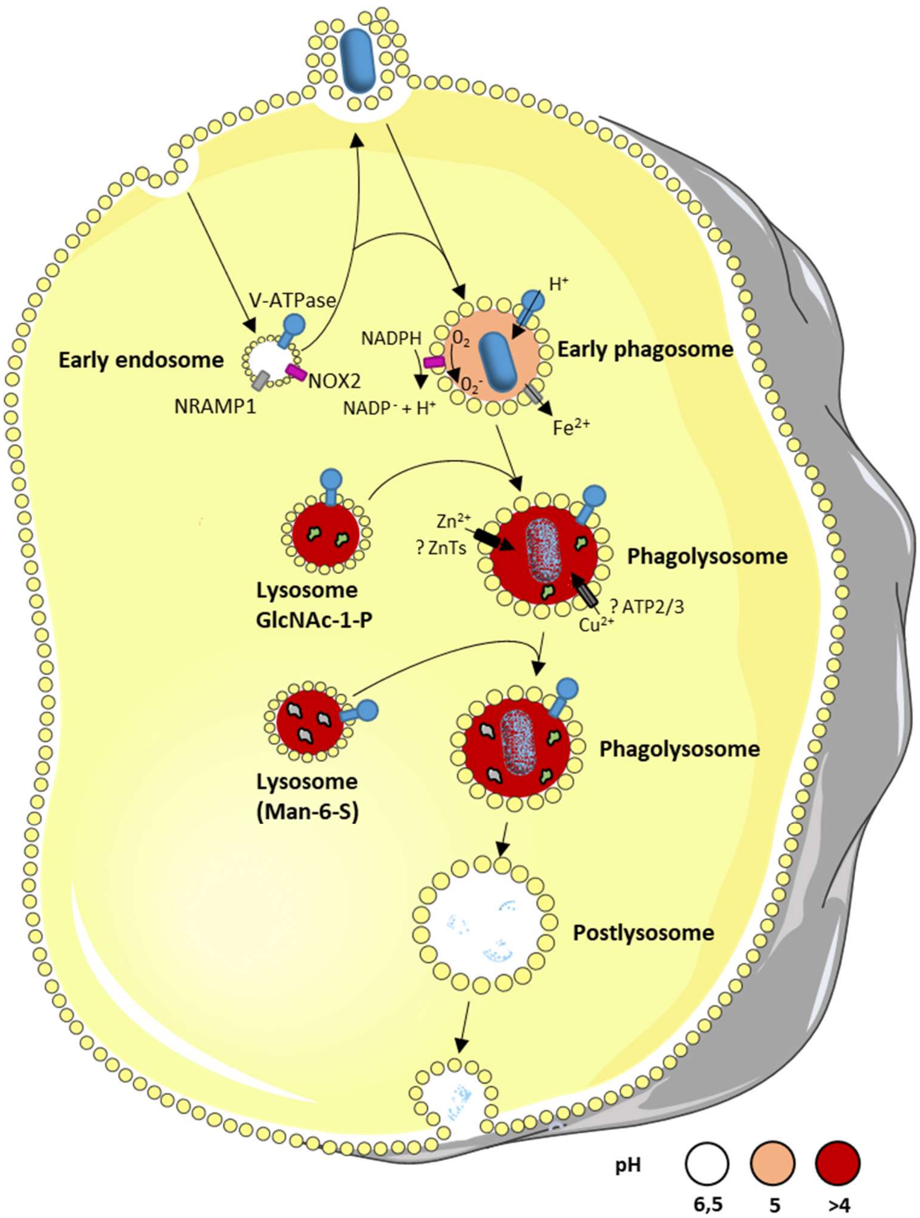

Fig.11 Intracellular killing in *Dictyostelium discoideum*

Like macrophage, intracellular killing in *Dictyostelium discoideum* follows at first a similar modus operandi: both the V-ATPase and the NOX2 complex are quickly delivered to the phagosome containing the bacteria. Transporters such as NRAMP1, depleting the phagosome of traces ions, are also quickly delivered to the phagosomes. Lysosomal enzymes delivery starts next within 3-5 min following phagocytosis via fusion with the lysosomes. Lysosomal enzymes are delivered in two waves, the first wave is detectable by the presence of GlcNAc-1-P labelled lysosomal enzymes, the second wave by Man-6-S labelled lysosomal enzymes. Once done the phagolysosome in *D. discoideum* reached its peak acidic pH, with mature lysosomal enzymes, active antimicrobial peptides, oxidative stress, and nutritional immunity. Metal poisoning is mentioned as a potential mechanism as *D. discoideum* possesses zinc and copper transporters. Later the V-ATPase will be removed from the phagolysosome and the remaining content exocytosed 40-60 min later.

Bacteria have evolved three strategies to overcome high copper concentrations: Sequestration, oxidation and export. *S. typhimurium* and *M. tuberculosis* can sequester copper in their periplasm by respectively producing CueP and MymT, two proteins capable of binding several copper atoms (Gold et al., 2008, Osman et al., 2010). Both bacteria encode also copper oxidizing proteins in their periplasm, respectively CueO and MmcO (Achard et al., 2010, Rowland and Niederweis, 2013). In addition, *M. tuberculosis* encodes MctB a copper export channel (Wolschendorf et al., 2011). As expected, mutant strains having lost one of these genes have lower pathogenicity that WT strains. This example demonstrates again the vast array of defense mechanisms developed by *M. tuberculosis* to resist intracellular killing.

The *D. discoideum* genome encodes only one CTR-type copper permease (*p80*), and three putative copper-translocating P-type ATPases *atp*1, *atp*2 and *atp*3 (Burlando et al., 2002). p80 localized at the plasma membrane and at the membrane of endosomes. p80 presence in the phagosome membrane increases during its maturation. Incubation of *D. discoideum* cells with bacteria leads to an increased expression of *p80*, but not upon incubation with only copper salts, suggesting copper transports may play a role in IC killing of bacteria (Hao et al., 2016). Additionally, Incubation of *D. discoideum* cells with bacteria leads to an increased expression of ATP2 and ATP3. ATP2 is orthologous to ATP7A, which pumps copper inside the phagosome lumen in mammalian cells, suggesting that copper trafficking is upregulated during phagocytosis and intracellular killing of bacteria in *D. discoideum* (Burlando et al., 2002). In summary, although the molecular mechanisms are not entirely elucidated, *D. discoideum* express the genes capable of performing copper poisoning and that expression of these genes is upregulated upon the presence of bacteria.

8. Xenophagy

Xenophagy refers to a specific degradation by autophagy of pathogens in the cytosol (Escoll et al., 2016). Autophagy is an intracellular process described as the degradation of a cargo in the cytosol, by forming around it an intracellular double-membrane vesicle (autophagosomes) derived from the ER, eventually fusing with lysosomes. Ultimately this process leads to degradation of the cargo and the inner membrane (Dikic and Elazar, 2018). During Xenophagy, recruitment of the ULK1 complex, Beclin1, and ATG16L1, initiates membrane nucleation of the phagophore that engulfs the intracellular bacteria, then ATG5–ATG12 associates with ATG16L1 and ATG5–ATG12–ATG16L1 binds LC3. Specific ubiquitin-binding adaptor such as p62 and NDP52 (Cemma et al., 2011) also bind LC3. Coordinated action of ATGs, LC3 and ubiquitin-binding adaptors allow the elongation and closure of nascent autophagosomes. This process requires membranes from the ER, the Golgi apparatus, the ER–mitochondria contact sites, or the plasma membrane to complete the autophagosome. Finally, the attachment of syntaxin 17 to the autophagosomal membrane enables the fusion with lysosomes and represents the final maturation step of autophagosomes into autolysosomes (Dikic and Elazar, 2018) (Fig.12).

Pathogens, which have evolved mechanisms to escape degradation within phagosomes, encounter xenophagy once they escape to the cytosol (Escoll et al., 2016). *M. tuberculosis* and *S. typhimurium* inhibit autophagy initiation signaling upstream of autophagosome formation (Shin et al., 2010, Tattoli et al., 2012). Some pathogens evade xenophagy later , such as *Shigella flexneri* which produces IcsB, a type III secretion effector, binding to the autophagy protein, ATG5 (Kayath et al., 2010). Binding ATG5 prevent the elongation of the nascent autophagosome around *Shigella flexneri.* Interestingly some pathogens promote autophagy: *Yersinia pseudotuberculosis* replicates intracellularly by subverting an autophagosome and prevents V-ATPase acidification. The resulting compartment is known as the *Yersinia*-containing vacuole (YCVs) (Moreau et al., 2010). Similarly, *Legionella pneumophila* promotes autophagy to increase the pool of nutriments available while simultaneously delaying autophagosome maturation to gain enough time to replicate and avoid fusion of the autophagosomes with lysosomes (Escoll et al., 2016). Subverting and/or resisting xenophagy is an efficient intracellular pathogen strategy for survival.

In *D. discoideum*, bacterial escape from the phagosome has been documented and triggers xenophagy (Mesquita et al., 2017). Many of the proteins involved in the process of autophagosome formation are conserved between mammalian cells and *D. discoideum* (Calvo-Garrido et al., 2010): The inductive stage depends on the UKL/Atg1 kinase complex and the class III PI3K complex, ATG12–ATG5 interacts with ATG16 and localizes to the phagophore membrane. Recruitment of ATG8 (LC3) is necessary for the elongation of the phagophore. Finally, ATG9 recruitment is necessary for lysosome fusion which represents the final maturation step of autophagosomes (Calvo-Garrido et al., 2010, Mesquita et al., 2017). In *D. discoideum*, the only selective autophagy receptor identified so far is p62/SQSTM1, which has been shown to recognize the intracellular pathogens *F. noatunensis* and *M. marinum* (Lampe et al., 2016, Gerstenmaier et al., 2015). However, both pathogens once freed from the phagosome behave differently. The majority of *F. noatunensis* replicates in the cytosol, but a small proportion of bacteria eventually succumb to autophagy, while *M. marinum* both avoids xenophagic killing and is ejected through the *D. discoideum* plasma membrane in an autophagy-dependent manner (Gerstenmaier et al., 2015). On the other hand, pathogens that escape the phagosome but cannot escape or block xenophagy in *D. discoideum* are digested in the autolysosomes, such as *S. enterica* and *S. aureus* (Jia et al., 2009, Pflaum et al., 2012) (Fig.12).

A few years ago, *D. discoideum* was proposed as a model system to study the interaction of phagocytes with yeasts (Koller et al., 2016). Axenic strains of *D. discoideum* can engulf yeasts. While testing IC killing of yeasts strains, mutant amoebae lacking autophagy proteins (ATG5, ATG6, ATG7, or ATG8) exhibited a killing defect (Koller et al., 2016). *atg*1 mutants, unlike the other mutants cannot produce autophagosomes, did not exhibit a killing defect. *S. cerevisiae*, *Candida albicans*, and *Candida* survival once phagocytosed by *atg1* mutant *D. discoideum* cells is lower than in WT of other autophagy proteins. Once potential explanation is that yeast use a non-lytic autophagy-dependent mechanism to exit the amoeba, like *M. marinum* (Pflaum et al., 2012).

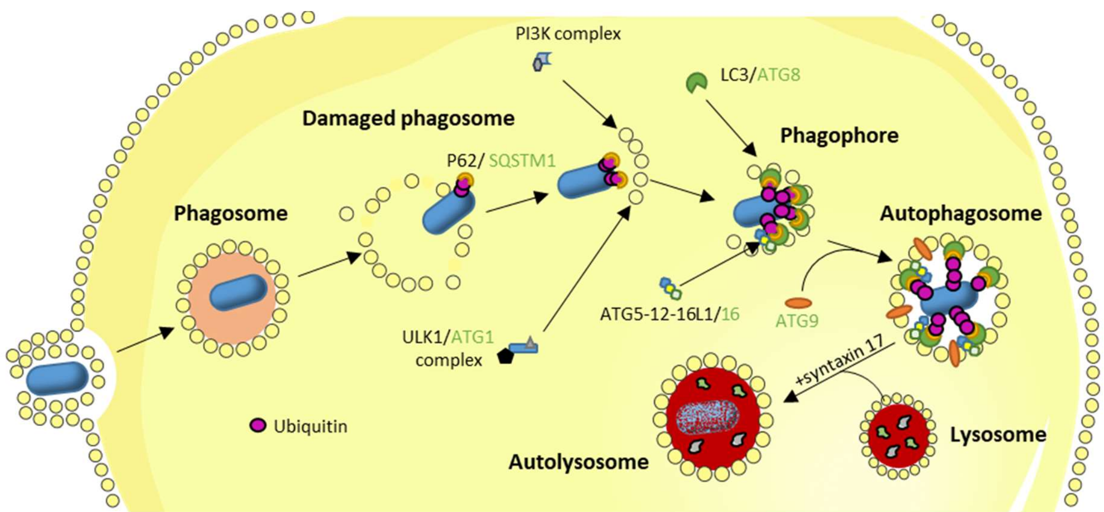

Fig.12 Xenophagy in mammalian and *D. discoideum*
Xenophagy refers to a specific degradation by autophagy of pathogens in the cytosol. Recruitment of ULK1 complex, and the PI3K complex initiate membrane nucleation of the phagophore that will engulf the intracellular bacteria. ATG5–ATG12 then associates with ATG16L1 and binds LC3. Specific ubiquitin-binding adaptor such as p62 and NDP52 binds LC3 too. Coordinated action of ATGs, LC3 and ubiquitin-binding adaptor allow elongation and closure of nascent autophagosomes. Finally, the attachment of syntaxin 17 to the autophagosome membrane enables the fusion with lysosomes and represents the final maturation step of autophagosomes into autolysosomes. In *D.discoideum* the mechanism is very similar. Homologs to mammalian effectors are in green for *D. discoideum*.

9. Unexplored mechanisms of IC pathogen recognition and killing in *D. discoideum*

Macrophages and other professional phagocytes in humans possess three categories of intracellular PRRs : nucleotide-binding and oligomerization domain (NOD)-like receptors (NLRs), retinoic acid inducible gene-I (RIG-I)-like receptors (RLRs), and absent-in-melanoma (AIM)-like receptors (ALRs).

The NLRs recognize various ligands from microbial pathogens (peptidoglycan, flagellin, viral RNA, fungal hyphae, etc.), host cells factors and environmental sources. Typically, they contain a NACHT domain, a N-terminal effector domain, and C-terminal leucine-rich repeats (LRRs). They are important player for autophagy, inflammation and response to cytokine (Kim et al., 2016). Unfortunately, direct evidence for NLRs binding bacterial cues or pathogen-containing vacuoles in *D. discoideum* is lacking.

RLRs are major components of antiviral and pathogen innate immune response as they detect RNA/DNA in the cytosol and results in the production of type I interferons (IFNs). For example, *L. pneumophila* secretes the Icm/Dot substrate SdhA to suppress type I IFN (IFN-α/β) production by interfering with the RIG-I/MDA5 pathway (Monroe et al., 2009). There again in *D. discoideum* RLRs have not been characterized.

ALRs are also DNA binding receptors thanks to their PYHIN domain (Ratsimandresy et al., 2013). Mice lacking AIM2, a canonical ALR, are unable to triggers production of the proinflammatory cytokines and suffer higher mortality during infections (Fernandes-Alnemri et al., 2010). Currently, no ALRs have been characterized in *D. discoideum*.

Macrophages also relies on immunity-related GTPases (IRGs) and guanylate-binding proteins (GBPs) to prevent the pathogens to survive in the cytosol (Fig.13). IRGs and GBPs cooperate to target NADPH oxidase, ATG proteins, and inflammasome complex to pathogen-containing vacuoles (Haldar et al., 2013). IRGs are split in two categories: the cytosolic GKS proteins on one side and the membrane-bound IRGM proteins on the other side. IRGM presence on membranes blocks GKS-GBPs oligomer binding. Therefore, GKS-GBPs oligomer only binds IRGM free vacuoles such as autophagosomes and pathogen-containing vacuoles (Haldar et al., 2013). GBS are IFN-induced GTPases, and 7 are expressed in human cells (Meunier and Broz, 2015, Tretina et al., 2019). GBPs have been shown to operate against at least 10 bacterial species. They trigger canonical or non-canonical inflammasome responses to control cytokine secretion and pyroptosis (Kim et al., 2016). For example, GBP1 and GBP7 assemble respectively p62/SQSTM1 and NADPH oxidase subunits for autophagic and oxidative immunity to intracellular bacteria (Kim et al., 2011). As of yet, IRGs and GBPs have not been studied on *D. discoideum*, but a homolog to GBP3 exists, and may perform immunity-related functions.

Macrophages possess also seven Tumor necrosis factor (TNF) receptor–associated factor (TRAF) proteins, (Park, 2018) (Fig.13). They are signaling molecules that can transduce signals from tumor necrosis factor receptor (TNF-R), TLRs, NLRs, RLRs, and even from cytokine receptor family, placing TRAFss at the heart of immunity-based signaling. They harbor usually two domains: (i) a RING domain at the N terminus, constituting the core of the ubiquitin ligase catalytic domain, (ii) a protein–protein interaction domain known as the TRAF domain which can serve as a scaffold to mediate interactions of various membrane receptors with diverse downstream effector molecules. In macrophages, TRAF6 notably is responsible for the decoration of pathogens and pathogen-containing vacuoles with polyubiquitin chains, which recruits GBP and p62, thus promoting autophagy (Tretina et al., 2019). In *D. discoideum*, 16 predicted TRAF proteins display both conserved domains, but none have been functionally characterized (Dunn et al., 2018).

Macrophages also exhibit Tripartite motif-containing proteins (TRIMs) which are involved in many biological processes including innate immunity, viral infection, carcinogenesis and development (Jiang et al., 2017)

(Fig.13). TRIMs contain a RING finger, one or two B-box motifs and a coiled-coil motif and are very numerous , above 80 members are found in humans (Jiang et al., 2017). During autophagy several TRIM proteins function as platforms for the assembly of autophagy regulators. They recognize ubiquitinated cargos via sequestosome-1-like receptors (Hatakeyama, 2017). Although TRIMs are often ubiquitinases, they can also recognize bacteria cargo intended for autolysosomes in an ubiquitin-independent manner, and mediate delivery via binding to LC3 (Kimura et al., 2016). A single homolog of TRIMs is identified in the *D. discoideum* genome. DdTRIM is an ortholog of human TRIM37. TRIM37 induces K63 polyubiquitination of TRAF2, which is an important activator of NF-κB signaling, and TRIM37 was the second member of the TRIM family (after TRIM5α) to be described as having anti-HIV-1 activity as its overexpression induced decreased viral replication and viral DNA synthesis (Brigant et al., 2019). Unravelling the role of the unique TRIM in *D. discoideum* may be much simpler that studying the 80 human TRIMs and may reveal the fundamental role of this family of proteins.

Last are the signal transducers and activators of transcription (STAT) proteins (Mogensen, 2019) (Fig.13). In macrophages, 7 STATs can transduce signals from the cytosol to the nucleus. STAT proteins consist of coiled coil (CC) domain, a DNA binding domain (DBD), and an SH2 domain that binds Janus kinases or other STATs. When cytokines or growth factors bind their receptors on at the plasma membrane, receptor-associated JAK kinases phosphorylate cytosolic STAT monomers. Phosphorylated STAT molecules form dimers that then translocate into the nucleus to bind their DNA targets (Mogensen, 2019). STATs deficiency has been implicated in numerous susceptibilities to infection. For example, STAT1 deficiency increases mycobacterial infections (Dupuis et al., 2001) and STAT3 deficiency increases susceptibility to *S. aureus* infection (Minegishi et al., 2007). In *D. discoideum*, 4 STATs have been identified: DstA-D (Kawata and Takefumi, 2011). DstA has been linked to cAMP sensing to trigger the development cycle. DstB function in growth is unclear but STATb mostly distinguish itself from the other STATs due to be constitutively dimerized, nuclear localized, and active, DstC responds to DIF-1 during development but also to hyperosmotic stress, heat shock, and oxidative stress. Finally, the function of DstD remains to be elucidated (Zhukovskayaet al., 2004, Kawata and Takefumi, 2011). Unfortunately, experimental data during microbial infection is lacking, therefore whether STATs proteins play a role in responses to bacterial cues is unknown in *D. discoideum*.

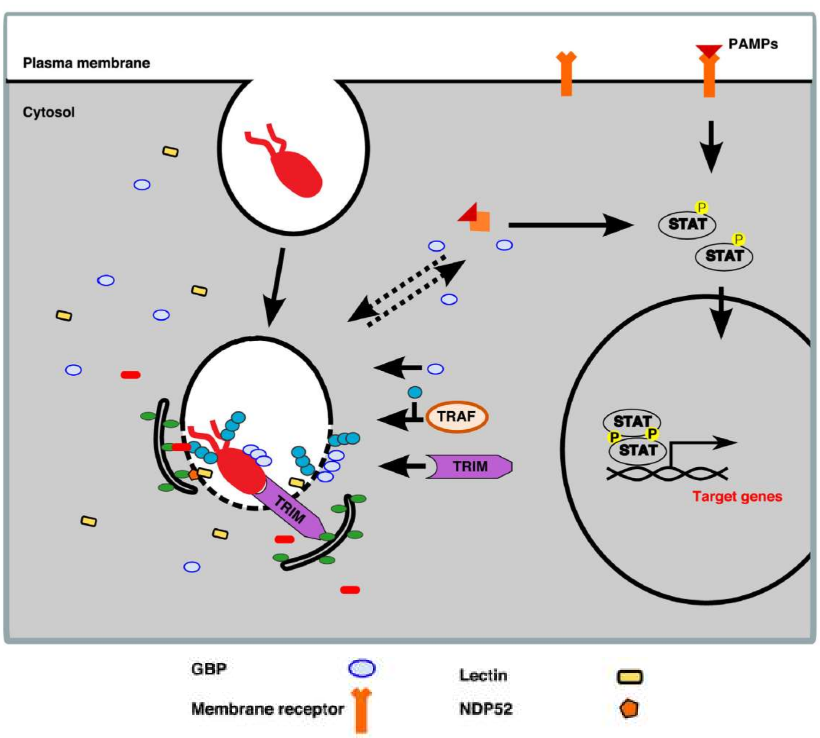

Fig.13 Unexplored mechanisms of IC killing in *D. discoideum*

MAMPs detection signal could be transduce through numerous cytosolic or plasma membrane receptors. For example, the STAT family could transduce the signal from both sources and enhance innate-immunity-related gene expression. Pathogen escaping the phagosome expose themselves to polyubiquitination by members of the TRAF family, thus recruiting the autophagy machinery. Moreover, ubiquitin-tagged membranes also promote the recruitment of GBP oligomers which recruits bacteria killing and clearance mechanisms. Furthermore, members of the TRIM family could detect and bind directly to the invading pathogen and mediate its degradation by autophagy. Dunn et al., 2018.

V. IC killing in *D. discoideum*: the case of *K. pneumonia*e

D. discoideum is an interesting model organism to study IC killing notably because it can be used for large scale screens. These screens can be used to identify bacterial virulence factor or host IC-killing mechanisms. In the first case, a screen can detect the presence or absence of a bacterial virulence factor by testing if bacterial strains impair *D. discoideum* growth (March et al., 2013). This strategy has also been used to identify inhibitors of virulence (Ouertatani-Sakouhi et al., 2017). In the second case, one can identify *D. discoideum* IC-killing mechanisms by identifying *D. discoideum* mutant strains that do not kill bacteria (Leiba et al., 2017).

A strain of *K. pneumoniae* has been extensively used as a food source for amoeba since 1937, but it was not until 1972 and the work of Brenner that the bacteria was classified as a *K. pneumoniae*. This strain, *Kp*Ge, is now sequenced (Lima et al., 2018). This strain is non-virulent and *D. discoideum* cells feed very efficiently on *Kp*GE. On the other hand, virulent strains of *K. pneumoniae* tend to inhibit growth of *D. discoideum* (March et al., 2012). No colony of *D. discoideum* grows on a lawn of *Kp*52145, but *D. discoideum* grow very efficiently of a capsule-defective mutant of *Kp*52145 (March et al., 2013). The versatility of the *K. pneumoniae* strain pathogenicity and ease of use of *D. discoideum* as a host model have fueled large scale mutagenesis screen to find IC killing related genes in *D. discoideum*.

1. *K. pneumoniae is heavily equipped to resist IC killing*

K. pneumoniae is a commensal enterobacteria found in the intestine but can be found ubiquitously in nature and is generally regarded as an opportunistic pathogen (Bengoechea et al., 2018). Carl Friedlander in 1882 isolated a bacterium from the lungs of patients who had died from pneumonia, and named it *K. pneumoniae* (Friedlander, 1882). Today, *K. pneumoniae* is a leading cause of fatal nosocomial infections and the number of hypervirulent strains of *K. pneumoniae* reports is increasing. Pneumonia was the first disease characterized by *K. pneumoniae* infection, but urinary tract infection, bloodstream infection, and sepsis are also commonly caused by *K. pneumoniae* (Bengoechea et al., 2018). *K. pneumoniae* -triggered pneumonia are now under heavy scrutiny as hypervirulent strains can lead to a mortality rate as high as 43% (Paganin et al., 2004). Even more worrying the occurrence of multi-drug resistant hypervirulent *K. pneumoniae* strains is rising (Yao et al., 2017).

K. pneumoniae are Gram-negative, non-motile, encapsulated, lactose-fermenting, facultative anaerobic, rod-shaped bacteria. *K. pneumoniae* colonizes the mucosal surfaces in humans, particularly the nasopharynx, the gastrointestinal tract, and urinary tract (Martin et al., 2018). Adhesion is mediated by type 1 pili, filamentous structures extending from the bacteria surface, and their ability to adhere to human mucosal or epithelial surfaces. Once *K. pneumoniae* adheres, it starts producing a biofilm, a gel-like structure embedding the bacteria, which provides protection against secreted AMPs and phagocytosis (Bellich et al., 2018). Phagocytosis by macrophages of *K. pneumoniae* encased in a biofilm is 2-times lower than in the absence of the biofilm (Rathore et al., 2019) and *K. pneumoniae* hypervirulent strains produced even higher amount of biofilm (Rathore et al., 2019). Another virulence trait of *K. pneumoniae* is the production a polysaccharide capsule, regarded as one of the most important virulence factors. Incubation of capsule-defective mutant *K. pneumoniae* strains with macrophages results in a 35-fold increase in phagocytosis compared to WT *K. pneumoniae* (Cortès et al., 2002). Nested in a capsule and in a biofilm, *K. pneumoniae* easily invades the host tissues and avoid phagocytosis by innate immune cells. It can cause severe sepsis, often fatal in case of multidrug resistant strains.

In macrophages or neutrophils, *K. pneumoniae* subverts several IC killing mechanisms. *K. pneumoniae* can withstand the phagosome pH of macrophages. *K. pneumoniae* growth is optimum at pH7 but only marginally affected by pH 6 or 5. At pH 4 the growth is arrested, but the bacteria are still viable (Abbas et al., 2014). In addition, *K. pneumoniae* uses a multitude of strategies to deflect AMPs: (i) An Outer membrane protein (OMP)-

dependent mechanism confers resistance to α-defensins is 2-times higher than in the WT (Llobet et al., 2009). (ii) The Sap (sensitivity to antimicrobial peptides) transporter, confers resistance to cathelicidin (Hsu et al., 2019), (iii) Efflux pumps such as AcrRAB, increase survival of *K. pneumoniae* mixed with human bronchoalveolar lavage fluid (Padilla et al., 2010). Like many pathogens, *K. pneumoniae* is equipped with a wide range of siderophores to chelate iron and resist nutritional immunity. There is a clear correlation between the number of siderophores encoded in the *K. pneumoniae* genome and the strain virulence. Hypervirulent *K. pneumoniae* strains can produce all the following siderophores: aerobactin (*iucABCD*, *iutA*), colibactin (*clbA-R*), salmochelin, yersiniabactin (*ybt*, *irp1*, *irp2*, *fyuA)* (Holt et al., 2015). In summary, *K. pneumoniae* strains are very well-equipped opportunistic pathogens. Not only do they evade phagocytosis, but they are also capable of withstanding pH, AMPs and nutritional immunity.

2. Role of Phg1A/Kil1

As mentioned previously, mutants of *D. discoideum* that are less efficient at killing *K. pneumoniae* can be isolated from random libraries of mutants. In 2000, identification of a mutant defective for phagocytosis led to the identification of Phg1A as a main actor in cell adhesion (Cornillon et al., 2000). Tested in 2005 for growth on *K. pneumoniae* lawn, *phg1A* mutant showed a severe growth defect (Benghezal et al., 2006). This defect was not due to reduced phagocytosis of *K. pneumoniae* but to the fact that phagocytosed bacteria survived much longer in *phg1A* KO cells than in WT cells (Benghezal et al., 2006).

Phg1A is a member of the TM9 family, defined by their 9 transmembrane domains and a high degree of conservation. It is not expected to be directly involved in IC killing but regulates sorting of proteins in the secretory pathway (Perrin et al., 2015). In *D. discoideum,* Phg1A regulates the surface expression of the integrin-like SibA, which is likely to account for its role in phagocytosis (Froquet et al., 2012). *Phg*1A mutant cells were transfected with a *D. discoideum* cDNA overexpression library and clones were selected for growth restoration on a *K. pneumoniae* lawn. *kil*1 was identified during this suppressor screen. Overexpression of *kil*1 in a phg1 mutant did not increase phagocytosis, but the intracellular killing of *K. pneumoniae* rose back to WT levels (Benghezal et al., 2006). The presence of Kil1 requires the presence of Phg1A (Benghezal et al., 2006). Kil1 is the main sulphotransferase in *D. discoideum*. Lysosomal enzymes with mannose-6-sulphate-containing epitope are undetectable by western blotting in *kil*1 KO cells (Le Coadic et al., 2013). In summary Phg1A is involved in phagocytosis because it assists transport of SibA to the cell surface, while its role in IC killing is due to its ability to stabilize the amount of Kil1 in the cell (Fig.14). The exact role of Kil1 in IC killing remains to be elucidated : it presumably modifies the sugars of proteins essential for intracellular killing, and this modification is essential either for their function or for their transport to phagosomes.

3. Role of Kil2

In 2010, *kil*2 mutant cells were identified as mutants growing poorly on a *K. pneumoniae* lawn but with no defect in phagocytosis (Lelong et al., 2010). Kil2 exhibits a strong similarity to members of the P-type ATPase superfamily. This family of transporters is involved in the active transport of a variety of cations across membranes. Like in *phg*1A and *kil*1 KO cells, the IC killing defect is specific to Gram- bacteria (Lelong et al., 2010). Like *kil*1 KO cells, the pH of the phagosomes is unaffected in *kil*2 KO cells, and the lysosomal enzymes are sorted normally (Lelong et al., 2010). The IC-killing defect of *kil*2 KO cells does not globally affect the physiology of the cells and is specific to a class of bacteria. Unlike Kil1, Kil2 is detectable in the membrane of purified phagosomes and its concentration increases during the phagosome maturation. To test which ion it could transport, inside or out of the phagosome, the authors exogenously added in the media $CaCl_2$, NaCl, KCl,

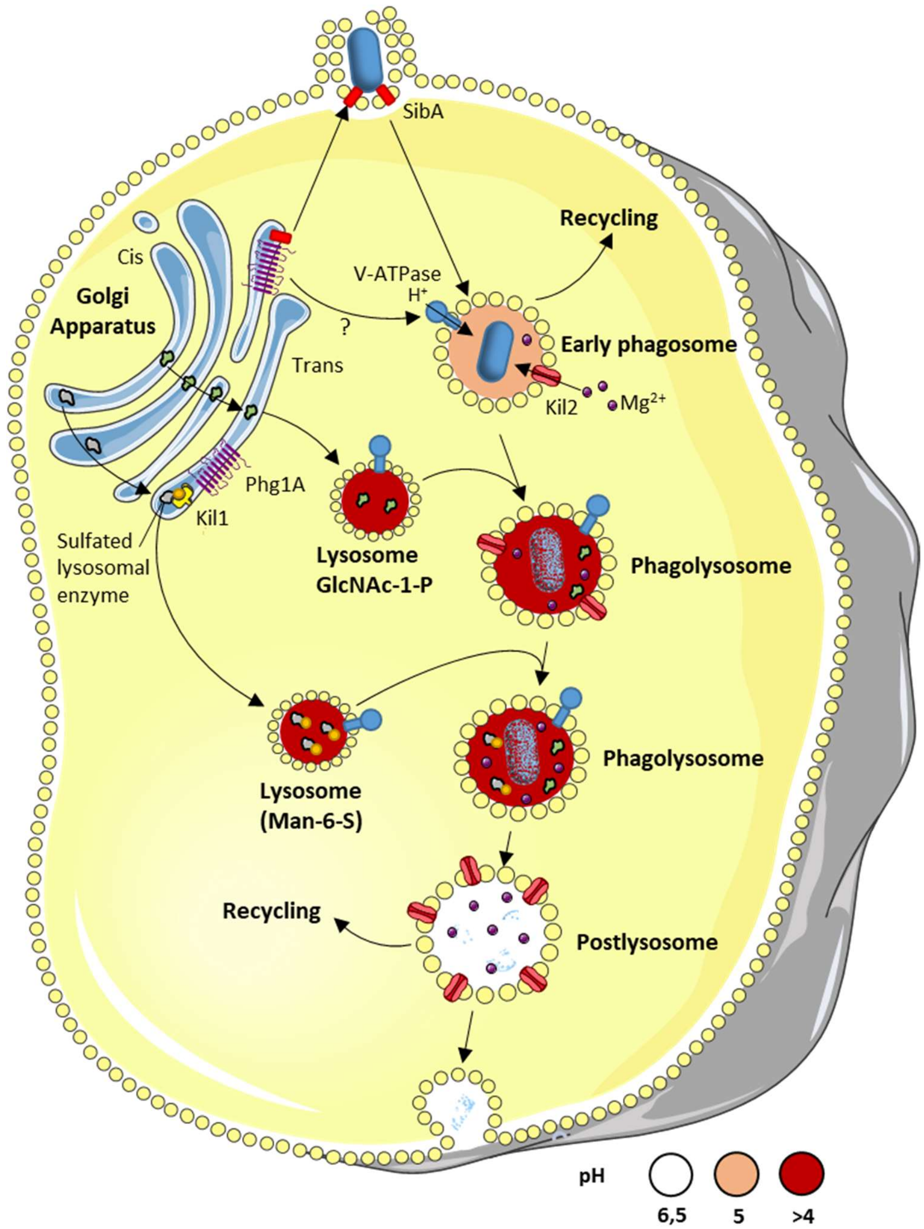

Fig.14 Phg1A/Kil1 and Kil2 role in *Kp* intracellular killing

Phg1A primary role in intracellular killing is to control the cellular amount of Kil1. Kil1 is as sulfotransferase in the Golgi apparatus. Most likely Kil1 sulfates lysosomal enzymes for proper delivery and function in lysosomes and phagolysosomes. Phg1A also affects cellular adhesion and phagocytosis due to its role in controlling surface expression of SibA, an integrin-like protein. Lastly, Phg1A impacts also pH in phagosomes, although it remains unclear how. Kil2 is a cation pump enchased in the phagosome membrane. Kil2 is quickly delivered to the phagosome and its concentration in the phagosome membrane increases along the maturation process. Kil2 function is to pump magnesium ions inside the phagosome lumen. Controlling magnesium levels directly affects protease activity. Kil2 and Kil1 activities are independent from each other.

$MnCl_2$, $FeSO_4$, $ZnCl_2$, $NiCl_2$ or $MgCl_2$ during IC killing assay with *kil*2 KO cells. Addition of $MgCl_2$ restored specifically efficient killing in *kil*2 KO cells. Mg^{2+} is a known cofactor for proteases, and the authors measured the proteolytic activity in the phagosomes. Beads covered with red proteolytic insensitive dye and green proteolytic sensitive dye were fed to the kil2 mutant. The fluorescence reading showed a lower green fluorescence intensity in kil2 mutant cell indicating a lower proteolytic activity in *kil*2 mutants. Proteolytic activity is restored in the presence or Mg^{2+}. To the best of our knowledge Kil2 is thus a Mg^{2+} pump responsible to maintain efficient proteolysis. (Fig.14)

The Kil1 sulphotransferase and the Kil2 cationic pump are two main proteins characterized and involved in the IC killing of *K. pneumoniae*. Three experiments classify them in distinct pathways: first overexpression of *kil*1 in a *kil*2 KO cells does not restore either growth on *K. pneumoniae* lawn or IC killing of *K. pneumoniae*. Second, Proteolytic capacity in the phagosome is impaired only in kil2 KO cells. Third, *kil*1 is normally expressed in *kil*2 KO cells.

OBJECTIVES OF MY THESIS

Intracellular killing within professional phagocytes is essential to protect the human body against foreign microorganisms. Although numerous mechanisms have been described, it remains unclear which of these mechanisms act predominantly and if we have discovered the whole spectrum of mechanisms. *D. discoideum* has been instrumental in studying intracellular killing of bacteria and notably represents a powerful model to discover new gene products involved in intracellular killing.

My first goal was to determine the kinetics of intracellular killing in *D. discoideum* to be able to compare precisely mutant and WT cells. A live-imaging IC killing assay at the single cell level was essential to discriminate uptake and motility defects from IC killing defect, and high resolution in time was needed to follow single bacterium fate once phagocytosed.

My second aim was to identify new gene products involved in intracellular killing. A random mutagenesis screen was performed by Jade Leiba and Ayman Sabra in 2014. Out of the screen two candidate genes *vps13*F and *lrrk*A were selected for further characterization. The main objective of my thesis was to characterize *vps*13F and *lrrk*A KOs, to unravel the role of these two gene products in IC killing and their relationship to *kil*1 and *kil*2.

MATERIALS AND METHODS

I. Media, buffers and solutions

HL5 • **Component (g/L)** • Peptone: 5 • Yeast Extract: 5 • Tryptone: 5 • KH_2PO_4: 1.2 • Na_2HPO_4 : 0.35 • Glucose: 10	SM agar • **Component (g/L)** • KH_2PO_4: 4.4 • Na_2HPO_4 : 2.0 • $MgSO_4$: 0.49 • Glucose: 7.5 • Bactopeptone: 10 • Yeast Extract: 1	LB • **Component (g/L)** • Tryptone: 10 • Yeast Extract: 5 • NaCl: 5
Sørensen buffer (SB) • **Component g/L** • KH_2PO_4: 9.985 g • Na_2HPO_4: 1.415 g • H_2O: Up to 500 ml For SBS: • Add 50 ml of 1M Sorbitol solution	Phosphate Buffer Saline (PBS) 10x • **Component g/L** • NaCl: 80 g • KCl: 2 g • Na_2HPO_4 : 14.4 g (anhydrous) • KH_2PO_4 : 2.4 g • H_2O: 800 ml • pH: 7.2 Adjust with HCl	TAE • **Component for 1 L** • Tris: 242 g in 500 ml of H_2O • EDTA 0.5 M pH 8.0: 100 ml • Glacial Acetic Acid: 57.1 ml • Adjust to 1 L with H_2O
$NaPO_4$ buffer 0.1M pH6.1: • **Component** • 0.1 M Na_2HPO_4 • 0.1 M NaH_2PO_4 Mix the two solutions: while measuring the pH. The ratio is about: 1 ml of sol.1 : 4 ml of sol.2. Filter sterile and keep this stock solution at 4°C	Electroporation buffer 500ml: • **Component g/L** • Sucrose 50mM : 8.56 g • $NaPO_4$ pH 6.1 10mM: 50 ml of 0.1 M stock solution • H_2O Adjust to 500ml. Filter sterile and keep at 4°C	100 mM Folic acid (For 10 ml) • **Component** • 0.44 g folic acid • Add 10 N NaOH until most of the solid folic acid dissolved, then add drop by drop of 1 N Na OH until everything dissolved. pH is around 7.8 Filter sterile store frozen and protected from light
SWL + Proteinase K 50 ml • KCl 50 mM: 2.5 ml (1M stock sol) • Tris pH 8.3 10 mM: 500 µl (1M stock sol) • $MgCl^2$ 2.5 mM: 125 µl (1M stock sol) • NP40 0.45 %: 225 µl • Tween 20 0.45 %: 225 µl • Adjust to 50 ml H_2O Keep at RT. • 1 µl of proteinase K in 25 µl SWL buffer		

II. Antibodies

a) *Primary antibodies*

Antibody description	*target*	*Publication/supplier*
H161	p80	PMID: 11831389
221-35-2	vatA	PMID: 9704504
169-477-5	talA	PMID: 7698984
H72	p25	PMID: 11831389
RB1	rhgA	PMID: 11220631

b) *Secondary antibodies*

Antibody description	*Method - Dilution*	*Supplier*
anti-rabbit/mouse Ig Alexa 488, 594, 647	10 mg/ml	2-5 µg/ml

III. Antibiotics

Antibiotic	*Stock concentration*	*Working concentration*
G418	10 mg/ml	2-5 µg/ml
Blasticidin S	10 mg/ml	3-5 µg/ml
Kanamycin	50 mg/ml	25-50 µg/ml
Ampicillin	100 mg/ml	100 µg/ml
Tetracycline	125 mg/ml	125 µg/ml
Spectinomycin	100 mg/ml	100 µg/ml

IV. *D. discoideum* cell lines

Antibody description	*Background*	*Source*
DHI	WT	Cosson Lab
*kil*2 KO	DHI	Lelong et al., 2010
*kil*1 KO	DHI	Benghezal et al., 2006
*vps13*F KO	DHI	Leiba et al., 2017
*lrrk*A KO	DHI	Bodinier et al., 2020
*kil*2-*vps13*F KO	DHI	Leiba et al., 2017
*kil2-lrrk*A KO	DHI	Bodinier et al., 2020
*kil1-vps13*F KO	DHI	Leiba et al., 2017
*kil1-lrrk*A KO	DHI	Bodinier et al., 2020
kil1-kil2 KO	DHI	Cosson Lab
fspA KO	DHI	Lima et al., 2013
far1 KO	AX2	Pan et al., 2016
far1 KO	DHI	Leiba et al., 2017
*Sib*A	DHI	Cornillon et al., 2006
*Tal*A KO	DHI	Cornillon et al., 2008
myoVII KO	DHI	Cornillon et al., 2008
vps13A	DHI	Leiba et al., 2017

V. Bacterial strains

Antibody description	*Antibiotic resistance*	*Source*
*K. pneumoniae Kp*GE	-	(Lima et al., 2018)
K. pneumoniae LM21	-	(Balestrino et al., 2008)
*Kp*GE-GFP	Amp	(Bodinier et al., 2020)
E. coli B/r	-	(Gerisch, 1959)
P. aeruginosa PT531	-	(Cosson et al., 2002)
B. subtilis 36.1	-	(Ratner & Newell, 1978)
B. subtilis 36.1 (Δhag amyE::Physpank - mCherry)	Spec	Professor D. Kearns (Indiana University, USA)
M. luteus	-	(Wilczynska & Fisher, 1994).

VI. Plasmids

Plasmid description	*Resistance*	*Source*
pZA2 (IPTG inducible ye-GFP)	Kan	addgene 97760
pZA2 (+ constitutive ye-GFP)	Kan	Modif: Bodinier et al., 2020

VII. Primers

Primer description	*Sequence*
BSR lost sense	5-TTGAGTGGAATGAGTTCTTCAATCG-3
BSR lost antisense	5-CATCATGTGGGAGCGGCAATTCG-3
G418 lost sense	5-TGGAGAGGCTATTCGGCTATGACT-3
G418 lost antisense	5-GATGCTCTTCGTCCAGATCATCCT-3
vps13A Loss 5-sense	5-TCAAACAGCTTCACCAGAATTAATA-3
vps13A Loss 5-antisense	5-CAAATTCAACCAATATCTTTAAGAAC-3
vsp13A int Loss sense	5-TGGATGGTTGATTAGATTTAGATTTG-3
vps13A int Loss antisense	5-TTGTTGTTGAGATGGAATAAATGATG-3
vps13A Loss 3-sense	5-TGGAATGTAATGGTTGGTGATCTAAAT-3
vps13A Loss 3-antisense	5-GAACCAATGATACAAACATCAACCAT-3
pSCba	5-AGAGACTTCCTGCCTCGTC-3
pSCbb	5-GCATTAGATGTAAAACAGCCAAAGAGT-3
vps13F Loss 5-sense	5-TGAAAATGATTCACAATCAGGTGGT-3
vps13F Loss 5-antisense	5-CGCTTATCAAAGAATTGTGGTGTCC-3
vsp13F int Loss sense	5-TTCAACAACAACTTCATCATCGTCA-3
vps13F int Loss antisens	5-GGTGAATTTGGTGGTTGCAATCTAA-3
vps13F Loss 3-sense	5-TTAGATTGCAACCACCAAATTCACC-3
vps13F Loss 3-antisense	5-TATCAGAGGGTGCATTTCCAAAGAA-3
BSRa	5-TCAAAAAGATAAAGCTGACCCGAAAGC-3
BSRb	5-TTCAAATAATAATTAACCAACCAAG-3
lrrkA Loss 5-sense	5-GATGCTTCATGAAGAAGCAGAG-3
lrrkA Loss 5-antisense	5-GATTGGCTGATAGATCAAGATCACG-3

lrrkA int Loss sense	5-CGTGATCCTTGATCTATCAGCCAATC-3
lrrkA int Loss antisens	5-ATTGGAAGTGCAGGGTTAACA-3
lrrkA Loss 3-sense	5-GAGGAACAGAAGTAGCAGTGAAAATCC-3
lrrkA Loss 3-antisense	5-TTGGTGACCCAGTTTGTTGTAGTTC-3
Constitutive promotor pZA2 5'	5-ACCGAATTCATTTTGACAGCTAGCTCAGTCCTAGGTATAATGCTAGCATTAAAGAGGAGAAATACTAGATGTCTAAAGGTGAAGAATTATTCACTGG-3
Constitutive promotor pZA2 3'	5-ATTAAGCTTTCATTTGTACAATTCATCCATACCATGGG-3

VIII. Cell culture

a) *D. discoideum cell culture :*

D. discoideum cells are cultivated at 22°C on Falcon Petri Dishes (BD Falcon) in HL5 supplemented with 125 µg/ml of Tetracycline.

b) *D. discoideum Growth test on bacteria:*

- Grow 100.10^4 cells/mL of *D. discoideum* cells culture
- Prepare overnight bacterial culture (colony in 3mL of LB 37°C)
- Prepare 24 wells plate containing SM agar medium: 2mL/well
- Put 50µL of bacteria /well
- Move circularly the plate to cover the entire medium with bacteria
- Dry the plate under the hood 2 or 3 hours
- Add 5µL containing Dictyo cells (10'000 – 1'000 – 100 – 10 cells/well)
  (10'000 cells/ 5µL = 200.10^4 cells/mL)
- Dry the plate for a few minutes
- Wrap the plate in aluminum paper
- Incubate at 21°C and follow the growth of Dictyo during several days.

c) *D. discoideum stocks :*

For freezing:

- Freezing medium: cold HL-5 medium + 10% DMSO.
- Centrifuge 10 ml of cell culture at a density of about 1 million per ml (1400 rpm, 5 min, 4 °C)
- aspirate all the supernatant, to remove all old medium.
- Resuspend cells gently in 1 ml cold freezing medium
- freeze slowly in a Nalgene cryobox (with isopropanol) in the -80 °C fridge.
- After one day, transfer the cryotubes to liquid nitrogen.

For thawing:

- Thaw rapidly in 37°C water bath
- Pour ice cube in 10 ml HL-5 medium.
- Centrifuge 1400 rpm 5 min
- Resuspend gently in HL-5 medium

d) *Bacterial liquid culture :*

- Scrape one colony with a sterile tip
- Put the tip in a 14ml tube containing 3 ml LB (with appropriate antibiotic if necessary
- 37C° degree, shaking, 16 hours.

e) *Bacterial stocks :*

For freezing:

- Transfer 500 µl of an overnight culture into a cryogenic vial, add 500 µl of 40-50% glycerol
- Freeze in liquid nitrogen and place at -80°C.

For thawing:

- scrape a bit of frozen bacteria onto a LB agar plate with the appropriate antibiotics.

IX. Generation of knock-out *D. discoideum* cells

a) *Primer design KO and screen*

Based on the pKOSG-iba-dicty1 protocol (Wiegand et al., 2011).

Design of primers for KO plasmid:

- Design 2 pairs of primers (forward and reverse) to amplify the left and right "arm" (flanking region) of the gene of interest (GOI)

Sequence of primer (5'-3'):

Left Arm Primer1 AGCGCGTCTCCAATG - unique RES - forward sequence left arm
Left Arm Primer2 AGCGCGTCTCCGTTG - reverse sequence left arm
Right Arm Primer1 AGCGCGTCTCCCTTC - forward sequence right arm
Right Arm Primer2 AGCGCGTCTCCTCCC - unique RES - reverse sequence right arm

- The primers optimal melting temperature is about 50-55°C
- The pairs of primers should amplify a product of about 500-700 bp.
- The primers LA1 and RA2 should be preferably outside the GOI

Design of primers for screen:

- One forward flanking primer: this primer is outside the GOI, upstream, and is further awayfrom the GOI compared to the LA1. This primer will be used together with the BsR_Reverse primer.
- One reverse flanking primer: same as for the forward, but downstream of the GOI. This primer is used together with the BsR_Forward primer.
- Two primers inside the gene: these primers will amplify a fragment inside the GOI that should be deleted in the KO (i.e. that amplify a fragment that is not present in the left or right arm).

b) *Plasmid cloning*

One-step cloning:

- Mix the following in total 25 µl:

pKOSG-IBA-Dicty	10 µl
PCR product Left Arm	15 ng
PCR product Right Arm	15 ng
Star Solution A1	1 µL

Star Solution A2	1 µL
Star Solution A3	1 µL

- Incubate 1 h at 30°C.
- Transform directly into electrocompetent *E. coli*

c) *Electroporation of D. discoideum cells*

- *D. discoideum* cells should be around 1.10^{6}cells/ml
- Incubate cells on ice 10 min.
- Centrifuge 2000 rpm, 4° C, 10 min
- Rinse 1x with ice-cold electroporation buffer (5mL)
- Count cells
- Centrifuge again 2000 rpm, 4°C, 10 min
- Resuspend at 20x10^6 cells / ml in ice-cold electroporation buffer
- In each electroporation cuvette (Gene Pulser Cuvette, 0.2 cm-gap) transfer 400µl of cell suspension and 20µg plasmid (Endo-free prep)
- Electroporate (Biorad : capacitance 3µF, 800V, time expected : 0.8 msec).
- Electroporate using the Biorad electroporation system fitted with the Rf module for square waves.
  Parameters: voltage 400 V
  frequency 50 Hz
  delivery time 2 ms (burst duration)
  time between pulses 1 s (burst interval)
  % Mod 100
  number of burst 4 or 5
- Add 1mL HL5 to cuvette. Incubate 30 min RT
- Transfer to a large plate containing 35 ml HL5
- When a G418 selection is envisaged, transfer into 2 plates (half of the cells per plate)
- Blasticidin (or Geneticin) is added about 24 hrs later
- For BSR & G418 selection, change the medium 6-7 days later
- continue the selection for another 6-7 days.

d) *KO clones selection*

Selection of clones by serial dilutions:

- Use confluent plate of mutants.
- Count 1000, 100, 50, 25, 12, 6, 3, 1 cells and plate them by serial dilutions in 96 well plates containing HL5 rich medium and the correct antibiotic.
- Wait 1 week until cells grow, and expand cells to 24 well plates for DNA extraction and PCR screening. Repeat if the dilution was not enough to reach a maximum or one colony per 96 well plate.

Selection of clones on Klebsiella lawns:

- Prepare first SM agar medium
- Thaw *Kp*GE on SM agar plates. Incubate O/N at 37°C.
- Prepare 3 SM agar plates for each pool:
  - One plate with 1000 Dicty cells + 300 µl of Klebsiella culture

- One plate with 100 Dicty cells + 300 µl of Klebsiella culture
- One plate with 10 Dicty cells + 300 µl of Klebsiella culture

- Use HL5 medium without antibiotics to dilute cells, spread the mix on the plate and gently swirl it. Let it try under the hood and put it at 22°C upside down. Plates are checked after about 2-3 days.
- Pick about 8-20 well-isolated plaques per pool by scraping the plaque with a tip and placing it in a 24 well already full with medium and 5 µg/ml of BsR. The next one/two days the plaques should be ready.
- Once cells are confluent, DNA is recovered from 24 well plates and screened

e) *Cre Lox system*

Material :

- 30 µg pDEX-NLS-cre vector
- Dicytostelium culture (1-2 x106/ml) in HL5 KO system IBA pKOSG
- Electroporation Buffer
- Specific oligonucleotides matching in the BSR cassette (to verify the excision) and in the Neo cassette (to verify the absence of the pDEX-NLS-cre vector eventually integrated in the Dictyostelium genome)

Procedure :

- Transfect *D. discoideum cells* with 30 µg pDEX-NLS-cre vector (not linearized) in Electroporation Buffer. Cf electroporation protocol.
- 24 hours later add the G418 selection to the medium. 15µg/ml (6 µl for 10 ml; stock : 25 mg/ml)
- 5-6 days from the adding of selection,
- Recover transfected cells dilutions to plate on Klebsiella culture, growing on SM agar (if your KO can grow on Klebsiella. If not, choose another way to select clones, limiting dilutions).
- Recover 1 ml of transfected cells (even if clones are not visible in the plate and recovering also dead cells) and after one wash with HL5, plate it on Klebsiella SM agar.
- Another ml of transfected cell will be diluted in this way :

  -1 :1000 / -1 :500 / -1 :300 / -1 :100
- When phagocytic plaques are evident (5-6 days later), pick-up cells with toothpicks and directly dilute them in 15 µl of SWL lysis Buffer.
- Lysis conditions in the PCR cycler:
  1. 4°C 2 min
  2. 95°C 2 min
  3. 4°C pause
- PCR the product to detect BSR and G418.

X. DNA-related protocols

a) *Extraction of genomic DNA (gDNA) from D. discoideum*

From liquid culture:

- Put $1 \cdot 10^6$ cells in an Eppendorf tube
- Centrifuge 2 min, 4000 rpm, 21°C
- Aspirate the supernatant.
- Resuspend the cell pellet in 200 µl of SWL+ Proteinase K, and transfer in a 200 µl PCR tube.
- Lysis is made in the PCR machine, with the following program :

  Step 1 : 4°C 2 minutes
  Step 2 : 95°C 5 minutes
  Step 3 : 4°C Pause

- For a 20 µl PCR reaction, use 2 µl of this lysate.

Clones growing in 96 well plates:
- For each clone to be tested, put 10 µl of SWL+PK per PCR tube.
- Remove almost all liquid from the 96 well, but leave about 50 µl of medium (1 or 2 drops).
- Resuspend cells in this little volume and transfer 10 µl of cell suspension in the PCR tube containing SWL+PK.
- Lysis is made in the PCR machine, same conditions as above.
- For a 20 µl PCR reaction, use 2 µl of this lysate.

From colonies growing on bacteria:
- For each prep, transfer 20 µl of SWL+PK per PCR tube.
- Pick dicty from colony with a yellow tip or a toothpick and transfer in the PCR tube.
- Lysis is made in the PCR machine, same conditions as above.
- For a 20 µl PCR reaction, use 2 µl of this lysate.

b) *PCR-GoTaq (Promega)*

For KO and mutants screening:	20 µl of PCR reaction
• 5x GoTaq buffer	4 µl
• 6.25x dNTP	3.2 µl
• Oligo 1 100 ng/µl	1.3 µl
• Oligo 2 100 ng/µl	1.3 µl
• GoTaq	0.1 µl
• Template (gDNA)	2 µl
• dH_2O	8.1 µl

PCR program
1) 95°C 2 min
2) 95°C 30 sec
3) 58°C 30 sec
4) 65°C 1 min 30 (for 1000 bp amplification) Return to step 2 for 40 cycles
5) 65°C 10 min (optional)
6) 4°C Pause

c) *Restriction enzyme digestion*

About 1 µg of DNA is used. In the case of diagnostic digestions to screen minipreps, 5 µl of miniprepped DNA are used.

Component	Volume
DNA	1 µg – 5 µL
Buffer 10x	2.5 µl
Enzyme	0.5 µl
H_2O	20µl

Incubate for 2 hours at 37°C. Up to 2 different enzymes were used per reaction.

d) *Isopropanol precipitation*

PCR product:

- NaOAc 0.3 M final
- 0.7 volumes isopropanol
- Centrifuge max speed at 4°C for 30 min.
- Remove supernatant carefully and wash 2 times in 75% EtOH
- Let the pellet air-dry and resuspend in H2O (approx. 20 µl). Measure the concentration with Nanodrop.

Plasmid:

This protocol yield plasmid which is fine for enzymatic digestion and sequencing if the bacteria in which the plasmid is propagated are free of nucleases (TOP10, SURE, DH5a...). It will not work for bacteria still containing nucleases (MC1061P3, BL21...)

- Grow 3 ml of bacteria overnight in LB + antibiotics
- Centr. 1 ml of culture, 6000 rpm, Eppendorf centrifuge, 2 min, RT
- Aspirate supernatant with a different tip for each culture
- Vortex pellet extensively (minimum 20-30 sec)
- Add 150µl Solution 1 (from commercial miniprep kits)
- Vortex until there are no visible aggregates
- Add 150µl Solution 2, immediately mix gently by inverting tubes several times.
- Leave 5 min at RT
- Add 150µl Solution 3. Mix by inverting and shaking the tubes.
- Centrifuge 5min 10000rpm 4°C
- Collect approx. 400µl supernatant and transfer to new tubes. As much as possible try not to transfer white precipitate
- Add 800µl EtOH
- Leave minimum 5min at RT
- Centrifuge 5min, 10000rpm, 4°C
- Pour supernatant and stand tubes inverted on paper towel
- Add 1ml 70% EtOH, vortex until pellet detaches from bottom
- Centrifuge 5min, 10000rpm, 4°C
- Pour supernatant and stand tubes inverted on paper towel
- Dry the pellet. Option: if you wash with 100% EtOH drying will be very fast.
- Resuspend in 50µl TE or autoclaved water.
- For analysis we usually use 5µl for enzymatic digestion in 20µl total volume (5µl miniprep DNA, 1-2µl of enzymes, 2µl of 10x buffer, complete to 20µl with autoclaved water-1h 37°C)

e) *Gel purification kit*

Protocol GeneJet Gel extraction kit (Qiagen):

- Excise gel slice containing the DNA fragment using a clean scalpel or razor blade.
- Place the gel slice into a pre-weighed 1.5 mL tube and weigh. Record the weight of the gel slice. Note.
- Add 1:1 volume of Binding Buffer to the gel slice (volume: weight) (e.g., add 100 µL of Binding Buffer for every 100 mg of agarose gel).

- Incubate the gel mixture at 50-60 °C for 10 min or until the gel slice is completely dissolved. Mix the tube by inversion every few minutes to facilitate the melting process.
- Check the color of the solution. A yellow color indicates an optimal pH for DNA binding
- Transfer up to 800 µL of the solubilized gel solution (from step 3 or 4) to the GeneJET purification column. Centrifuge for 1 min. Discard the flow-through and place the column back into the same collection tube.
- Add 700 µL of Wash Buffer (diluted with ethanol as described on p. 3) to the GeneJET purification column. Centrifuge for 1 min. Discard the flow-through and place the column back into the same collection tube.
- Centrifuge the empty GeneJET purification column for an additional 1 min to completely remove residual wash buffer.
- Transfer the GeneJET purification column into a clean 1.5 mL microcentrifuge tube (not included).
- Add 50 µL of Elution Buffer to the center of the purification column membrane. Centrifuge for 1 min.
- Discard the GeneJET purification column and store the purified DNA at -20 °C.

f) *DNA ligation*

New England Biolabs protocol:

- Set up the following reaction in a microcentrifuge tube on ice. (T4 DNA Ligase should be added last

COMPONENT	20 µl REACTION
T4 DNA Ligase Buffer (10X)*	2 µl
Vector DNA (4 kb)	50 ng (0.020 pmol)
Insert DNA (1 kb)	37.5 ng (0.060 pmol)
Nuclease-free water	to 20 µl

- Gently mix the reaction by pipetting up and down and microfuge briefly
- For cohesive (sticky) ends, incubate at 16°C overnight or room temperature for 10 minutes
- For blunt ends or single base overhangs, incubate at 16°C overnight or room temperature for 2 hours (alternatively, high concentration T4 DNA Ligase can be used in a 10 minute ligation)
- Heat inactivate at 65°C for 10 minutes
- Chill on ice and transform 1-5 µl of the reaction into 50 µl competent cells

g) *Transformation competent E. coli*

Preparation of cells:

- Inoculate 1l of Super-broth with 1/100 volume of a fresh O.N. culture
- Grow cells at 37°C with vigorous shaking to an OD_{600} of 0.5 to 0.6. It might take less than 2 hrs.
- Pour into prechilled 500 ml centrifuge flasks, cool on ice 15-30 min. Centrifuge in a cold rotor at 4000 rpm for 15 min
- Resuspend pellets in 1 liter precooled Electroporation buffer (EB)- Centrifuge as in 3-/ Repeat with 500 EB
- Resuspend in 100 ml of precooled EB- Centrifuge in the bench-top centrifuge (15 min, 3000 rpm)
- Resuspend in a final volume of 3-4 ml in precooled EB. Aliquot in precooled Eppendorf tubes, freeze in an EtOH-dry ice bath, store at -70°C. The cells are good for at least 6 months under these conditions

Electrotransformation:

- Thaw the cells on ice
- In a pre-chilled eppendorf tube, mix 40 µl of cell suspension with 1 µl DNA 20ng/µl. DNA (from ligations for example) must be precipitated and resuspended in dH2O before use (No salts !)

- Swith on Gene Pulser II
- Set gene pulser at 25 µF (GenePulser II Capacitance) and 1.7 kV (Gene Pulser II, press Set Volt, it will light up). Set the pulse controler to 200 Ohms on Low range, and High range to infinite (OO).
- Transfer the mixture of cells and DNA to a cold 0.1 cm electroporation cuvette and shake suspension to bottom of cuvette. Dry the cuvette very carefully and place in a safety chamber, push the slide into the chamber until the cuvette is seated between the contacts in the base of the chamber.
- Pulse once by pressing the two red buttons on the Gene Pulser II until you hear a Bip (a few sec). It should produce a time constant of 4,5 to 5 ms. (The field strength will be 17 kV/cm).
- Remove the cuvette and immediately add 1 ml SOC medium (or LB) to the cuvette. (Rapid addition of SOC is important to maximize the recovery of transformants). Put back on ice.
- Transfer the cell suspension to an eppendorf tube (or a1,7x, 100mm polypropylene tube) and incubate at 37°C for 1 hour, shaking at 225 rpm.
- Centrifuge (5min 6000 rpm), aspirate medium, add 300µl SOC.
- Plate on selective medium (LB-Amp).

XI. Phagocytosis assay

Use cells kept well diluted in culture for at least 2 medium changes. When cells become more confluent than $5x10^5$ cells/ml their ability to phagocytose in HL5 decreases strongly. Ideally on the day of the experiment cells are at 200-300.000 cells/ml for phagocytosis.

- Transfer 1 ml of cell culture in a 1.5 ml Eppendorf.
- Centrifuge 4000 RPM, 2', RT, Eppendorf centrifuge.
- Resuspend cells in 700 µl HL5 containing:

- FITC latex beads	1µm/0.2 µm/0.05 µm	1µl/ml / 4µl/ml / 6µl/ml
- Ka-TRITC		10µl/ml
- DH5α-Rhodamine		10µl/ml
- Alexa647-dextran (stock 2mg/ml, use 1:200)		2.5µl/ml

- 20', 21°C, + shaking 200 RPM (tubes horizontal)
- Centrifuge 4000 RPM, 2', 4°C.
- Wash 1ml ice-cold HL5+Azide 0.1% (for bacteria wash 2x1ml SB).
- Resuspend cells in 100µl HL5+Azide 0.1% ice-cold.
- Use FACS machine for analysis

XII. Live microscopy

a) *Killing assay*

Sample preparation:

- Count *D. discoideum cells*: Aim for 700’000 cells/mL the day of the experiment.
- In 1.5 ml Eppendorf take 1mL Dictyo
- In 1.5 ml Eppendorf take 1mL of O/N KpGE-GFP culture
- Centrifuge both 4000rpm 2min RT
- Wash 1mL SB-sorb (1uL SB50x + 5mL sorbitol 1M → 50mL H20)

- Centrifuge 4000rpm 2min RT
- Resuspend Dictyo in 300uL SB-sorb
- Resuspend KpGE-GFP in 1mL SB-sorb with 1:100 dilution
- Put 150uL KpGE-GFP in each IBIDI well (4max)
- Wait 5 minutes
- Add 100uL Dictyo

Microscope

- Objective 40x oil
- Select Brightfield channel: Exposure 50msec Gain 5
- Set Lampe brightness 17%
- Select GFP channel: Exposure 140msec Gain 64 Sola 9%
- Acquisition: Time 2hours interval 30sec (241 points) Lambda Brighfield and GFP Z: 5 steps 3µm steps range 10um XY: select 4 positions
- Put oil on objective
- Place plate and move plate to put oil everywhere (avoid loss of focus)
- Set PFS (autofocus)
- Chose name for the file
- Turn all ambient light off
- Run the movie

When the movie is done:

- Create maximum intensity profile in z to maximize GFP signal detection
- Save/Export to TIFF with Resize 60%

On Fiji

- Deinterleave the stack (Image>Stacks>Tools>Deinterleave)
- Apply new Lookup table on the GFP channel (On GFP movie Image>Lookup Tables > Fire)
- Image>Adjust>Brightness and contrast>Auto Reduce Brightness
- Merge channels

Analysis:

- Use Prism
- Use Kaplan-Meyer survival curve
- Select at random 30-60 phagocytosis events per film
- For each bacterium followed, register the time spent inside the amoeba until the fluorescence vanished. For each bacterium that was exocytosed during the assay or for which the movie finished before the vanishing of fluorescence register these events as censored.
- Draw the curve

b) *Beads preparation for pH and proteolysis:*

(Sattler et al., 2013)

- Wash 50 mg of 3µm carboxylated silica particles three times with 1 mL of PBS by brief vortexing and spin at 2,000 × g for 60 s in a tabletop centrifuge

- Resuspend beads in 700 µ L of PBS (pH 7.2) containing 17.5 mg of cyanamide (concentration 25 mg/mL).
- Incubate at room temperature with shaking for 15 min
- Remove cyanamide by washing as in step 1 twice with coupling buffer
- Incubate overnight with agitation at 4°C in 1 mL of coupling buffer containing:
    - (a) 5 mg of defatted BSA (see Note 11) for the pH-sensitive reporter beads.
    - (b) 1 mg of DQgreen-labeled BSA and 250 mg of defatted BSA for the proteolysis reporter beads.
- Wash beads twice with quenching buffer to quench unreacted cyanamide.
- Wash beads twice with coupling buffer to remove soluble amine groups
- Resuspend beads in 700 µ L of coupling buffer and add:
    - (a) For the pH-sensitive reporter beads: 20 µ L of FITC and 20 µ L of Alexa 594 succinimidyl ester stocks (for each total amount 0.25 mg)
    - (b) For the proteolysis reporter beads: 20 µ L Alexa 594 succinimidyl ester (total amount 0.25 mg)
- Incubate for 1h at room temperature with shaking to allow labelling of BSA with fluorophores
- Wash particles once with quenching buffer and twice with PBS
- Resuspend in 1 mL of PBS with 0.01% w/v sodium azide as a preservative
- Store at 4°C in the dark and avoid drying of the particles
- Before adding beads to cells wash with PBS to remove sodium azide

c) *Proteolysis assay*

Sample preparation:

- Count *D. discoideum cells*: Aim for 700’000 cells/mL the day of the experiment.
- In 1.5 ml Eppendorf take 1mL Dictyo
- Centrifuge 4000rpm 2min RT
- Wash 1mL SB-sorb (1uL SB50x + 5mL sorbitol 1M → 50mL H20)
- Centrifuge 4000rpm 2min RT
- Resuspend Dictyo in 300uL SB-sorb
- Add 100uL Dictyo in each well
- Add 200ul SBS
- Add 10 ul 1:100 proteolysis beads dilution
- Wait 5 minutes

Microscope

- Objective 40x oil
- Select Brightfield channel: Exposure 50msec Gain 5
- Set Lampe brightness 17%
- Select GFP channel: Exposure 140msec Gain 64 Sola 9%
- Select RFP channel: Exposure 30 ms Gain 64 Sola 3%
- Acquisition: Time 3 hours Lambda Brighfield and GFP and RFP Z: 5 steps 3µm steps range 10um XY: select 4 positions
- Put oil on objective
- Place plate and move plate to put oil under all well (avoid loss of focus)
- Set PFS (autofocus)

- Chose name for the file
- Turn all ambient light off
- Run the movie

When the movie is done:
- Create maximum intensity profile in z for all fluorescence channel signal detection
- Save/Export to TIFF with Resize 60%

On Fiji
- Deinterleave the stack (Image>Stacks>Tools>Deinterleave)
- Select randomly 15 beads
- Draw a circle zone on the first frame of phagocytosis for the first bead
- Drag the circle at every frame on the bead position and register the “Area of interest”
- When for a bead the series of position is registered configure the measurement for average value
- Press “Measure” in each channel and register the fluorescence in both GFP and RFP channel at each position on an Excel file
- Compute the ration GFP fluorescence/RFP fluorescence
- Open prism and paste the list of ratios over time.
- Repeat for every bead

d) *Phagosomal pH assay*

Sample preparation:
- Count *D. discoideum cells*: Aim for 700’000 cells/mL the day of the experiment.
- In 1.5 ml Eppendorf take 1mL Dictyo
- Centrifuge 4000rpm 2min RT
- Wash 1mL SB-sorb (1uL SB50x + 5mL sorbitol 1M → 50mL H20)
- Centrifuge 4000rpm 2min RT
- Resuspend Dictyo in 300uL SB-sorb
- Add 100uL Dictyo in each well
- Add 200ul SBS
- Add 10 ul 1:100 proteolysis pH beads dilution
- Wait 5 minutes

Microscope
- Objective 40x oil
- Select Brightfield channel: Exposure 50msec Gain 5
- Set Lampe brightness 17%
- Select GFP channel: Exposure 140msec Gain 64 Sola 9%
- Select RFP channel: Exposure 30 ms Gain 64 Sola 3%
- Acquisition: Time 3 hours Lambda Brighfield and GFP and RFP Z: 5 steps 3µm steps range 10um XY: select 4 positions
- Put oil on objective
- Place plate and move plate to put oil under all well (avoid loss of focus)
- Set PFS (autofocus)
- Chose name for the file
- Turn all ambient light off

- Run the movie

When the movie is done:

- Create maximum intensity profile in z for all fluorescence channel signal detection
- Save/Export to TIFF with Resize 60%

On Fiji

- Deinterleave the stack (Image>Stacks>Tools>Deinterleave)
- Select randomly 15 beads
- Draw a circle zone on the first frame of phagocytosis for the first bead
- Drag the circle at every frame on the bead position and register the “Area of interest”
- When for a bead the series of position is registered configure the measurement for average value
- Press “Measure” in each channel and register the fluorescence in both GFP and RFP channel at each position on an Excel file
- Compute the ration GFP fluorescence/RFP fluorescence
- Open prism and paste the list of ratios over time.
- Repeat for every bead

e) *Motility assay:*

Cell culture:

- One 100 mm Petri dish at 10-20.104 cells/ml in HL5.Ideally, cell culture concentration should be at between 40.104 cells/ml and 80.104 cells/ml the day of the experiment.

Cell preparation

- Count the cells.
- In an Eppendorf tube put 20.104 cells + 1 ml SBsorbitol.
- Centrifuge 2 min, 4000 rpm, RT. Aspirate supernatant.
- Wash pellet with 1 ml SBsorbitol. Centrifuge 2 min, 4000 rpm, RT. Aspirate supernatant.
- Resuspend cells in 1 ml SBsorbitol.

In a 96 well plate : (µclear plate, black, Greiner cat no 655090)

- Put 100 µl of cell suspension per well (= 2.104 ¢).
- Allow cells to attach for 30 min RT (cell culture room).
- Aspirate supernatant VERY SLOWLY, and resupend cells gently in :
- 100 µl SBsorbitol : control
- 100 µl in SBsorbitol + 1 mM Folate (1 µl of 100mM stock) or 1:100 Bacteria final
- Incubate 20 minutes RT (cell culture room).

Imaging:

- ImageXpress XL or Nikon Eclipse T*i*2 equipped with a DS-Qi2 camera (obj 10x)
- Image cells for 30 minutes, one picture every 15 seconds.
- Assemble pictures into a movie and save as .stk file.

Analysis:

- Use Metamorph “Track Points” tool
- Follow 15 individual cells during all the duration of the movie.
- Calculate average distance and persistence for each condition tested.

f) *RICM Spreading assay*

<u>Material:</u>

- Amoeba cell culture: optimal between $0.5x10^6$ cells/ml and $1x10^6$ cells/ml
- Media: HL5, SB or SBS
- Glass bottom wells dishes
- SRIC or RICM objective

<u>Sample preparation:</u>

- Transfer 1ml of cell culture in an Eppendorf
- Centrifuge 4000 rpm, 2 min
- Rinse with 1ml of your desired medium
- Centrifuge again 4000 rpm, 2 min
- Resuspend in the corrected volume to have around 1 $x10^6$ cells/ml final concentration.
- Deposit in a Glass bottom wells dishes the volume desired:
  In 8 wells ibidi glass bottom dishes [10 ul – 200 ul]

<u>Microscope:</u>

- Open fully the diaphragm for the fluorescent light input
- Launch the Nikon software
- Set the objective on "oil 60x"
- Set the Brightfield channel to select the field of interest
- Set SRIC/RICM setting to adjust the "Z" (You should dark spots on a bright background)
- Set "PFS" on
- Acquisition: <u>Time:</u> it depends whether it is just a picture or a movie <u>Lambda:</u> Brightfield and SRIC/RICM <u>Z:</u> 5 steps 3µm steps range 10um <u>XY:</u> select 4 positions for movies
- Run for picture or movie

<u>Image analysis:</u>

For picture analysis:

- Open Software: ImageJ
- Remove the background (Process>Remove background)
  Click on "preview" and select the "rolling radius" that keep your dark spots but smooth the background
- Click on Image/Threshold
  Click on light background
  Apply (it generally selects the best fit but you can adjust the window)
- Click on "Analysis/set measurement"
  Choose "area"
- Click on "Analysis/Analyse particle »
  Select : 2-infitiny
  Select : Show outline
  Select : Display Results
  Select : Clear results
  Press "ok"
- In the result window you will have listed the area of each dot.

For movie analysis:

- Import movie or image in: Matlab
- Load the following algorithms:
  - Dictyotrack
  - DictyoAnalyze
  - Area_comparison
  - Global Analysisv2
- To select the time frame, modify the “t_window = [value start value end]” in “Area_comparison”
- Run the “threshold” detection algorithm
- Once all amoebae are correctly selected, click on “Analysis”
- Pressing “Save” will generate the excel file with all relevant data
  - Position
  - Surface Area global
  - Surface retracted
  - Surface expanded

XIII. Cell fixation and Immunofluorescence

Immunofluorescence (Actin/p80/H-ATPase):

- Cells grown in HL5 (not filtrated) to a maximum of about $1.0X10^6$ cell/ml
- Plate About 500 000 cells on glass coverslips (not ethanol sterilized) for 3 hours in about 500 µl of HL5 (fresh medium). Manipulate carefully the six-well plate to do not spill the medium off of the coverslip.
- Fix in paraformaldehyde 4% final in HL5 30 min at RT (minimum of 200 µl of fixation solution, not more than 500 µl to do not spill the solution off of the coverslip)
- Rinse with 2ml of 1x PBS-NH4Cl 40mM. Cells can be kept in this solution for a while. (Stock is 2M = 50X, 200 µl in 10 ml or 300µl in 15 ml)
- Replace 1x PBS-NH4Cl 40mM by 2ml of plain 1x PBS.
- Permeabilize cells with Saponin**:** PBS+0.1% saponin (PBS-Sapo), 5 min (Stock is 5% = 50X, 200 µl in 10 ml or 300µl in 15 ml)
- Incubate in PBS-BSA (0.2%) at least 5 min (Stock is 20% = 100X)
- Incubate coverslip in new dry six-well plate for 45 minutes with 100µl first antibody solution (anti-H-ATPase [221-35-2] diluted 1:4 in PBS-BSA)
- Rinse 3x PBS-BSA (1ml), last rinse leave 5min
- Incubate coverslip in new dry six-well plate for 30 minutes with 100 µl secondary fluorescent antibody (Alexa Fluor 547 [red] diluted 1:600 = 5µl aliquot in 3ml of PBS-BSA)
- Rinse 3x PBS-BSA, last rinse leave 5min
- Incubate coverslip in new dry six-well plate for 30 minutes with **50 µl** of Alexa Fluor 488-coupled H161 antibody (Antibody diluted 1:300 in PBS-BSA)
- Rinse 3x PBS-BSA, last rinse leave 5min
- Rinse 1x PBS
- Mount in moewiol with DABCO (8µl per coverslip)

RESULTS

I. VPS13F alters intracellular killing in a Kil2-independent manner in *D. discoideum*

1. Early characterization of Vps13F.

Out of the random mutagenesis done to identify killing-defective mutant cells, *vps13F* was the first gene to be identified and properly inactivated. Like Kil1 and Kil2, vps13F is not a direct effector of killing since it is a cytosolic protein. Based on its homology with the previously characterized yeast Vps13, Vps13F was expected to be involved in intracellular transport.

The main highlights of this study are:

- We characterized a new IC-killing defective mutant: *vps*13F KO
- We showed that vps13F activity is independent of Kil2.
- We showed that IC killing can be stimulated by addition of exogenous folate.
- Use of live imaging for IC killing provided sufficient precision to measure the median IC killing time in WT cells for *K. pneumoniae* : 7.5min, and 18min in *vps13*F KO cells.

When we studied *vps13F* KO cells we applied the same rationale as when studying *kil2* KO cells (Lelong et al., 2010). Kil2 has the features of a cation pump so it is likely that the ion addition that restores the IC killing could be what the pump transports. In a similar fashion, we hypothesized that if addition of folate stimulates IC killing in *vps13F* KO cells then Vps13F plays a role in the folate sensing pathway. As will be discussed below, our later studies changed our interpretation of these results. Our current hypothesis is that vps13F is independent of the folate-sensing pathway.

2. Vps13F links bacterial recognition and intracellular killing in *Dictyostelium*

Published: Cell Microbiol. 2017 Jul; 19(7): e12722.

Jade Leiba[1,*], Ayman Sabra[1,*], **Romain Bodinier[1]**, Anna Marchetti[1], Wanessa C. Lima[1], Astrid Melotti[1], Jackie Perrin[1], Frederic Burdet[2], Marco Pagni[2], Thierry Soldati[3], Emmanuelle Lelong[4], Pierre Cosson[1]

Affiliations:
[1]Department of Cell Physiology and Metabolism, Faculty of Medicine, University of Geneva, 1 rue Michel Servet, CH-1211, Geneva 4, Switzerland.
[2]Vital-IT, Swiss Institute of Bioinformatics, University of Lausanne, Lausanne, Switzerland.
[3]Department of Biochemistry, University of Geneva, Geneva CH-1211, Switzerland.
[4]Genomic Research Laboratory, Division of Infectious Diseases, Geneva University Hospitals, Geneva CH-1211, Switzerland.
*These authors contributed equally to this work
Corresponding author: Pierre.Cosson@unige.ch

Personal contribution:

Figure + legends:

Object:	Analysis	Quantification	Figure	Text	Revision
Fig1	AS/JL/**RB**	AS/JL/**RB**	JL	AS/JL	JL/**RB**/PC
Fig5	JL/**RB**	JL/**RB**	JL	JL/**RB**	JL/**RB**/PC
Fig7	JL/**RB**	JL/**RB**	JL	JL/**RB**	JL/**RB**/PC
Fig10	JL/**RB**	JL/**RB**	JL	JL/**RB**	JL/**RB**/PC

Manuscript:
Introduction/Discussion**:**

Object:	Text	Revision
Abstract	JL/AS/PC	JL/AS/**RB**/PC
Introduction	JL/AS/PC	JL/AS/**RB**/PC
Discussion	JL/AS/PC	JL/AS/**RB**/PC

Materials & Methods:

Object:	Development	Qualification	Text	Revision
Intracellular killing assay	**RB**	JL/**RB**	**RB**	JL/**RB**

Results:

Object:	Text	Revision
Fig1	JL/**RB**/PC	JL/**RB**/PC
Fig5	JL/**RB**/PC	JL/**RB**/PC
Fig7	JL/**RB**/PC	JL/**RB**/PC
Fig10	JL/**RB**/PC	JL/**RB**/PC

Received: 7 September 2016 | Revised: 6 January 2017 | Accepted: 6 January 2017

DOI: 10.1111/cmi.12722

WILEY

RESEARCH ARTICLE

Vps13F links bacterial recognition and intracellular killing in *Dictyostelium*

Jade Leiba[1]* | Ayman Sabra[1]* | Romain Bodinier[1] | Anna Marchetti[1] | Wanessa C. Lima[1] | Astrid Melotti[1] | Jackie Perrin[1] | Frederic Burdet[2] | Marco Pagni[2] | Thierry Soldati[3] | Emmanuelle Lelong[4] | Pierre Cosson[1]

[1] Department of Cell Physiology and Metabolism, Faculty of Medicine, University of Geneva, Geneva, Switzerland

[2] Vital-IT, Swiss Institute of Bioinformatics, University of Lausanne, Lausanne, Switzerland

[3] Department of Biochemistry, University of Geneva, Geneva, Switzerland

[4] Genomic Research Laboratory, Division of Infectious Diseases, Geneva University Hospitals, Geneva, Switzerland

Correspondence

Pierre Cosson, Department of Cell Physiology and Metabolism, Faculty of Medicine, University of Geneva, 1 rue Michel Servet, CH-1211, Geneva 4, Switzerland.

Email: pierre.cosson@unige.ch

Funding information

Swiss National Science Foundation, Grant/Award Number: 31003A_153326 to PC

Abstract

Bacterial sensing, ingestion, and killing by phagocytic cells are essential processes to protect the human body from infectious microorganisms. The cellular mechanisms involved in intracellular killing, their relative importance, and their specificity towards different bacteria are however poorly defined. In this study, we used *Dictyostelium discoideum*, a phagocytic cell model amenable to genetic analysis, to identify new gene products involved in intracellular killing. A random genetic screen led us to identify the role of Vps13F in intracellular killing of *Klebsiella pneumoniae*. *Vps13F* knock-out (KO) cells exhibited a delayed intracellular killing of *K. pneumoniae*, although the general organization of the phagocytic and endocytic pathway appeared largely unaffected. Transcriptomic analysis revealed that *vps13F* KO cells may be functionally similar to previously characterized *fspA* KO cells, shown to be defective in folate sensing. Indeed, *vps13F* KO cells showed a decreased chemokinetic response to various stimulants, suggesting a direct or indirect role of Vps13F in intracellular signaling. Overstimulation with excess folate restored efficient killing in *vps13F* KO cells. Finally, genetic inactivation of Far1, the folate receptor, resulted in inefficient intracellular killing of *K. pneumoniae*. Together, these observations show that stimulation of *Dictyostelium* by bacterial folate is necessary for rapid intracellular killing of *K. pneumoniae*.

1 | INTRODUCTION

Phagocytic cells play a key role in the elimination of invading microorganisms in the human body. These cells ingest many different types of bacteria and eliminate them in phagosomes. In neutrophils and macrophages, phagocytosis is accompanied by a burst in the production of superoxide, and the oxidative burst is thought to play a key role in killing ingested bacteria, because free radicals can react with and damage virtually any biological molecule (Silva, 2010). The evidence implicating free radicals in intracellular killing of bacteria is mostly based on the analysis of patients in which NOX2, which produces superoxide ions, is partially or totally inactivated by mutations. Loss of NOX2 activity results in a disease called chronic granulomatous disease (CGD), characterized by an increased susceptibility to infections with fungi and with a subset of catalase-positive bacteria (Goldblatt & Thrasher, 2000). In addition, it has been observed that neutrophils from CGD patients are less efficient at killing *Staphylococcus aureus* in vitro (Ellson et al., 2006). It is not clear why certain bacteria and not others are more prone to mount infections in these patients. Oxidative burst and free radical productions were also reported to play important roles to protect macrophages against infection with *Salmonella* (Rushing & Slauch, 2011). Although these observations have brought to light the role of free radicals in the elimination of ingested bacteria, it is also clear that other killing mechanisms must exist: they presumably account for the fact that CGD patients are not prone to infections with all bacteria.

A number of additional mechanisms have been implicated in intracellular killing, in particular exposure to the acidic pH of phagolysosomes and activity of lytic lysosomal enzymes and of antibacterial molecules such as defensins, cathelicidins and histatins (De Smet & Contreras, 2005; Zanetti, 2005). In neutrophils, the

*These authors contributed equally to this work myeloperoxidase-mediated halogenation as well as the cathepsin G, elastase, and proteinase 3 also contribute to the killing of bacteria (Segal, 2005). Other mechanisms such as the generation of DNA and lytic enzymes that complex by dying neutrophils (NETs: Neutrophil Extracellular Traps) may in addition account for extracellular killing of bacteria (Papayannopoulos & Zychlinsky, 2009). The relative importance of these different killing mechanisms is not fully known, and it is also not clear if different bacteria are killed by different mechanisms. It has for example been shown that elastase knock-out mice are highly susceptible to infections with *Candida albicans*, *Klebsiella pneumoniae*, and *Escherichia coli* but not with *S. aureus*, whereas mice lacking cathepsin G were highly susceptible to *S. aureus* (Belaaouaj et al., 1998; Reeves et al., 2002). In these mice, microbial killing was abolished despite a normal oxidative burst, suggesting that free radicals and other antimicrobial mechanisms act synergistically, and that their relative importance in the control of infections depends on the infecting pathogen.

Dictyostelium discoideum is a free-living unicellular organism continuously engaged in bacterial ingestion and killing. Its haploid genome makes it easily amenable to genetic analysis, and it has been used to study many facets of cell biology, in particular cellular motility, phagocytosis, and organization of the endocytic pathway. In addition, *Dictyostelium* provides a good model to study interactions between phagocytic eukaryotic cells and pathogenic or nonpathogenic bacteria (Cosson & Lima, 2014; Cosson & Soldati, 2008). Characterization of mutants with decreased ability to kill ingested bacteria allowed the identification of new gene products involved in intracellular bacterial killing. For example, Kil2, a phagosomal P-type ATPase presumably transporting Mg^{2+} ions into the phagosome, is essential for intracellular killing of *K. pneumoniae* bacteria (Lelong et al., 2011). *Kil2* knock-out (KO) cells still kill efficiently ingested *Pseudomonas aeruginosa* or *Bacillus subtilis*, suggesting that different bacteria are killed by different mechanisms (Lelong et al., 2011).

In this study, we isolated a new *Dictyostelium* mutant defective for intracellular killing of *K. pneumoniae*. Detailed analysis revealed that *vps13F* KO cells are partially defective in bacterial recognition and as a consequence, fail to efficiently kill ingested *K. pneumoniae* bacteria. These results provide the first evidence that over a time scale of a few minutes, recognition of ingested bacteria is necessary to ensure efficient intracellular killing.

2 | RESULTS

2.1 | Vps13F is involved in the interaction between *Dictyostelium* and *Klebsiella pneumoniae*

We previously identified Kil2 as a gene product essential for efficient intracellular killing of nonpathogenic, noncapsulated *K. pneumoniae* (Lelong et al., 2011). In order to identify new gene products involved in intracellular killing of bacteria that could potentially exhibit a functional redundancy with Kil2, we created, in *kil2* KO cells, a library of random mutants by restriction enzyme-mediated insertion (REMI). We then tested individual clones for their ability to grow on six different nonpathogenic bacteria (*Micrococcus luteus*, *B. subtilis*, *E. coli* B/r, *K. pneumoniae*, *K. pneumoniae* LM21, and *P. aeruginosa*) and selected double mutants defective for growth on at least one bacteria. This study is dedicated to the analysis of one mutant strain initially seen to exhibit a defect for growth on *K. pneumoniae*. The mutagenic vector recovered from this strain, together with the flanking genomic sequences, was found to be inserted in the *vps13F* gene (Figure S1A). In order to ascertain that the growth defect of this original insertional mutant strain was caused by the disruption of the *vps13F* gene, we deleted in the parental strain a large portion of the *vps13F* gene by homologous recombination. Three individual *vps13F* KO clones were selected (Figure S1 B, C, and D), and they all exhibited similar phenotypes, detailed below. Three clones of double *kil2–vps13F* KO were also generated and analyzed in parallel.

We first compared the ability of *kil2-vps13F* KO cells to grow in the presence of *K. pneumoniae* with that of its parental single *kil2* KO. For this, a defined number of *Dictyostelium* cells (from 10 to 10,000) was deposited on a lawn of *K. pneumoniae* bacteria, and *Dictyostelium* growth was observed after 5 days (Figure 1A). Wild-type (WT) *Dictyostelium* cells grew rapidly in the presence of *K. pneumoniae*, and *kil2* KO cells grew less efficiently, as previously described (Lelong et al., 2011). When combined with a mutation in *kil2*, disruption of the *vps13F* gene created a strong additional growth defect (Figure 1A). In a WT background, *vps13F* inactivation only slightly delayed growth on *K. pneumoniae* (Figure 1A). When tested on a wider array of bacteria, the growth defect created by *vps13F* inactivation in the *kil2* KO background was seen when cells were exposed to *K. pneumoniae*, to a mucoid strain of *E. coli* B/r, and to *M. luteus* (Figure 1B). Growth of all these KO strains was identical to that of WT cells in liquid HL5 medium, suggesting that the genetic inactivation of *vps13F* created a specific defect in the interaction of *Dictyostelium* cells with *K. pneumoniae* and a few other bacteria.

Interestingly, a separate genetic screen performed in a WT background also yielded a mutation in a gene of the Vps13F family (Figure S2): *vps13A* KO cells grew inefficiently in the presence of *M. luteus* but as efficiently as WT cells in the presence of other bacteria (Figure 1B). This indicates that different members of the Vps13F family have distinct functions during *Dictyostelium* growth in the presence of different bacteria.

Although mutations in vacuolar protein sorting 13 (*Vps13*) genes have already been studied in a number of organisms, the function of Vps13 proteins is still poorly understood. Vps13 was first identified in *Saccharomyces cerevisiae*, which encodes a single member of the family. Its mutation causes a defect in the sorting of lysosomal enzymes, and more specifically, in vesicular transport between the vacuole and the Golgi apparatus (Brickner & Fuller, 1997, Redding, Brickner, Marschall, Nichols, & Fuller, 1996). The human Vps13 family is composed of four members: Vps13A (also called Chorein), Vps13B, Vps13C, and Vps13D. Mutations in Vps13A and Vps13B result in rare neurological diseases, respectively, chorea-acanthocytosis (Rampoldi et al., 2001; Ueno et al., 2001) and Cohen syndrome (Kolehmainen et al., 2003). In both cases, the large size of these proteins and the lack of well-characterized domains or motifs in their structure made their functional characterization difficult. To date the molecular function of Vps13 proteins is still poorly understood, as well as their specific involvement in these genetic diseases. The *Dictyostelium* Vps13 family comprises six members, and one of them, Vps13C (also called TipC),

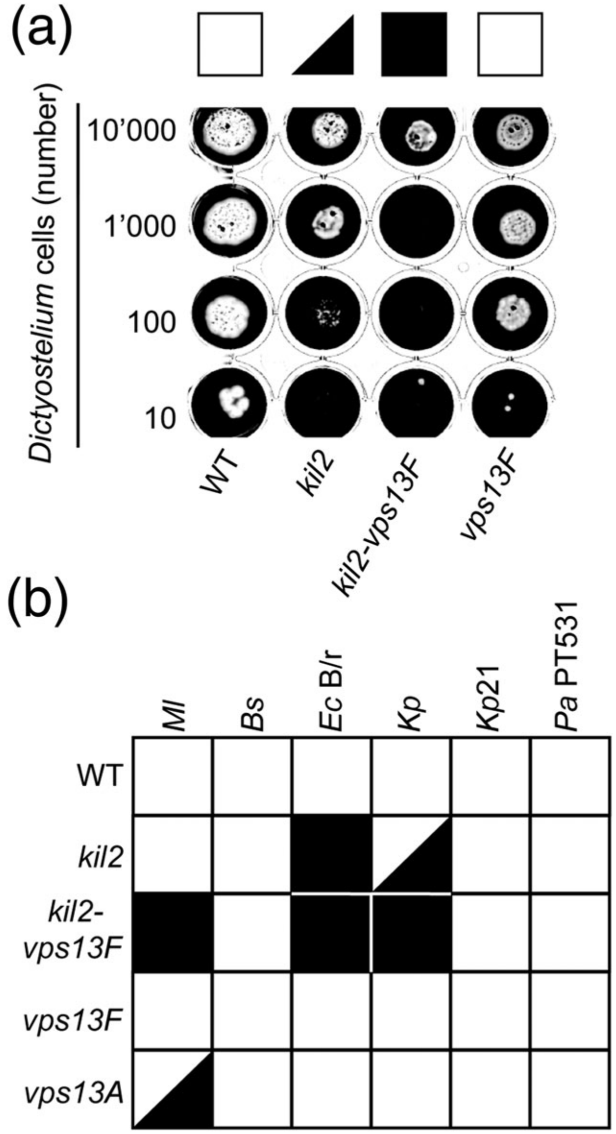

FIGURE 1 *Vps13F* and *vps13A* KO cells exhibit specific growth defects in the presence of different bacteria. (a) To quantify the ability of *Dictyostelium* mutants to feed upon *Klebsiella pneumoniae*, *Dictyostelium* cells (10,000, 1,000, 100, or 10 cells) were applied onto a lawn of *K. pneumoniae*. After five days, wild-type (WT) *Dictyostelium* cells created phagocytic plaques (white) in the bacterial lawn. *Kil2* KO cells grew slower than WT cells on *K. pneumoniae* and double *kil2–vps13F* KO cells presented an even more pronounced growth defect. *Vps13F* KO cells grew slightly slower that WT cells, but this growth defect is less pronounced than that of *kil2* KO cells. (b) Growth of Dictyostelium cells on several bacterial species was assessed as shown in (a) in four independent experiments and scored from 4 (efficient growth) to 0 (no growth). A white square indicates an average score of 4–3, a black triangle a score of 3–2, and a black square a score of 2–0. Double *kil2–vps13F* KO cells presented a severe growth defect on *Escherichia coli B/r*, *K. pneumoniae* and *M. luteus*. *Vps13A* KO cells grew poorly on *M. luteus*. (Bs = *Bacillus subtilis*; Ec B/r = *Escherichia coli* B/r; Kp = *K. pneumoniae*; Kp21 = *Klebsiella pneumoniae* LM21; Ml = *Micrococcus luteus*, Pa PT531 = *Pseudomonas aeruginosa* PT531)

was proposed recently to play a role in autophagy (Munoz-Braceras, Calvo, & Escalante, 2015).

The six *Dictyostelium* Vps13 proteins show relatively low overall primary sequence similarity with each other (between 25% and 40%), but their domain structure is conserved and essentially identical to that of human and yeast proteins (Figure 2A), with six conserved domains: (a) an N-terminal domain, also called Chorein domain, (b) a second N-terminal domain, (c) a repeated coiled region, (d) an an SHORT-ROOT (SHR)-binding domain shown in plants to bind the SHR transcription factor (Koizumi & Gallagher, 2013), (e) a C-terminal domain, and (f) a second C-terminal autophagy-related domain (also found in the Atg2 protein). The molecular functions of these domains remain essentially unelucidated in all species. Vps13 proteins have no transmembrane domain or signal peptide sequences, suggesting that they are neither secreted nor present in intracellular organelles.

Phylogenetic reconstructions using the proteins from *Dictyostelium*, human, and yeast suggest that paralogs were generated by duplication independently after divergence of Amoebozoae and of Metazoa (Figure 2B). Each of the six *D. discoideum* paralogs have orthologs in two other *Dictyostelium* species (*D. purpureum* and *D. fasciculatum*), indicating that the duplications occurred before the speciation of the Dictyostelid group. *Dictyostelium* Vps13A and D are close, as well as C/E and B/F. The human proteins show a large degree of divergence, as evidenced by the long branch lengths between the four orthologs (Figure 2B).

2.2 | Defective killing of *K. pneumoniae* in *vps13F* KO cells

In order to test the putative role of Vps13F in phagocytosis and macropinocytosis, WT and *vps13F* KO cells were incubated in the presence of fluorescent latex beads, of fluorescently-labeled *K. pneumoniae*, or of a fluorescent dextran. Phagocytosis of latex beads and of *K. pneumoniae* was unaffected in *vps13F* KO cells compared to WT cells, as well as fluid-phase uptake of dextran by macropinocytosis (Figure 3). *Kil2* KO and *kil2–vps13F* KO cells both showed a minor defect in phagocytosis of latex beads compared to WT cells (Figure 3).

We next tested whether ingested bacteria were efficiently killed in *vps13F* KO cells. For this, we followed the fate of internalized *K. pneumoniae* bacteria expressing Green Fluorescent Protein (GFP) (*Kp*-GFP). As described previously (Benghezal et al., 2006; Lelong et al., 2011), killing of *Kp*-GFP bacteria results in extinction of the GFP fluorescence. We first incubated *Dictyostelium* cells with an excess of *Kp*-GFP bacteria (10 bacteria per *Dictyostelium*) and measured the intracellular accumulation of fluorescent bacteria by flow cytometry. In WT cells, accumulation of intracellular fluorescent bacteria reached a maximum after approximately 15 min, then decreased as extracellular bacteria were gradually ingested and killed (Figure 4). In *vps13F* KO cells, the maximal intracellular fluorescence was also reached after 15 min, but it was significantly higher than in WT cells (Figure 4), suggesting that internalized bacteria remained fluorescent longer in *vps13F* KO cells than in WT cells.

We next visualized phagocytosis and intracellular killing of individual GFP-expressing *K. pneumoniae*, as previously described (Delince et al., 2016). For this, we imaged directly *Dictyostelium* cells phagocytosing and killing *Kp*-GFP and measured the time between ingestion and killing of individual bacteria. Two representative movies are shown (Figure 5A): in these instances, extinction of GFP fluorescence occurred approximately 3 min after phagocytosis in WT

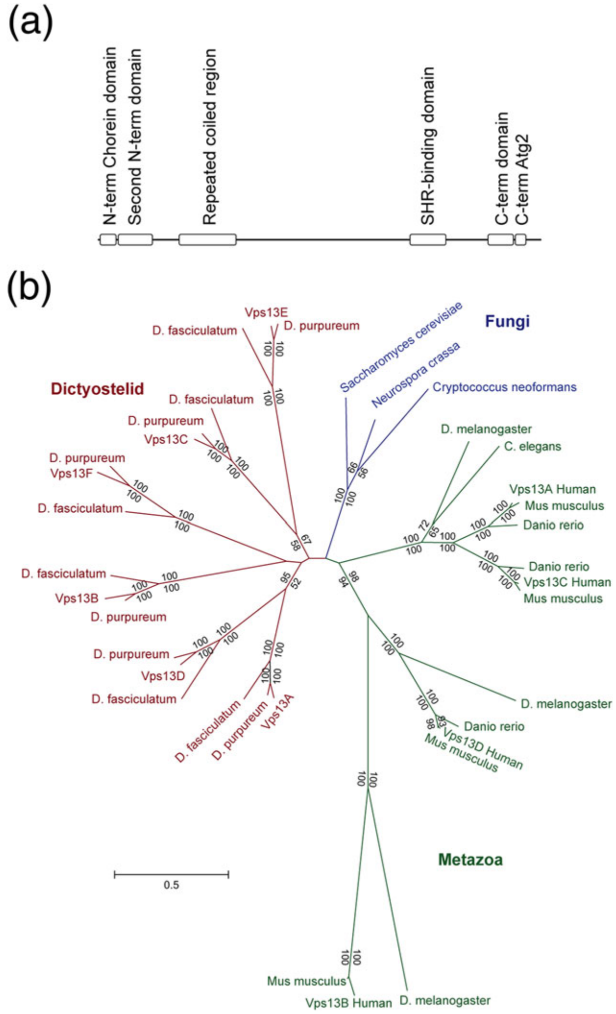

FIGURE 2 The Vps13F family. (a) Proteins of the vacuolar protein sorting 13 family share a similar domain organization. On the basis of primary sequence analysis, *Dictyostelium* proteins share the same six conserved domains present in human and yeast proteins: two N-terminal domains (the first one corresponding to the Chorein domain), a repeated coiled region, an SHR-binding domain, and two C-terminal domains (the last one corresponding to an autophagy or Atg2-related domain). (b) Unrooted maximum-likelihood phylogenetic tree of Vps13F proteins from dictyostelid, fungi, and metazoan species. Numbers at the nodes indicate the percentage of bootstrap support (upper values for the maximum-likelihood tree and lower values for the neighbor-joining tree; only numbers above 50% are shown)

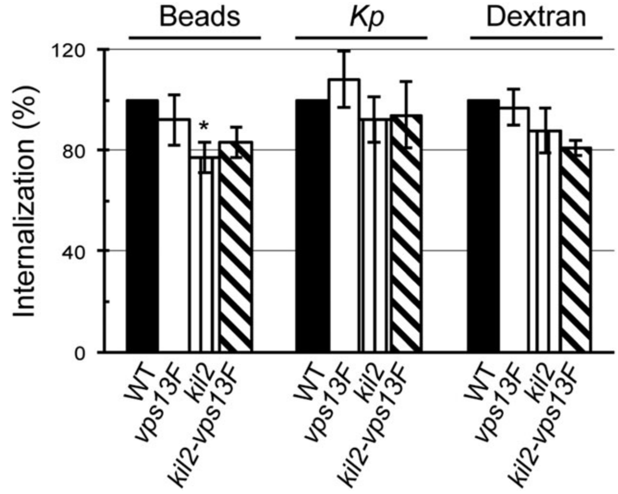

FIGURE 3 Phagocytosis and macropinocytosis are not defective in *vps13F* KO cells. Wild-type (WT) or knock-out (KO) cells were incubated for 20 min with fluorescent latex beads, heat-inactivated *Klebsiella pneumoniae*, or dextran. The internalized fluorescence was measured by flow cytometry. Mean fluorescence was plotted for each strain and expressed as a function of internalization in WT cells. Macropinocytosis of dextran and phagocytosis of beads or bacteria were as efficient in *vps13F* KO as in WT cells (mean ± SEM; 5 and 7 independent experiments for WT and KO respectively). *Kil2–vps13F* KO cells exhibited a minor defect in phagocytosis of latex beads compared to WT cells, as also seen in *kil2* KO cells ($p < .05$)

cells, while GFP fluorescence persisted for 13 min in *vps13F* KO cells (Figure 5A). The time required for fluorescence extinction was quantified for a large number of bacteria (>100) in at least three independent experiments and plotted as a Kaplan–Meyer survival curve. The curves generated in three independent experiments for WT and *vps13F* KO cells are shown (Figure 5B), as well as the curves combining the results of the three experiments for the WT and seven experiments for *vps13F* KO (Figure 5C). *Vps13F* KO cells killed internalized bacteria significantly slower than WT cells (Figure 5C). The average survival time of internalized bacteria was 7.6 min in WT and 22.1 min in *vps13F* KO cells. Note that the average survival time (7.6 min for WT cells) is significantly higher than the median killing time (5.0 min) due to the fact that a small number of ingested bacteria remain fluorescent for extended periods of time (>30 min), as previously observed (Delince et al., 2016).

Finally, in order to assess directly the viability of bacteria in *Dictyostelium* cells, we incubated WT or *vps13F* KO cells with a small number of *K. pneumoniae* (200 *Dictyostelium* cells per bacteria) to ensure optimal phagocytosis. At various times, an aliquot of the suspension was collected, the *Dictyostelium* cells were killed, and the surviving (intracellular and extracellular) bacteria plated on agar where they formed colonies after an overnight incubation at 37 °C. WT cells internalized bacteria over a period of 6 h and phagocytosed bacteria are rapidly killed as previously observed (Benghezal et al., 2006; Lelong et al., 2011; Lima, Balestrino, Forestier, & Cosson, 2014; Figure 6A). In *vps13F* KO cells, bacteria survived longer: after 2 h of incubation with *vps13F* KO cells; 64% of bacteria were still alive, against 45% in the presence of WT cells (Figure 6A). Because *K. pneumoniae* are phagocytosed as efficiently in *vps13F* KO cells and in WT cells (Figure 3), these results confirm the proposal that intracellular killing of *K. pneumoniae* is delayed in *vps13F* KO cells compared to WT cells. In summary, three different assays indicate that intracellular killing of *K. pneumoniae* is slower in *vps13F* KO cells than in WT cells. We also tested the survival of *B. subtilis* upon incubation with *Dictyostelium* cells and observed no difference in survival of ingested *B. subtilis* in *vps13F* KO cells (Figure 6B).

We then compared the killing defect observed in *vps13F* KO cells with that in *kil2* KO cells: intracellular killing was significantly slower in *kil2* KO cells than in *vps13F* KO cells, and it was even slower in the double *kil2-vps13F* KO cells (Figure 7; average survival time: 7.6 min in WT cells, 22.1 min in *vps13F* KO, 48.5 min in *kil2* KO and 85 min in *kil2-vps13F* KO cells). The fact that genetic inactivation of *vps13F* conferred an additional killing defect to a *kil2* KO cell suggests that

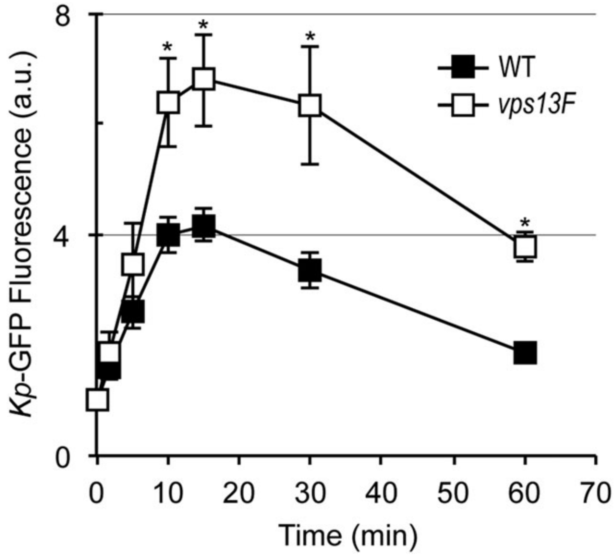

FIGURE 4 Intracellular accumulation of live *Klebsiella pneumoniae* in *vps13F* KO cells. Wild-type or *vps13F* KO *Dictyostelium* cells were incubated in the presence of *K. pneumoniae* expressing GFP (10 bacteria per *Dictyostelium*). At the indicated time, an aliquot was collected, and the fluorescence associated with cells was determined by flow cytometry. The number of intracellular fluorescent bacteria increased gradually and reached a plateau after 15 minutes, when internalization and killing rates equilibrated. Intracellular fluorescence then decreased gradually as extracellular bacteria were depleted. *Vps13F* KO cells accumulated more intracellular fluorescence than WT cells, suggesting that genetic inactivation of *vps13F* causes a defect in intracellular killing of *K. pneumoniae*. (mean ± SEM; *: $p < .05$; student t test; $n = 7$)

the two proteins function in different pathways in the killing process. Interestingly, *vps13A* KO cells did not exhibit significant defects in ingestion or intracellular killing of *K. pneumoniae* (Figure S3), confirming the specificity of the *vps13F* KO killing defect. As observed previously with other mutants unable to kill efficiently bacteria (e.g., *kil2* KO cells), both *vps13F* KO and *kil2*–*vps13F* KO cells grew as efficiently as WT cells in the presence of heat-killed bacteria (Figure S4).

2.3 | The organization of the phagocytic and endocytic pathways is not affected in *vps13F* KO cells

In order to account for the defective killing of *K. pneumoniae*, we first checked the organization and function of the endocytic and phagocytic pathway in *vps13F* KO cells. Acidification of the endocytic pathway was analyzed by measuring extinction of internalized Oregon green-labeled dextran as previously described (Marchetti, Lelong, & Cosson, 2009) and was found to be unaffected in *vps13F* KO cells: after an 18-min pulse, internalized fluid phase was found in the very acidic endosomes, from which it was transferred after approximately 30 min to less acidic postlysosomes (Figure 8A and Figure S5). The morphology of the main endocytic compartments was assessed by immunofluorescence with antibodies against p80, a marker of lysosomes and postlysosomes; p25, a marker of the cell surface and of recycling endosomes; and rhesus, a marker of the contractile vacuole. No gross defects in endosomal morphology and sorting were detected (Figure S6).

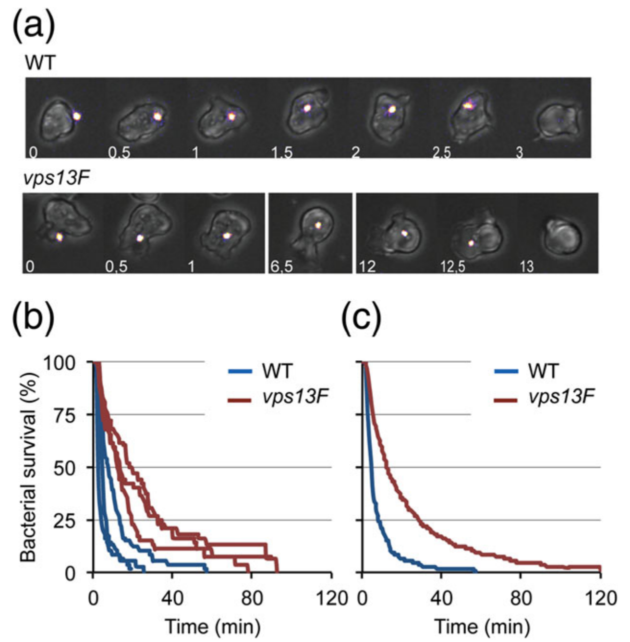

FIGURE 5 **Impaired intracellular killing of *Klebsiella pneumoniae* in *vps13F* KO cells.** To visualize ingestion and intracellular killing of individual *K. pneumoniae*, *Dictyostelium* cells were incubated with GFP-expressing *K. pneumoniae* (*Kp*-GFP) at a ratio of 1:3 in PB-Sorbitol for a total duration of 2 h. Cells were imaged every 30 sec by phase contrast and fluorescence microscopy. (a) Representative, successive images showing a WT cell that kills an individual *Kp*-GFP in 3 min. Below, representative images showing a *vps13F* KO cell killing a *Kp*-GFP in 13 min. (b) The time between phagocytosis and fluorescence extinction of each phagocytosed bacterium was determined and the probability of bacterial survival is represented as a Kaplan–Meyer estimator. Survival curves of ingested *K. pneumoniae* collected in three independent experiments in WT cells (blue) and KO cells (red). (c) Survival curves of ingested *K. pneumoniae* combining results of three independent experiments in WT cells (blue) and seven in *vps13F* KO (red). Intracellular killing is significantly slower in *vps13F* KO cells compared to WT cells ($p < 10^{-4}$; log-rank test; number of ingested bacteria is 228 for WT and 457 for *vps13F* KO cells)

Silica beads coated with Bovine Serum Albumin (BSA) coupled to DQ green were used to assess the activity of lysosomal proteases inside phagosomes as previously described (Lelong et al., 2011; Sattler, Monroy, & Soldati, 2013). In *vps13F* KO, like in WT cells, degradation of BSA-released DQ green and dequenched its fluorescence (Figure 8B). The fact that no difference was seen between WT and *vps13F* KO cells indicates that beads were transferred with similar kinetics to acidic compartments where they were processed by active proteases. Alterations in phagosome maturation and acidification, in protease delivery to phagosomes, or in protease activity would all be expected to delay proteolytic digestion in phagosomes.

We also tested the levels of glycosidases in cells and in the cell supernatant: in WT and in *vps13F* KO cells, intracellular levels of N-acetyl β-glucosaminidase and α-mannosidase were indistinguishable, and only minor amounts of enzymes were detected in the cell supernatant (Figure 8C), indicating that their intracellular sorting was not grossly perturbed.

Finally, we measured by Western blots the intracellular level of several proteins previously shown to participate in phagocytosis and

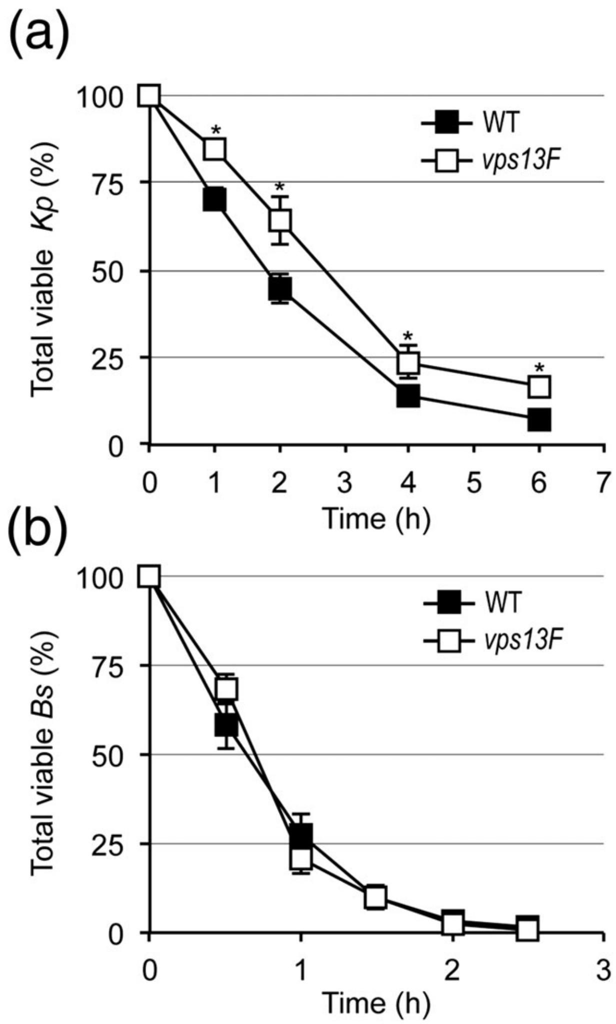

FIGURE 6 *Vps13F* KO cells are defective for killing *Klebsiella pneumoniae* but not *Bacillus subtilis*. (a) WT or KO *Dictyostelium* were mixed with *K. pneumoniae* (200 *Dictyostelium* cells per bacteria to ensure optimal phagocytosis). At the indicated times, an aliquot of the mixture was collected, *Dictyostelium* cells were lysed, the bacteria were plated on LB-agar, and the total (extracellular and intracellular) number of remaining viable bacteria was evaluated by counting colony forming units (CFUs). Results are expressed as a percentage of CFUs at time 0 (mean ± SEM; *: $p < .01$; student *t* test; $n = 12$ for WT or 16 for *vps13F* KO). (b) Intracellular killing of *B. subtilis* was assessed as described in (a). No significant difference was detected between WT and *vps13F* KO cells ($n = 4$)

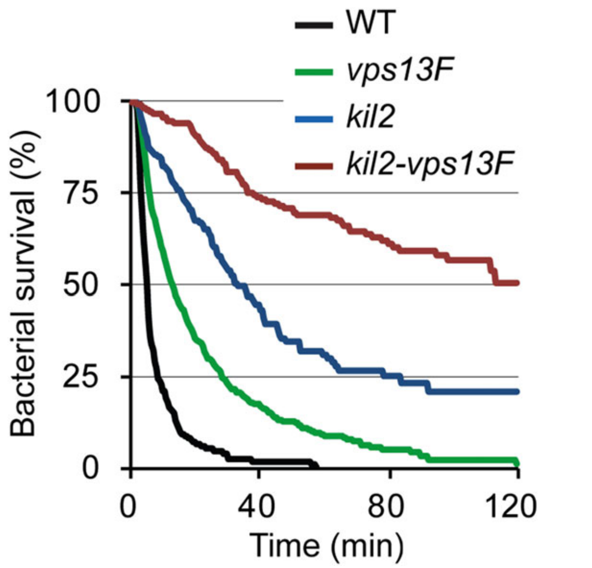

FIGURE 7 Deletion of *vps13F* in *kil2* KO cells strongly impacts intracellular killing of *Klebsiella pneumoniae*. Intracellular killing of individual *Kp*-GFP by amoeba cells was visualized as described in Figure 5 in WT, *vps13F*, *kil2*, and *kil2–vps13F* KO cells. Intracellular survival of ingested *Kp*-GFP was significantly longer in *kil2* KO cells than in *vps13F* KO cells, and significantly longer in *kil2–vps13F* KO cells than in *kil2* KO cells ($p < 10^{-4}$; log-rank test; number of ingested bacteria is 198 for *kil2* and 194 for *kil2–vps13F* KO). The sets of data for WT and *vps13F* KO cells are the same as presented in Figure 5C

intracellular killing: the cellular levels of SibA (Froquet et al., 2012), Phg1A (Le Coadic et al., 2013), Kil1, and Kil2 were identical in WT and in *vps13F* KO cells, as well as the level of Far1 (Figure 8D and Figure S7).

In summary, all our observations indicate that the organization and function of the endocytic and phagocytic pathways are unaffected by genetic inactivation of *vps13F*, suggesting that the role of Vps13F in intracellular killing of *Klebsiella* is linked to another, more subtle functional alteration.

2.4 | The killing defect of *vps13F* KO cells is linked to defective bacterial sensing

We next analyzed by RNA sequencing the transcription profile of *vps13F* KO cells and compared it to that of WT and of other KO cells defective for growth in the presence of *K. pneumoniae*: *kil2* (Lelong et al., 2011), *kil1* (Benghezal et al., 2006), *phg1A* (Cornillon et al., 2000), and *fspA* KO cells (Lima et al., 2014). Compared to the experimental variability, the effects of the genetic inactivations were too subtle to be clearly visible from a global expression analysis including all genes. Analysis was thus conducted on a subset of 927 genes, differently regulated in at least one of the pairwise combinations of strains (see experimental procedures). Principal Component Analysis (PCA) revealed that *vps13F* KO cells clustered together with *fspA* KO cells in all three combinations of the first three principal components (Figure 9A), while WT and the other KO cells clustered separately. Although the biological mechanism at play is unclear, this observation suggested that the transcriptional profile of *vps13F* KO cells is more similar to that of *fspA* KO cells than of *kil1*, *kil2*, or *phg1a* KO cells, and led us to analyze if phenotypic traits observed in *fspA* KO cells were also found in *vps13F* KO cells.

Previous results showed that *fspA* KO cells have a defect in sensing folate (Lima et al., 2014), and that folate is the main feature of noncapsulated *K. pneumoniae* recognized by *Dictyostelium* (Lima et al., 2014). This result led us to test the ability of *vps13F* KO cells to respond to various stimuli.

Dictyostelium cells respond to various stimuli by increasing their random velocity. This can be observed after exposure to folate or to different bacteria (*K. pneumoniae*, *B. subtilis*, and *M. luteus*; Lima et al., 2014). In this assay, unstimulated *vps13F* KO cells exhibited a random motility identical to that of WT cells (Figure 9B). Upon stimulation with *K. pneumoniae* or with *M. luteus*, a 2.4-fold increase of motility was observed in WT cells. In these conditions, motility of *vps13F* KO cells also increased significantly (1.5 fold) but to a lesser extent than seen

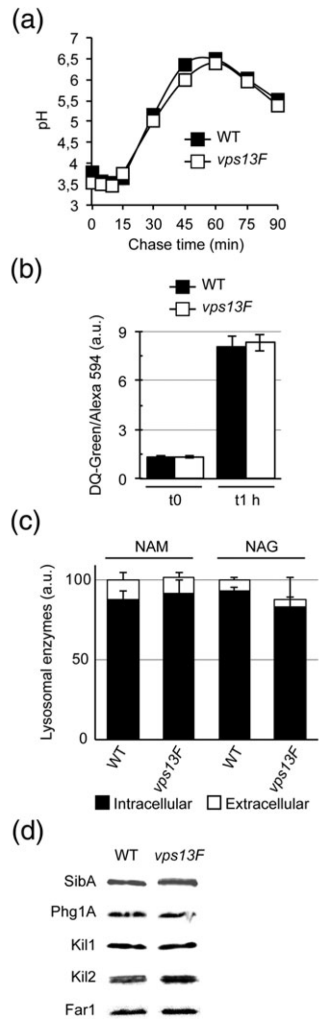

FIGURE 8 The organization of the endocytic pathway is not altered in *vps13F* KO cells. (a) Kinetics of endosomal acidification and reneutralization in *vps13F* KO and in wild-type (WT) cells are identical. To assess acidification in endosomal compartments, cells were allowed to engulf for 18 min two fluorescent dextrans, then washed and incubated further for the indicated chase times. Intracellular fluorescence was measured by flow cytometry. The endosomal pH was estimated by the fluorescence ratio of the two internalized probes. This experiment was repeated 3 times with identical results. (b) Phagosomal proteolysis is not defective in *vps13F* KO cells. Cells were incubated with latex beads coupled to BSA labeled with DQ-green for 15 min, then incubated further for 0 or 1 h. At time 0, internalized beads exhibited low fluorescence. Intracellular proteolysis of BSA released DQ-green fluorescence and revealed the intra-phagosomal proteolysis of BSA. Results are expressed as the ratio of DQ-Green/Alexa-594 (mean ± SEM; 3 independent experiments). (c) After 3 days of culture in HL5 medium, *Dictyostelium* cells were recovered by centrifugation, and the activity of two lysosomal enzymes (NAG = N-acetyl β-glucosaminidase; NAM = α-mannosidase) was measured in cell pellets and in supernatants using chromogenic substrates. The total activity of lysosomal enzymes was very similar in *vps13F* KO and in WT cells. In both cells, only a small fraction of lysosomal enzymes was secreted (mean ± SEM; 3 independent experiments). (d) Cell lysates of WT and *vps13F* KO cells were migrated on polyacrylamide gels, transferred to nitrocellulose, and analyzed by Western-blot using antibodies against SibA (209 kDa), Phg1A (55 kDa), Kil1 (56 kDa), Kil2 (131 kDa), and Far1 (70 kDa) proteins (quantification in Figure S7). No significant difference was seen between WT and *vps13F* KO cells

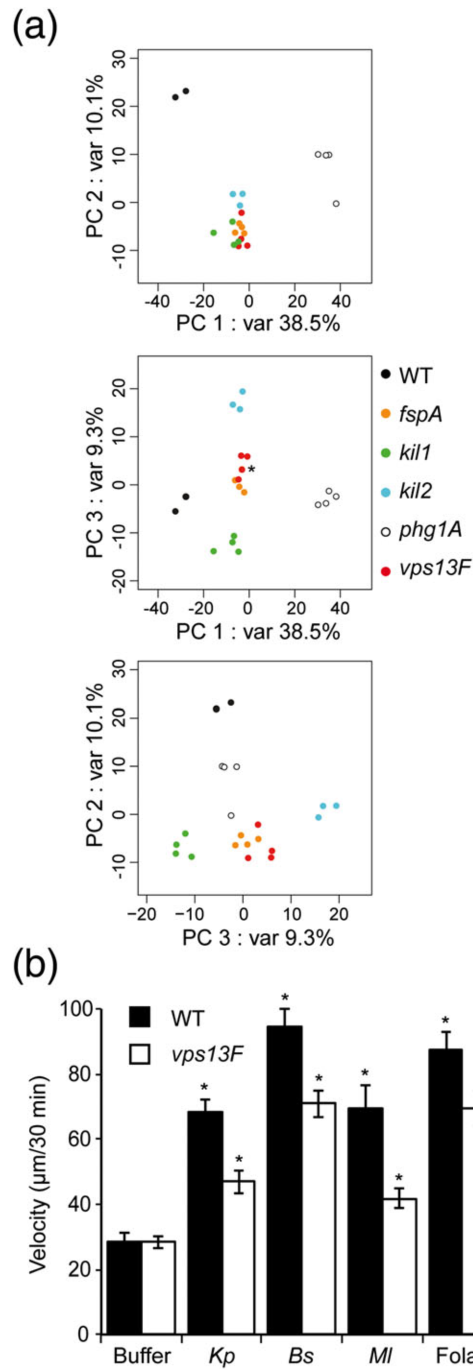

FIGURE 9 Sensing of bacteria and folate is defective in *vps13F* KO cells. (a) Principal component analysis, done on a subset of 927 genes, showing the three first principal components (explaining 57.9% of the variance). This analysis suggested that *vps13F* KO cells were most closely related to *fspA* KO cells (var = variance; *: the dot corresponding to the fourth *fspA* replicate is hidden behind the *vps13F* dot). (b) Cells were imaged during 30 min in the absence or presence of bacteria (*Klebsiella pneumoniae*, *Bacillus subtilis*, *Micrococcus luteus*) or folate (1 mM). Individual cell trajectories of 15 cells were tracked to measure cell motility in response to stimulants. Differences between each condition within the same cell type and between *vps13F* KO and WT strains were statistically significant (mean ± SEM; *: $p < .05$; student *t* test; n = 14 to 30 independent experiments)

for WT cells (Figure 9B). Addition of *B. subtilis* or of a high folate concentration (1 mM) increased even more the motility of WT cells (3 fold). *Vps13F* KO cells responded to these more efficient stimulants

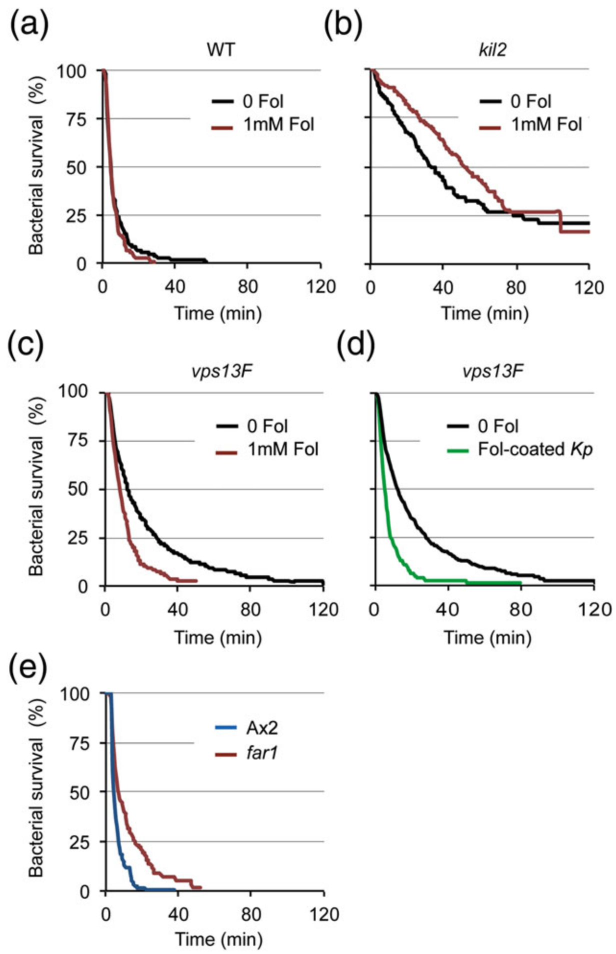

FIGURE 10 Intracellular killing of *Klebsiella* by *vps13F* KO cells is stimulated by a high concentration of folate. (a-c). As in Figure 5, intracellular killing of individual *Kp*-GFP by amoeba cells was visualized in (a) wild-type (WT) cells, (b) *kil2* KO cells, or (c) *vps13F* KO cells in the presence (red curves) or absence (black curves) of folate (1 mM). In these experiments, folate was directly added in the medium containing cells and bacteria, and imaging was initiated 5 min later. Stimulation with folate significantly accelerated intracellular killing in *vps13F* KO cells but not in WT or *kil2* KO cells ($p < 10^{-4}$; log-rank test; number of ingested bacteria with folate is 350 for *vps13F*, 200 for WT, and 264 for *kil2* KO cells). The sets of data for WT, *vps13F* KO and *kil2* KO cells incubated in the absence of folate are the same as presented in Figure 5c and Figure 7. (d) *Kp*-GFP bacteria were preincubated for 15 min with 1 mM folate, washed with PB-Sorbitol, and mixed with *vps13F* KO cells before analysis. In *vps13F* KO cells, intracellular killing of *Kp*-GFP coated with folate was significantly faster than killing of untreated *Kp*-GFP ($p < 10^{-4}$; log-rank test; number of ingested bacteria coated with folate is 161). The set of data for killing of untreated *Kp*-GFP is the same as presented in Figure 5c. (e) Intracellular survival of *Kp*-GFP in Ax2 cells (blue) and *far1* KO cells (red). Genetic alteration of the Far1 folate receptor significantly impaired intracellular killing of *Klebsiella pneumoniae* ($p < 10^{-4}$; log-rank test; number of ingested bacteria is 197 for Ax2 and 206 for *far1* KO cells)

by increasing 2.4 fold their random motility (Figure 9B). Thus with all stimulants tested, motility of *vps13F* KO cells increased significantly less than observed in WT cells. These experiments suggest that *vps13F* KO cells respond less efficiently to extracellular stimuli, and in particular to Far1-dependent folate stimulation. Note that strong stimuli (*B. subtilis*, or a high folate concentration) are sufficient to stimulate *vps13F* KO cells to the same extent as WT cells stimulated with *K. pneumoniae* or *M. luteus*.

We next tested the hypothesis that inefficient killing of *Klebsiella* in *vps13F* KO cells resulted from the inability of *vps13F* KO cells to efficiently respond to the presence of *K. pneumoniae*. For this, we assessed intracellular survival of *K. pneumoniae* in cells that were simultaneously exposed to a high concentration of extracellular folate (1 mM). Exposure to folate did not significantly increase killing efficiency in WT cells (Figure 10A), or in *kil2* KO cells (Figure 10B). Strikingly, in *vps13F* KO cells, exposure to folate restored an efficient killing of ingested *K. pneumoniae* (Figure 10C; average survival time: 22.1 min without folate and 10.7 min in the presence of folate). Note that in this assay, the folate was added to *Dictyostelium* cells at the same time as the bacteria, and a few minutes before imaging. This indicates that the effect of folate on intracellular killing can be observed within minutes of exposure to folate. This result suggests that the slow killing observed in *vps13F* KO cells is due to the fact that these cells are not properly stimulated upon phagocytosis of *K. pneumoniae*. We next assessed intracellular survival of *K. pneumoniae* preincubated with folate prior to their ingestion. For this, *K. pneumoniae* were preincubated with 1 mM folate for 15 min, washed, then incubated with *vps13F* KO cells in the absence of excess folate. In these conditions, efficient killing of ingested *K. pneumoniae* was restored (Figure 10D; average survival time: 8.23 min for folate-coated *K. pneumoniae*). The level of folate secreted by *K. pneumoniae* is presumably not sufficient to induce efficient killing in *vps13F* KO cells, but a higher level of folate can overcome this sensing defect.

Together, these observations suggest that upon ingestion of *K. pneumoniae* by *Dictyostelium*, sensing of folate is required to ensure rapid intracellular killing. To test this hypothesis directly, we assessed intracellular killing of *K. pneumoniae* in cells genetically inactivated for the Far1 folate receptor (Pan, Xu, Chen, & Jin, 2016). Remarkably, *far1* KO cells also showed a significant defect in intracellular killing of *K. pneumoniae* compared to their parental cell line (Figure 10E; average survival time: 6.1 min in Ax2 and 12.3 min in *far1* KO cells).

3 | DISCUSSION

In this study, we identified Vps13F as a new gene product involved in intracellular killing of *K. pneumoniae* bacteria by *Dictyostelium* amoeba. Our key finding, based on the analysis of *vps13F* KO cells, is that efficient intracellular killing of *K. pneumoniae* requires cells to sense and to respond to the bacteria that they are ingesting. In the case of *K. pneumoniae*, and as suggested by our previous studies, the main factor allowing *Dictyostelium* cells to sense the presence of *K. pneumoniae* is the folate secreted by the bacteria.

More specifically, we showed that *vps13F* KO cells respond poorly to extracellular stimulation, suggesting that in these cells inefficient killing of *K. pneumoniae* is due to a defective sensing of ingested bacteria. Indeed, *vps13F* KO cells overstimulated with a high concentration of folate kill ingested *K. pneumoniae* as efficiently as WT cells do. Restoration of killing can be achieved by adding folate to the medium during the ingestion of *K. pneumoniae*, but it is even more efficient to preincubate shortly the *K. pneumoniae* with folate prior to their encounter with *Dictyostelium*. The critical role of folate sensing in stimulating intracellular killing was further demonstrated by showing that genetic inactivation of the folate receptor also resulted in inefficient intracellular killing of ingested *K. pneumoniae*. Recent results have shown that *Dictyostelium* senses folate during phagocytosis of bacteria or folate-coated particles and that this stimulates phagocytosis (Pan et al., 2016). The current study brings these results one step further by showing that after phagocytosis, folate sensing also stimulates the subsequent killing of *K. pneumoniae*. A working model for intracellular killing of *K. pneumoniae* bacteria is proposed (Figure 11).

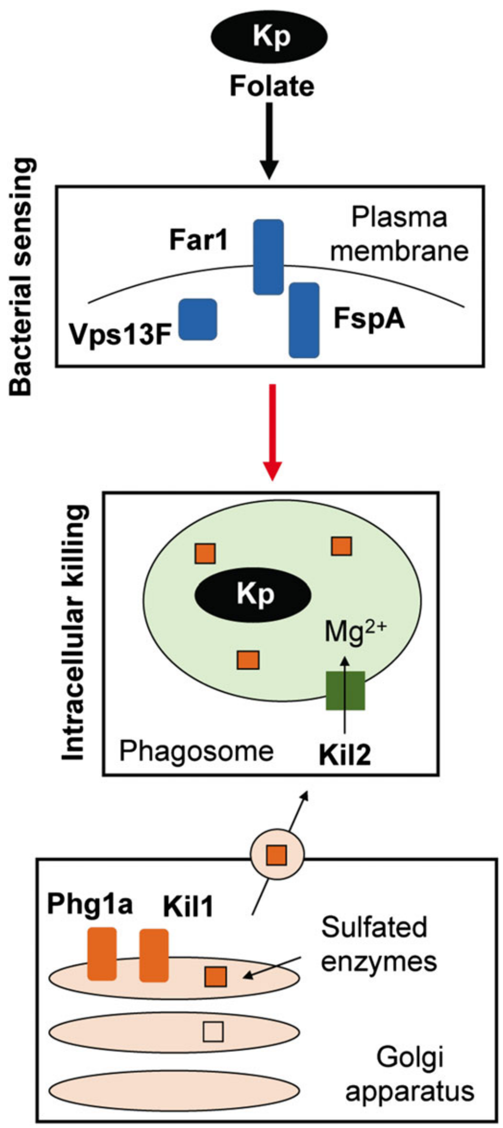

FIGURE 11 Intracellular killing of *Klebsiella pneumoniae*: a working model. All *Dictyostelium* gene products involved in intracellular killing of *K. pneumoniae* are depicted in this scheme. In the Golgi apparatus, Phg1 ensures efficient sorting of Kil1, a sulfotransferase sulfating lysosomal enzymes essential for efficient killing. In the phagosome, Mg^{2+} ions transported by Kil2 are necessary for optimal activity of lytic enzymes. The current study indicates that three gene products (Far1, FspA, and Vps13F) are involved in sensing of bacterial folate and are also essential for efficient killing of *K. pneumoniae*. Identifying the lytic enzymes specifically involved in killing of *K. pneumoniae* and their regulation is one of our next goals

One previous study has shown that *Dictyostelium* cells modify their gene expression patterns following exposure to different bacteria (Nasser et al., 2013). This allows them to adapt to changes in their source of nutrients. However, changes in gene expression occured over a time frame of several hours, while the effect of folate on the kinetics of intracellular killing observed in this study is almost immediate. It is likely that the very rapid sensing of bacteria and slower modifications of gene expression patterns both contribute to ensure optimal adaptation of *Dictyostelium* to changes in its environment and food supply.

Defective growth of *kil2–vps13F* KO cells was apparent in the presence of *K. pneumoniae*, as well as of a mucoid strain of *E. coli* (*E. coli* B/r), and of *M. luteus*, but not in the presence of other bacterial species like *B. subtilis* and *P. aeruginosa*, or even in the presence of another strain of *K. pneumoniae* (capsulated *K. pneumoniae* LM21). This phenotype suggests that phenotypic features of a bacterial strain (such as the composition of its cell surface and resistance to various bactericidal mechanisms) are more important than their species to determine their intracellular processing by *Dictyostelium* cells. We only measured the effect of genetic inactivation of *vps13F* on intracellular killing of *K. pneumoniae* and of *B. subtilis*, as these are for the moment the only bacteria for which assays measuring intracellular killing have been developed. As observed before with other mutants defective in intracellular killing (*phg1a*, *kil1*, and *kil2* KO cells; Le Coadic et al., 2013; Lelong et al., 2011), alteration of the *vps13F* gene affects intracellular killing of *K. pneumoniae*, but not of *B. subtilis*, suggesting that the molecular mechanisms engaged in intracellular killing of different bacteria are largely distinct. Together, these new results reinforce the notion that molecular mechanisms responsible for intracellular killing of bacteria exhibit a high degree of specificity.

Our results do not identify the exact molecular role of Vps13F in response to extracellular stimulants. Because Vps13 has been proposed to play a role in intracellular sorting in *S. cerevisiae*, one possibility would be that genetic inactivation of *vps13F* in *Dictyostelium* perturbs intracellular transport of one or several molecules critical for sensing. Existing knowledge on the cellular function of Vps13F proteins is, however, very succinct. It is equally possible that the main role of Vps13 is to participate directly in intracellular activation, and that its function in intracellular sorting in *S. cerevisiae* was an indirect effect of an alteration of intracellular signaling. Our study indicates that a certain degree of specificity exists between different members of the family, because genetic inactivation of *vps13A* and *vps13F* in *Dictyostelium* resulted in radically different phenotypes. More detailed studies will be necessary to determine the exact mode of action of Vps13F proteins.

Concerning the strategy followed in this study, the *vps13F* insertional mutant was identified by screening a library of random mutants generated in a *kil2* KO background. The underlying assumption was that there is a certain degree of redundancy in mechanisms ensuring the intracellular killing of bacteria, and in this case more specifically of *K. pneumoniae*. Consequently, the role of certain gene products in intracellular killing may become more apparent when other killing mechanisms are inactivated. This hypothesis is confirmed by our results: the *vps13F* insertional mutant would not have been selected if it had been created in a WT background: it exhibits a significant but limited killing defect, which is not sufficient to cause a major growth defect in the presence of *K. pneumoniae* bacteria. On the contrary, genetic inactivation of *vps13F* in a *kil2* KO background causes a strong additional growth defect in the presence of *K. pneumoniae*. In further studies, analysis of double or triple KO cells may be necessary to determine the role and the relative importance of various gene products in intracellular killing of different types of bacteria.

4 | EXPERIMENTAL PROCEDURES

4.1 | Cell culture and strains

Dictyostelium cells were grown in HL5 medium at 21 °C (Cornillon, Olie, & Golstein, 1998) and subcultured twice a week to maintain a density below 10^6 cells/ml.

Unless specified, *Dictyostelium* cells used in this study were all derived from the DH1–10 subclone (Cornillon et al., 2000) of the *D. discoideum* strain DH1 (Caterina, Milne, & Devreotes, 1994), referred to in this study as wild-type (WT). The *phg1A* (Cornillon et al., 2000), *kil2* (Lelong et al., 2011) and *fspA* (Lima et al., 2014) KO strains were described previously. In this study, we created a new *kil2* KO strain by deleting a sequence of the *kil2* gene in DH1–10 and replacing it with a Blasticidin S Resistance (BSR) cassette (Figure S8). The BSR cassette was then excised by extrachromosomal expression of Cre (Linkner, Nordholz, Junemann, Winterhoff, & Faix, 2012). This new *kil2* KO strain behaved in the same manner as the previously published *kil2* KO strain (Lelong et al., 2011), and it was used as a starting point for mutagenesis (see below). Ax2 and *far1* KO strains were a kind gift of Dr. Miao Pan and Pr. Jin Tian (National Institute of Health, MD, USA; Pan et al., 2016).

Bacterial strains were grown overnight in Lysogeny broth (LB) medium at 37 °C. Bacteria used were uncapsulated *K. pneumoniae* laboratory strain (Benghezal et al., 2006), capsulated *K. pneumoniae* LM21 (Balestrino, Ghigo, Charbonnel, Haagensen, & Forestier, 2008), *E. coli* B/r (Gerisch, 1959) and *P. aeruginosa* PT531 (Cosson et al., 2002), *B. subtilis* 36.1 (Ratner & Newell, 1978), and *M. luteus* (Wilczynska & Fisher, 1994).

4.2 | Screening for growth-deficient *Dictyostelium* mutants

To isolate *Dictyostelium* mutants that are specifically unable to grow in the presence of bacteria, *kil2* KO cells were mutagenized by restriction-enzyme–mediated insertion of the pSC plasmid and screened as previously described (Cornillon et al., 2000; Lelong et al., 2011; Figure S1). Briefly, individual mutant cells were cloned in 96 well plates using a cell sorter. Overall, 10,000 individual clones were tested for their ability to grow efficiently on several bacteria: *M. luteus*, *B. subtilis*, *E. coli* B/r, *K. pneumoniae*, *K. pneumoniae* LM21, and *P. aeruginosa* PT531. Mutants that grew poorly on at least one of the tested bacteria were selected and expanded, and their genomic DNA was extracted. To identify the site of insertion of the pSC plasmid in each mutant, genomic DNA was digested with ClaI, self-ligated, transformed in *E. coli* SURE, and sequenced. Mutants in which the plasmid was inserted in a coding region were selected for further analysis. The *vps13F* mutant was isolated in a *kil2* KO background, while the *vps13A* mutant was identified in a WT background (Figures S1 and S2).

A KO plasmid was constructed to replace a sequence in the *vps13F* gene with a BSR cassette, in both WT and *kil2* KO strains (Figure S1), to generate simple *vps13F* KO and double *kil2*–*vps13F* KO cells. Individual clones were identified by polymerase chain reaction (PCR) (Figure S1). Three independent clones of each KO cells were obtained and yielded identical results in this study.

The plasmid recovered from the *Dictyostelium* genome after plasmid rescue and containing the genomic region flanking the insertion site in *vps13A* was used to create new *vps13A* KO (Figure S2). Three independent clones were obtained, but only one was used in this study.

4.3 | Growth of *Dictyostelium* in the presence of bacteria

Dictyostelium cells were grown in the presence of bacteria as described previously (Froquet, Lelong, Marchetti, & Cosson, 2009). Briefly, 50 μl of an overnight bacterial culture were plated on 2 ml of SM-agar in each well of a 24-well plate. Alternatively, to test the growth of *Dictyostelium* in the presence of dead bacteria, an overnight culture of *K. pneumoniae* (7 ml) was boiled for 4 h at 95 °C, pelleted, resuspended in 200 μl and applied in each well. Then, 10, 100, 1,000 or 10,000 *Dictyostelium* cells were added on top of the bacterial lawn. Growth of *Dictyostelium* generated phagocytic plaques after 4–7 days of incubation at 21 °C. Quantification of the extent of the growth defect was done by scoring the growth of *Dictyostelium* strains on each bacteria in at least four independent experiments. For each experiment, growth was scored from 4 (efficient growth) to 0 (no growth). For each bacteria tested, the average score of *Dictyostelium* growth was calculated.

4.4 | Phagocytosis and macropinocytosis

To measure efficiency of phagocytosis, 3×10^5 *Dictyostelium* cells were washed once, resuspended in 1 ml of Phosphate Buffer (PB: 2 mM Na_2HPO_4, 14.7 mM KH_2PO_4, pH 6.5) supplemented with 100 mM sorbitol (PB-Sorbitol) and incubated for 20 min with 1 μl FITC latex beads (Fluoresbrite plain YG 1 micron, Polysciences), or with 5×10^7 glutaraldehyde-fixed *K. pneumoniae* labeled with rhodamine at a multiplicity of infection of 1:200. To assess macropinocytosis, cells were incubated in PB-Sorbitol containing 10 μg/ml Alexa-647 Dextran (Life Technologies) for 20 min. Then, cells were washed in ice cold HL5 supplemented with 0.1% NaN_3 and internalized fluorescence was measured by flow cytometry. Mean fluorescence was plotted for each strain.

4.5 | Intracellular killing of bacteria

Three methods were used to measure intracellular killing of bacteria. First, as previously described (Benghezal et al., 2006), cells were mixed with a small number of bacteria (200 *Dictyostelium* cells for 1 *K. pneumoniae*) and incubated at 21 °C in PB-Sorbitol. Aliquots were taken at different time points, cells were lysed, and bacteria were plated on LB-agar. The number of colony-forming units decreased as bacteria were ingested and killed.

A second method (Benghezal et al., 2006) was to incubate *Dictyostelium* cells with a larger number of GFP-expressing

K. pneumoniae (*Kp*-GFP, 10 bacteria per *Dictyostelium* cells) and to measure by flow cytometry the accumulation of GFP fluorescence in cells. For this, bacteria were grown overnight in LB supplemented with 100 μg/ml of ampicillin, and washed once with PB-Sorbitol. *Dictyostelium* cells (10^5) were washed with PB-Sorbitol, mixed with 10^6 bacteria in 1 ml PB-Sorbitol and incubated at 21 °C. At the indicated times (0–60 min), a 100 μl aliquot was collected. Then, cells were washed in ice cold HL5 supplemented with 0.1% NaN_3 and internalized GFP fluorescence was measured by flow cytometry.

To measure phagocytosis and intracellular killing of individual bacteria (Delince et al., 2016) *Kp*-GFP bacteria were mixed with *Dictyostelium* cells at a ratio of 3:1 in PB-Sorbitol, deposited on a glass slide (Fluorodish, World Precision Instruments, Inc.) for 10 min, then imaged every 30 sec for 2 h with a videotime lapse (Zeiss Axiovert 200 M). At each time, one picture (phase contrast and GFP fluorescence) was taken in four successive focal planes (step size 3 μm) to image the whole cell volume. The Metamorph software was used to extract images, and ImageJ to compile and analyze movies. Survival analysis of phagocytosed fluorescent bacteria was computed using the Kaplan–Meier estimator. Statistical comparisons between Kaplan–Meier curves were done using the log-rank test. We rejected the null hypothesis if the *p* value was below 10^{-3}. Statistical analysis was done using XLSTAT (Version 2016.03.31333). For each condition, the number of ingested bacteria is indicated and at least three independent experiments were performed.

4.6 | Chemokinetic response to folate and bacteria

For chemokinetic measurements, 2×10^4 *Dictyostelium* cells were allowed to attach to the polystyrene bottom of one well of a 96-well microplate (Cell culture microplate PS F-bottom, μclear, Greiner bio-one) for 20 min in 100 μl of PB-Sorbitol with or without supplementation of 1 mM folate, or of bacteria (1:1000 *v*/v., from an overnight culture washed twice in PB-Sorbitol). Cells were then imaged every 15 sec during 30 min using the widefield plate reader ImageXpress XL with a 10X S Fluor objective. The images were acquired with a CoolSnap HQ camera (Photometrics) and movies assembled with Metamorph. Track point tool of Metamorph was used to track individual trajectories and total distance of 15 cells for each experiment and to calculate velocity.

4.7 | Organization of endosomal and lysosomal pathways

Kinetics of endosomal acidification were assessed by flow cytometry as previously described (Marchetti et al., 2009). Endosomal pH was determined by fluorescence levels of two internalized dextrans, one coupled to pH-sensitive fluorophore and the other coupled to pH-insensitive fluorophore. The activity of lysosomal glycosidases in cells and in supernatant was measured as previously described (Le Coadic et al., 2013) using a colorimetric assay.

The activity of phagosomal proteases was measured as previously described (Lelong et al., 2011; Sattler et al., 2013), using silica beads coupled to Alexa-594 red fluorescent succinimidyl ester (Molecular Probes) and to BSA labeled with DQ-green (490 nm, Molecular Probes) at a self-quenching concentration. Cells were allowed to engulf beads in phosphate buffer for 15 min, then aliquots collected after 0 or 1 h. Upon proteolysis, green fluorescence was released and measured by flow cytometry.

4.8 | Immunolabeling

To perform immunofluorescence analysis, 10^6 cells were let to adhere to a glass coverslip for 30 min in HL5 medium. Then, *Dictyostelium* cells were fixed with 4% paraformaldehyde for 30 min, washed, permeabilized with methanol at −20°C for 2 min, and labeled with the indicated primary antibody in phosphate buffer with 0.2% bovine serum albumin for 1 h. Permeabilized cells were labeled with markers of endosomal compartments (p80, p25) and of the contractile vacuole (Rhesus). Cells were stained with the corresponding Alexa-488 fluorescent secondary antibodies for 1 h and observed by LSM700 confocal microscopy (Carl Zeiss).

To determine the levels of cellular proteins, 10^6 cells were resuspended in 10 μl of 0.103 g/ml sucrose, 5 × 10–2 M Tris, pH 6.8, 5 × 10–3 M EDTA, 0.5 mg/ml bromophenol blue, 2% SDS, and proteins were separated by electrophoresis on an SDS-polyacrylamide gel. Proteins were then transferred to a nitrocellulose membrane for immunodetection using anti-Phg1A (Blanc, Zufferey, & Cosson, 2014), anti-SibA (Cornillon et al., 2006), anti-Kil1 (Benghezal et al., 2006), and anti-Kil2 (Lelong et al., 2011) primary antibodies. Horseradish-peroxidase-coupled antimouse (for anti-SibA and anti-Phg1A) and antirabbit (for anti-Kil1 and anti-Kil2) antibodies were used as secondary antibodies. A recombinant anti-Far1 antibody was generated by the Geneva Antibody Facility (http://www.unige.ch/antibodies; reference MRB 168).

4.9 | Sequence and Phylogenetic analysis

Protein sequences of Vps13F homologs from a diverse group of organisms were aligned using the K-align algorithm (Lassmann, Frings, & Sonnhammer, 2009). The alignment was then manually refined in order to remove regions that were hyper variable or with gaps. Phylogenetic trees were generated using MEGA 6.0 (Tamura, Stecher, Peterson, Filipski, & Kumar, 2013). Genetic distances were computed using the Jones-Taylor-Thornton algorithm, and Neighbor-Joining (NJ) was used to generate distance-based phylogenetic trees. Maximum-likelihood (ML) phylogenetic estimates were obtained with the Le_Gascuel_2008 model. Sequence evolution model was selected using the "find best model option" in MEGA 6.0. Bootstrap assessment of tree topology with 100 replicates was performed to find the support for the inferred clades. Similar topologies were found for the two phylogenetic methods employed; the star-shaped, unrooted tree displayed in Figure 2B corresponds to the maximum-likelihood topology (with bootstrap values for both ML and NJ trees shown). The organisms and the accession codes of the proteins investigated in the phylogenetic analysis are shown in Table S2.

4.10 | RNA sequencing and analysis

RNA was isolated from at least 5×10^6 *Dictyostelium* cells using the Direct-zol RNA MiniPrep kit (Zymo Research, # R2052). The quality of RNA was confirmed with a Bioanalyzer (Agilent, RNA 6000 Nano Kit # G2938–90037). Libraries were constructed from 100 ng of RNA using the Ovation Universal RNA-Seq System kit (Nugen, # 0343). The quality of the libraries was verified by TapeStation (Agilent, High Sensitivity D1000 ScreenTape, # 5067–5584). Samples were pooled and run in single read 50 flow cell (Illumina, # 15022187) and run on a Hiseq 2500 (Illumina).

From six different *Dictyostelium* strains, 21 libraries were analyzed: WT (2 replicates), *fspA* (4 replicates), *kil1* (4 replicates), *kil2* (3 replicates), *phg1A* (4 replicates), and *vps13F* (4 replicates) KO cells. 50 nt singe-end reads were mapped to the *Dictyostelium discoideum* genome (2009, downloaded from dictybase) using tophat (version 2.0.13) and bowtie2 (version 2.2.4) softwares. As the RNASeq data is stranded, parameter library-type was set to fr-secondstrand. Multihits were not allowed, by using option --max-multihits 1. The other parameters were default. The read counts per gene were generated using HTSeq software (version 0.6.1) and the GFF annotation downloaded from dictybase (February 2015). Options for htseq-count were -t exon --stranded = yes -m union. The counts were then imported in R (version 3.2.2). The genes were filtered for minimal expression, by removing genes with an average through all samples lower than 5 reads. Normalization factors to scale the libraries sizes were calculated using edgeR. The read counts were then log transformed and variance stabilized using voom. The log-transformed counts were then batch corrected for date effect using the R package sva and the ComBat function. The experimental design (mutation) was provided to the ComBat algorithm.

A differential expression analysis was then performed on these batch-corrected data using the R package limma. All the comparisons 2 by 2 were performed between the 6 conditions, so in total 15 comparisons. The genes having an adjusted p-value lower than 0.05 and an absolute log fold change above 1.5 were considered differentially expressed. The union of these genes was then taken for the following of the analysis. The principal component analysis were generated using the R function prcomp, with centering and scaling the data. The 3 first principal components were considered and plotted versus each other.

ACKNOWLEDGEMENTS

This work was supported by the Swiss National Science Foundation (grant 31003A_153326 to PC). The present study has been in part supported by HostPathX, a Research, Technology and Development project grant from SystemsX.ch to MP, TS and PC. The TS laboratory is also supported by the Swiss National Science Foundation.

REFERENCES

Balestrino, D., Ghigo, J. M., Charbonnel, N., Haagensen, J. A., & Forestier, C. (2008). The characterization of functions involved in the establishment and maturation of *Klebsiella pneumoniae* in vitro biofilm reveals dual roles for surface exopolysaccharides. *Environmental Microbiology*, *10*, 685–701.

Belaaouaj, A., McCarthy, R., Baumann, M., Gao, Z., Ley, T. J., Abraham, S. N., & Shapiro, S. D. (1998). Mice lacking neutrophil elastase reveal impaired host defense against gram negative bacterial sepsis. *Nature Medicine*, *4*, 615–618.

Benghezal, M., Fauvarque, M.O., Tournebize, R., Froquet, R., Marchetti, A., Bergeret, E., … Cosson, C. (2006). Specific host genes required for the killing of Klebsiella bacteria by phagocytes. *Cellular Microbiology 8*, 139–148.

Blanc, C., Zufferey, M., & Cosson, P. (2014). Use of in vivo biotinylated GST fusion proteins to select recombinant antibodies. *ALTEX*, *31*, 37–42.

Brickner, J. H., & Fuller, R. S. (1997). SOI1 encodes a novel, conserved protein that promotes TGN-endosomal cycling of Kex2p and other membrane proteins by modulating the function of two TGN localization signals. *The Journal of Cell Biology*, *139*, 23–36.

Caterina, M. J., Milne, J. L., & Devreotes, P. N. (1994). Mutation of the third intracellular loop of the cAMP receptor, cAR1, of Dictyostelium yields mutants impaired in multiple signaling pathways. *The Journal of Biological Chemistry*, *269*, 1523–1532.

Cornillon, S., Gebbie, L., Benghezal, M., Nair, P., Keller, S., Wehrle-Haller, B., … Cosson, P. (2006). An adhesion molecule in free-living Dictyostelium amoebae with integrin beta features. *EMBO Reports*, *7*, 617–621.

Cornillon, S., Olie, R. A., & Golstein, P. (1998). An insertional mutagenesis approach to Dictyostelium cell death. *Cell Death and Differentiation*, *5*, 416–425.

Cornillon, S., Pech, E., Benghezal, M., Ravanel, K., Gaynor, E., Letourneur, F., … Cosson, P. (2000). Phg1p is a nine-transmembrane protein superfamily member involved in dictyostelium adhesion and phagocytosis. *The Journal of Biological Chemistry*, *275*, 34287–34292.

Cosson, P., & Lima, W. C. (2014). Intracellular killing of bacteria: Is Dictyostelium a model macrophage or an alien? *Cellular Microbiology*, *16*, 816–823.

Cosson, P., & Soldati, T. (2008). Eat, kill or die: when amoeba meets bacteria. *Current Opinion in Microbiology*, *11*, 271–276.

Cosson, P., Zulianello, L., Join-Lambert, O., Faurisson, F., Gebbie, L., Benghezal, M., … Köhler, T. (2002). Pseudomonas aeruginosa virulence analyzed in a Dictyostelium discoideum host system. *Journal of Bacteriology*, *184*, 3027–3033.

De Smet, K., & Contreras, R. (2005). Human antimicrobial peptides: defensins, cathelicidins and histatins. *Biotechnology Letters*, *27*, 1337–1347.

Delince, M. J., Bureau, J. B., Lopez-Jimenez, A. T., Cosson, P., Soldati, T., & McKinney, J. D. (2016). A microfluidic cell-trapping device for single-cell tracking of host–microbe interactions. *Lab on a Chip*, *16*, 3276–3285.

Ellson, C. D., Davidson, K., Ferguson, G. J., O'Connor, R., Stephens, L. R., & Hawkins, P. T. (2006). Neutrophils from p40phox−/− mice exhibit severe defects in NADPH oxidase regulation and oxidant-dependent bacterial killing. *The Journal of Experimental Medicine*, *203*, 1927–1937.

Froquet, R., le Coadic, M., Perrin, J., Cherix, N., Cornillon, S., & Cosson, P. (2012). TM9/Phg1 and SadA proteins control surface expression and stability of SibA adhesion molecules in Dictyostelium. *Molecular Biology of the Cell*, *23*, 679–686.

Froquet, R., Lelong, E., Marchetti, A., & Cosson, P. (2009). Dictyostelium discoideum: A model host to measure bacterial virulence. *Nature Protocols*, *4*, 25–30.

Gerisch, G. (1959). Ein submerskulturverfahren fuer entwicklungsphysiologische untersuchungen an Dictyostelium discoideum. *Naturwissenschaften*, *46*, 654–656.

Goldblatt, D., & Thrasher, A. J. (2000). Chronic granulomatous disease. *Clinical and Experimental Immunology*, *122*, 1–9.

Koizumi, K., & Gallagher, K. L. (2013). Identification of SHRUBBY, a SHORT-ROOT and SCARECROW interacting protein that controls root growth and radial patterning. *Development*, *140*, 1292–1300.

Kolehmainen, J., Black, G. C., Saarinen, A., Chandler, K., Clayton-Smith, J., Traskelin, A. L., … Lehesjoki, A. E. (2003). Cohen syndrome is caused by mutations in a novel gene, COH1, encoding a transmembrane protein with a presumed role in vesicle-mediated sorting and intracellular protein transport. *American Journal of Human Genetics*, *72*, 1359–1369.

Lassmann, T., Frings, O., & Sonnhammer, E. L. (2009). Kalign2: High-performance multiple alignment of protein and nucleotide sequences allowing external features. *Nucleic Acids Research*, *37*, 858–865.

Le Coadic, M., Froquet, R., Lima, W. C., Dias, M., Marchetti, A., & Cosson, P. (2013). Phg1/TM9 proteins control intracellular killing of bacteria by determining cellular levels of the Kil1 sulfotransferase in Dictyostelium. *PloS One*, *8*, e53259.

Lelong, E., Marchetti, A., Gueho, A., Lima, W. C., Sattler, N., Molmeret, M., … Cosson, P. (2011). Role of magnesium and a phagosomal P-type ATPase in intracellular bacterial killing. *Cellular Microbiology*, *13*, 246–258.

Lima, W. C., Balestrino, D., Forestier, C., & Cosson, P. (2014). Two distinct sensing pathways allow recognition of *Klebsiella pneumoniae* by Dictyostelium amoebae. *Cellular Microbiology*, *16*, 311–323.

Linkner, J., Nordholz, B., Junemann, A., Winterhoff, M., & Faix, J. (2012). Highly effective removal of floxed Blasticidin S resistance cassettes from Dictyostelium discoideum mutants by extrachromosomal expression of Cre. *European Journal of Cell Biology*, *91*, 156–160.

Marchetti, A., Lelong, E., & Cosson, P. (2009). A measure of endosomal pH by flow cytometry in Dictyostelium. *BMC Research Notes*, *2*, 7.

Munoz-Braceras, S., Calvo, R., & Escalante, R. (2015). TipC and the chorea-acanthocytosis protein VPS13A regulate autophagy in Dictyostelium and human HeLa cells. *Autophagy*, *11*, 918–927.

Nasser, W., Santhanam, B., Miranda, E. R., Parikh, A., Juneja, K., Rot, G., … Kuspa, A. (2013). Bacterial discrimination by dictyostelid amoebae reveals the complexity of ancient interspecies interactions. *Current Biology*, *23*, 862–872.

Pan, M., Xu, X., Chen, Y., & Jin, T. (2016). Identification of a chemoattractant G-protein-coupled receptor for folic acid that controls both chemotaxis and phagocytosis. *Developmental Cell*, *36*, 428–439.

Papayannopoulos, V., & Zychlinsky, A. (2009). NETs: A new strategy for using old weapons. *Trends in Immunology*, *30*, 513–521.

Rampoldi, L., Dobson-Stone, C., Rubio, J. P., Danek, A., Chalmers, R. M., Wood, N. W., … Monaco, A. P. (2001). A conserved sorting-associated protein is mutant in chorea-acanthocytosis. *Nature Genetics*, *28*, 119–120.

Ratner, D. I., & Newell, P. C. (1978). Linkage analysis in Dictyostelium discoideum using multiply marked tester strains: establishment of linkage group VII and the reassessment of earlier linkage data. *Journal of General Microbiology*, *109*, 225–236.

Redding, K., Brickner, J. H., Marschall, L. G., Nichols, J. W., & Fuller, R. S. (1996). Allele-specific suppression of a defective trans-Golgi network (TGN) localization signal in Kex2p identifies three genes involved in localization of TGN transmembrane proteins. *Molecular and Cellular Biology*, *16*, 6208–6217.

Reeves, E. P., Lu, H., Jacobs, H. L., Messina, C. G., Bolsover, S., Gabella, G., … Segal, A. W. (2002). Killing activity of neutrophils is mediated through activation of proteases by K+ flux. *Nature*, *416*, 291–297.

Rushing, M. D., & Slauch, J. M. (2011). Either periplasmic tethering or protease resistance is sufficient to allow a SodC to protect Salmonella enterica serovar Typhimurium from phagocytic superoxide. *Molecular Microbiology*, *82*, 952–963.

Sattler, N., Monroy, R., & Soldati, T. (2013). Quantitative analysis of phagocytosis and phagosome maturation. *Methods in Molecular Biology*, *983*, 383–402.

Segal, A. W. (2005). How neutrophils kill microbes. *Annual Review of Immunology*, *23*, 197–223.

Silva, M. T. (2010). When two is better than one: Macrophages and neutrophils work in concert in innate immunity as complementary and cooperative partners of a myeloid phagocyte system. *Journal of Leukocyte Biology*, *87*, 93–106.

Tamura, K., Stecher, G., Peterson, D., Filipski, A., & Kumar, S. (2013). MEGA6: Molecular Evolutionary Genetics Analysis version 6.0. *Molecular Biology and Evolution*, *30*, 2725–2729.

Ueno, S., Maruki, Y., Nakamura, M., Tomemori, Y., Kamae, K., Tanabe, H., … Sano, A. (2001). The gene encoding a newly discovered protein, chorein, is mutated in chorea-acanthocytosis. *Nature Genetics*, *28*, 121–122.

Wilczynska, Z., & Fisher, P. R. (1994). Analysis of a complex plasmid insertion in a phototaxis-deficient transformant of Dictyostelium discoideum selected on a Micrococcus luteus lawn. *Plasmid*, *32*, 182–194.

Zanetti, M. (2005). The role of cathelicidins in the innate host defenses of mammals. *Current Issues in Molecular Biology*, *7*, 179–196.

SUPPORTING INFORMATION

Additional Supporting Information may be found online in the supporting information tab for this article.

How to cite this article: Leiba J, Sabra A, Bodinier R et al. Vps13F links bacterial recognition and intracellular killing in *Dictyostelium*. *Cellular Microbiology*. 2017;19:e12722. https://doi.org/10.1111/cmi.12722

3. Manuscript: Vps13F supplementary data

Figure S1. Isolation and generation of *vps13F* KO cells.

A. Schematic representation of the *vps13F* insertional mutant obtained by REMI mutagenesis, with the mutagenic plasmid pSC inserted 7'144 nucleotides (nt) after the start codon.

B. The site of insertion was identified by digestion of genomic DNA with ClaI, which allowed the recovery of the mutagenic plasmid with the genomic flanking regions of *vps13F*.

C. Schematic representation of the *vps13F* gene in WT or KO cells. To create a new *vps13F* KO, we deleted 909 nt of the genomic sequence, 1'752 nt downstream of the *vps13F* start codon and replaced this portion with a blasticidin resistance cassette by homologous recombination. Arrows indicate the positions of the oligonucleotides used to identify KO cells.

D-E. Identification of *vps13F* KO cells was done by PCR using distinct pairs of oligonucleotides to verify both loss and gain of signal.

Figure S2. Isolation and generation of *vps13A* KO cells.

A. Schematic representation of the *vps13A* insertional mutant obtained by REMI mutagenesis, with the mutagenic plasmid pSC inserted 5'151 nt after the start codon.

B. The site of insertion was identified by digestion of genomic DNA with ClaI, which allowed the recovery of the mutagenic plasmid with the genomic flanking regions of *vps13A*. We used this same plasmid to transfect WT cells in order to create a new *vps13A* KO by homologous recombination.

C. Schematic representation of the *vps13A* gene in KO cells. Arrows indicate positions of the oligonucleotides used to identify KO cells.

D. Identification of *vps13A* KO cells was done by PCR using distinct pairs of oligonucleotides to verify the expected size of PCR products.

Figure S3. Phagocytosis, macropinocytosis, and intracellular killing of *K. pneumoniae* or *B. subtilis* are not defective in *vps13A* KO cells.

A. Internalization of fluorescent latex beads, of rhodamine-labeled glutaraldehyde-fixed *K. pneumoniae* and of fluorescent Dextrans in PB-Sorbitol was assessed by flow cytometry (mean ± SEM; 3 independent experiments). Differences in phagocytosis of fixed *K. pneumoniae* between WT and KO cells were not significant.

B. *Kp*-GFP survival curve in WT or in *vps13A* KO cells (number of ingested bacteria is 228 for WT and 224 for *vps13A* KO cells). The set of data for WT is the same as presented in Fig. 5C.

Figure S4. Vps13F is not required for growth in the presence of heat-killed *Klebsiella*.

WT, *kil2* KO, *kil2-vps13F* KO and *vps13F* KO cells were seeded on a lawn of heat-killed *Klebsiella* bacteria. All cells analyzed grew comparably in these conditions.

Figure S5. The endosomal pH in WT and in *vps13F* KO cells is similar.

To measure endosomal pH, *Dictyostelium* cells were allowed to endocytose during 18 min a mixture of dextrans coupled to Oregon Green 488 (OG, pH-sensitive) and to Alexa 647 (A-647, pH-insensitive). Flow cytometry was used to measure levels of intracellular fluorescence, at different chase time points after 18 min of endocytosis. The intracellular fluorescence of both probes exhibited the same profile in WT and mutant cells. This experiment was repeated 3 times with identical results.

Figure S6. General organization of cellular compartments is similar in *vps13F* KO and WT cells.

Immunofluorescence was used to label p25, p80, and Rhesus proteins, in order to detect distinct pericentriolar compartments, endosomes, and the contractile vacuole respectively. Confocal images are shown. Scale bar 5 µm.

Figure S7. Western-blot analysis of Far1 expression.

A. Western-blot analysis of Far1 protein expression in Ax2, *far1* KO, WT (DH1) and *vps13F* KO strains. Cells were allowed to grow at a density of $3x10^5$ cells/ml. $1.3x10^6$ cells were suspended in 20 µl of 2x sample buffer and loaded on a 10% SDS-PAGE gel. After migration and transfer of proteins on a Nitrocellulose membrane, the latter was blocked overnight with PBS-Tween (0.1%)-milk (7%) at 4°C. The next day, the membrane was washed twice in PBS-Tween for 30 sec and incubated overnight at 4°C in the presence of the primary antibody (MRB168) in PBS-Tween. The next day, after three 5-min washes with PBS-Tween-milk the membrane was incubated for 2 h in the presence of the secondary antibody (HRP-coupled anti-mouse Ig) diluted 1/3000 in PBS-Tween-milk. Finally, after five washes with PBS-Tween the ECL solution was added to reveal the presence of the Far1 protein.

B. Quantification of Western-blot analysis of SibA, Phg1A, Kil1, Kil2 and Far1 proteins in *vps13F* KO and WT strains. The relative abundance of each protein in *vps13F* KO cells and WT cells was determined in two to four independent experiments using the ImageJ software. The quantifications corresponding to gels shown in Fig. 8D are marked in red. The small increase in Kil2 levels observed in *vps13F KO* cells is not significant (p=0.31; Student t-test, n=4).

Figure S8. Isolation and generation of *kil2* KO cells.

A. Schematic representation of the *kil2* gene in WT or KO cells. To create a new *kil2* KO, we deleted 1'646 nt of the genomic sequence, 798 nt downstream of the *kil2* start codon and replaced this portion with a blasticidin resistance cassette by homologous recombination. Arrows indicate positions of the oligonucleotides used to identify KO cells.

B. Identification of *kil2* KO cells was done by PCR using distinct pairs of oligonucleotides to verify both loss and gain of signals.

Table S1. List of species and corresponding gene accession codes used for phylogenetic analysis (Fig. 2B).

Protein	Organism	Accession ID
Vps13A	*D. discoideum*	XP_637643
Vps13B	*D. discoideum*	XP_644147
Vps13C	*D. discoideum*	XP_647570
Vps13D	*D. discoideum*	XP_637675
Vps13E	*D. discoideum*	XP_647037
Vps13F	*D. discoideum*	XP_637397
Vps13A	*D. purpureum*	XP_003286357
Vps13B	*D. purpureum*	XP_003292820
Vps13C	*D. purpureum*	XP_003293812
Vps13D	*D. purpureum*	XP_003290022
Vps13E	*D. purpureum*	XP_003291063
Vps13F	*D. purpureum*	XP_003293882
Vps13A	*D. fasciculatum*	XP_004358813
Vps13B	*D. fasciculatum*	XP_004363054
Vps13C	*D. fasciculatum*	XP_004361633
Vps13D	*D. fasciculatum*	XP_004358786
Vps13E	*D. fasciculatum*	XP_004359975
Vps13F	*D. fasciculatum*	XP_004358101
Vps13A	*Homo sapiens*	NP_150648
Vps13B	*Homo sapiens*	NP_060360
Vps13C	*Homo sapiens*	NP_065872
Vps13D	*Homo sapiens*	NP_056193
Vps13A	*Mus musculus*	NP_766616
Vps13B	*Mus musculus*	NP_796125
Vps13C	*Mus musculus*	NP_796158
Vps13D	*Mus musculus*	NP_001263431
Vps13A	*Danio rerio*	NP_001112365
Vps13C	*Danio rerio*	XP_009301518
Vps13D	*Danio rerio*	XP_001919988
Vps13	*Caenorhabditis elegans*	NP_740899
Vps13A	*Drosophila melanogaster*	NP_610299
Vps13B	*Drosophila melanogaster*	NP_729825
Vps13C	*Drosophila melanogaster*	NP_651753
Vps13	*Saccharomyces cerevisiae*	NP_013060
Vps13	*Cryptococcus neoformans*	XP_012052436
Vps13	*Neurospora crassa*	XP_960097

Figure S1:

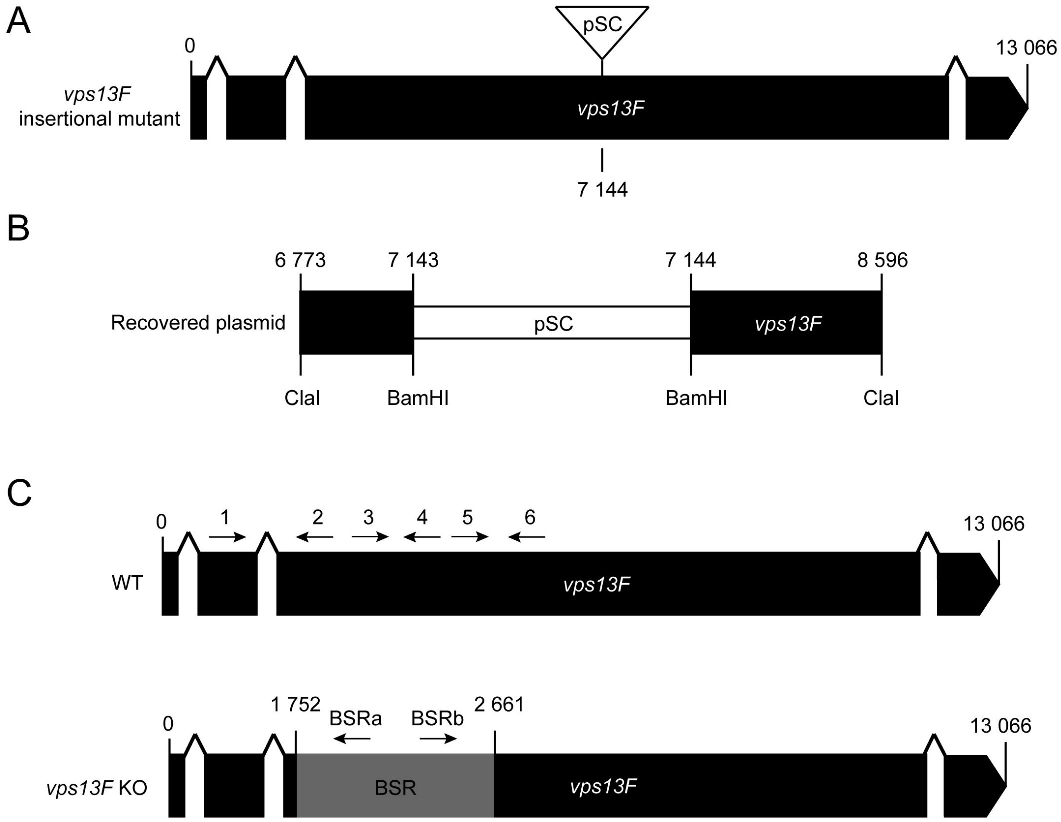

D

Oligos	Sequence
1	TGAAAATGATTCACAATCAGGTGGT
2	CGCTTATCAAAGAATTGTGGTGTCC
3	TTCAACAACAACTTCATCATCGTCA
4	GGTGAATTTGGTGGTTGCAATCTAA
5	TTAGATTGCAACCACCAAATTCACC
6	TATCAGAGGGTGCATTTCCAAAGAA
BSRa	TCAAAAAGATAAAGCTGACCCGAAAGC
BSRb	TTCAAATAATAATTAACCAACCCAAG

	Well	Oligos pair	Size WT (bp)	Size KO (bp)
Loss of signal	1	1+2	865	0
	2	3+4	774	0
	3	5+6	513	0
Gain of signal	4	1+BSRa	0	890
	5	BSRb+6	0	934

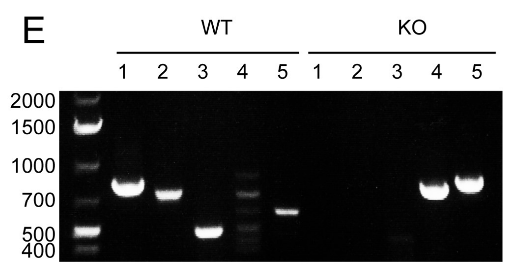

Figure S2:

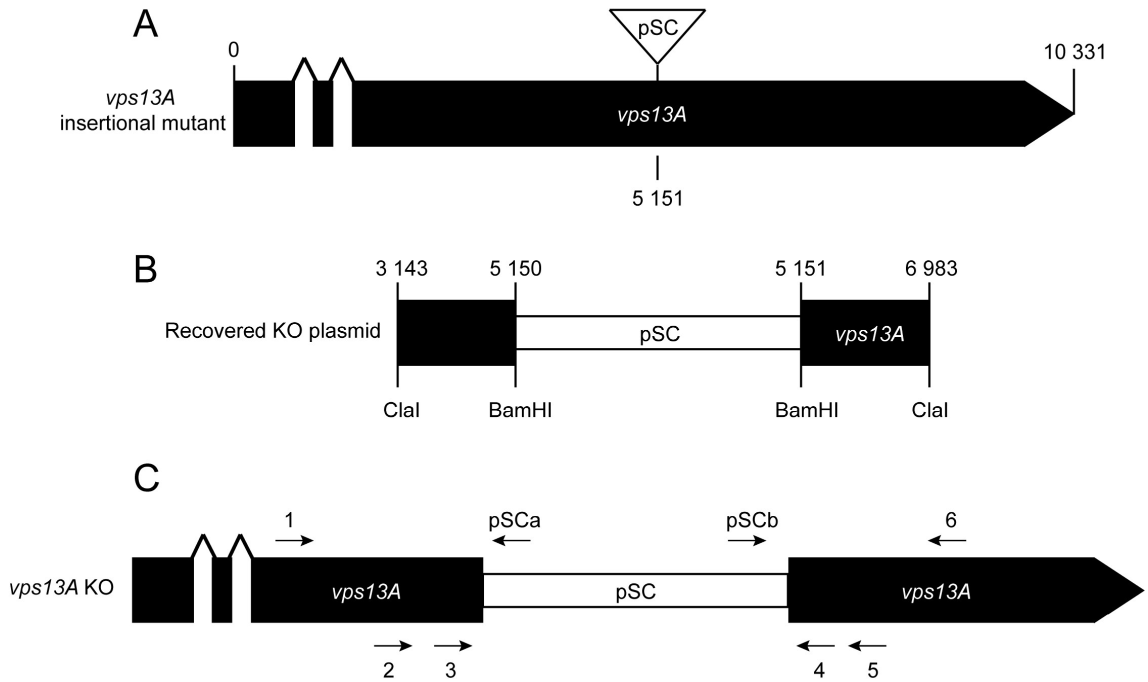

D

Oligos	Sequence
1	TCAAACAGCTTCACCAGAATTTAATA
2	CAAATTCAACCAATATCTTTAAGAAC
3	TGGATGTTGATTTAGATTTAGATTTG
4	TTGTTGTTGAGATGGAATAAATGATG
5	TGAATGTAATGGTTGGTGATCTAAAT
6	GAACCAATGATACAAACATACCAACT
pSCa	AGAGACTTCCTGCCTCGTC
pSCb	GCATTAGATGTAAAACAGCCAAAGAGT

	Oligos pair	Size WT (bp)	Size KO (bp)
	2+4	368	4103
	2+5	558	4293
	3+4	146	3881
	3+5	336	4071
Gain of signal	1+pSCa	0	2091
	pSCb+6	0	1982

Figure S3:

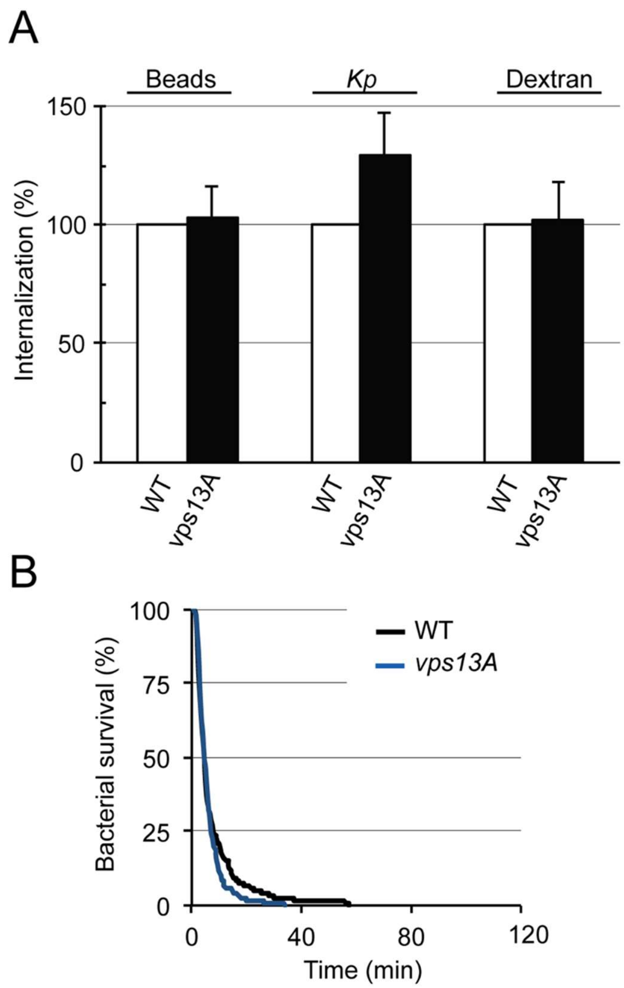

Figure S4:

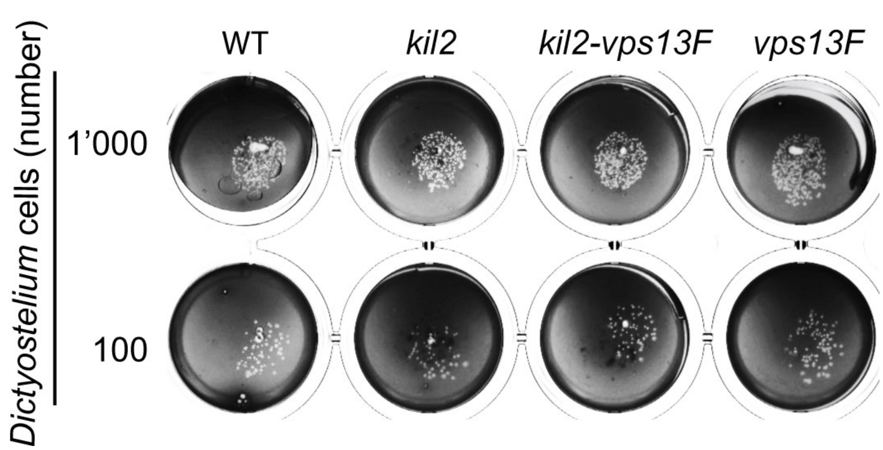

Figure S5:

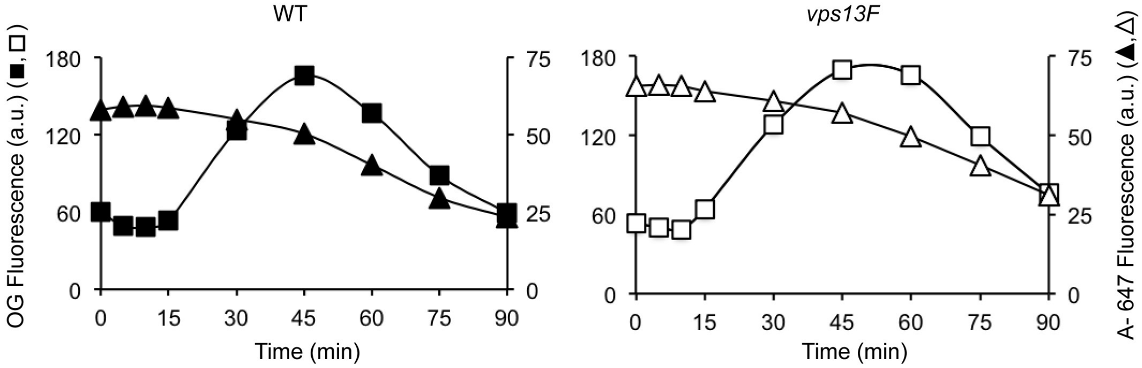

Figure S6:

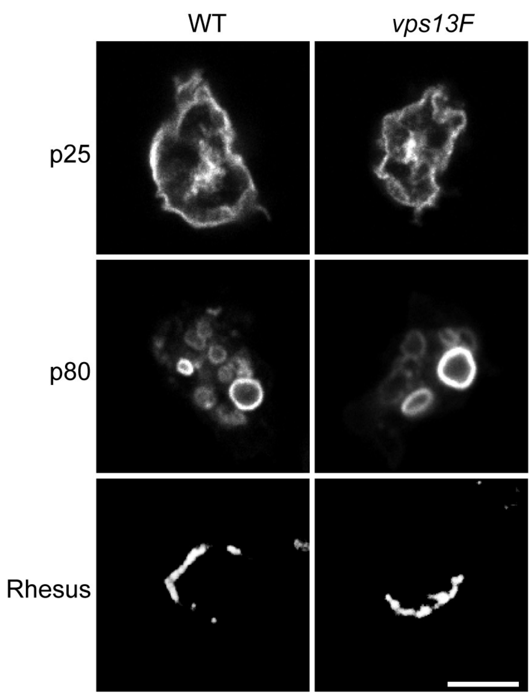

Figure S7:

A

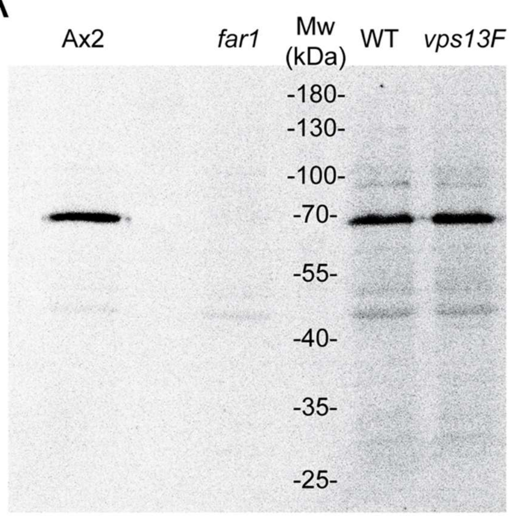

B

	vps13F / WT
SibA	0.92
	1.05
Phg1A	0.96
	0.91
Kil1	0.87
	0.98
Kil2	1.69
	0.81
	1.28
	1.1
Far1	1.09
	1.21

Figure S8:

A

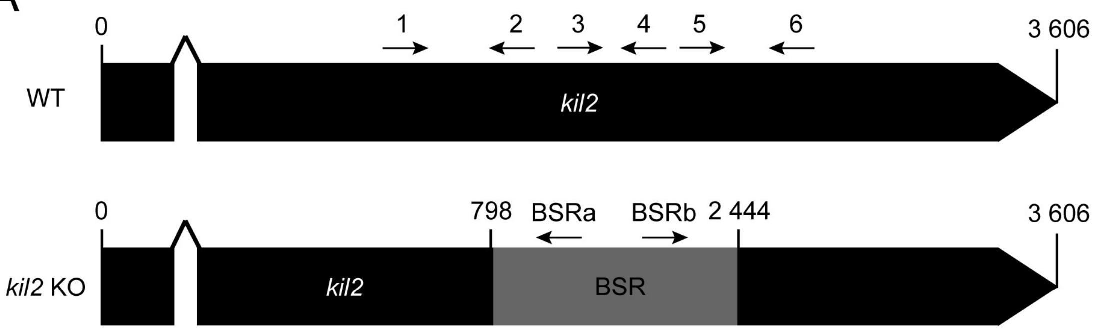

B

Oligos	Sequence
1	GTTACAATGAACCAAATGATCCTTTAG
2	CATCTCTTAACACTGTCACATCACATC
3	AAAGTATTCATTGGAGGAGTGTTCAGG
4	ACAATAGACTTCAACTTTACCTGCCAT
5	TGGTAAACCAACAATGGTAGAATGG
6	TTGTAAACCAACAATGGTAGAATGG
BSRa	TCAAAAAGATAAAGCTGACCCGAAAGC
BSRb	TTCAAATAATAATTAACCAACCCAAG

	Oligos pair	Size WT (bp)	Size KO (bp)
Loss of signal	1+2	834	0
	3+4	487	0
	5+6	1127	0
Gain of signal	1+BSRa	0	831
	BSRb+6	0	1275

II. LrrkA alters intracellular killing in a Kil2-dependent manner in *D. discoideum*

1. First characterization of LrrkA KO mutant

*lrrk*A is the second gene identified in the random mutagenesis that revealed *vps13*F. Like Vps13F, LrrkA does not have any feature that would suggest that it acts as a direct effector of IC killing. Sequence analysis displays the features of a cytosolic kinase.

The main highlights of this study are:

- We characterized a new mutant defective in IC-killing: *drkD* KO
- Based on sequence analysis we renamed *drk*D into *lrrk*A. Indeed, *drk*D shares very little similarities with *drk*A, B and C but several with the LRRK family.
- We showed that Kil2 activity depends on LrrkA.
- We showed that fAR1 is implicated in intracellular killing unravelling a fAR1-LrrkA-Kil2 pathway allowing extracellular folate to control intracellular killing.

It was already established that folate regulates phagocytosis and chemotaxis. Our observations revealed that it also regulates IC killing. These observations strongly reinforce the hypothesis that *D. discoideum* can sense and answer specifically to different bacterial cues. Unfortunately, we were not able to identify the molecular targets phosphorylated by LrrkA. Further detailed genetic and biochemical studies will be necessary to establish the precise molecular organization of the pathway allowing folate to regulate intracellular killing.

2. LrrkA, a kinase with Leucine-Rich Repeats links folate sensing with Kil2 activity and intracellular killing

Published: Cell Microbiol. 2020, Jan

Romain Bodinier[1], Jade Leiba[1], Ayman Sabra[1], Tania N. Jauslin[1], Otmane Lamrabet[1], Cyril Guilhen[1], Anna Marchetti[1], Yumi Iwade[2], Takefumi Kawata[2], Wanessa C. Lima[1], Pierre Cosson[1‡]

Affiliations:
[1]Department of Cell Physiology and Metabolism, Faculty of Medicine, University of Geneva, Geneva, Switzerland
[2] Department of Biology, Faculty of Science, Toho University, 2-2-1 Miyama, Funabashi, Chiba 274-8510, Japan
[‡]Author for correspondence: pierre.cosson@unige.ch

Key Words: LrrkA, DrkD, intracellular killing, *Klebsiella pneumoniae*, magnesium, Kil2, *Dictyostelium*

Personal contribution:

Figure + legends:

Object:	Analysis	Quantification	Figure	Text	Revision
Fig1	AS/JL/**RB**	AS/JL/**RB**	**RB**	**RB**	AS/JL/**RB**
Fig2	WL	WL	**RB**	WL/**RB**	WL/**RB**/PC
Fig3	AM/JL/**RB**	AM/JL/**RB**	**RB**	**RB**	**RB**/PC
Fig4	**RB**	**RB**	**RB**	**RB**	**RB**/PC
Fig5	JL/**RB**	JL/**RB**	**RB**	**RB**	**RB**/PC
Fig6	**RB**	**RB**	**RB**	**RB**	**RB**/PC
Fig7	**RB**	**RB**	**RB**	**RB**	**RB**/PC
Fig8	**RB**	**RB**	**RB**	**RB**	**RB**/PC
Fig9			**RB**/PC	**RB**/PC	**RB**/PC
FigS1 D)	**RB**	**RB**	**RB**	**RB**	**RB**/PC
FigS2	**RB**	**RB**	**RB**	**RB**	**RB**/PC

Manuscript:

Introduction/Discussion**:**

Object:	Text	Revision
Abstract	**RB**/PC	JL/AS/**RB**/PC
Introduction	**RB**/PC	JL/AS/**RB**/PC
Discussion	**RB**/PC	JL/AS/**RB**/PC

Materials & Methods:

Object:	Text	Revision
All / except WL:Phylogeny, CG:lysosozyme activity and YI: Autophosphorylation assay)	**RB**	**RB**/PC

Results:

Object:	Text	Revision
ALL	**RB**/PC	**RB**/PC

Received: 9 July 2019 | Revised: 20 September 2019 | Accepted: 3 October 2019

DOI: 10.1111/cmi.13129

RESEARCH ARTICLE

WILEY

LrrkA, a kinase with leucine-rich repeats, links folate sensing with Kil2 activity and intracellular killing

Romain Bodinier[1] | Jade Leiba[1] | Ayman Sabra[1] | Tania N. Jauslin[1] | Otmane Lamrabet[1] | Cyril Guilhen[1] | Anna Marchetti[1] | Yumi Iwade[2] | Takefumi Kawata[2] | Wanessa C. Lima[1] | Pierre Cosson[1]

[1] Department of Cell Physiology and Metabolism, Faculty of Medicine, University of Geneva, Geneva, Switzerland

[2] Department of Biology, Faculty of Science, Toho University, Funabashi, Japan

Correspondence
Pierre Cosson, Department of Cell Physiology and Metabolism, Faculty of Medicine, University of Geneva, Geneva, Switzerland.
Email: pierre.cosson@unige.ch

Funding information
Schweizerischer Nationalfonds zur Förderung der Wissenschaftlichen Forschung, Grant/Award Number: 31003A_172951

Abstract

Phagocytic cells ingest bacteria by phagocytosis and kill them efficiently inside phagolysosomes. The molecular mechanisms involved in intracellular killing and their regulation are complex and still incompletely understood. *Dictyostelium discoideum* has been used as a model to discover and to study new gene products involved in intracellular killing of ingested bacteria. In this study, we performed random mutagenesis of *Dictyostelium* cells and isolated a mutant defective for growth on bacteria. This mutant is characterized by the genetic inactivation of the *lrrkA* gene, which encodes a protein with a kinase domain and leucine-rich repeats. *LrrkA* knockout (KO) cells kill ingested *Klebsiella pneumoniae* bacteria inefficiently. This defect is not additive to the killing defect observed in *kil2* KO cells, suggesting that the function of Kil2 is partially controlled by LrrkA. Indeed, *lrrkA* KO cells exhibit a phenotype similar to that of *kil2* KO cells: Intraphagosomal proteolysis is inefficient, and both intraphagosomal killing and proteolysis are restored upon exogenous supplementation with magnesium ions. Bacterially secreted folate stimulates intracellular killing in *Dictyostelium* cells, but this stimulation is lost in cells with genetic inactivation of *kil2*, *lrrkA*, or *far1*. Together, these results indicate that the stimulation of intracellular killing by folate involves Far1 (the cell surface receptor for folate), LrrkA, and Kil2. This study is the first identification of a signalling pathway regulating intraphagosomal bacterial killing in *Dictyostelium* cells.

KEYWORDS

Dictyostelium, DrkD, intracellular killing, Kil2, *Klebsiella pneumoniae*, LrrkA, magnesium

1 | INTRODUCTION

Phagocytosis is used by both mammalian cells and environmental amoebae to ingest microorganisms, in particular bacteria. In mammals, one of the main functions of specialised phagocytic cells (e.g., neutrophils and macrophages) is to eliminate invading microorganisms and to protect the body against infections. Amoebae use phagocytosis to feed upon other microorganisms. In both mammalian cells and amoebae, intracellular destruction of ingested microorganisms is one of the first events following phagocytosis. To achieve this goal, ingested bacteria are rapidly transferred into acidic phagolysosomes, equipped to perform efficient killing. Phagocytosis, phagosome maturation, and intracellular bacterial killing are complex and interdependent processes involving multiple gene products. Consequently, our understanding of the molecular mechanisms ensuring intracellular killing is still largely incomplete (Dunn et al., 2017).

The *Dictyostelium discoideum* amoeba has been an instrumental model to study the molecular mechanisms controlling the dynamics of the actin cytoskeleton, phagocytosis, and intracellular killing of bacteria (Cosson & Soldati, 2008; Mori, Mode, & Pieters, 2018; Stuelten, Parent, & Montell, 2018). To the best of our current knowledge, molecular mechanisms involved in ingestion and killing of bacteria are largely similar in *Dictyostelium* and mammalian cells (Cosson & Soldati, 2008). Due to the relative ease with which haploid *Dictyostelium* cells can be grown, observed, and genetically altered, they have been largely used to discover and analyse the role of specific gene products in various facets of the phagocytic process. Identification of mutants with interesting phenotypic alterations has notably been a powerful method to discover new gene products involved in phagocytosis and intracellular killing.

One relatively easy way to identify *Dictyostelium* mutants with interesting phenotypic defects is to test their ability to grow in the presence of bacteria. Defects in various facets of phagocytosis (e.g., phagocytosis or intracellular bacterial killing) were indeed found to reduce the ability of *Dictyostelium* cells to feed upon various bacteria. This strategy has been successfully used to identify gene products involved in phagocytosis like SpdA (Dias et al., 2016) or in intracellular killing like Kil1 (Benghezal et al., 2006) Kil2 (Lelong et al., 2011) and Vps13F (Leiba et al., 2017). Importantly, growth in the presence of bacteria can be affected in many different manners, for example, by mutations decreasing the ability of the cell to recognise bacteria, to ingest them, to kill them, to digest them, or to make use of the nutrients. Defects in cellular motility, cell division, or gene expression could also modify the ability of a cell to grow in the presence of bacteria. As detailed in Section 3, from a practical point of view, this means that isolating mutants unable to grow in the presence of bacteria is a practical method to isolate interesting new mutants but a very poor method to characterize mutants.

In this study, we isolated and characterized a new *Dictyostelium* mutant unable to grow in the presence of Gram-positive bacteria. The *lrrkA* (formerly *drkD*) gene, disrupted in this mutant, encodes a kinase with leucine-rich repeats (LRRs). Our results reveal that LrrkA plays a key role in a pathway activating intracellular killing in response to folate.

2 | RESULTS

2.1 | *LrrkA* knockout cells are unable to feed upon Gram-positive bacteria

In order to identify new gene products implicated in ingestion and killing of bacteria, we previously created a collection of random insertional mutants in a *kil2* knockout (KO) cell line (Leiba et al., 2017). We then tested the ability of individual clones to grow on a lawn of nonpathogenic strains of various bacterial species (*Klebsiella pneumoniae*, *Micrococcus luteus*, *Bacillus subtilis*, *Escherichia coli*, and *Pseudomonas aeruginosa*). We isolated in this manner a mutant clone unable to feed upon *M. luteus* and *B. subtilis*. We purified the genomic DNA of the mutant cells, digested it with ClaI, self-ligated DNA fragments, and transformed them into competent bacteria. This led to the isolation of the inserted pSC plasmid with the genomic flanking regions (Figure S1a). Sequencing revealed that the mutagenic plasmid was inserted in the coding sequence of the *drkD* gene at position 1,782 (Figure S1a). As detailed below, this gene was renamed *lrrkA* in this study and in the dictyBase database.

In order to ascertain that the phenotype of the original mutant was due solely to the insertion of the plasmid in the *lrrkA* gene, we created deletion mutants where a part of the *lrrkA* gene was deleted. Specifically, we generated by homologous recombination three *lrrkA* KO clones as well as two *kil2–lrrkA* double KO clones (Figure S1b–d). These independent mutant clones were characterized in parallel and yielded indistinguishable phenotypes in all assays described below.

In order to precisely assess the ability of *Dictyostelium* cells to feed upon various bacteria, we deposited increasing numbers of cells (10 to 10,000) on a lawn of bacteria. After a few days, wild-type (WT) *Dictyostelium* cells eliminated bacteria and created visible phagocytic plaques in bacterial lawns of *K. pneumoniae* and *B. subtilis* (Figure 1a). *LrrkA* KO cells grew as efficiently as WT cells on *K. pneumoniae*, but they were unable to feed upon *B. subtilis* (Figure 1a). We also assessed growth of *lrrkA* KO cells on a wider range of bacteria (*M. luteus*, a Kp21 *K. pneumoniae* strain, *E. coli*, and one nonpathogenic *P. aeruginosa* strain), and this analysis revealed that *lrrkA* KO cells were unable to feed upon the two Gram-positive bacteria tested but showed no defect when grown on a lawn of Gram-negative bacteria (Figure 1b).

2.2 | LrrkA is a kinase with LRRs and no Roc GTPase domain

The *lrrkA* gene analysed in this study was originally named *drkD*. The Drk family as originally defined contained four kinases characterized by the presence of a conserved putative kinase domain (Araki et al., 1998). However, there are notable differences between DrkA, DrkB, and DrkC on one side and DrkD on the other side. First, DrkA, DrkB, and DrkC have a signal peptide and a transmembrane domain, both absent in DrkD (Figure 2a). Second, DrkD contains seven LRRs, not found in DrkA, DrkB, and DrkC (Figure 2a). Third, the size of DrkD (1,288 residues) differs widely from that of DrkA, DrkB, and DrkC (642–749 residues; Figure 2a). Consequently, we propose to move DrkD out of the Drk family and to rename it LrrkA (LRR kinase).

Cytosolic kinases containing LRRs are found in a variety of species over the whole evolutionary tree (Figure 2b). There are, for example, eight LRR-containing kinases in the unicellular ciliate *Paramecium tetraurelia* and 35 in the plant *Arabidopsis thaliana*. Although the phylogenetic relationships remain to be determined, a variation on this basic structure appeared after the divergence of plants: Starting at this point, some LRR-containing kinases contain in addition a Roc/COR GTPase domain, and they are often referred to as Roco kinases. In Mycetozoa (including *D. discoideum*) and Acanthomyxids (*Acanthamoeba castellanii*), many LRR-containing kinases can be found, some of which belong to the Roco subfamily (Figure 2b). In animals, LRR-containing kinases are less numerous, and they all belong to the Roco subfamily. In human, there are only two Roco kinases,

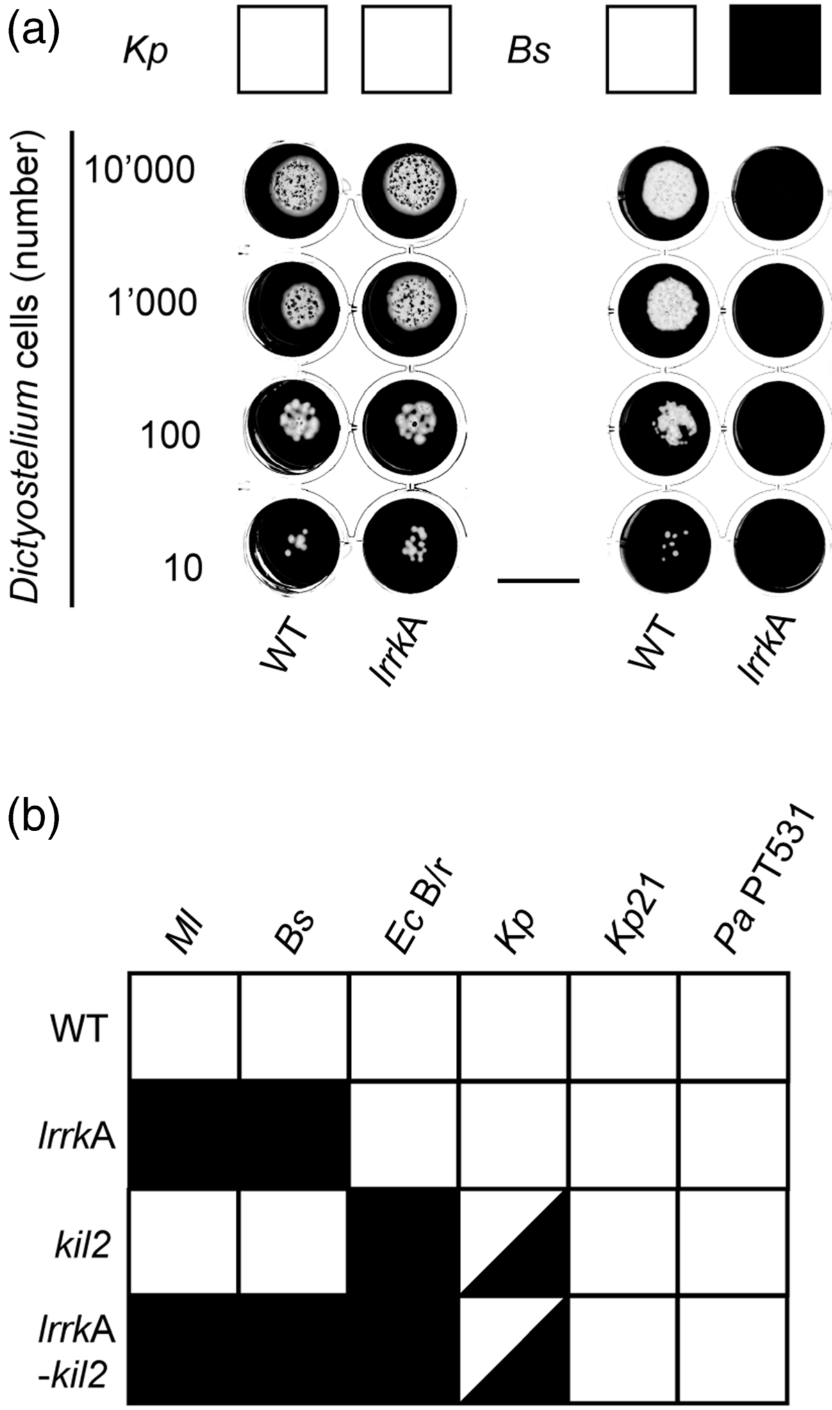

FIGURE 1 *lrrkA* knockout (KO) cells are unable to feed upon Gram-positive bacteria. (a) To determine the ability of *Dictyostelium* cells to feed upon *Klebsiella pneumoniae* (*KpGe* strain), *Dictyostelium* cells (10,000, 1,000, 100, or 10 cells) were deposited on a lawn of *KpGe*. After 4 days, wild-type (WT) *Dictyostelium* cells created phagocytic plaques (white) in the bacterial lawn (black). *LrrkA* KO cells grew as well as WT cells on *K. pneumoniae* but were unable to grow on *Bacillus subtilis*. A white square indicates a growth comparable with that of WT cells, and a black square indicates a defective growth. (b) Several bacterial species were assessed as described above. *LrrkA* KO cells grew very poorly on both Gram-positive bacteria tested (*Micrococcus luteus* and *B. subtilis*) but normally on other bacteria. *Bs*, *B. subtilis*; *Ec B/r*, *Escherichia coli B/r*; *Kp*, *K. pneumoniae KpGe*; *Kp21*, *K. pneumoniae* LM21; *Ml*, *M. luteus*; *Pa* PT531, *Pseudomonas aeruginosa* PT531. Scale bar: 1.5 cm

named LRRK1 and LRRK2 (Figures 2b and S2). We did not identify LRR-containing kinases in fungi (*Saccharomyces cerevisiae*, *Paramicrosporidium saccamoebae*, and *Ustilago bromivora*; Figure 2b). A more complete description of Roco proteins, including proteins devoid of a kinase domain, was recently published (Wauters, Versees, & Kortholt, 2019).

Note that the classification of LRR kinases and Roco kinases is not devoid of some ambiguity, because Roco kinases can contain incomplete Roc/COR domains, or be devoid of LRRs. In *Dictyostelium*, we identified a total of 13 LRR kinases (Figure S2):

- LrrkA.
- DDB_G0278509 has an overall structure similar to that of LrrkA. Primary sequence analysis revealed one kinase domain, 13 LRRs, and no other functional domains. We consequently named it LrrkB.
- DDB_G0278909 contains one kinase domain, six LRRs, and 13 HEAT repeats. The kinase domain misses a catalytic aspartate and is expected to be inactive.
- Eight Roco kinases contain a full Roc/COR domain and LRRs (Roco 1–6, 8, and 11).

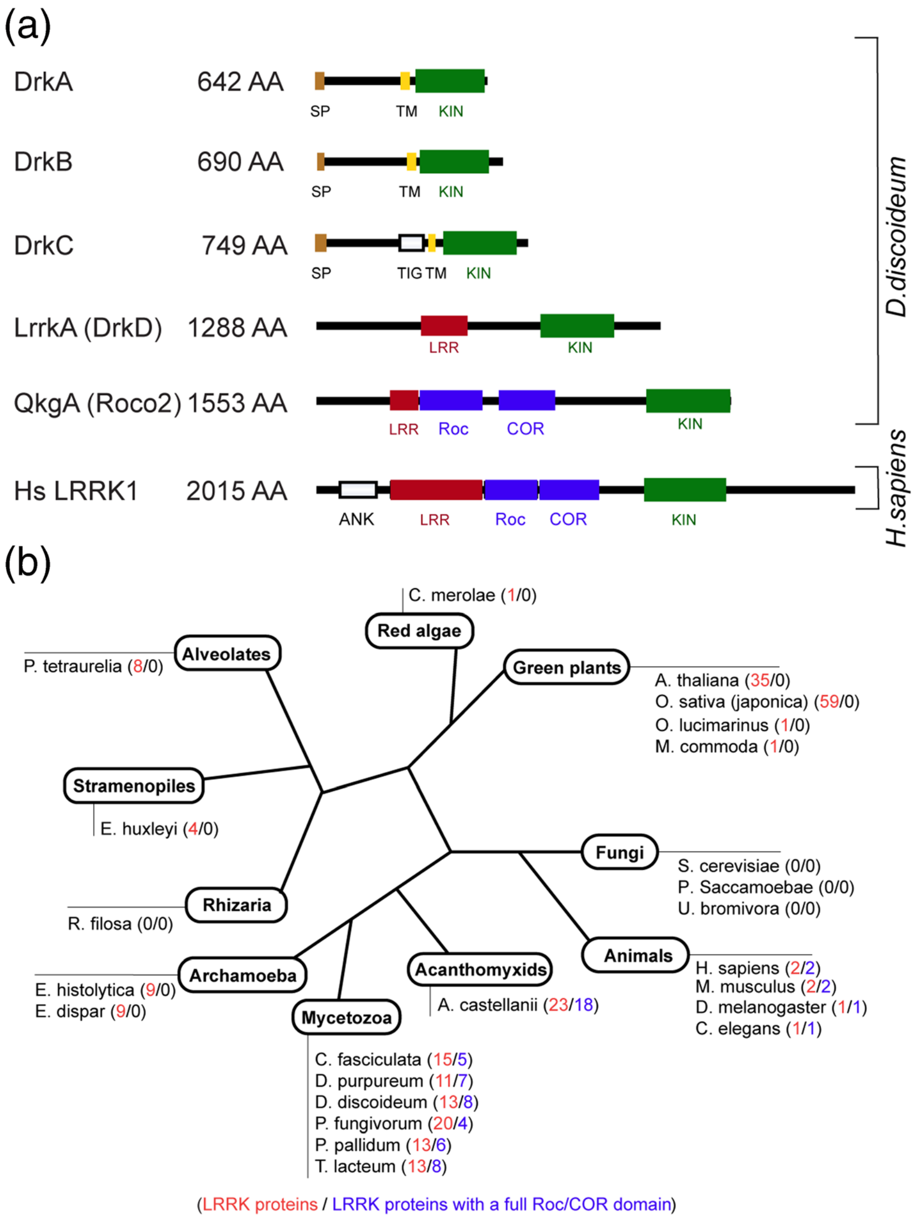

FIGURE 2 DrkD/LrrkA belongs to the family of leucine-rich repeat (LRR) kinases. (a) Organisation of functional domains of DrkA–DrkD, of the *Dictyostelium* ROCO2 kinase, and of the human LRR kinase 1. DrkA, DrkB, and DrkC contain a putative signal peptide and a putative transmembrane domain situated N-terminally of the kinase domain. LrrkA/DrkD, Roco 2, and human LRRK1 contain LRRs and a kinase domain. In addition, ROCO proteins (Roco 2 and human LRRK1) contain a Roc and a Cor domain. (b) Schematic phylogenetic tree representing the number of LRR kinases (with or without a Roc/COR domain) in eukaryotes (indicated in red) and the number of LRR kinases containing a full Roc/COR domain (indicated in blue)

- Two kinases classified as Roco kinases (Roco 9 and 10) contain LRRs but an incomplete or absent Roc/COR domain.
- Roco 7 has been classified as a Roco kinase. It contains an incomplete Roc/COR domain and no LRRs and is thus strictly speaking not an LRR kinase.

In order to verify that LrrkA has a functional kinase domain, we expressed myc-tagged LrrkA, both WT, and a catalytically inactive version (K877A). After immunoprecipitation of LrrkA–myc with an anti-myc antibody, anti-phosphoserine antibodies revealed that a serine is phosphorylated in LrrkA but not in the inactive mutant (Figure S3). No tyrosine phosphorylation was detected with an anti-phosphotyrosine antibody. These results suggest that LrrkA is a serine (and presumably a serine/threonine) kinase and that it is capable of autophosphorylation.

2.3 | The structure and pH of phagocytic compartments is unaffected in *lrrkA* KO cells

Many mutants showing a reduced ability to feed on bacteria exhibit a defect in the structure or function of the endocytic or phagocytic pathways. Consequently, we first checked whether the basic structure

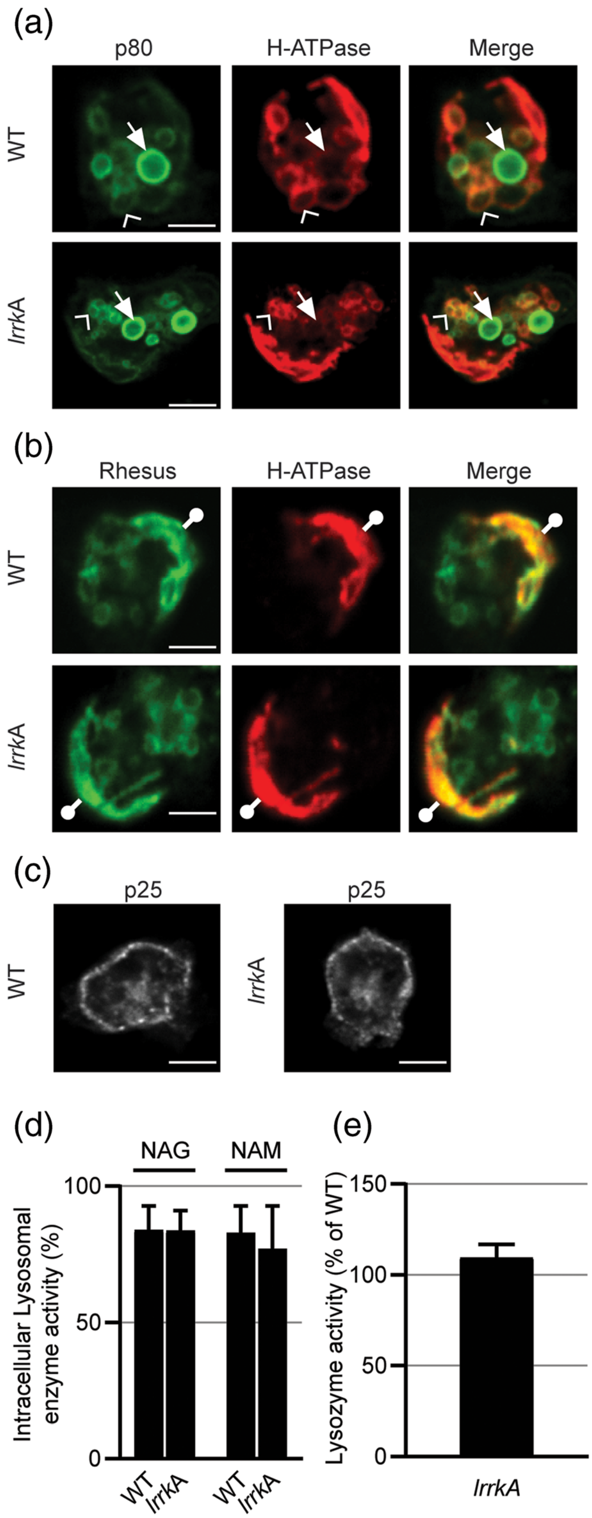

FIGURE 3 General organisation of cellular compartments is similar in *lrrkA* knockout (KO) and in wild-type (WT) cells. (a) Immunofluorescence labelling of p80 and H^+-ATPase allowed to identify lysosomes (arrowheads; $p80^+$ and H^+-$ATPase^+$) and post-lysosomes (arrows; $p80^+$ and H^+-$ATPase^-$). (b) Immunofluorescence labelling of rhesus and H^+-ATPase allowed to identify contractile vacuole (circles with bar; $rhesus^+$ and H^+-$ATPase^+$). (c) Immunofluorescence labelling of recycling endosomes enriched in p25. Scale bar in (a–c): 5 μm. (d) Intracellular retention of lysosomal glycosidases is as efficient in WT as in *lrrkA* KO cells. After 4 days of culture in HL5 medium, *Dictyostelium* cells were recovered by centrifugation, and the activity of two lysosomal enzymes (NAG, *N*-acetyl-β-glucosaminidase; NAM, α-mannosidase) was measured in cell pellets and in supernatants using chromogenic substrates. The percentage of intracellular glycosidase activity was not different for WT and *lrrkA* KO cells (mean ± standard error of the mean, $N = 7$, paired Student's t test, NAG $p = .948$, NAM $p = .492$). (e) Intracellular levels of lysozyme activity are similar in WT and *lrrkA* KO cells (mean ± standard error of the mean, paired Student's t test, $N = 5$, $p = .251$)

of the phagocytic pathway was perturbed in *lrrkA* KO cells. For this, we visualised the structure of the endocytic pathway by immunofluorescence, using antibodies against the main endocytic compartments. The structure of the contractile vacuole, visualised with an anti-rhesus antibody (Benghezal, Gotthardt, Cornillon, & Cosson, 2001), of recycling endosomes (p25 positive; Charette, Mercanti, Letourneur, Bennett, & Cosson, 2006), of lysosomes (p80 positive and H^+-ATPase positive; Ravanel et al., 2001), and of post-lysosomes (p80 high and H^+-ATPase negative; Ravanel et al., 2001) was indistinguishable in *lrrkA* KO and in WT cells (Figure 3a–c).

We next assessed the intracellular retention of two lysosomal glycosidases (α-mannosidase and *N*-acetyl-glucosaminidase) and found no difference between WT and *lrrkA* KO cells (Figure 3d), suggesting that lysosomal targeting is not grossly deficient in *lrrkA* KO cells. Finally, the activity of intracellular lysozymes, hydrolytic enzymes potentially implicated in intracellular killing in phagocytic cells (Muller et al., 2005), was indistinguishable in WT and in *lrrkA* KO cells (Figure 3e).

We then measured the pH of phagosomes after ingestion of beads coupled to two fluorophores, one of which (FITC) is extinguished at low pH, whereas the other one (Alexa Dextran 594) is not. In WT cells, a very rapid acidification was observed after formation of the phagosome (Figure 4a), and this very acidic pH was maintained for more than 30 min, that is, largely after intracellular killing was completed. Interestingly, a calibration curve of fluorescence extinction at low pH indicated that FITC coupled to beads was quenched gradually between pH 2 and 8 (Figure 4b). This behaviour differs from that of FITC coupled to a soluble dextran, which is completely quenched at pH 5 or below (Marchetti, Lelong, & Cosson, 2009). This allows us to extrapolate that the pH in phagosomes may be as low as 2.5, in agreement with previous results suggesting that *Dictyostelium* lysosomes are exceptionally acidic (inferior to 3.5; Marchetti et al., 2009). In *lrrkA* KO cells, acidification kinetics were indistinguishable from those in WT cells (Figure 4a), revealing that at least in beads-containing phagosomes, acidification is not perturbed in *lrrkA* KO cells.

In summary, immunofluorescence analysis and pH measurement did not reveal major defects in the structure and organisation of the endocytic pathway in *lrrkA* KO cells.

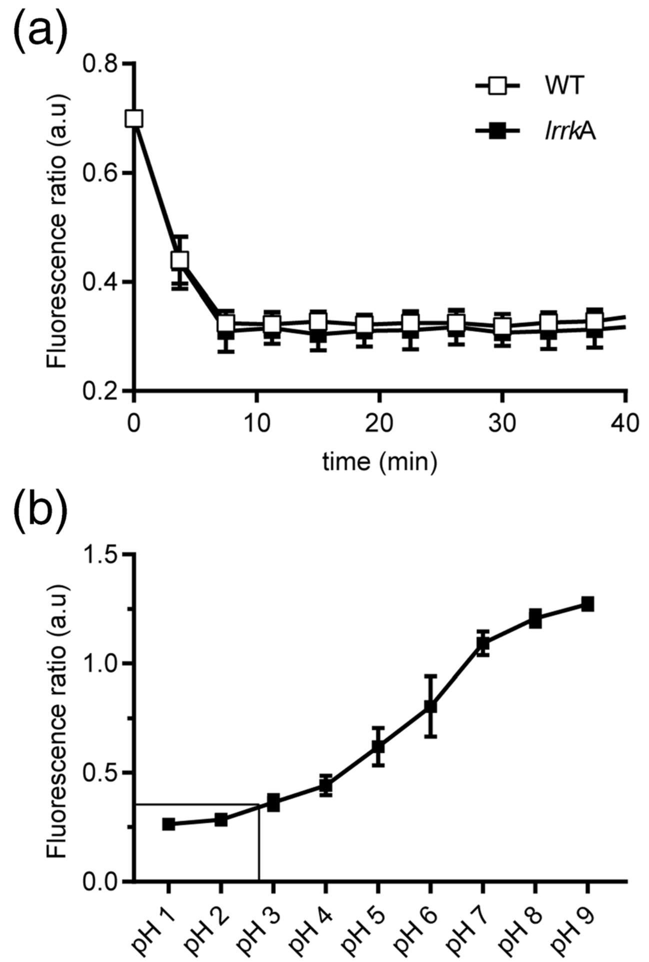

FIGURE 4 Acidification of phagosomes is unaffected in *lrrkA* knockout (KO) cells. (a) Wild-type (WT) and *lrrkA* KO cells were allowed to internalise 3-μm-diameter beads coated with two fluorophores (pH-sensitive FITC and pH-insensitive Alexa 594) and imaged every 75 s for 3 hr. The pH was deduced from the fluorescence 488/594 nm ratio (mean ± standard error of the mean, *N* = 4, *n* = 40 beads for each strain). The kinetics of acidification and the pH value in phagolysosomes were identical in *lrrkA* KO and in WT cells. The fluorescence ratio in acidic phagolysosomes is 0.324. (b) Calibration curve of the pH-sensitive beads in buffer ranging from pH 1 to 9. The dynamic range allows to discriminate variations of pH from 2 to 8 (mean ± standard error of the mean, *N* = 3, *n* = 100 beads per pH). A fluorescence ratio of 0.324 corresponds to a pH value between 2.5 and 3

2.4 | *LrrkA* KO cells are defective for intracellular killing of *K. pneumoniae* bacteria

The fact that *lrrkA* KO cells grow poorly in the presence of some bacteria may be due to their inability to kill efficiently ingested bacteria. In order to test this hypothesis, cells were allowed to ingest GFP-expressing *K. pneumoniae* bacteria, and the survival of the bacteria was monitored as previously described (Leiba et al., 2017). Previous experiments have established that loss of fluorescence accompanies loss of bacterial viability (Lelong et al., 2011). Using this assay, WT cells were found to kill ingested *K. pneumoniae* shortly after phagocytosis (Figure 5a; median killing time 6 min). In *lrrkA* KO cells, intracellular killing was significantly slower (Figure 5a; median killing time 14 min). This delay in intracellular killing was highly reproducible in multiple experiments (Figure 5b). As previously described (Lelong et al., 2011), intracellular killing was also delayed in *kil2* KO cells (Figure 5b). Remarkably, the effect of the two mutations was not additive: Killing was not slower in *kil2–lrrkA* double KO cells than in *kil2* KO cells (Figure 5b). This observation suggests that Kil2 and LrrkA play partially redundant roles in intracellular killing. On the contrary, *kil1–lrrkA* double KO cells killed bacteria even slower than *kil1* KO cells (Figure 5b), suggesting that Kil1 and LrrkA do not play redundant roles in intracellular killing.

We also tested in a similar manner the ability of *lrrkA* KO cells to kill ingested *B. subtilis* expressing a fluorescent mCherry. Interestingly, *lrrkA* KO cells killed these Gram-positive bacteria as efficiently as WT cells (Figure S4). This result indicates that different killing mechanisms are involved in the killing of *K. pneumoniae* and *B.*

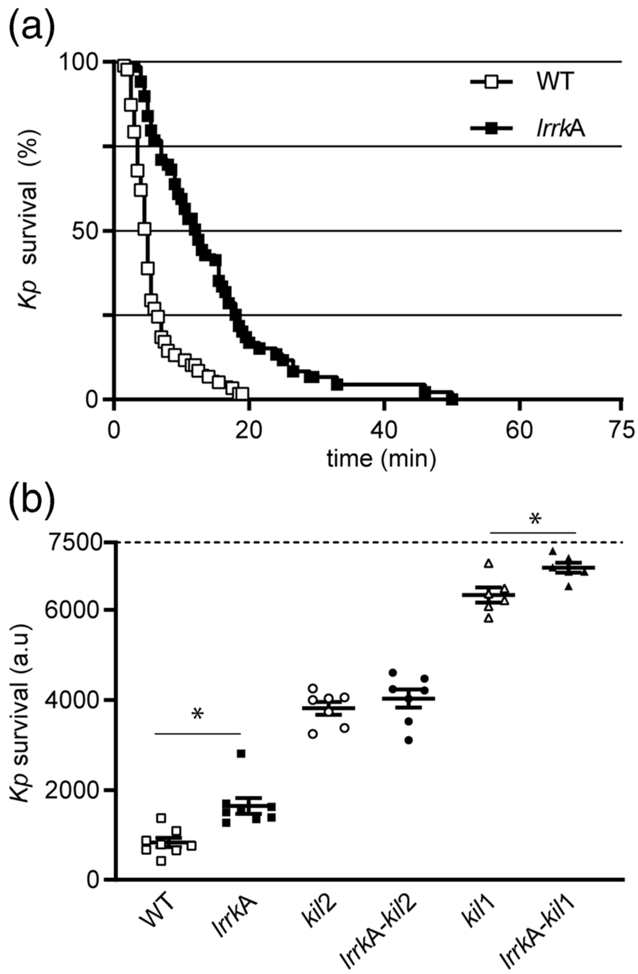

FIGURE 5 Intracellular killing of *Klebsiella pneumoniae* is impaired in *lrrkA* knockout (KO) cells. *Dictyostelium* cells were incubated with GFP-expressing *K. pneumoniae* (Kp-GFP) in phosphate buffer–sorbitol for 2 hr. Cells were observed by phase-contrast and fluorescence microscopy, and the ingestion and intracellular killing of Kp-GFP were monitored. (a) The probability of bacterial survival following ingestion is represented as a Kaplan–Meyer estimator for one experiment in wild-type (WT) cells (white squares) and *lrrkA* KO cells (black squares). (b) For each experiment, the survival of bacteria was determined by measuring the area under the survival curve from 0 to 75 min. Each dot is the result of a separate experiment. Intracellular killing was significantly slower in *lrrkA* KO cells and in *kil2* KO cells than in WT cells (p = .013; paired Student's t test, N = 8 independent experiments). Intracellular killing was not slower in *lrrkA–kil2* KO cells than in *kil2* KO cells (p = .510; paired Student's t test, N = 7 independent experiments), but it was significantly slower in *lrrkA–kil1* KO cells than in *kil1* KO cells ($p = 4.10^{-4}$; paired Student's t test, N = 6 independent experiments). Total number of events observed: WT = 351, *lrrkA* = 496, *kil2* = 274, *lrrkA–kil2* = 252, *kil1* = 120, and *lrrkA–kil1* = 120

subtilis. It is at first glance surprising that *lrrkA* KO cells are unable to grow in the presence of Gram-positive bacteria, although they can kill them normally. Similarly, it is surprising that *lrrkA* KO cells grow normally in the presence of *K. pneumoniae* bacteria, while they kill them inefficiently. This lack of congruence between these two assays is discussed in Section 3.

2.5 | Phagosomal proteolysis is defective in *lrrkA* KO cells

Previous experiments have shown that the killing defect observed in *kil2* KO cells is accompanied by a defective activity of proteases in phagosomes (Lelong et al., 2011). If LrrkA and Kil2 do play redundant roles, a similar phenotype may be expected in *lrrkA* KO cells. In order to test the activity of proteases in phagosomes, cells were allowed to ingest silica beads coated with Alexa Fluor 594 and DQ Green-labelled BSA at a self-quenching concentration. Proteolysis releases DQ Green from the beads and increases its fluorescence (Sattler, Monroy, & Soldati, 2013; Figure 6a). Quantification of the images obtained by fluorescence microscopy confirmed that phagosomal proteolysis was less efficient in *kil2* KO cells than in WT cells (Figure 6b).

Proteolysis was also less efficient in *lrrkA* KO cells than in WT cells, although the defect was less pronounced than in *kil2* KO cells (Figure 6b). Proteolysis was however not slower in *kil2–lrrkA* double KO cells than in *kil2* KO cells (Figure 6b). These results suggest that Kil2 and LrrkA play partially redundant roles in controlling proteolysis in *Dictyostelium* phagosomes.

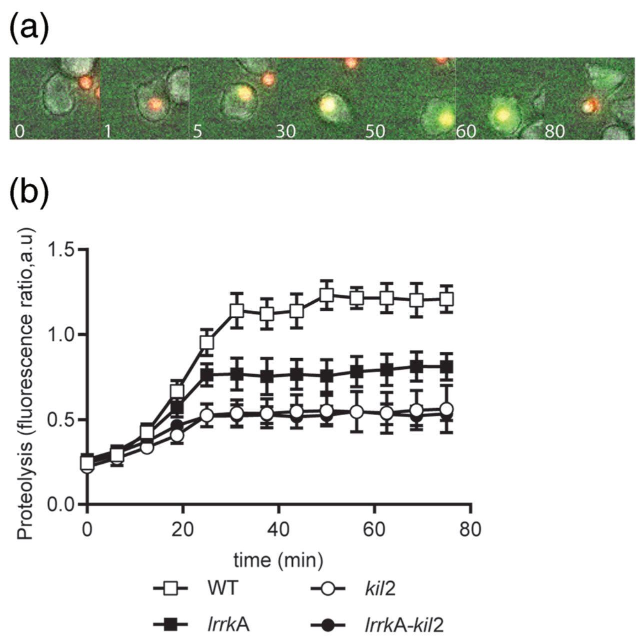

FIGURE 6 Proteolytic activity in phagosomes is reduced in *lrrkA* knockout (KO) cells. (a) Cells were allowed to internalise beads coated with a quenched fluorophore (DQ™ Green BSA) and a proteolysis-insensitive dye (Alexa 594) and were imaged every 75 s. Representative, successive pictures of a wild-type (WT) cell ingesting a bead and processing it over 80 min are shown. Upon degradation of BSA by proteases, the DQ™ Green is released in phagosomes, and the corresponding fluorescence increases. (b) To quantify proteolysis, we plotted the 488/594-nm fluorescence ratio as a function of time following phagocytosis. In all cells, DQ green fluorescence reached a plateau approximately 40 min after phagocytosis. The fluorescence ratio was lower in *lrrkA* KO cells than in WT cells and even lower in *kil2* KO cells or in *kil2–lrrkA* KO cells (mean ± standard error of the mean, N = 4, n = 40 beads for each strain)

2.6 | Magnesium supplementation alleviates the killing and proteolysis defects of *lrrkA* KO cells

It has been previously proposed that Kil2 stimulates intraphagosomal proteolysis by pumping magnesium ions into the phagosome. This proposal is mainly based on the observation that exogenous addition of magnesium restores normal intraphagosomal killing and proteolysis in *kil2* KO cells (Lelong et al., 2011). We consequently determined the effect of exogenous magnesium on intracellular killing and proteolysis in WT, *kil2*, and *lrrkA* KO cells (Figure 7). Addition of exogenous magnesium restored efficient killing in *lrrkA* KO cells (Figure 7a). As previously reported, exogenous magnesium also greatly stimulated killing in *kil2* KO cells. An identical effect was observed in *kil2–lrrkA* double KO cells (Figure 7a).

Exogenous magnesium also restored normal phagosomal proteolysis in *lrrkA* KO cells, *kil2* KO cells, and *lrrkA–kil2* double KO cells (Figure 7b). These results further suggest that LrrkA and Kil2 play redundant roles in the control of magnesium-dependent phagosomal proteolysis and bacterial killing.

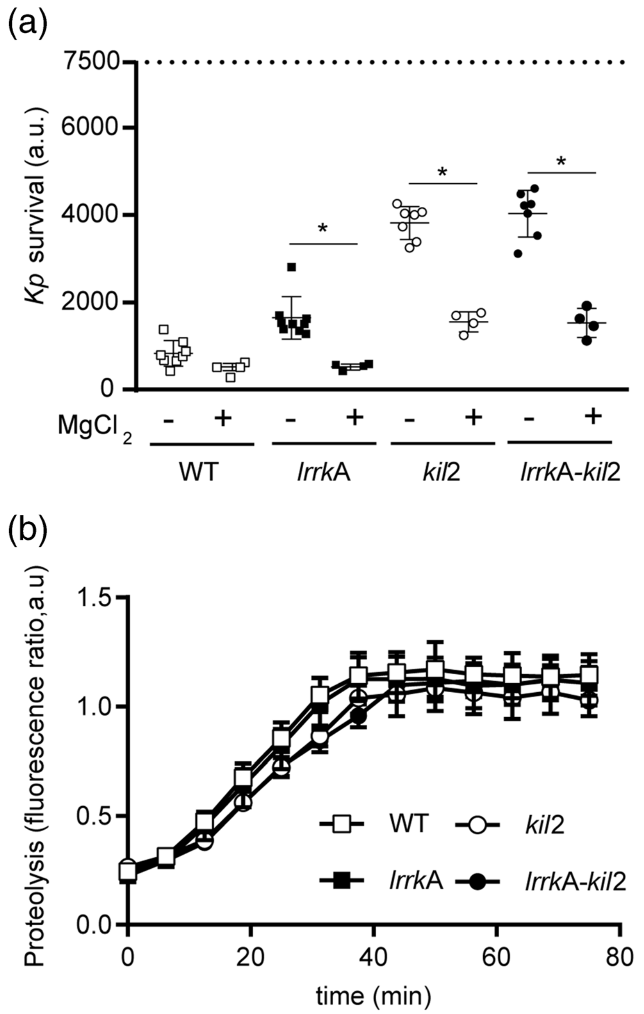

FIGURE 7 Exogenous addition of magnesium restores intracellular killing and proteolytic activity in *lrrkA* knockout (KO), *kil2* KO, and *lrrkA–kil2* KO cells. (a) Intracellular killing of *Klebsiella pneumoniae* was determined in wild-type (WT), *lrrkA* KO, *kil*2 KO, and *lrrkA–kil*2 KO cells in the presence or absence of $MgCl_2$ (1 mM), as described in Figure 5. In these experiments, $MgCl_2$ was directly added in the medium containing cells and bacteria. Exogenous $MgCl_2$ accelerated significantly intracellular killing in all mutant cells ($p < 10^{-4}$; paired Student's *t* test, $N = 5$ independent experiments). (b) Proteolytic activity was measured in phagosomes in the presence of 1 mM of $MgCl_2$ as detailed in Figure 6. Normal levels of phagosomal proteolytic activity were restored in all mutant cells by addition of exogeneous magnesium

2.7 | Stimulation of intracellular killing by folate requires Far1, LrrkA, and Kil2

The results presented above suggest that LrrkA can modulate Kil2 activity and intraphagosomal killing. Little is known about the regulation of intracellular killing mechanisms in *Dictyostelium* in response to extracellular cues. We recently reported that folate, which is synthesized and secreted by many bacteria, can stimulate killing (Leiba et al., 2017). This effect was initially detected in killing-deficient *vps13F* KO cells: Upon exposure to folate, efficient killing was restored in *vps13F* KO cells (Leiba et al., 2017). Our previous results have also shown that folate does not stimulate intracellular killing in *kil2* KO cells (Leiba et al., 2017; Figure 8), suggesting that Kil2 may be necessary for the response to folate. If LrrkA stimulates Kil2 activity, it may represent a missing link between folate sensing and Kil2 activity. To test this hypothesis, we measured the ability of folate to stimulate intracellular killing of ingested *K. pneumoniae* in various mutant cells.

As previously reported for *vps13F* KO cells, folate stimulated intracellular killing in *kil1* KO cells (Figure 8). Remarkably, intracellular killing was not stimulated (and actually inhibited) in *lrrkA* KO cells upon exposure to folate (Figure 8). Far1 has been identified as the main folate receptor at the cell surface (Pan, Xu, Chen, & Jin, 2016), and intracellular killing was also not stimulated by folate in *far1* KO cells (Figure 8).

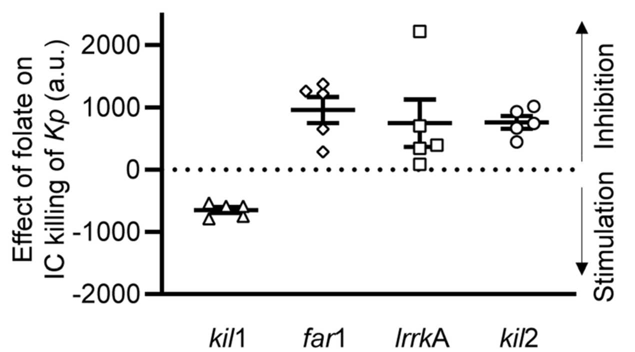

FIGURE 8 Far1, LrrkA, and Kil2 participate in a folate-sensitive pathway stimulating intracellular killing. Intracellular (IC) killing of *Klebsiella pneumoniae* (Kp) was determined in *far1* knockout (KO), *lrrkA* KO, *kil*2 KO, and *kil1* KO cells in the presence or absence of folate (1 mM), as described in Figure 5 ($N = 5$). Each dot represents the difference of area under the curve for each strain with or without folate. All values above zero indicate that the addition of folate slowed intracellular killing. Conversely a value below zero indicates that addition of folate accelerated intracellular killing. Folate stimulated intracellular killing in *kil1* KO cells but not in *far1* KO, *lrrkA* KO, and *kil2* KO cells, revealing the role of Far1, LrrkA, and Kil2 in increasing killing upon folate sensing

Taken together, these results reveal the existence of a signalling pathway where folate is recognised at the cell surface by the Far1 receptor, leading to the sequential activation of LrrkA and Kil2 and ultimately to the activation of intraphagosomal killing of bacteria (Figure 9).

3 | DISCUSSION

In this study, we identified a new molecular mechanism controlling intracellular killing of *K. pneumoniae*. LrrkA is a kinase with LRRs, and its genetic ablation results in a markedly slower intracellular killing of ingested *K. pneumoniae*, although the overall structure of the phagocytic pathway is not defective in these cells. Genetic analysis of *kil2*–*lrrkA* double KO cells, as well as analysis of the phenotype of *lrrkA* KO cells indicate that LrrkA stimulates the activity of Kil2, a putative magnesium transporter in the phagosomal membrane. Magnesium is essential for optimal activity of phagosomal proteases and for efficient killing of ingested *K. pneumoniae*. In addition, our results indicate that LrrkA links the sensing of bacterially secreted folate to the activity of Kil2 and intracellular killing. A schematic description of the roles of folate, LrrkA, Kil2, magnesium ions, and proteases in intraphagosomal killing of bacteria is depicted in Figure 9. It is logical to assume that *Dictyostelium* uses bacterial-sensing mechanisms to adapt intraphagosomal killing to the ingested bacteria, but to our knowledge, this is the first study suggesting the existence of a folate-sensing pathway stimulating intracellular killing.

In order to propose a unified model, we have been led to revisit the interpretation of previously published results (Leiba et al., 2017). According to our current interpretation, the fact that intracellular killing is stimulated by folate in *vps13F* KO cells but not in *kil2* KO cells indicates that Vps13F is not involved in stimulation of intracellular killing by folate, whereas Kil2 is. Similarly, Far1 and LrrkA are essential for the stimulation of intracellular killing by folate, whereas Kil1 is not. Moreover, the fact that *kil2*–*vps13F* double KO cells are more defective in intracellular killing than *kil2* KO cells indicates that the function of Kil2 is not dependent on Vps13F. According to this new interpretation, we suggest that Kil1 and Vps13F play a role in intracellular killing distinct from that of Far1, Kil2, and LrrkA: while the folate–Far1–LrrkA–Kil2 pathway controls ionic composition of phagosomes, Kil1 and Vps13F may play a role in the modification and phagosomal targeting of lysosomal enzymes involved in killing (Figure 9). Although this model accounts for the results presented in this study, we are fully aware that the proposed scheme is overly simple and that it will most probably be refined by further studies.

Screening for mutants exhibiting defective growth in the presence of bacteria has proven a powerful method to identify mutants defective in intracellular killing, but we would like to point out the difficulty in interpreting precisely the results of these growth assays. For example, in the current study, *lrrkA* KO cells were shown to grow efficiently on a lawn of *K. pneumoniae* but not on a lawn of *B. subtilis*. Simple logic would lead to predict that *lrrkA* KO cells kill *K. pneumoniae* efficiently and *B. subtilis* inefficiently. The opposite result is reported in this study. This is not the first case of a discrepancy between assays measuring different facets of *Dictyostelium* physiology: For example, *kil1* KO cells kill *K. pneumoniae* very poorly, yet they grow almost as efficiently as WT cells on a lawn of *K. pneumoniae* (Le Coadic et al., 2013). These results stress the fact that these two assays (growth in the presence of bacteria and killing of bacteria) measure different parameters in different situations. To measure killing, we use cells growing exponentially in rich liquid medium and measure over a short time (2 hr maximum) their ability to kill ingested bacteria. On the contrary, growth in the presence of bacteria is assessed over a period of 5 to 10 days. During that time, *Dictyostelium* cells must achieve numerous functions to be able to grow: sense, ingest, kill, and digest bacteria and also migrate on the plate, grow, divide, and so forth. Any alteration in one or several of these functions can potentially alter in a highly unpredictable way the final outcome. In addition, previous studies have shown that the pattern of gene expression is profoundly different in *Dictyostelium* cells growing in HL5 medium and on a lawn of bacteria and also differs depending on the bacterial species forming the lawn (Nasser et al., 2013). Consequently, the relative importance of any given gene product may vary significantly between these different conditions. To obtain meaningful comparisons, we have chosen to focus on a standard invariant growth condition, that is, cells growing in HL5 medium. It may be of interest in future studies to establish if the mechanisms allowing efficient killing are significantly modulated when *Dictyostelium* cells are grown continuously in the presence of bacteria. This may allow to reconcile the results obtained in growth assays with those obtained during more precise characterization of *Dictyostelium* mutants. From a practical perspective, the fact that a mutant cell is not capable of feeding upon

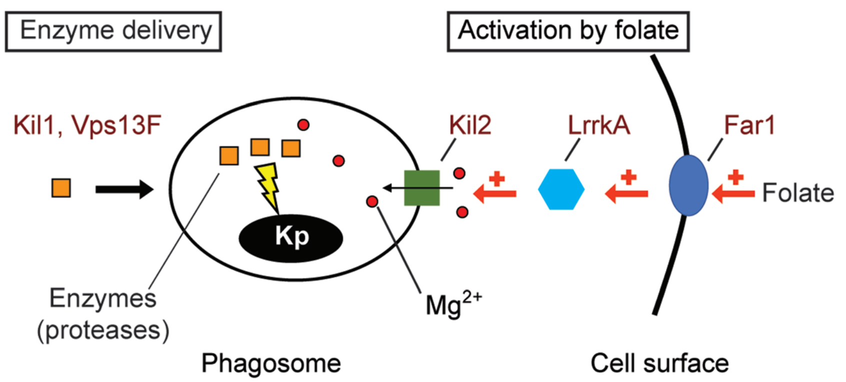

FIGURE 9 Intracellular killing of *Klebsiella pneumoniae*. This simple scheme describes our working model incorporating the results described in this study. Folate activates Far1, which activates LrrkA, resulting in the stimulation of the activity of Kil2 and transfer of magnesium ions (Mg^{2+}) from the cytosol to the phagosomal lumen. In the presence of increased levels of magnesium ions, lysosomal enzymes kill more efficiently ingested *K. pneumoniae* bacteria (Kp). Kil1 and Vps13F play a distinct role in the delivery of properly modified enzymes (notably proteases) to phagosomes

given bacteria is often indicative of a defect in the structure or function of the phagocytic pathway. It cannot however be equated with specific alterations in cell physiology, such as an inability to kill specific bacteria. Specific assays must be used to measure alterations in various facets of *Dictyostelium* physiology.

Finally, this study reveals a high degree of specificity in the mechanisms controlling intracellular killing of different bacteria: Killing of *K. pneumoniae* is slower in *lrrkA* KO cells than in WT cells, but killing of *B. subtilis* is not affected. Similar results were reported previously when the phenotype of *kil1* and *kil2* KO mutants was analysed (Benghezal et al., 2006; Lelong et al., 2011). Overall, our current knowledge strongly suggests that *Dictyostelium* uses vastly different mechanisms to kill different types of bacteria. Although our knowledge of the intracellular mechanisms controlling intracellular killing of *K. pneumoniae* is growing, the mechanisms controlling intracellular killing of other bacteria remain to be identified.

It is not easy to compare the function of *Dictyostelium* LrrkA with human Lrr kinases, because the family of Lrr kinases is more diverse in *Dictyostelium* than in human. The function of LRRK2 has been most intensely studied in human cells because it has been identified as a risk factor for sporadic Parkinson's disease (Lill, 2016). LRRK2 has been detected in several intracellular locations and linked to a range of functions. It has been proposed to be associated with mitochondria where it interacts with DLP1 and regulates mitochondrial dynamics and function (Wang et al., 2012). On endosomal compartments, LRRK2 may associate with NAADP receptors and regulate lysosomal calcium homeostasis and autophagy (Gomez-Suaga et al., 2012). In human macrophages, LRRK2 associates with the class III phosphatidylinositol-3 kinase complex and Rubicon and inhibits the maturation of phagosomes containing *Mycobacterium tuberculosis* bacteria (Hartlova et al., 2018). Detailed studies will be necessary to establish if *Dictyostelium* LrrkA recapitulates some of the functions of human LRRK2 or whether Lrr kinases control different cellular functions in human and in *Dictyostelium* cells.

4 | EXPERIMENTAL PROCEDURES

4.1 | Strains and cell culture

Dictyostelium cells were grown at 21°C in HL5 medium (Froquet, Lelong, Marchetti, & Cosson, 2009). *Dictyostelium* cells used in this study were all derived from the DH1-10 parental strain (Cornillon et al., 2000), referred to in this study as WT. The *kil2* KO and *kil1* KO strains were described previously (Leiba et al., 2017).

Bacterial strains were grown overnight in Luria–Bertani medium at 37°C. Bacteria used were uncapsulated *K. pneumoniae* KpGe (Lima et al., 2018), capsulated *K. pneumoniae* LM21 (Balestrino, Ghigo, Charbonnel, Haagensen, & Forestier, 2008), *P. aeruginosa* PT531 (Cosson et al., 2002), *E. coli* B/r, *B. subtilis* 36.1, and *M. luteus* (Benghezal et al., 2006). To generate fluorescent *K. pneumoniae* bacteria, the KpGe strain of *K. pneumoniae* was transfected with a plasmid constitutively expressing codon-optimised yeast-enhanced GFP (ye-GFP) and conferring resistance to kanamycin. For this, ye-GFP was amplified by PCR from pZA2 (addgene 97760; using as oligos: Oligo1: ACCGAATTCATTTTGACAGCTAGCTCAGTCCTAGGTATAAT GCTAGCATTAAAGAGGAGAAATACTAGATGTCTAAAGGTGAAGAA-TTATTCACTGG and Oligo2: ATTAAGCTTTCATTTGTACAATTCATCC ATACCATGGG). The PCR fragment (765 bp) was cloned into pZA2 (*Eco*RI/*Hind*III), thus switching the IPTG inducible promotor, pLac, to the strong synthetic constitutive promoter contained in Oligo1. A flagella-less *B. subtilis* expressing mCherry (DK4214 Δhag *amyE*::$P_{hyspank}$-*mCherry spec*) was a kind gift of Professor D. Kearns (Indiana University, USA).

4.2 | Screening for growth-deficient *Dictyostelium* mutants

Dictyostelium mutants unable to grow in the presence of bacteria were isolated as described previously (Leiba et al., 2017). Briefly, *kil2* KO cells were mutagenised by restriction enzyme-mediated insertion (REMI) of the pSC plasmid, a variant of pUCBsrΔBamHI (Adachi, Hasebe, Yoshinaga, Ohta, & Sutoh, 1994) with a modified polylinker (Figure S1e). Individual mutant cells were deposited in HL5-containing 96-well plates using a cell sorter, grown for 10 days, and then tested for their ability to grow efficiently on several bacteria: *M. luteus*, *B. subtilis*, *E. coli* B/r, *K. pneumoniae* KpGe, *K. pneumoniae* LM21, and *P. aeruginosa* PT531. Mutants that grew poorly on at least one of the tested bacteria were selected and further characterized.

A KO plasmid was constructed to replace a sequence in the *lrrkA* gene with a blasticidin-resistance cassette, in WT, *kil1* KO, or *kil2* KO strains (Figure S1). Individual *lrrkA* KO clones were identified by PCR (Figure S1). At least two independent clones of each mutant were obtained and yielded identical results in this study.

4.3 | Growth of *Dictyostelium* in the presence of bacteria

Dictyostelium cells were grown in the presence of bacteria as described previously (Froquet et al., 2009; Leiba et al., 2017). Briefly, 50 μl of an overnight bacterial culture was plated on 2 ml of Standard Medium (SM, for 1 l: 10 g peptone, 1 g yeast extract, 2.2 g KH2PO4, 1 g K2HPO4, 1 g MgSO4 : 7H2O, 10g glucose) agar in each well of a 24-well plate. Then, 10, 100, 1,000, or 10,000 *Dictyostelium* cells were added on top of the bacterial lawn. Growth of *Dictyostelium* generated phagocytic plaques after 4–7 days of incubation at 21°C.

4.4 | Intracellular killing of bacteria

To visualise phagocytosis and intracellular killing of individual bacteria, *K. pneumoniae* bacteria constitutively expressing a fluorescent GFP were mixed with *Dictyostelium* cells at a ratio of 3:1 in phosphate buffer (PB: 2 mM of Na_2HPO_4 and 14.7 mM of KH_2PO_4, pH 6.0) supplemented with 100 mM of sorbitol, deposited on an eight-well slide (Ibidi μ-slide 8 well Glass Bottom, 80827) for 10 min, and then imaged every 30 s for 2 hr with a videotime lapse (Nikon Eclipse T*i*2 equipped with a DS-Qi2 camera) as described previously (Froquet et al., 2009;

Leiba et al., 2017). At each time, one picture (phase contrast and GFP fluorescence) was taken in five successive focal planes (step size 3 μm) to image the whole-cell volume. Four samples were analysed in parallel in this set-up, generating paired series of measures. The Nikon NIS software (NIS Element AR 5.02.00) was used to extract images, and FiJi (v1.52j) was used to compile and analyse movies. Survival of at least 30 phagocytosed fluorescent bacteria was computed using the Kaplan–Meier estimator. In each experiment, the area under the survival curve was calculated, and a number between 1 (very rapid killing) and 7,500 (no killing) was obtained. To compare two conditions meaningfully (e.g., mutant vs. WT or not treated vs. folate treated), at least five independent experiments were performed and compared. Statistical comparisons were done with a paired Student's *t* test.

4.5 | Sequence analysis

Domain searches were done with Interpro, TMHMM v.2.0, and SignalP v.4.1 servers. Searches for domains with a structure similar to LrrkA were done on the UniProt server using the following syntax: (ipr032675 OR ipr003591 OR ipr001611; ipr011009 OR ipr000719 OR ipr001245) NOT (keyword:transmembrane OR annotation:(type: transmem)).

4.6 | Organisation and function of endosomal and lysosomal pathways

To perform immunofluorescence analysis, 10^6 *Dictyostelium* cells were let to adhere to a glass coverslip for 30 min in HL5 medium. Cells were then fixed with 4% paraformaldehyde for 30 min, washed, permeabilised with methanol at −20°C for 2 min, and labelled with the indicated primary antibody in PBS containing 0.2% BSA for 1 hr. For this, antibodies against p80 (H161), p25 (H72; Ravanel et al., 2001), vacuolar H^+-ATPase (221-35-2), and rhesus (Benghezal et al., 2001) were used. Cells were then stained with fluorescent secondary antibodies for 1 hr and observed by LSM800 confocal microscopy (Carl Zeiss).

To determine the pH of phagosomes, we used pH-sensitive bifluorescent beads as previously described (Sattler et al., 2013). Carboxylated silica beads (3 μm; Kisker Biotech; PSI-3.0COOH) were coupled with both a green pH-sensitive fluorescent probe (FITC) and a pH-insensitive probe (Alexa 594 succinimidyl ester; Thermo Fisher A20004). They were mixed with *Dictyostelium* cells at a ratio of 5:1 in PB–sorbitol, deposited on an eight-well slide (Ibidi μ-slide 8 well Glass Bottom, 80827) for 10 min, and then imaged every 75 s for 3 hr with a videotime lapse (Nikon Eclipse T*i*2 equipped with a DS-Qi2 camera) as described above.

To measure the proteolytic activity in phagosomes, we used proteolysis-sensitive bifluorescent beads (Sattler et al., 2013). Three-micrometer carboxylated silica beads (Kisker Biotech; PSI-3.0COOH) were coupled with both a proteolysis-sensitive probe (DQ™ Green BSA; Thermo Fisher D12050) and a proteolysis-insensitive probe (Alexa 594 succinimidyl ester; Thermo Fisher A20004).

The activity of lysosomal glycosidases in cells and supernatants was measured as previously described (Le Coadic et al., 2013) using a colorimetric assay. Briefly, cells were grown to a density of 2×10^6 cells per ml. Cells and medium were separated by centrifugation (1,500 *g*, 2 min), and the glycosidase activity (*N*-acetyl-β-glucosaminidase and α-mannosidase) revealed using chromogenic substrates (*p*-nitrophenyl-*N*-acetyl-β-D-glucosamide and *p*-nitrophenyl-α-D-mannopyranoside, respectively). Release of *para*-nitrophenol upon glycolysis was measured by spectrophotometry (405 nm).

4.7 | Lysozyme activity

To measure lysozyme activity, 2.5×10^8 *Dictyostelium* cells were washed twice in PB buffer and lysed with 600 μl of lysis buffer (50 mM of sodium PB pH 3, 0.5% Triton X-100, 20 μg ml^{-1} of leupeptin, 10 μg ml^{-1} of aprotinin, and 18 μg ml^{-1} of phenylmethylsulfonyl fluoride [PMSF]). The suspension was centrifuged (30,000 *g* during 10 min at 4°C), and the supernatant was collected and diluted in lysis buffer. Muramidase activity was assessed by mixing in a microtitre plate 100 μl of cell lysate with 100 μl of heat-killed *Micrococcus lysodeikticus* (Sigma) suspended in 50 mM of PB (pH 3) to a final optical density at 450 nm of 0.5. The decrease in turbidity (optical density at 450 nm) after 2 hr of incubation at 21°C was measured with a spectrophotometer plate reader and used to determine the muramidase activity of *lrrk*A KO cells relative to their WT counterparts.

4.8 | Autophosphorylation of LrrkA

4.8.1 | Construction of vectors for expression of tagged LrrkA proteins

A DNA fragment corresponding to the entire open reading frame of *lrrkA* was amplified by PCR using cDNAs as template. The amplified fragment was subcloned into pCR-Blunt II-TOPO (Invitrogen). The coding sequence was then subcloned in pLD1ΔBX-myc (Kawata et al., 2015) to yield an expression vector encoding LrrkA tagged with the myc epitope.

For point mutation of the conserved ATP-binding site (Hanks & Hunter, 1995; lysine residue at 878) of the LrrkA kinase domain, an inverse PCR was performed with KOD plus Mutagenesis Kit (TOYOBO, Osaka, Japan) according to the manufacturer's instruction. The LrrkA (K878A) fragment was purified and ligated as above into pLD1ΔBX-myc. The resultant vectors were transformed into *lrrkA* KO cells to produce LrrkA–Myc and LrrkA (K878A)–Myc, a kinase-dead form of LrrkA.

Immunoprecipitation of Myc-tagged LrrkA was performed as previously described (Araki et al., 1998): Cells (6.0×10^8) were washed twice in KK2 buffer (16.5 mM of KH_2PO_4 and 3.8 mM of K_2HPO_4, pH 6.2), suspended in KK2 buffer at a density of 2×10^7 cells per ml, and shaken for 4 hr at 150 r.p.m., followed by addition of cAMP (Tokyo chemical industry, Tokyo, Japan) to achieve a final concentration of 5 mM, and further shaken for 15 min. Cells were harvested and lysed in 6 ml of mNP40 lysis buffer (50 mM of Tris–HCl (pH 8.0), 150 ml of NaCl, 1.0% (v/v) Nonidet P-40, 50 mM of NaF, 2 mM of EDTA (pH 8.0), 2 mM of Na pyrophosphate, 2 mM of benzamidine, 1 μg/ml of pepstatin, 1 mM of PMSF, and complete EDTA-free protease inhibitor mixture [Roche Diagnostics]) for 10 min on ice. After preclearing by centrifugation, the supernatant was incubated with anti-Myc antibody for 2–3 hr at 4°C with gentle rocking, followed by additional 2–3 hr of incubation with Dynabeads Protein-G (Thermo Fisher Scientific). Alternatively, the supernatant was directly incubated with anti-Myc tag magnetic beads (M047-9, MBL International Co.) for 2 hr. Beads were washed four times in mNP40 buffer, and proteins were eluted by boiling in SDS gel sample buffer and then subjected to Western blot analysis.

The primary antibodies used in the experiments were anti-phosphotyrosine antibody 4G10 (Merck Millipore) for general phosphotyrosine modification, anti-phosphoserine antibody A8G9 (Abnova), and anti-Myc antibody 9E10 (Wako Pure Chemical, Osaka, Japan) for Myc-tagged proteins. Alkaline phosphatase-conjugated anti-mouse IgG (H + L) antibody (S372B, Promega) or anti-rabbit IgG (Fc) antibody (S373B, Promega) was used as the secondary antibody for Western blot analysis. Proteins were detected using the Western Blue® Stabilized Substrate for Alkaline Phosphatase (S3841, Promega).

ORCID

Jade Leiba https://orcid.org/0000-0001-8751-1169
Takefumi Kawata https://orcid.org/0000-0002-3685-4492
Pierre Cosson https://orcid.org/0000-0002-4881-0358

REFERENCES

Adachi, H., Hasebe, T., Yoshinaga, K., Ohta, T., & Sutoh, K. (1994). Isolation of *Dictyostelium discoideum* cytokinesis mutants by restriction enzyme-mediated integration of the blasticidin S resistance marker. *Biochem Biophys Res Commun*, *205*(3), 1808–1814.

Araki, T., Gamper, M., Early, A., Fukuzawa, M., Abe, T., Kawata, T., … Williams, J. G. (1998). Developmentally and spatially regulated activation of a *Dictyostelium* STAT protein by a serpentine receptor. *EMBO J*, *17*(14), 4018–4028. https://doi.org/10.1093/emboj/17.14.4018

Balestrino, D., Ghigo, J. M., Charbonnel, N., Haagensen, J. A., & Forestier, C. (2008). The characterization of functions involved in the establishment and maturation of *Klebsiella pneumoniae* in vitro biofilm reveals dual roles for surface exopolysaccharides. *Environ Microbiol*, *10*(3), 685–701. https://doi.org/10.1111/j.1462-2920.2007.01491.x

Benghezal, M., Fauvarque, M. O., Tournebize, R., Froquet, R., Marchetti, A., Bergeret, E., … Cosson, P. (2006). Specific host genes required for the killing of *Klebsiella* bacteria by phagocytes. *Cell Microbiol*, *8*(1), 139–148. https://doi.org/10.1111/j.1462-5822.2005.00607.x

Benghezal, M., Gotthardt, D., Cornillon, S., & Cosson, P. (2001). Localization of the Rh50-like protein to the contractile vacuole in *Dictyostelium*. *Immunogenetics*, *52*(3-4), 284–288. https://doi.org/10.1007/s002510000279

Charette, S. J., Mercanti, V., Letourneur, F., Bennett, N., & Cosson, P. (2006). A role for adaptor protein-3 complex in the organization of the endocytic pathway in *Dictyostelium*. *Traffic*, *7*(11), 1528–1538. https://doi.org/10.1111/j.1600-0854.2006.00478.x

Cornillon, S., Pech, E., Benghezal, M., Ravanel, K., Gaynor, E., Letourneur, F., … Cosson, P. (2000). Phg1p is a nine-transmembrane protein superfamily member involved in *Dictyostelium* adhesion and phagocytosis. *J Biol Chem*, *275*(44), 34287–34292. https://doi.org/10.1074/jbc.M006725200

Cosson, P., & Soldati, T. (2008). Eat, kill or die: When amoeba meets bacteria. *Curr Opin Microbiol*, *11*(3), 271–276. https://doi.org/10.1016/j.mib.2008.05.005

Cosson, P., Zulianello, L., Join-Lambert, O., Faurisson, F., Gebbie, L., Benghezal, M., … Kohler, T. (2002). *Pseudomonas aeruginosa* virulence analyzed in a *Dictyostelium discoideum* host system. *J Bacteriol*, *184*(11), 3027–3033. https://doi.org/10.1128/jb.184.11.3027-3033.2002

Dias, M., Brochetta, C., Marchetti, A., Bodinier, R., Bruckert, F., & Cosson, P. (2016). Role of SpdA in cell spreading and phagocytosis in *Dictyostelium*. *PLoS One*, *11*(8), e0160376. https://doi.org/10.1371/journal.pone.0160376

Dunn, J. D., Bosmani, C., Barisch, C., Raykov, L., Lefrancois, L. H., Cardenal-Munoz, E., … Soldati, T. (2017). Eat prey, live: *Dictyostelium discoideum* as a model for cell-autonomous defenses. *Front Immunol*, *8*, 1906.

Froquet, R., Lelong, E., Marchetti, A., & Cosson, P. (2009). *Dictyostelium discoideum*: A model host to measure bacterial virulence. *Nat Protoc*, *4*(1), 25–30. https://doi.org/10.1038/nprot.2008.212

Gomez-Suaga, P., Luzon-Toro, B., Churamani, D., Zhang, L., Bloor-Young, D., Patel, S., … Hilfiker, S. (2012). Leucine-rich repeat kinase 2 regulates autophagy through a calcium-dependent pathway involving NAADP. *Hum Mol Genet*, *21*(3), 511–525. https://doi.org/10.1093/hmg/ddr481

Hanks, S. K., & Hunter, T. (1995). Protein kinases 6. The eukaryotic protein kinase superfamily: Kinase (catalytic) domain structure and classification. *FASEB J*, *9*(8), 576–596.

Hartlova, A., Herbst, S., Peltier, J., Rodgers, A., Bilkei-Gorzo, O., Fearns, A., … Gutierrez, M. G. (2018). LRRK2 is a negative regulator of *Mycobacterium tuberculosis* phagosome maturation in macrophages. *EMBO J*, *37*(12), e98694.

Kawata, T., Nakamura, Y., Saga, Y., Iwade, Y., Ishikawa, M., Sakurai, A., & Shimada, N. (2015). Implications of expansin-like 3 gene in *Dictyostelium* morphogenesis. *Springerplus*, *4*, 190.

Le Coadic, M., Froquet, R., Lima, W. C., Dias, M., Marchetti, A., & Cosson, P. (2013). Phg1/TM9 proteins control intracellular killing of bacteria by determining cellular levels of the Kil1 sulfotransferase in *Dictyostelium*. *PLoS One*, *8*(1), e53259.

Leiba, J., Sabra, A., Bodinier, R., Marchetti, A., Lima, W. C., Melotti, A., … Cosson, P. (2017). Vps13F links bacterial recognition and intracellular killing in *Dictyostelium*. *Cell Microbiol*, *19*(7), e12722.

Lelong, E., Marchetti, A., Gueho, A., Lima, W. C., Sattler, N., Molmeret, M., … Cosson, P. (2011). Role of magnesium and a phagosomal P-type ATPase in intracellular bacterial killing. *Cell Microbiol*, *13*(2), 246–258. https://doi.org/10.1111/j.1462-5822.2010.01532.x

Lill, C. M. (2016). Genetics of Parkinson's disease. *Mol Cell Probes*, *30*(6), 386–396.

Lima, W. C., Pillonel, T., Bertelli, C., Ifrid, E., Greub, G., & Cosson, P. (2018). Genome sequencing and functional characterization of the non-pathogenic *Klebsiella pneumoniae* KpGe bacteria. *Microbes Infect.*, *20*(5), 293–301.

Marchetti, A., Lelong, E., & Cosson, P. (2009). A measure of endosomal pH by flow cytometry in *Dictyostelium*. *BMC Res Notes*, *2*, 7.

Mori, M., Mode, R., & Pieters, J. (2018). From phagocytes to immune defense: Roles for Coronin proteins in *Dictyostelium* and mammalian immunity. *Front Cell Infect Microbiol*, *8*, 77.

Muller, I., Subert, N., Otto, H., Herbst, R., Ruhling, H., Maniak, M., & Leippe, M. (2005). A *Dictyostelium* mutant with reduced lysozyme levels compensates by increased phagocytic activity. *J Biol Chem*, *280*(11), 10435–10443. https://doi.org/10.1074/jbc.M411445200

Nasser, W., Santhanam, B., Miranda, E. R., Parikh, A., Juneja, K., Rot, G., … Kuspa, A. (2013). Bacterial discrimination by dictyostelid amoebae reveals the complexity of ancient interspecies interactions. *Curr Biol*, *23*(10), 862–872.

Pan, M., Xu, X., Chen, Y., & Jin, T. (2016). Identification of a chemoattractant G-protein-coupled receptor for folic acid that controls both chemotaxis and phagocytosis. *Dev Cell*, *36*(4), 428–439. https://doi.org/10.1016/j.devcel.2016.01.012

Ravanel, K., de Chassey, B., Cornillon, S., Benghezal, M., Zulianello, L., Gebbie, L., … Cosson, P. (2001). Membrane sorting in the endocytic and phagocytic pathway of *Dictyostelium discoideum*. *Eur J Cell Biol*, *80*(12), 754–764. https://doi.org/10.1078/0171-9335-00215

Sattler, N., Monroy, R., & Soldati, T. (2013). Quantitative analysis of phagocytosis and phagosome maturation. *Methods Mol Biol*, *983*, 383–402. https://doi.org/10.1007/978-1-62703-302-2_21

Stuelten, C. H., Parent, C. A., & Montell, D. J. (2018). Cell motility in cancer invasion and metastasis: Insights from simple model organisms. *Nat Rev Cancer*, *18*(5), 296–312.

Wang, X., Yan, M. H., Fujioka, H., Liu, J., Wilson-Delfosse, A., Chen, S. G., … Zhu, X. (2012). LRRK2 regulates mitochondrial dynamics and function through direct interaction with DLP1. *Hum Mol Genet*, *21*(9), 1931–1944.

Wauters, L., Versees, W., & Kortholt, A. (2019). Roco proteins: GTPases with a baroque structure and mechanism. *Int J Mol Sci*, *20*(1), 147.

SUPPORTING INFORMATION

Additional supporting information may be found online in the Supporting Information section at the end of the article.

How to cite this article: Bodinier R, Leiba J, Sabra A, et al. LrrkA, a kinase with leucine-rich repeats, links folate sensing with Kil2 activity and intracellular killing. *Cellular Microbiology*. 2020;22:e13129. https://doi.org/10.1111/cmi.13129

3. Manuscript: LrrkA IC killing supplementary data

Figure S1. **Isolation and generation of *lrrkA* KO cells.**
(A) Schematic representation of the lrrkA insertional mutant obtained by REMI mutagenesis, with the mutagenic pSC plasmid inserted 1'782 nucleotides (nt) after the start codon of lrrkA. The site of insertion was identified by digestion of genomic DNA with ClaI, which allowed the recovery of the mutagenic plasmid with the genomic flanking regions of lrrkA. (B) Schematic representation of the lrrkA gene in WT and in KO cells. To create lrrkA KO cells, we deleted 880 nt of the genomic sequence, 1'048 nt downstream of the lrrkA start codon and replaced this portion with a blasticidin resistance cassette by homologous recombination. Arrows indicate the positions of the oligonucleotides used to identify KO cells. (C-D) Identification of lrrkA KO cells was done by PCR using distinct pairs of oligonucleotides to verify both loss and gain of signal. Three independent lrrkA KO clones were identified. (E) Structure of the pSC plasmid. The overall structure of the plasmid is indicated, as well as the sequence of the cloning site.

Figure S2. **Detailed structure of all Dictyostelium LRR kinase proteins.** The main functional domains present in each protein are indicated. Note that Roco7 is strictly speaking not an LRR kinase, since it lacks LRRs. The structure of the human LRRK1 and 2 is also shown for comparison. Domains were drawn using "Illustrator for Biological Sequences" (http://ibs.biocuckoo.org).

Figure S3. LrrkA is capable of self-phosphorylation on a serine residue.
Cells expressing either LrrkA-Myc (WT) or LrrkA(K877A)-Myc were harvested and starved in KK2 buffer for 4 h. After starvation, cAMP was added and incubated further 15 min. Myc-tagged LrrkA was immunoprecipitated with the 9E10 anti-myc antibody, and the precipitated samples were subjected to Western blot analysis. The blot was probed with anti-phosphoserine antibody A8G9 (upper row; pSer), anti-phosphotyrosine antibody 4G10 (middle row; pTyr), or 9E10 (lower row; c-Myc).

Figure S4. Intracellular killing of *B. subtilis* is unaffected in *lrrkA* KO cells.
Dictyostelium cells were incubated with mCherry-expressing *B. subtilis* PB-sorbitol for 2 h. Cells were observed by phase contrast and fluorescence microscopy, and the ingestion and intracellular killing of *Bs* monitored. (A) The probability of bacterial survival following ingestion is represented as a Kaplan-Meyer estimator for one experiment in WT cells (n=91 ingested bacteria) (white squares) and *lrrkA* KO cells (n=76) (black squares). (B) For three independent experiments, the survival of bacteria was determined by measuring the area under the survival curve from 0 to 75 min. Intracellular killing was not different in WT and *lrrkA* KO cells (Wilcoxon matched-pairs rank test, N=3, p=0.75)

Figure S1.

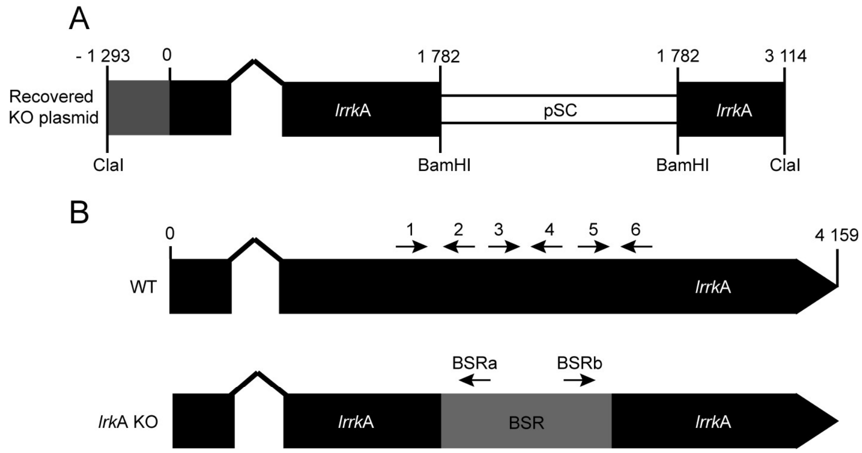

C

Oligos	Sequence
1	GATGCTTCATGAAGAAGCAGAG
2	GATTGGCTGATAGATCAAGATCACG
3	CGTGATCTTGATCTATCAGCCAATC
4	ATTGGTGGAAGTGCAGGGTTAACA
5	GAGGAACAGAAGTAGCAGTGAAAATGC
6	TTGGTGACCCAGTTTGTTGTAGTTG
BSRa	TCAAAAAGATAAAGCTGACCCGAAAGC
BSRb	TTCAAATAATAATTAACCAACCCAAG

	Oligos pair	Size WT (bp)	Size KO (bp)
Loss of signal	1+2	590	0
	3+4	515	0
	5+6	1152	0
Gain of signal	1+BSRa	0	638
	BSRb+6	0	1187

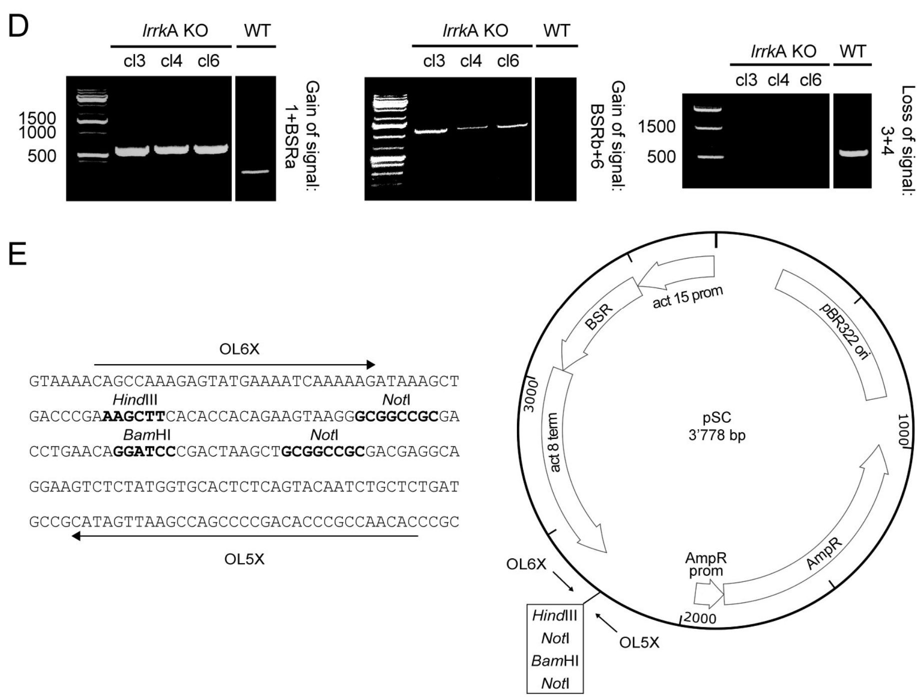

Figure S2.

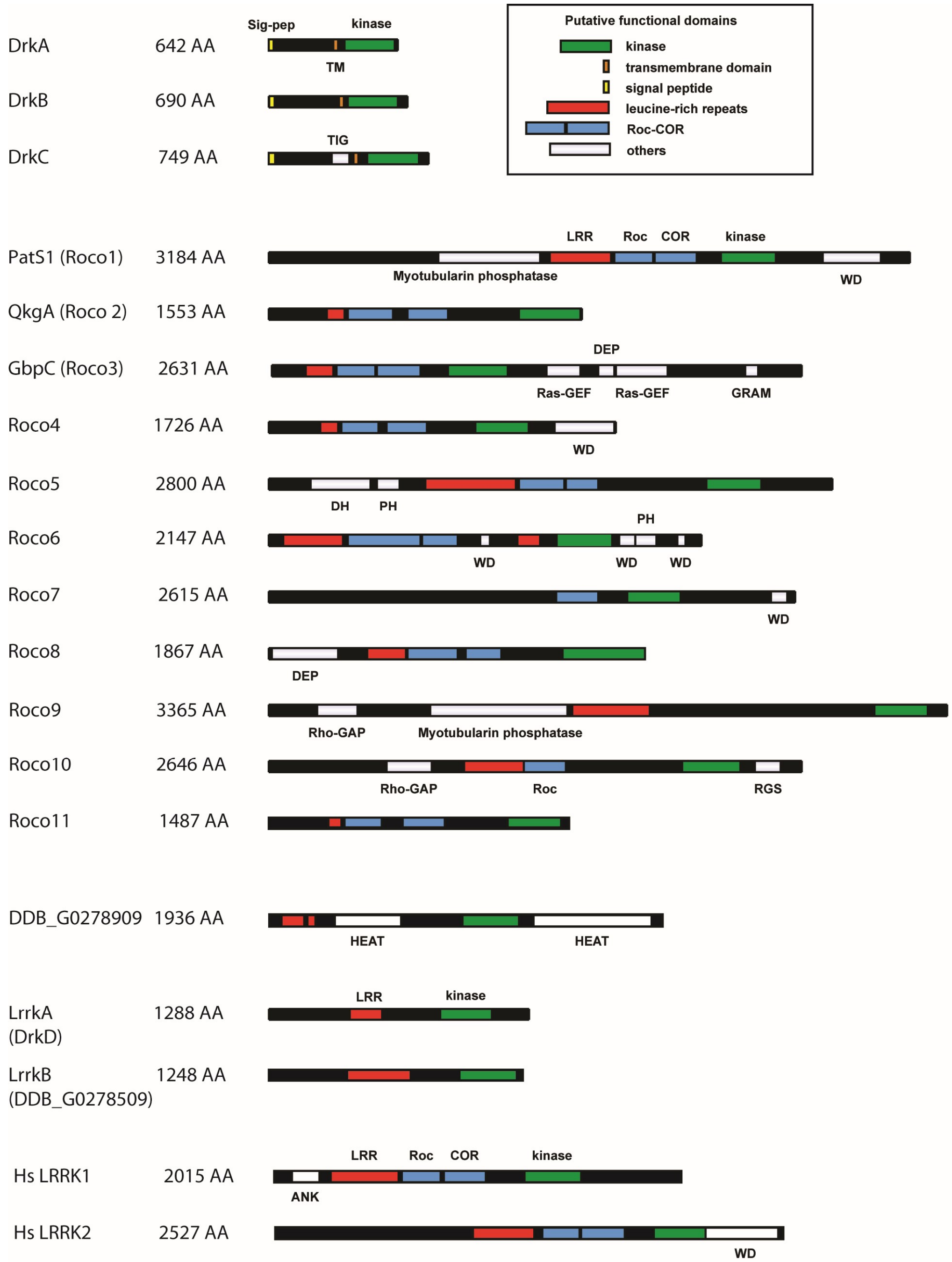
Putative functional domains
kinase
transmembrane domain
signal peptide
leucine-rich repeats
Roc-COR
others
DrkA 642 AA
Sig-pep
kinase
TM
DrkB 690 AA
DrkC 749 AA
TIG
PatS1 (Roco1) 3184 AA
LRR
Roc
COR
kinase
Myotubularin phosphatase
WD
QkgA (Roco 2) 1553 AA
GbpC (Roco3) 2631 AA
DEP
Ras-GEF
Ras-GEF
GRAM
Roco4 1726 AA
WD
Roco5 2800 AA
DH
PH
Roco6 2147 AA
PH
WD
WD
WD
Roco7 2615 AA
WD
Roco8 1867 AA
DEP
Roco9 3365 AA
Rho-GAP
Myotubularin phosphatase
Roco10 2646 AA
Rho-GAP
Roc
RGS
Roco11 1487 AA
DDB_G0278909 1936 AA
HEAT
HEAT
LrrkA (DrkD) 1288 AA
LRR
kinase
LrrkB (DDB_G0278509) 1248 AA
Hs LRRK1 2015 AA
LRR
Roc
COR
kinase
ANK
Hs LRRK2 2527 AA
WD

Figure S3.

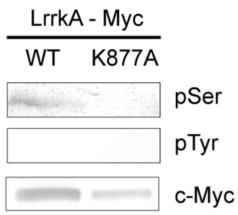

Figure S4.

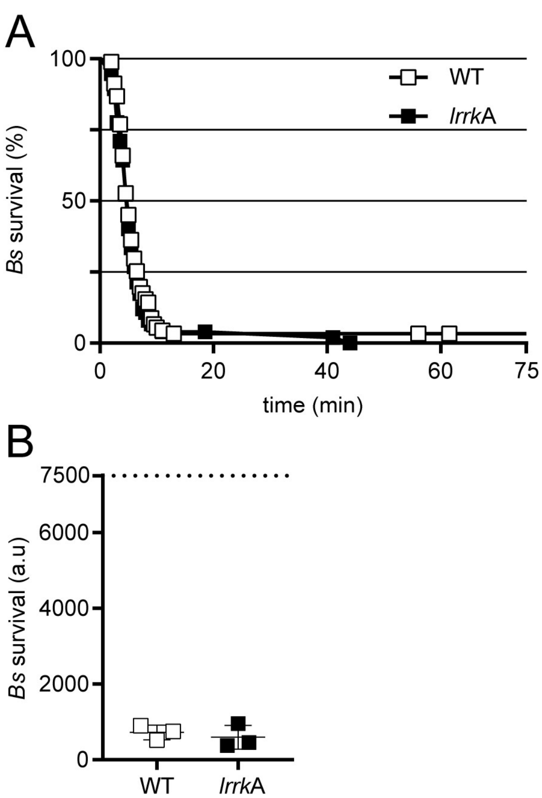

III. LrrkA is a folate-sensitive motility switch

1. LrrkA regulates multiple cellular functions.

In this second study on LrrkA, we focused on cellular motility and phagocytosis. *LrrkA* KO cells exhibit no major alteration in the spatial distribution of the actin cytoskeleton or in the organization of the endocytic pathway. Yet we observed that these cells showed altered kinetics of phagocytosis and cellular motility. Our results suggest that LrrkA acts as a switch between a folate activated state and a resting state. This allows cells to regulate in a coordinated manner phagocytosis, cellular motility and intracellular killing of ingested bacteria in response to extracellular folate. It will be interesting in the future to test if LrrkA is necessary for response to AMPc, another chemoattractant, to test whether LrrkA is a shared element in folate and cAMP signalling cascades.

The main highlights of this study are:

- *lrrkA* KO cells phagocytose more efficiently than WT cells. This phenotype is not due to impaired quorum sensing. Rather it is cell-autonomous and represents a dysregulation of the pathway allowing folate to regulate phagocytosis and cellular motility.
- Control of gene transcription by folate stimulation is independent of LrrkA.
- TalinA and MyoVII, two cytoskeletal proteins which interact together, are involved in the pathway linking folate sensing by Far1 and cellular motility.

This study increases the number of potential LrrkA targets. In the future it will be interesting to study the dynamics of the actin cytoskeleton in cells exposed to folate, in order to better define how LrrkA regulates cellular motility and phagocytosis.

2. LrrkA relays folate activation and controls cell motility and phagocytosis

Status: *In preparation*

Romain Bodinier[1], Ayman Sabra[1], Jade Leiba[1], Anna Marchetti[1], Otmane Lamrabet[1], Vedrana F. Mileta[2], Igor Weber[2], Pierre Cosson[1]

Affiliations:
[1]Department of Cell Physiology and Metabolism, Faculty of Medicine, University of Geneva, Geneva, Switzerland
[2] Ruder Boskovic Institute, Division of Molecular Biology, Zagreb, Croatia
‡Author for correspondence: pierre.cosson@unige.ch

Key Words: LrrkA, DrkD, phagocytosis, motility, *Dictyostelium*
Running title: *Dictyostelium* LrrkA, a folate-regulated inhibitor of motility

Personal contribution:

Figure + legends:

Object:	Analysis	Quantification	Figure	Text	Revision
Fig1	AS/JL/AM/**RB**	AS/JL/AM/**RB**	**RB**	**RB**	AS/JL/AM/**RB**
Fig5	**RB**	**RB**	**RB**	**RB**	**RB**/PC
Fig7	**RB**	**RB**	**RB**	**RB**	**RB**/PC
Fig10			**RB**/PC	**RB**/PC	**RB**/PC
Fig5	JL/**RB**	JL/**RB**	**RB**	**RB**	**RB**/PC

Manuscript:
Introduction/Discussion**:**

Object:	Text	Revision
Abstract	**RB**/PC	JL/AS/**RB**/PC
Introduction	**RB**/PC	JL/AS/**RB**/PC
Discussion	**RB**/PC	JL/AS/**RB**/PC

Materials & Methods:

Object:	Text	Revision
All / except VM: Motility, AS/AM: Cell autonomous experiment and OL:RT-PCR	**RB**	**RB**/PC

Results:

Object:	Text	Revision
ALL	**RB**/PC	**RB**/PC

Summary

LrrkA is a *Dictyostelium discoideum* kinase with leucine-rich repeats. It has been suggested that LrrkA stimulates Kil2 and intra-phagosomal killing of ingested bacteria in response to folate. In this study we show that genetic inactivation of *lrrkA* causes a previously unnoticed phenotype: *lrrkA* KO cells exhibit enhanced phagocytosis and cell motility. This phenotype is cell autonomous and is not due to an abnormal response to inhibitory quorum-sensing factors secreted by *D. discoideum* in its medium. Parental *D. discoideum* show enhanced phagocytosis and motility when exposed to folate, but this stimulation is lost in *lrrkA* KO cells, as well as in *far1*, *myoVII* and *talA* KO cells. On the contrary, *lrrkA* KO cells regulate gene transcription in response to folate in a manner indistinguishable from WT cells. Overall our results suggest the existence of a folate signaling pathway inhibiting motility and phagocytosis and implicating Far1 (the surface folate receptor), LrrkA, MyoVII and TalA. In non-stimulated cells LrrkA inhibits cell motility and phagocytosis, while in the presence of folate this inhibition is lost and LrrkA stimulates intracellular killing. This branching signaling pathway provides a mechanism by which *D. discoideum* encountering bacterially secreted folate migrates, engulfs and kills bacteria more efficiently.

Introduction

The initial contact between a cell and a substrate is a key element that determines the ability of the cell to adhere and spread on the substrate, and depending on its size to ingest it by phagocytosis (if it is small enough), or to move on its surface [1]. Cell adhesion, spreading and motility involve massive changes in cell shape, which are carried out by a dynamic reorganization of the actin cytoskeleton. Actin-driven changes in cell shape can also lead to the enclosure of a large volume of extracellular medium, and its capture within an intracellular macropinosome, although in this situation the process of reshaping and ingestion is not driven by adhesion to a substrate [2].

Phagocytosis is used by both mammalian cells (e.g. neutrophils and macrophages) and environmental amoebae as a mean to ingest microorganisms, in particular bacteria. Ingested bacteria are then transferred into acidic phago-lysosomes, where they are killed and digested. In mammals one of the main functions of phagocytic cells is to destroy invading microorganisms and to protect the body against infections. Amoebae use phagocytosis to feed upon other microorganisms. Phagocytosis, phagosome maturation and intracellular bacterial killing are complex processes involving multiple gene products. Our vision of the role of individual gene products in these processes is largely incomplete.

Dictyostelium discoideum has been an instrumental model to study the molecular mechanisms controlling the dynamics of the actin cytoskeleton, phagocytosis and intracellular killing of bacteria [3-5]. Due to the relative ease with which these haploid cells can be grown, observed, and genetically altered, they have proven instrumental to discover and analyze the role of multiple gene products in various facets of these cellular processes. For example, characterization of adhesion-defective *Dictyostelium* mutant cells led to the discovery that SibA, a molecule with integrin features, is a surface adhesion molecule essential for efficient phagocytosis of certain substrates [6]. Not all adhesion-defective mutants reveal gene products playing a direct role in cellular adhesion: for example Phg1A controls cell surface expression of SibA, and its genetic inactivation thus results indirectly in a cell adhesion defect [7]. To the best of our knowledge, molecular mechanisms involved in ingestion and killing of bacteria are largely similar in *Dictyostelium* and mammalian cells [3].

One relatively easy way to identify *Dictyostelium* mutants with interesting phenotypic defects is to test their ability to feed upon bacteria. Defects in various facets of phagocytosis (e.g. spreading to a substrate, intracellular bacterial killing...) were indeed found to reduce the ability of *Dictyostelium* cells to feed upon various bacteria.

This has been used successfully as a means to identify gene products involved in cell spreading on a substrate and phagocytosis like SpdA [8], or intracellular killing like Kil2 [9].

In a recent study, we characterized a new *Dictyostelium* mutant unable to feed upon *Bacillus subtilis* bacteria. *LrrkA* KO cells were initially identified in a random screen as mutants exhibiting defective ability to grow on a lawn of gram-positive *B. subtilis* (Bodinier et al., 2020). The *lrrkA* gene, affected in this mutant, encodes a kinase associated with leucine-rich repeats. Our earlier results revealed that a signaling pathway implicating Far1 (the cell surface folate receptor), LrrkA and Kil2 (a putative magnesium transporter in the phagosomal membrane) stimulates intracellular killing in response to extracellular folate. In this study we show that LrrkA also controls phagocytosis and cell motility. Since LrrkA is endowed with the ability to control both phagocytosis, cell motility and intracellular killing it has the capacity to co-regulate these functions.

Results

***lrrkA* KO cells phagocytose particles more efficiently than WT cells**

LrrkA KO cells were initially shown to present a defect in intra-phagosomal killing (Bodinier et al., 2020). Beyond this defect, *lrrkA* KO cells did not exhibit any major alteration of the structure of the endocytic pathway (Bodinier et al., 2020). The overall structure of endocytic compartments appeared unaffected, as well as the acidic pH of lysosomes (Bodinier et al., 2020), but this left open the possibility that kinetic parameters such as endocytosis were modified. In order to test the ability of *lrrkA* KO cells to perform phagocytosis, WT or mutant cells were incubated in the presence of fluorescent latex beads for 20 min in HL5 medium, and the number of internalized beads was then determined by flow cytometry (Fig. 1A). Interestingly, *lrrkA* KO cells phagocytosed beads more efficiently than WT cells (171% of WT ± 12; mean ± SEM, N=7; $p<0.01$, Mann-Whitney test). On the contrary, *lrrkA* KO cells did not ingest a fluid phase marker (fluorescent dextran) more efficiently than WT cells (104% of WT ± 14; mean ± SEM; N=7; p=0.70, Mann-Whitney test). We also assessed phagocytosis of beads over a period of 2 h, and observed that *lrrkA* KO cells ingest beads more efficiently than WT cells at all times, even after 5 min of internalization (Fig. 1B). The fact that phagocytosis is increased upon *lrrkA* genetic inactivation while macropinocytosis is not, suggests that an increase in cell size is not responsible for the increased phagocytosis. We verified this by measuring directly cell size using two different techniques: image-based analysis (Tali cytometer) and electric current exclusion (CASY analyzer). Both techniques revealed that the size of *lrrkA* KO cells was essentially identical to that of WT cells: 100% ± 0.2 (average ± SEM; n=3) for image analysis 97.6% ± 0.2 (n=3) for electric current exclusion. Staining of the actin cytoskeleton also failed to reveal any gross anomaly of the actin cytoskeleton in *lrrkA* KO cells (Fig. S1).

The increased phagocytosis of *lrrkA* KO cells is cell autonomous

Phagocytosis is a highly regulated process in *D. discoideum*. In particular, previous studies have shown that accumulation of (unidentified) quorum-sensing factors in cell culture medium can modulate significantly cell adhesion, phagocytosis and cell motility in *D. discoideum* [10, 11].
A modification in the secretion of quorum-sensing factors could in principle result in a modification of phagocytosis rates. We first studied whether the medium in which *lrrkA* KO cells grew contained more quorum-sending factors than the medium in which WT cells grew. For this we grew *lrrkA* KO or WT cells to the same density and collected the cell supernatants. WT cells were then exposed for 4 h to increasing concentrations of these two supernatants, and their rate of phagocytosis measured. The rates of phagocytosis were identical for cells exposed to supernatants from *lrrkA* KO and from WT cells (Fig. 2) indicating that both supernatants contained the same amounts of quorum-sensing factors.

We then tested whether the phenotype of *lrrkA* KO cells is cell-autonomous. For this, we co-cultured WT cells expressing GFP and *lrrkA* KO cells for 6 days. We then incubated the mixed population with rhodamine-labeled polystyrene beads and analyzed uptake of beads by flow cytometry. GFP-expressing WT cells can readily be distinguished from *lrrkA* KO cells based on the fluorescence of GFP (Fig. 3A) and the phagocytosis of beads analyzed for the two populations of cells (Fig. 3B). *LrrkA* KO cells mixed with GFP-expressing WT cells exhibited a higher level of phagocytosis (150% of WT ± 4; mean ± SEM; N=6; $p<0.01$, Mann-Whitney test) (Fig. 3C). This result confirms the fact that the phenotype of *lrrkA* KO cells is cell-autonomous and not influenced by the conditions (medium, cell density, and contact with other cells…) in which the cells are grown.

A modification in the cellular response to quorum-sensing factors could in principle result in a cell-autonomous modification of phagocytosis rates. To test this possibility, we exposed *lrrkA* KO and WT cells for 4 h to an increasing concentration of quorum-sensing factors then measured their ability to perform phagocytosis. At all concentrations of quorum-sensing factors tested, including in the absence of quorum-sensing factors, *lrrkA* KO cells phagocytosed more efficiently than WT cells (Fig. 4A). Moreover, when the rates of phagocytosis were compared between *lrrkA* KO and WT cells incubated in the same conditions, the phenotype was quantitatively virtually identical in all conditions, with *lrrkA* KO cells ingesting approximately two time more efficiently than WT cells (Fig. 4B). These observations suggest that *lrrkA* KO cells respond normally to quorum-sensing factors.

LrrkA controls interaction of *D. discoideum* with its substrate

Mutations can alter phagocytosis either by modifying the level of the phagocytic receptor(s) or by modifying the cytosolic machinery involved in phagocytosis. SibA is the phagocytic receptor responsible for phagocytosis of beads in HL5, while it is dispensable in phosphate buffer where other (unidentified) receptors are engaged (Benghezal, 2003 #20). We compared by Western blot the amount of SibA found in *lrrkA* KO and WT cells and did not detect any significant difference (Fig. S2). We then measured phagocytosis in phosphate buffer for WT or mutant cells. *LrrkA* KO cells phagocytosed more efficiently than WT cells both in HL5 medium and in phosphate buffer (Fig. 5A). Genetic inactivation of Talin A (*talA*) and Myosin VII (*myoVII*) inhibited phagocytosis in both HL5 medium and PB, while genetic inactivation of SibA inhibited phagocytosis only in HL5 (Fig. 5A).

In many mutants, alterations in the phagocytic process result from alterations in the interaction between the phagocytosed particle and the phagocytic cell. However, the phagocytic event is transient and difficult to visualize, and it is much easier to characterize the interaction of *D. discoideum* with a surface to gain an understanding of its ability to interact with a substrate. In order to measure the ability of *lrrkA* KO cells to interact tightly with their substrate, we visualized and measured their zone of contact with a glass surface by interference reflection microscopy (IRM, Fig. 5B). The contact area was larger for *lrrkA* KO cells than for WT cell, both in HL5 and in phosphate buffer (Fig. 5C). *TalA* and *myoVII* KO cells exhibited defective spreading in both HL5 and phosphate buffer, while *sibA* KO cells spread less efficiently than WT cells in HL5, but normally in phosphate buffer (Fig. 6B).

Together these results indicate that LrrkA regulates negatively the cytosolic machinery engaged in cellular adhesion and phagocytosis and is not specifically involved in the function of SibA.

***LrrkA* KO cells exhibit an increased motility**

An alteration of the interaction between cells and their substrate can modify their ability to move. We first determined the random motility of WT and *lrrkA* KO cells on a glass substrate in HL5 by taking pictures every 10 sec. This revealed a major increase in motility of *lrrkA* KO cells compared to WT cells when considering either mean square displacement (Fig. 6A) or instantaneous speed (Fig. 6B). More precisely, it is typical for *D. discoideum* cells that on short time scales they move in a rectilinear fashion, whereas on longer time scales they display typical random motility. The crossover scale between the two regimes is around 2 min and is similar for both WT and *lrrkA* KO cells. We also observed a major increase in motility of *lrrkA* KO cells compared to WT cells when analyzed in phosphate buffer (Fig. 6C).

Folate stimulates phagocytosis and motility via a Far1-LrrkA pathway

Our recent results indicated that LrrkA participates in a signaling pathway linking Far1, the folate receptor to Kil2, and allowing folate to stimulate intracellular killing (Bodinier et al., 2020). We thus tested the ability of various mutant cells to modify their motility in response to folate. For this we measured random cell motility in phosphate buffer supplemented or not with 1mM folate. As previously described (Lima, 2014 #21), folate stimulated motility of WT and of *kil2* KO cells (Fig. 7). Unstimulated *lrrkA* KO cells were more mobile than WT cells, but their motility did not increase upon addition of folate (Fig. 7). Unstimulated *far1* KO cells, devoid of folate receptor, exhibited normal motility but did not respond to the addition of folate (Fig. 7). In *talA* or *myoVII* KO cells, the unstimulated motility was reduced, and the cells failed to respond to folate (Fig. 7). Together these results suggest that LrrkA relays a folate activation signal from Far1 to TalA/MyoVII, allowing cells to increase their motility in the presence of folate.

LrrkA is dispensable for the transcriptional response to folate

We have recently studied by RNA sequencing the transcription profiles of D. discoideum cells exposed to various stimuli, in particular folate (Lamrabet et al., submitted). This allowed us to define a set of ten genes whose expression varies upon exposure to folate (Fig. S3). We first validated these results by preparing RNA from WT *D. discoideum* cells exposed to folate or not. This experiment confirmed that the expression of the selected set of genes is regulated by folate (Fig. S3). We then measured the expression of these genes in WT, far1 or lrrkA KO cells (Fig. 8). In *far1* KO cells, gene expression was not modified by exposure to folate, confirming that folate sensing relies critically on the Far1 receptor. On the contrary, lrrkA KO cells responded to folate in a manner indistinguishable from WT cells (Fig. 8), indicating that LrrkA does not play a critical role in gene regulation upon folate exposure.

DISCUSSION

In this study, we describe a new role for LrrkA, as a negative regulator of cell motility and phagocytosis. This inhibitory function is detected in cells growing in HL5 medium, as well as in phosphate buffer. Our results lead us to propose a model where LrrkA functions in two modes, as schematized in Fig. 9. In the absence of folate, LrrkA fails to stimulate killing. In addition, it inhibits motility and phagocytosis, as evidenced by the fact that its genetic inactivation leads to an increase in phagocytosis and motility in these conditions. In the presence of a high concentration of folate (1mM), which in the environment is secreted by bacteria, Far1 activates LrrkA thus suppressing its inhibitory effect on phagocytosis and motility and allowing it to stimulate intracellular killing via activation of Kil2. This dual role allows LrrkA to coordinate capture, internalization and killing of bacteria, and represents a mechanism for rapid adaptation to changes in the amoeba environment.

Materials and Methods

Strains and cell culture

Dictyostelium cells were grown at 21°C in HL5 medium (Froquet et al., 2009). *Dictyostelium* cells were all derived from the DH1-10 parental strain (Cornillon et al., 2000), referred to in this study as wild-type (WT). *lrrk*A KO, *far*1 KO, *kil*2 KO, *sib*A KO, *tal*A KO and *myo*VII KO were described previously (Bodinier et al., 2020; Pan et al., 2016; Lelong et al., 2011; Froquet et al., 2012; Tsujioka et al., 2008; Gebbie et al., 2004).

Phagocytosis and macropinocytosis

To measure efficiency of phagocytosis, $3x10^5$ *Dictyostelium* cells were washed once, resuspended in either 1 ml of HL5 or 1 ml of phosphate buffer (PB: 2 mM Na_2HPO_4, 14.7 mM KH_2PO_4, pH 6.5) and incubated for 30 min with 1 µl FITC latex beads (Fluoresbrite plain YG 1 micron, Polysciences). To assess macropinocytosis, cells were incubated in either HL5 or PB containing 10 µg/ml Alexa-647 Dextran (Life Technologies) for 30 min. Then, cells were washed in ice cold HL5 supplemented with 0.1% NaN_3 and internalized fluorescence was measured by flow cytometry. Mean fluorescence was plotted for each strain.
For phagocytosis kinetic measurements, cells were resuspended in 1 ml of HL5, mixed with 1 µl FITC latex beads and a 100 µl of the suspension was taken at each time point. Cells were then washed, and phagocytosis was analyzed as mentioned above.

Cell autonomous

Conditioned medium experiments: Cells incubated 4 h in conditioned medium in 6-well plates (450'000 cells per condition in 1.5ml) then recover the cells, phagocytosis 5min with beads in fresh HL5

Cell volume measurement

We measured cell size based on electric current exclusion (CASY technology), using a CASY 1 cell counter [8] as previously described [8]. The Tali image-based cytometer (ThermoFischer Scientific) was also used to measure automatically the size of cells based on pictures of cell suspension.

Motility assay

To assess the motility of *Dictyostelium* cells, 1.10^5 cells were washed once and resuspended in 1 ml PBS (PB + 100 mM Sorbitol). 100 µl was deposit in 96 wells plates with treated bottom (Greiner Bio one ref:655090). Either 100 µl of PBS or PBS + 1 mM folate was added to each well. For imaging we used a Nikon Eclipse T*i*2 equipped with a DS-Qi2 camera, and image the cells every 15 seconds for 30min. Image were analyzed with the software MetaMorph (Molecular Devices) using the "Track points" function. Measure of mean square displacement and speed plots were done in HL5.

Immunofluorescence

To perform immunofluorescence analysis, 10^6 *Dictyostelium* cells were let to adhere to a glass coverslip for 30 min in HL5 medium. Cells were then fixed with 4% paraformaldehyde for 30 min, washed, permeabilized with methanol at -20°C for 2 min and labeled with the indicated primary antibody in PB containing 0.2% bovine serum albumin for 1 h. For this, antibodies against actin were used. Cells were then stained with fluorescent secondary antibodies for 1 h and observed by LSM800 confocal microscopy (Carl Zeiss).

Cell spreading

To measure the spreading surface of *Dictyostelium* cells, $5\text{-}10.10^5$ cells were washed once and resuspended in either 1 ml HL5 or 1 ml SB. A 50 µl drop was deposited for each strain on a glass-bottom fluorodish (WPI, inc; ref: FD35-100). A Zeiss Axio Observer Z1 equipped with a Neofluar 63x / 1.25 Oil Ph3 Antiflex objective for

RICM measurement was used for imaging. The cells were imaged once after 30 min incubation in the media. Quantification of the cell speading surface was done using FiJi (v1.52j).

Western-blot

To determine the levels of cellular proteins, 1.10^6 cells were resuspended in 10 µl of sample buffer (0.103 g/ml sucrose, 5.10 mM Tris, pH 6.8, 5.10 mM EDTA, 0.5 mg/ml bromophenol blue, 2% SDS), and proteins were separated by electrophoresis on an SDS-polyacrylamide gel. Proteins were then transferred to a nitrocellulose membrane for immunodetection using anti-SibA [6], anti-TalinA [12] and anti-PDI [9] primary antibodies. Horseradish-peroxidase-coupled anti-mouse (for anti-TalinA and anti-PDI) and anti-rabbit (for anti-SibA) antibodies were used as secondary antibodies.

RT-PCR

To be completed by Otmane Lamrabet for experimental conditions. primer sequences can be found in Fig S3.

FIGURE LEGENDS

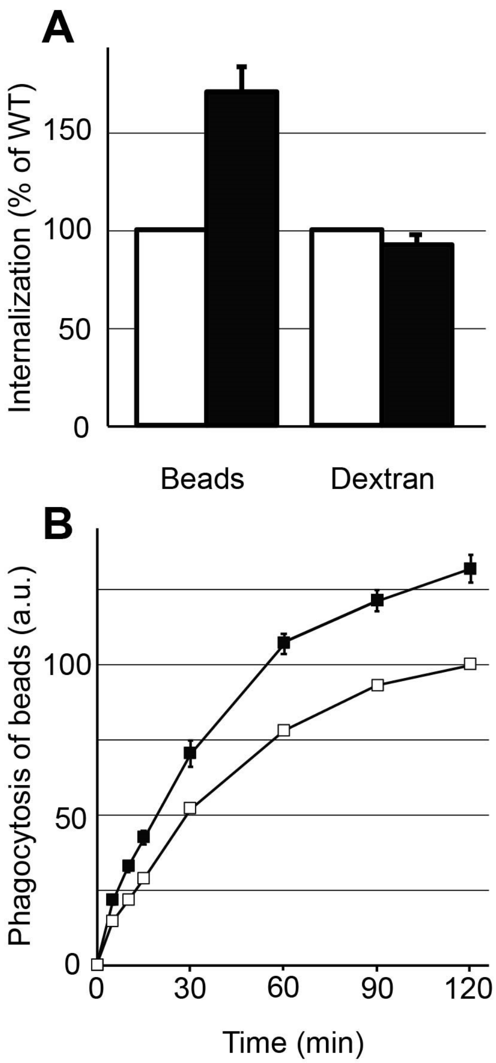

Figure 1. Genetic inactivation of *lrrkA* stimulates phagocytosis. A. *D. discoideum* cells (WT or *lrrkA* KO) were incubated for 20 min in HL5 medium containing either fluorescent polystyrene beads, or a fluorescent dextran. Internalization of beads or of dextran was measured in 7 independent experiments and averaged. B. *D. discoideum* cells (WT or *lrrkA* KO) were incubated for the indicated time in HL5 medium containing fluorescent polystyrene beads. The average and SEM at each time are indicated. *LrrkA* KO cells phagocytosed beads was significantly more than WT cells at all times ($p<0.01$, $N=9$, Mann-Whitney test).

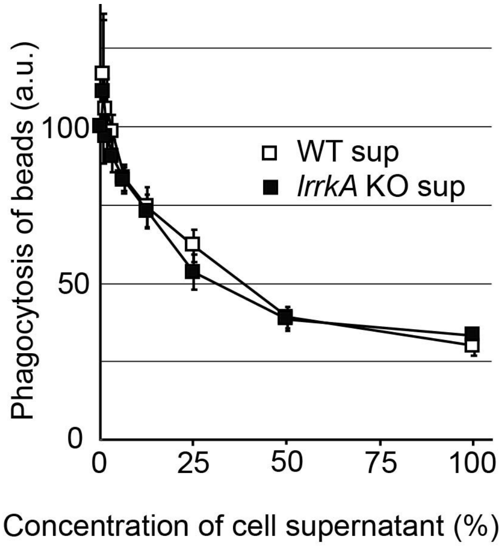

Figure 2. Secretion of quorum-sensing factors by *lrrkA* KO cells. Cell supernatants from WT or lrrkA KO cells grown at the same density were incubated with WT cells for 4 h, then they were incubated with polystyrene beads and phagocytosed measured as described in the legend to figure 1 (average ± SEM, N=3 independent experiments). Cells incubated in fresh medium phagocytosed beads approximately four times more efficiently than cells incubated in pure cell supernatants containing concentrated quorum-sensing factors. Cell supernatants diluted with fresh medium were also assessed to evaluate more precisely the quorum-sensing activity. The supernatant of *lrrkA* KO cells exhibited exactly the same inhibitory effect on phagocytosis as the supernatant of WT cells.

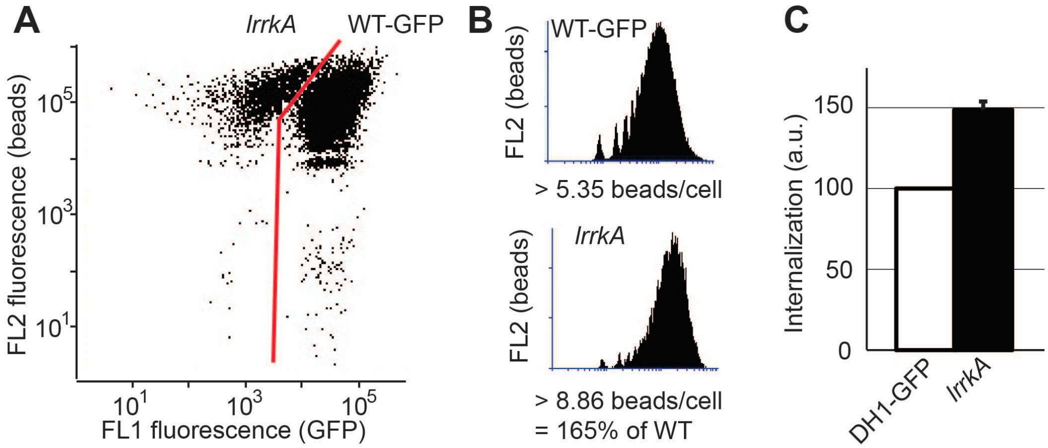

Figure 3. The phenotype of *lrrkA* KO cells is cell-autonomous. WT cells expressing GFP were mixed with *lrrkA* KO cells and co-cultured for six days. The mixed population of cells was then incubated with rhodamine-labeled polystyrene beads for 20 min, washed, and analyzed by flow cytometry. A. Based on the GFP fluorescence, WT cells were easily distinguished from lrrkA cells. B. Phagocytosis of beads was determined for WT and lrrkA KO cells. Even when mixed with WT cells, *lrrkA* KO cells exhibited significantly more phagocytic activity (average ± SEM; p<0.01, N=6, Mann-Whitney test).

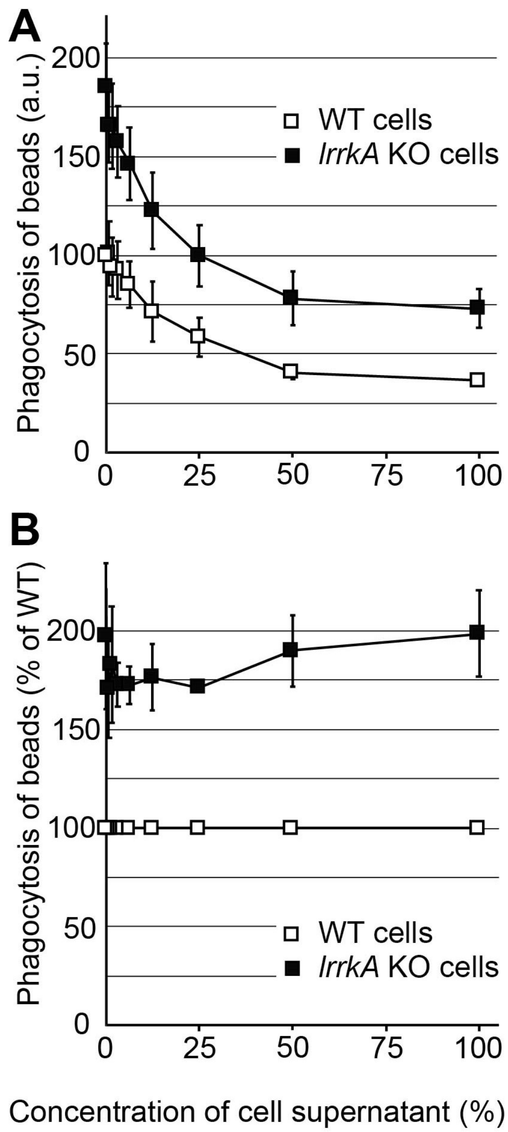

Figure 4. Response of *lrrkA* KO cells to secreted quorum-sensing factors. WT or *lrrkA* KO cells were incubated for 4 h with a cellular supernatant of WT cells. The ability of the cells to ingest polystyrene beads was then measured as described in the legend to figure 1. Both WT and *lrrkA* KO cells incubated in fresh medium phagocytosed beads more efficiently than cells incubated in pure cell supernatants containing concentrated quorum-sensing factors. At all concentrations of quorum-sensing factors, *lrrkA* KO cells phagocytosed beads more efficiently than WT cells (average ± SEM, N=3 independent experiments). B. For each condition, phagocytosis by lrrkA KO cells was represented as a percentage of WT phagocytosis in the same condition. In all conditions, *lrrkA* KO cells phagocytosed 1.5 to 2 times more beads than WT cells.

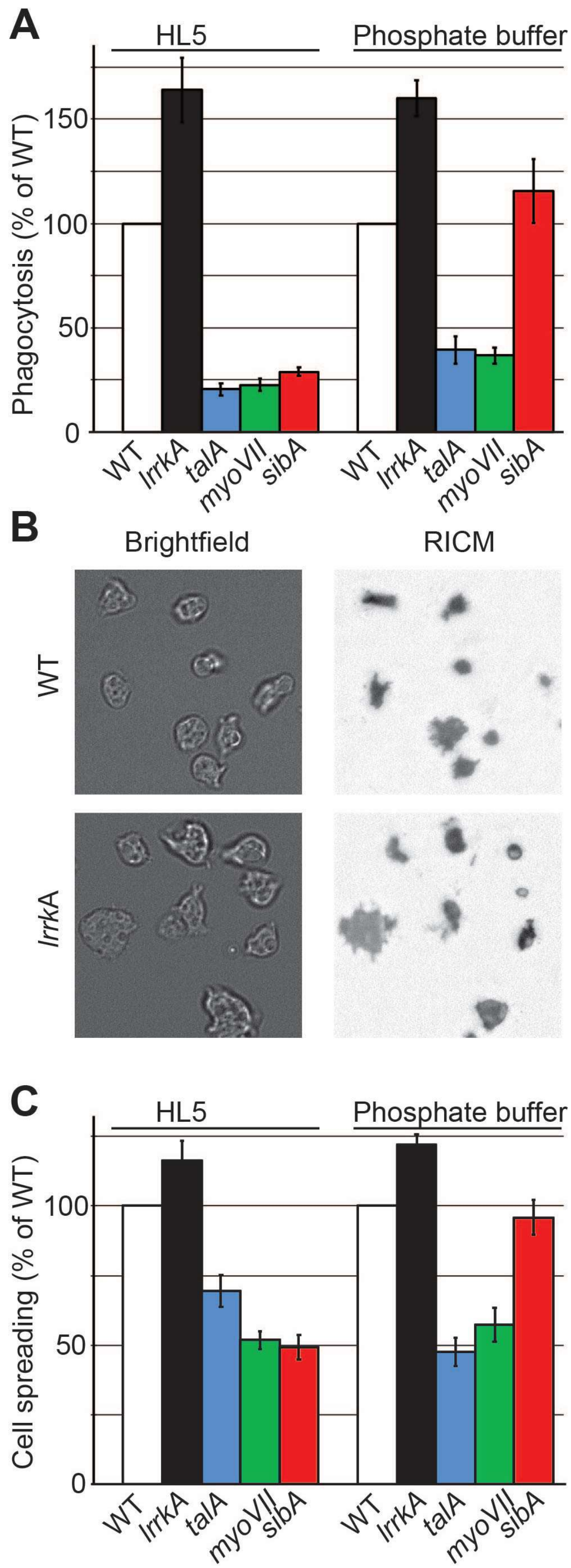

Figure 5. Genetic inactivation of lrrkA stimulates interaction with substrates in HL5 and in phosphate buffer. A. Phagocytosis of polystyrene beads was measured for the indicated mutant cells as described in the legend to figure 1. LrrkA KO cells phagocytosed more efficiently than WT cells both in HL5 and in phosphate buffer (PB). B. Brightfield and interference reflection pictures of WT and *lrrkA* KO cells (her in HL5) allow to visualize the contact area between cells and their substratum. C. Spreading of WT and mutant cells on their substrate in HL5 and in SB reflects their ability to phagocytose particles. The contact surface between WT *D. discoideum* and the glass substrate was 62 μm^2 and 87 μm^2 in HL5 and SB, respectively.

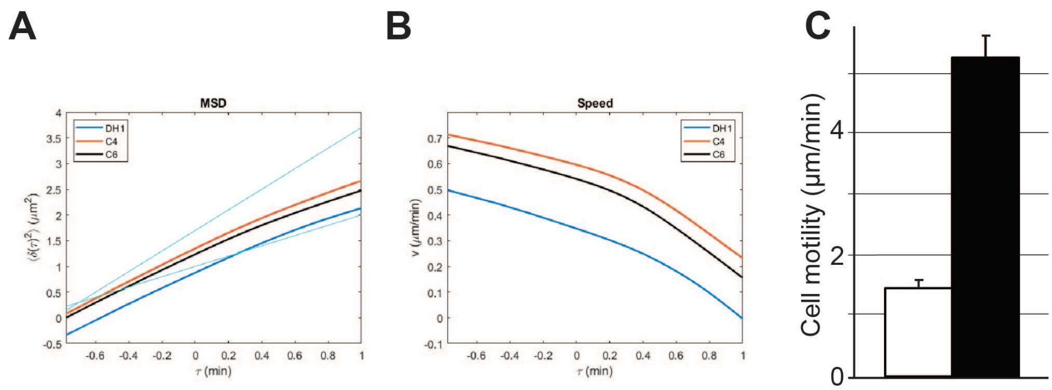

Figure 6. Cell motility is strongly increased by genetic inactivation of *lrrkA*. A. For the trajectories of more than 100 cells in 3 independent experiments the mean-square displacement was determined as a measure of the time interval. details B. details C. Random motility of WT or *lrrkA* KO cells on a substrate was measured in phosphate buffer. Motility was significantly higher in *lrrkA* KO cells than in WT cells ($p<0.01$, N=13, Mann-Whitney test)

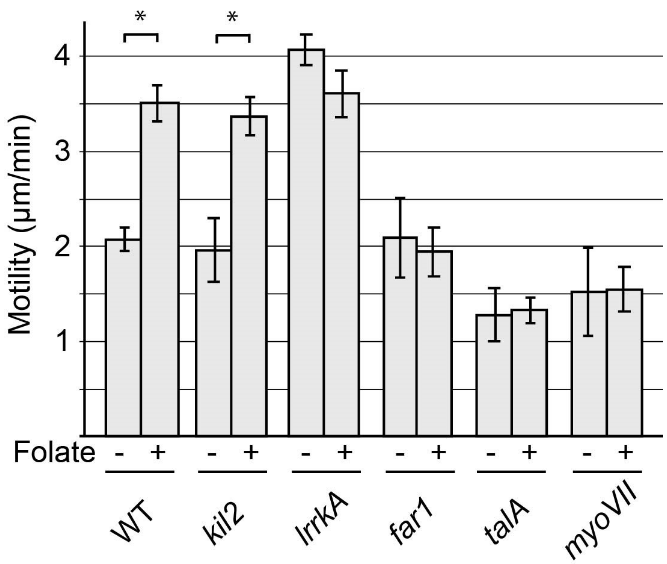

Figure 7. Stimulation of cell motility by folate is perturbed in *lrrkA* KO cells. Random motility of WT or mutant cells on a substrate was measured in the presence or absence of folate as described in the legend to figure 6. Motility increased significantly in WT cells or in *kil2* KO cells upon exposure to folate. In *lrrkA* KO cells, cell motility was high even in the absence of folate and was not further elevated upon folate treatment. In far1, talA and myoVII KO cells folate failed to stimulate cell motility. *: p<0.01, student t test. For each condition, the motility of at least 100 cells in at least 3 independent experiments was analyzed.

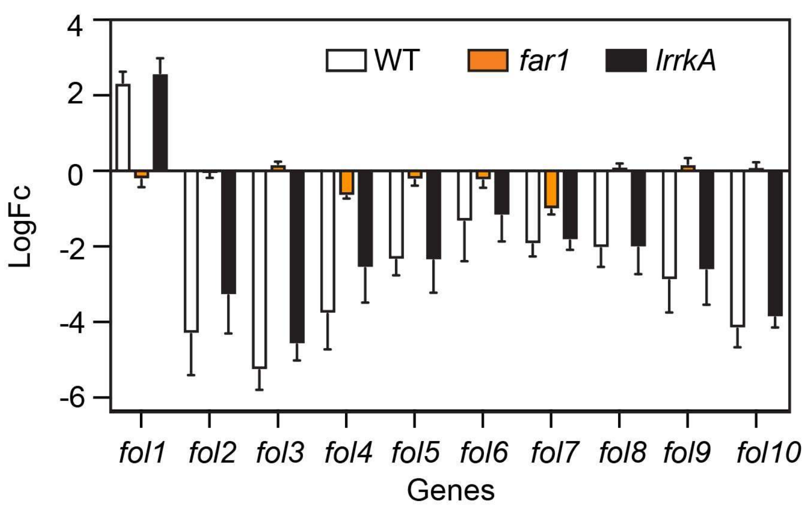

Figure 8. Folate controls gene transcription is independent of LrrkA. We measured by RT-PCR the levels of various RNAs in cells exposed or not to folate. The average and SEM of three independent experiments are shown. As previously observed, the transcription of genes *fol1*-*fol10* is altered when cells are exposed to folate. This regulation is essentially lost in *far1* KO cells. On the contrary, in *lrrkA* KO cells transcriptional response to folate is indistinguishable from that observed in WT cells. For each condition, the motility of at least 100 cells in at least 3 independent experiments was analyzed.

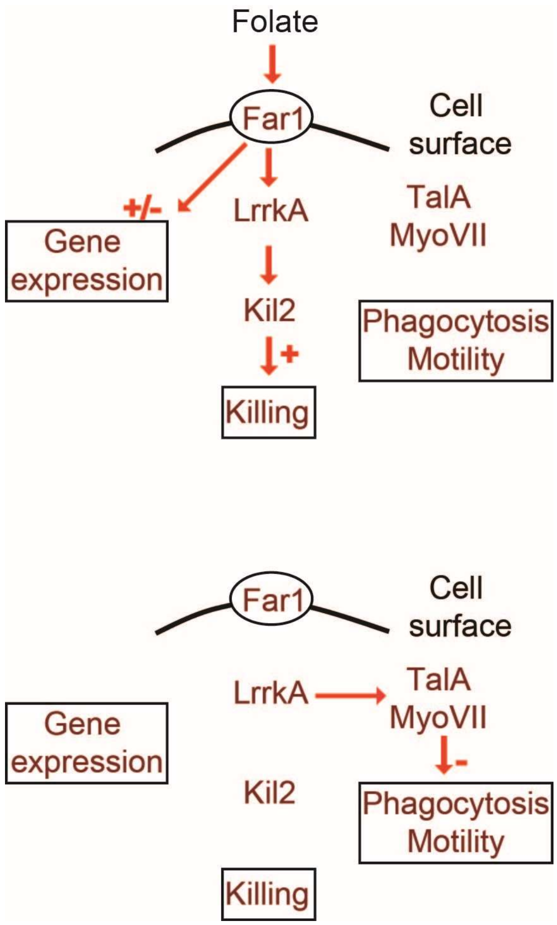

Figure 9. Cellular response to folate. This schematic overview proposes an overall interpretation of the results presented in this manuscript and in previous publications. Far1, the cell surface receptor for folate is essential for all cellular responses to folate. The LrrkA-Kil2 pathway stimulates intracellular killing in response to folate. The LrrkA-Talin/MyoVII pathway inhibits cell motility in the absence of folate. Transcriptional response operates in a manner independent on LrrkA.

REFERENCES

1. Cougoule C, Wiedemann A, Lim J, Caron E. Phagocytosis, an alternative model system for the study of cell adhesion. Semin Cell Dev Biol. 2004;15(6):679-89. doi: 10.1016/j.semcdb.2004.09.001. PubMed PMID: 15561587.

2. Buckley CM, King JS. Drinking problems: mechanisms of macropinosome formation and maturation. FEBS J. 2017;284(22):3778-90. doi: 10.1111/febs.14115. PubMed PMID: 28544479.

3. Cosson P, Soldati T. Eat, kill or die: when amoeba meets bacteria. Curr Opin Microbiol. 2008;11(3):271-6. doi: 10.1016/j.mib.2008.05.005. PubMed PMID: 18550419.

4. Mori M, Mode R, Pieters J. From Phagocytes to Immune Defense: Roles for Coronin Proteins in Dictyostelium and Mammalian Immunity. Front Cell Infect Microbiol. 2018;8:77. doi: 10.3389/fcimb.2018.00077. PubMed PMID: 29623258; PubMed Central PMCID: PMCPMC5874285.

5. Stuelten CH, Parent CA, Montell DJ. Cell motility in cancer invasion and metastasis: insights from simple model organisms. Nat Rev Cancer. 2018;18(5):296-312. doi: 10.1038/nrc.2018.15. PubMed PMID: 29546880.

6. Cornillon S, Gebbie L, Benghezal M, Nair P, Keller S, Wehrle-Haller B, et al. An adhesion molecule in free-living Dictyostelium amoebae with integrin beta features. EMBO Rep. 2006;7(6):617-21. doi: 10.1038/sj.embor.7400701. PubMed PMID: 16699495; PubMed Central PMCID: PMCPMC1479592.

7. Froquet R, le Coadic M, Perrin J, Cherix N, Cornillon S, Cosson P. TM9/Phg1 and SadA proteins control surface expression and stability of SibA adhesion molecules in Dictyostelium. Mol Biol Cell. 2012;23(4):679-86. doi: 10.1091/mbc.E11-04-0338. PubMed PMID: 22219373; PubMed Central PMCID: PMCPMC3279395.

8. Dias M, Brochetta C, Marchetti A, Bodinier R, Bruckert F, Cosson P. Role of SpdA in Cell Spreading and Phagocytosis in Dictyostelium. PLoS One. 2016;11(8):e0160376. doi: 10.1371/journal.pone.0160376. PubMed PMID: 27512991; PubMed Central PMCID: PMCPMC4981364.

9. Lelong E, Marchetti A, Gueho A, Lima WC, Sattler N, Molmeret M, et al. Role of magnesium and a phagosomal P-type ATPase in intracellular bacterial killing. Cell Microbiol. 2011;13(2):246-58. doi: 10.1111/j.1462-5822.2010.01532.x. PubMed PMID: 21040356.

10. Cornillon S, Froquet R, Cosson P. Involvement of Sib proteins in the regulation of cellular adhesion in Dictyostelium discoideum. Eukaryot Cell. 2008;7(9):1600-5. Epub 2008/08/05. doi: 10.1128/EC.00155-08. PubMed PMID: 18676957; PubMed Central PMCID: PMCPMC2547077.

11. Gole L, Riviere C, Hayakawa Y, Rieu JP. A quorum-sensing factor in vegetative Dictyostelium discoideum cells revealed by quantitative migration analysis. PLoS One. 2011;6(11):e26901. Epub 2011/11/11. doi: 10.1371/journal.pone.0026901. PubMed PMID: 22073217; PubMed Central PMCID: PMCPMC3207821.

12. Benghezal M, Fauvarque MO, Tournebize R, Froquet R, Marchetti A, Bergeret E, et al. Specific host genes required for the killing of Klebsiella bacteria by phagocytes. Cell Microbiol. 2006;8(1):139-48. doi: 10.1111/j.1462-5822.2005.00607.x. PubMed PMID: 16367873.

3. Manuscript: LrrkA phagocytosis supplementary data

Figure S1. Morphology of the actin cytoskeleton in WT and *lrrkA* KO cells. WT and *lrrkA* KO were allowed to adhere to a glass coverslip, then fixed, permeabilized and stained with fluorescent phalloidin to reveal the structure of the actin cytoskeleton. Three pictures are shown for WT and for *lrrkA* KO cells. The morphology of the actin cytoskeleton appeared highly similar in WT and *lrrkA* KO cells. Bar: 10µm.

Figure S2. Cellular levels of SibA, PDI and Talin are similar in WT and *lrrkA* KO cells. A. Cellular proteins were separated on an SDS-polyacrylamide gel, transferred to nitrocellulose, and the indicated proteins were detected with specific antibodies. B. The intensity of the signal was determined in several independent experiments and is indicated as a ratio of the signal in *lrrkA* KO and WT cells. The quantification of the experiment shown in A are indicated in red. The amount of SibA, Talin and PDI was indistinguishable in *lrrkA* KO and WT cells.

Figure S3. Regulation of gene expression by folate. *D. discoideum* WT cells grown in HL5 were exposed or not to 1mM folate for 4h. RNA-Seq analysis allowed the identification of 10 genes for which transcription was significantly altered by exposure to folate (Lamrabet et al., in preparation) A. For each gene considered (*fol1* to *fol10*), the gene identity and name are indicated, as well as the pair of primers used for RT-PCR and the size of the amplicon. B. For the 10 genes analyzed, RT-PCR analysis confirmed the results obtained by RNA-Seq.

Figure S1.

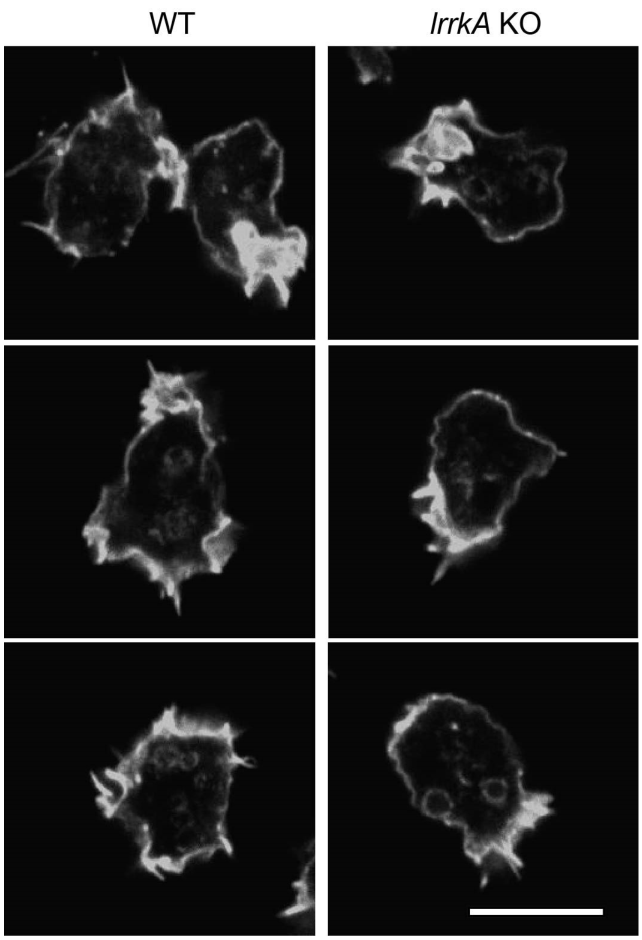

Figure S2.

A

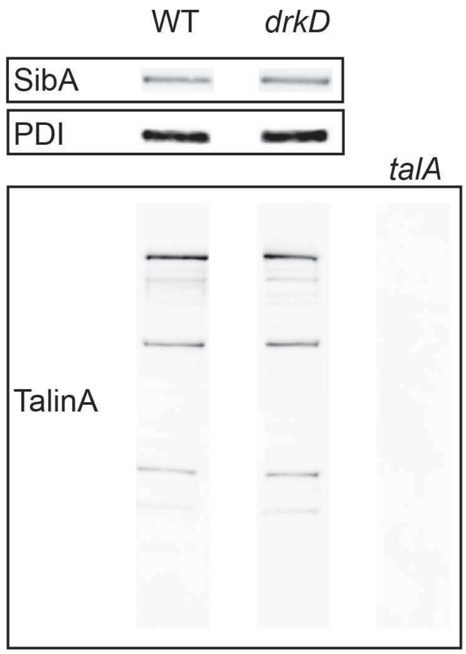

B

	lrrkA/ WT
SibA	0.82
	1.60
	1.23
	1.07
Talin	0.88
	1.01
PDI	0.93
	1.03
	1.09

Figure S3.

A

Gene	DDB Id	Name	Forward primer	Reverse primer	Size (bp)
fol1	G0282461	*grlC*	CATTGTTAACAGCACAAGTTG	CATTAAATCCTTCAACTACCAA	123
fol2	G0272030		GTCACCCTTTCATTCTCATCAG	GCAATTTGCATATATTTTGAATGG	146
fol3	G0293208		GGTTCATGTCAAGGAAGTTGTTC	GTTGATGGATTCCATGATGCAT	146
fol4	G0286015	*gmsA*	GTCACCAACCGAACAACAAA	CATTCCATTTTAATGCTGGAAT	104
fol5	G0271684	*grlA*	GTGGTGATTGGAGTGATATGGG	GAATCTTCAATTGCTTGTTTGG	145
fol6	G0275559		GCAATTACTCGTAATCCAGCAG	CCGAATTTTTCCATTGTCTGTT	137
fol7	G0289485	*vacA*	GAAGCCAATACATTATCATCTG	GTCTTTCAGAGGATTCATTGG	109
fol8	G0272244	*grlG*	CCAAGGAAAAGTAAATGTTGAA	GCCTTCATACATTTTGGCAAT	187
fol9	G0282459	*grlH*	CAGCCAATGTAAATGATATGGG	ACATGCGACAGTATGACCTTG	200
fol10	G0285995	*pdsA*	CCCATCAACAAGAAGATTGTGA	ATTCCAATTCTCTGGTGTATAATAA	143

B

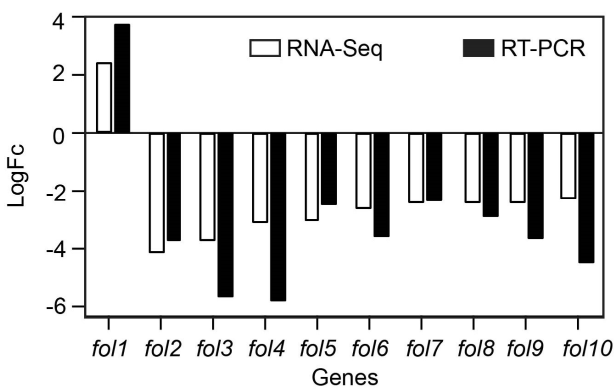

DISCUSSION

I. The advantages to go “Live"

In the recent years, our laboratory has developed live-cell imaging procedures. This has provided us with new insights on the interplay between the Kil1 and Kil2 pathways. It also allowed us to assess the role of phagosome acidification and proteolytic activity during IC killing of *K. pneumoniae*.

1. A better understanding of *K. pneumoniae* Kil1/Kil2 IC killing pathways

The development of an assay allowing direct visualization of IC killing has enabled us to better analyze the phenotypes of *D. discoideum* mutant cells defective in IC killing. As a reminder the test routinely used in early characterization of killing-defective mutants was designed as follows: *D. discoideum* cells and bacteria were mixed at a MOI of 0.1, aliquots were taken every hour, the *D. discoideum* cells were lysed and plated on LB-agar and the remaining bacteria colony-forming units were measured the following day. We then developed a live-imaging assay, where we observed a single *D. discoideum* cell interacting with a single fluorescent bacterium. This allowed us to measure the time between phagocytosis of an individual bacteria and the extinction of its fluorescence, an event presumed to indicate bacterial death. This assay bypassed two main limitations of our early studies: (i) This assay measured both phagocytosis and IC killing. It allowed the detection of the IC killing defect of *lrrkA* KO cells that was masked by the increased phagocytosis. In the CFU based assay described above, *lrrkA* KO cells killed *K. pneumoniae* more efficiently than WT cells (data not published), but this was due to faster phagocytosis of bacteria. The 75% increase in phagocytosis compensated the *lrrk*A KO cells IC killing phenotype; (ii) The sensitivity of the assay was significantly increased. This was also essential to reveal small killing defects in *fspA* and *far1* KO cells which would have gone undetected otherwise (Leiba et al., 2017; Bodinier et al., 2020). Moreover, the assay also provided a more quantitative measure of intracellular killing defects: in our original CFU assay *kil1*, *phg1a* and *kil2* KO cells displayed indistinguishable IC killing defects (Le Coadic et al., 2013). Our new assay revealed that *phg1A* KO cells and *kil1* KO cells have much more significant killing defect than *kil2* KO cells.

The ability to measure quantitatively IC killing enabled us to analyze double KO mutants to evaluate the functional links between different genes products. This type of analysis allowed us to define each individual gene as either Kil1-dependent or Kil2-dependent. Interestingly Δ*kil*1Δ*kil*2 double KO cells lost virtually its entire ability to kill ingested *K. pneumoniae* (data not published). This revealed that *K. pneumoniae* intracellular killing in *D. discoideum* depends virtually entirely on Kil1 and Kil2.

2. Limitations of the new IC killing assay

Obviously, using a fluorophore as a death marker comes with limitations. The eGFP expressed in *K. pneumoniae* is potentially sensitive to pH, proteolytic degradation and chlorination, and we cannot today determine which of these mechanisms is responsible for loss of GFP fluorescence. Nonetheless, The GFP is expressed in the cytosol of the bacteria, any of the three abovementioned alterations would require that the bacteria membrane is disrupted and no longer protects the bacterial cytosol from the degradative environment of the phagosome. Use of *kil*1 and *kil*2 KO cells showed that GFP quenching or degradation was severely diminished in these mutants, suggesting that the bacteria retained longer its membrane integrity. A recent study has observed the extinction of GFP fluorescence in GFP-expressing *E. coli* and *S. aureus* strains phagocytosed by macrophages and revealed that it is well-correlated with bacterial death (Flannagan and Heinrichs, 2018). Addition of another dye such as propidium iodide which stains DNA only when the bacterial membrane is breached, could provide a direct measure on bacterial membrane integrity (Thurston et al., 2016). Obviously, to determine the exact correlation between the fluorescence extinction and bacterial death will require further investigation. Experiments currently made in our laboratory are trying to determine whether the ability of bacteria to replicate disappears before, after, or concomitant with loss of GFP fluorescence.

Another question remains unanswered: do *D. discoideum* cells have a finite capacity for intracellular killing? When cells ingest multiple bacteria, is their killing activity reduced? This would leave *D. discoideum* exposed to pathogens or unable to feed properly when confronted with numerous bacteria Indeed, macrophages do fail to match sustained phagocytosis with sustained microbial killing when exposed to large inocula of *S. aureus* (Jubrail et al., 2015). In our current experimental setup, it is difficult to establish whether the IC killing level decreases with the number of bacteria ingested (Leiba et al., 2017, Bodinier et al., 2020). Specific experiments could be designed to answer this question.

3. *K. pneumoniae* is presumably not killed directly by acid exposure.

The exact role of pH in IC killing is still controversial. Inhibitors of the V-ATPase inhibit acidification, maturation of the phagosome and IC killing at the same time. As described in the introduction, numerous pathogens, like *S. aureus* or *M. tuberculosis*, see their virulence reduced when unable to counter the acidification of phagosomes. But is the lack of an acidic pH in phagosomes enough to prevent IC killing or does it act by halting the phagosomal maturation process?

Virulent *K. pneumoniae* strains ingested by macrophages are found in a compartment positive for the acidotropic probe LysoTracker (Cano et al., 2015) which does not fuse with TR-dextran labeled lysosomes. This observation suggests that *K. pneumoniae* can subvert the maturation process without altering the phagosome acidification. Since *K. pneumoniae* is strongly resistant to acidic pH, one might argue that the pH in macrophages is not acidic enough to kill the bacteria. In *D. discoideum* the phagosomal pH was reported to be at least 1 pH unit lower than in macrophages, approximately 3.5-4 (Dunn et al., 2018) but this assessment was done using a population-based assay. In our experiments we measured a phagosomal pH of 2.8 (Bodinier et al., 2020). In principle, a pH below 3 ensures that *K. pneumoniae* growth is at least halted. We should however take into consideration the observation that *kil1* KO cells are strongly defective for IC killing of *K. pneumoniae*, while the phagosomal pH remains unaffected. Thus, even the extreme acidity of the *D. discoideum* phagosome is not sufficient to ensure efficient killing. In *D. discoideum* the acidic pH probably only provides a secondary barrier to prevent growth of *K. pneumoniae* rather than being bactericidal.

Of course, it must be kept in mind that *D. discoideum* in its natural environment encounters numerous microorganisms that may not all have the same tolerance for pH as *K. pneumoniae*. It will be essential in the future to extend our observations of IC killing to other bacteria in order to determine if an acidic pH can be sufficient to kill certain bacteria in phagosomes.

4. Proteolysis in the maturing phagosome.

We used fluorescent beads to measure proteolysis in phagosomes. In initial experiments, fluorescent beads were mixed with *D. discoideum* cells then centrifuged to try to synchronize phagocytosis and the whole well fluorescence was measured in a plate reader (Russel et al., 2009). The continuous increase in fluorescence over 3 hours observed by the authors reflected in part the asynchronous phagocytosis of beads by *D. discoideum* cells. In our live-imaging assay at single cell level (Bodinier et al., 2020), we showed that proteolysis is detectable in the minutes following phagocytosis, it persists for 40min, then it reaches a plateau until exocytosis of the beads. The transfer to postlysosomes occurs around 40min after phagocytosis and may explain the plateau; the proteases may no longer be present, or the product of proteolysis may fail to accumulate in the postlysosome.

*Kil*2 KO cells also show a decreased rate of phagosomal proteolysis compared to WT cells. Exogenous addition of Mg^{2+} completely corrected the defect. In *lrrk*A KO cells phagosomal proteolysis is also reduced in the absence of exogenous Mg^{2+}. This could be due to a lower level of Kil2 in the phagosomes or to a lower activity of Kil2. Does Kil2 need to be phosphorylated by LrrkA to be fully functional? Further experiments to quantify Kil2 concentration in the phagosome of *lrrkA* KO cells will be necessary to answer this question, and to determine if Kil2 is phosphorylated in a LrrkA-dependent manner.

II. LrrkA is involved in sensing, motility and phagocytosis in *D. discoideum*.

To orchestrate efficient nutrient intake *D. discoideum* must sense bacteria, chase them, ingest them and kill them. Folate is the best studied bacterial cue that may trigger cytoskeleton remodeling, increased motility and directionally (Pan et al., 1972, Pan et al., 2016).

1. Folate, an essential signal

Folate is a byproduct of bacterial metabolism which attracts *D. discoideum* (Pan et al., 1972). *D. discoideum* when presented with a source of folate increased its mobility and directionality toward the source (Rifkin et al., 2006). Two membrane receptors were phosphorylated immediately after exposure to folate and shown to act as folate receptors: fAR1 and fAR2 (Pan et al., 2016). F*ar1* KO cells exhibit a loss of folate chemotaxis towards folate, confirming the main role of fAR1 in folate signaling. In addition, our group also identified previously *fsp*A as an essential element in folate sensing (Lima et al., 2013), but its role in this process remains to be established.

We tested both *far*1 and *fspA* KO mutant cells with our live imaging IC killing assay to check if a defect in sensing or response to folate affects IC killing. Both mutants were defective for intracellular killing (Leiba et al., 2017; Bodinier et al., 2020). Although the IC killing defect was relatively minor this observation revealed that mutants defective in folate sensing are also defective in IC killing. This may provide *D. discoideum* cells with the ability to stimulate rapidly intracellular killing via a fAR1/FspA/LrrkA folate-sensing pathway. Interestingly *fsp*A KO cells are defective for folate sensing but have an intact capsule sensing mechanism, as well as an intact *B. subtilis* sensing (Lima et al., 2013). *D. discoideum* can probably sense several distinct bacterial cues with different signaling pathways.

2. LrrkA, a pivotal kinase in the folate-sensing pathway

Far1 KO, *lrrkA* KO and *kil2* KO cells do not increase IC killing in response to folate stimulation identifying them as elements in a folate-sensing pathway stimulating IC killing. fAR1 the surface receptor activates the folate signaling pathway, LrrkA the cytosolic kinase participates in transducing the signal, and Kil2 the phagosome pump, which activity is regulated by LrrkA, regulates luminal magnesium concentration to increase proteolytic activities.

LrrkA was not only necessary to relay the folate activation signal to Kil2, we also observed in *lrrkA* KO cells an increased phagocytosis and cellular motility. LrrkA is likely among the first proteins activated by fAR1, in parallel or subsequently to the arrestin AdcC. AdcC is a key adaptor protein that controls the fate of cell-surface membrane proteins and modulates downstream signaling cascades (Mas et al., 2018). LrrkA downregulates motility when folate is not present. Most likely LrrkA inhibits actin cytoskeleton remodeling via TalinA and MyoVII. In the future we should also investigate the functional interaction of LrrkA with TalinB, since TalinB localizes at the leading edge of migrating cells.

3. LrrkA could integrate LPS and cAMP signals.

Recently Pan described that LPS sensing is another feature of the fAR1 receptor (Pan et al., 2018). In the future it will be very interesting to determine if LPS stimulates IC killing in *far1* KO, *lrrkA* KO and *kil2* KO cells. This will allow to determine if this signaling pathway responds identically to folate and to LPS.

Measuring the response of *lrrk*A KO cells to cAMP would also be of interest: cAMP is a chemoattractant during the development cycle of *D. discoideum*. The cAMP receptor is a G-protein-linked surface receptor, like fAR1, named cAR1 (Dormann et al., 2001). Upon activation of both cAMP and folate, the AdcC translocates to the surface (Mas et al., 2018). Upon cAMP activation cells increase directional motility toward the source. It is possible that a similar signal transduction machinery is stimulated by cAR1 and fAR1 and LrrkA may thus be involved in multiple sensing pathways.

III. VPS13F exhibits only a subset of Vps13p functions.

The canonical *vps*13 gene was first discovered in yeast during the initial screen to select mutants defective in the sorting of vacuolar proteases. (Bankaitis et al., 1986). Functionally, vps13Δ mutants exhibit four vacuolar proteases mislocalizations: CPY (Bankaitis et al., 1986), PrA (Rothman et al., 1989), PrB (Rothman et al., 1989) and Pep4 (Robinson et al., 1988). Mislocalization of vacuolar proteins indicates the implication of Vps13p in the Golgi-to-vacuole transport via a specific pathway, indeed Vps13p is required both for transport from the trans-Golgi network (TGN) to the late endosome/prevacuolar compartment and for TGN homotypic fusion (De et al., 2017). Another potential role is linked to bypassing the endoplasmic reticulum–mitochondria encounter structure (ERMES) complex. The ERMES complex tethers the mitochondria to the endoplasmic reticulum (Kornmann et al., 2009). The ERMES complex has yet an undefined role, and has been lost in metazoans (Wideman et al., 2013). Nonetheless ERMES mutants are lethal when combined with *vps*39Δ, *vps*13Δ, *crd*1Δ, or any vCLAMP subunit mutants. Intriguingly, a domain at the C-terminus of VPS13 mediate a function that can compensate for ERMES defect (Park et al., 2016).

In human cells, a sequence homology study at genome scale with VPS13p revealed 4 genes in total in the human genome: VPS13A (CHAC), VPS13B (COH1), VPS13C, VPS13D (Velayos-Baeza et al., 2004). Mutations in VPS13A trigger a rare neurodegenerative disease: chorea-acanthocytosis. Mutations in VPS13B trigger the Cohen syndrome. Mutations in VPS13C correlate with early onset severe parkinsonism (Lesage et al., 2016). Lastly, mutations in VPS13D trigger ataxia with spasticity (Seong et al., 2018). Vps13A and Vps13C act as lipid transporters at organelle contact sites (Kumar et al., 2017, Muñoz-Braceras et al., 2019). Vps13C and Vps13D affect mitochondria morphology: silencing of VPS13C leads to mitochondrial fragmentation (Lesage et al., 2016) and mitochondria are larger in VPS13D mutant cells (Anding et al., 2018). Overall the duplication event of the yeast gene VPS13p led to a partial partitioning of its function. A mutation in each of the genes is not compensated by the other but phenotypes are not unrelated, and we expect a similar situation in *D. discoideum* .

D. discoideum genome encodes 6 Vps13 proteins: Vps13A to F. Vps13C (TipC) is the only characterized member of the family and is involved in autophagosome closure (Muñoz-Braceras et al., 2015). Like numerous autophagy mutants in *D. discoideum,* the *vps13C* KO defect leads to abnormal multicellular development.

Vps13F KO cells exhibit normal multicellular development. We do not suspect Vps13F to be involved in autophagy. Regarding mitochondria, *vps13F* KO cells exhibit a mitochondria network similar to the WT (data not published) suggesting that Vps13F does probably not affect mitochondria either. Unfortunately, we were unable to locate Vps13F in *D. discoideum.* Nonetheless Vps13F contains 3 lipid binding domains: (i) the ATG_C autophagy-related protein C-terminal domain, (ii) the APT1 domain, (iii) the PH pleckstrin homology are typically docking sites for phosphatidylinositol lipids (Kaminska et al., 2016). Consequently, Vps13F presence at contact points between organelles is highly likely. Although exact localization at organelle contact sites is elusive, we suspect Vps13F to be implicated in trafficking of lysosomal enzymes as *vps13F* KO cells exhibit an IC killing defect without major alterations of the endocytic pathway. Proteomic studies to identify missing enzymes delivered to phagosomes in *vps13*F KO cells remain to be performed. Like in yeast, we do not expect numerous lysosomal enzymes to be mislocated as the IC killing defect is relatively small compared to *kil*2 or *kil*1 KO cells. Finally, it appeared clearly also through their effect on *D. discoideum* growth that Vps13A and Vps13F have different functions (Leiba et al., 2017).

IV. LrrkA may share several functions as LRRK2

LRRK (leucine-rich repeat kinase) is a family of kinases widely spread in eukaryotes. In plants and amoeba particularly, the family bloomed (Bodinier et al., 2020). In human, the LRRK family has only 2 members: LRRK1 and LRRK2. More specifically they are ROCO kinases. ROCO kinases form a subfamily of LRRK, characterized by the presence of the so-called ROC (Ras of complex proteins)/COR (C-terminal of ROC) domains. Mutations in LRRK2 were studied extensively because they are involved in the pathogenesis of familial Parkinson's disease (Zimprich et al., 2004). LRRK2 is also involved in intracellular killing in mice through its implication in lysozyme sorting in Paneth cell (Rocha et al., 2015), but mutations in LRRK2 also cause a defect in migration of immune cells to the gut, lower ROS production, and decrease lysozyme secretion in the intestinal lumen leading to Crohn's disease pathogenesis (Zhang et al., 2015, Rocha and al., 2018). The decreased lysozyme secretion results from a failure to recruit Nod2 onto lysozyme-containing dense core vesicles leading to lysosomal degradation of lysozyme. This failure occurs either in the absence of LRRK2 or absence of commensal bacteria in the gut (Zhang et al., 2015). Although the link between presence of bacteria and LRRK2 remains elusive, LRRK2 is part of a response to bacterial cues and bacterial killing.

In *D. discoideum* the function of LRRKs is only partially understood and they were not previously described as involved in intracellular killing in vegetative cells (van Egmond et al., 2010). The exact role of LrrkA in *D. discoideum* is unclear also, but our results indicate that it links sensing, motility and bacterial killing. LrrkA may perform some of the functions linked to bacterial sensing and killing performed by LRRK2. *Lrrk*A KO cells in *D. discoideum* exhibit an excess of motility, but the question of directionally has not been tackled. It is likely that chemotaxis towards folate is impaired in *lrrk*A KO cells. This impaired chemotaxis could mimic the migration defect of immune cells to the gut in *lrrk2* mutant mice. Regarding ROS production, we have not measured ROS production in *lrrkA* KO cells, but we do not suspect a defect in ROS production since multicellular development requires ROS production and is unaffected. Lastly, concerning lysozyme secretion, it is possible that among the 22 putative lysozymes in *D. discoideum* some are secreted (Lamrabet et al., 2020). Testing for lysozyme activity in a filtered culture media could help us answer the question of whether some are secreted, and which are affected by *lrrk*A KO.

REFERENCES

1.Abbas, S. Z. et al. Isolation and characterization of arsenic resistant bacteria from wastewater. Braz J Microbiol 45, 1309–1315 (2015).
2.Abo, A. et al. Activation of the NADPH oxidase involves the small GTP-binding protein p21rac1. Nature 353, 668–670 (1991).
3.Achard, M. E. S. et al. The Multi-Copper-Ion Oxidase CueO of Salmonella enterica Serovar Typhimurium Is Required for Systemic Virulence. Infect Immun 78, 2312–2319 (2010).
4.Allen, L. A. & Aderem, A. Molecular definition of distinct cytoskeletal structures involved in complement- and Fc receptor-mediated phagocytosis in macrophages. J. Exp. Med. 184, 627–637 (1996).
5.Allen, L.-A. H., Beecher, B. R., Lynch, J. T., Rohner, O. V. & Wittine, L. M. Helicobacter pylori Disrupts NADPH Oxidase Targeting in Human Neutrophils to Induce Extracellular Superoxide Release. The Journal of Immunology 174, 3658–3667 (2005).
6.Anding, A. L. et al. Vps13D Encodes a Ubiquitin-Binding Protein that Is Required for the Regulation of Mitochondrial Size and Clearance. Curr. Biol. 28, 287-295.e6 (2018).
7.Anjard, C., Consortium, the D. S. & Loomis, W. F. Evolutionary Analyses of ABC Transporters of Dictyostelium discoideum. Eukaryotic Cell 1, 643–652 (2002).
8.Arai, Y. et al. Uric acid induces NADPH oxidase-independent neutrophil extracellular trap formation. Biochem. Biophys. Res. Commun. 443, 556–561 (2014).
9.Bajno, L. et al. Focal exocytosis of VAMP3-containing vesicles at sites of phagosome formation. J. Cell Biol. 149, 697–706 (2000).
10.Baldauf, S. L., Roger, A. J., Wenk-Siefert, I. & Doolittle, W. F. A Kingdom-Level Phylogeny of Eukaryotes Based on Combined Protein Data. Science 290, 972–977 (2000).
11.Banchereau, J. et al. Immunobiology of dendritic cells. Annu. Rev. Immunol. 18, 767–811 (2000).
12.Bankaitis, V. A., Johnson, L. M. & Emr, S. D. Isolation of yeast mutants defective in protein targeting to the vacuole. Proc. Natl. Acad. Sci. U.S.A. 83, 9075–9079 (1986).
13.Barrera, G. Oxidative Stress and Lipid Peroxidation Products in Cancer Progression and Therapy. ISRN Oncol 2012, (2012).
14.Bellich, B. et al. Influence of Bacterial Biofilm Polysaccharide Structure on Interactions with Antimicrobial Peptides: A Study on Klebsiella pneumoniae. Int J Mol Sci 19, (2018).
15.Benghezal, M. et al. Specific host genes required for the killing of Klebsiella bacteria by phagocytes. Cellular Microbiology 8, 139–148 (2006).
16.Bengoechea, J. A. & Sa Pessoa, J. Klebsiella pneumoniae infection biology: living to counteract host defences. FEMS Microbiol Rev 43, 123–144 (2019).
17.Bera, A., Biswas, R., Herbert, S. & Götz, F. The presence of peptidoglycan O-acetyltransferase in various staphylococcal species correlates with lysozyme resistance and pathogenicity. Infect. Immun. 74, 4598–4604 (2006).
18.Berendes, H., Bridges, R. A. & Good, R. A. A fatal granulomatosus of childhood: the clinical study of a new syndrome. Minn Med 40, 309–312 (1957).
19.Besold, A. N., Culbertson, E. M. & Culotta, V. C. The Yin and Yang of copper during infection. J. Biol. Inorg. Chem. 21, 137–144 (2016).
20.Blanz, J. et al. Mannose 6-phosphate-independent Lysosomal Sorting of LIMP-2. Traffic 16, 1127–1136 (2015).
21.Bloomfield, G. & Pears, C. Superoxide signalling required for multicellular development of Dictyostelium. J. Cell. Sci. 116, 3387–3397 (2003).
22.Bloomfield, G. et al. Neurofibromin controls macropinocytosis and phagocytosis in Dictyostelium. Elife 4, (2015).
23.Blott, E. J. & Griffiths, G. M. Secretory lysosomes. Nat Rev Mol Cell Biol 3, 122–131 (2002).
24.Boe, D. M., Curtis, B. J., Chen, M. M., Ippolito, J. A. & Kovacs, E. J. Extracellular traps and macrophages: new roles for the versatile phagocyte. J. Leukoc. Biol. 97, 1023–1035 (2015).
25.Bohdanowicz, M., Balkin, D. M., De Camilli, P. & Grinstein, S. Recruitment of OCRL and Inpp5B to phagosomes by Rab5 and APPL1 depletes phosphoinositides and attenuates Akt signaling. Mol. Biol. Cell 23, 176–187 (2012).
26.Bohdanowicz, M. & Grinstein, S. Role of Phospholipids in Endocytosis, Phagocytosis, and Macropinocytosis. Physiological Reviews 93, 69–106 (2013).

27.Boman, H. G. Peptide antibiotics and their role in innate immunity. Annu. Rev. Immunol. 13, 61–92 (1995).
28.Boom, W. H. et al. Human immunity to M. tuberculosis: T cell subsets and antigen processing. Tuberculosis (Edinb) 83, 98–106 (2003).
29.Bose, T., Cieślar-Pobuda, A. & Wiechec, E. Role of ion channels in regulating Ca 2+ homeostasis during the interplay between immune and cancer cells. Cell Death Dis 6, e1648–e1648 (2015).
30.Botelho, R. J. et al. Localized Biphasic Changes in Phosphatidylinositol-4,5-Bisphosphate at Sites of Phagocytosis. J Cell Biol 151, 1353–1368 (2000).
31.Botella, H. et al. Mycobacterial p(1)-type ATPases mediate resistance to zinc poisoning in human macrophages. Cell Host Microbe 10, 248–259 (2011).
32.Bozzaro, S. & Eichinger, L. The Professional Phagocyte Dictyostelium discoideum as a Model Host for Bacterial Pathogens. Curr Drug Targets 12, 942–954 (2011).
33.Brefeld, O. Dictyostelium mucoroïdes. Ein neuer Organismus aus der Verwandtschaft der Myxomyceten. Archiv der Pharmazie 193, 94–95 (1870).
34.Brickner, J. H. & Fuller, R. S. SOI1 Encodes a Novel, Conserved Protein That Promotes TGN–Endosomal Cycling of Kex2p and Other Membrane Proteins by Modulating the Function of Two TGN Localization Signals. J Cell Biol 139, 23–36 (1997).
35.Brigant, B., Metzinger-Le Meuth, V., Rochette, J. & Metzinger, L. TRIMming down to TRIM37: Relevance to Inflammation, Cardiovascular Disorders, and Cancer in MULIBREY Nanism. Int J Mol Sci 20, (2018).
36.Brinkmann, V. et al. Neutrophil extracellular traps kill bacteria. Science 303, 1532–1535 (2004).
37.Bucci, C., Thomsen, P., Nicoziani, P., McCarthy, J. & van Deurs, B. Rab7: a key to lysosome biogenesis. Mol. Biol. Cell 11, 467–480 (2000).
38.Buckley, C. M. et al. WASH drives early recycling from macropinosomes and phagosomes to maintain surface phagocytic receptors. PNAS 113, E5906–E5915 (2016).
39.Buckley, C. M. et al. PIKfyve/Fab1 is required for efficient V-ATPase and hydrolase delivery to phagosomes, phagosomal killing, and restriction of Legionella infection. PLoS Pathog. 15, e1007551 (2019).
40.Buckley, C. M. et al. Co-ordinated Ras and Rac activity shapes macropinocytic cups and enables phagocytosis of geometrically diverse bacteria. bioRxiv 763748 (2019) doi:10.1101/763748.
41.Buracco, S. et al. Dictyostelium Nramp1, which is structurally and functionally similar to mammalian DMT1 transporter, mediates phagosomal iron efflux. J. Cell. Sci. 128, 3304–3316 (2015).
42.Burlando, B. et al. Occurrence of Cu-ATPase in Dictyostelium: Possible Role in Resistance to Copper. Biochemical and Biophysical Research Communications 291, 476–483 (2002).
43.Buvelot, H., Jaquet, V. & Krause, K.-H. Mammalian NADPH Oxidases. Methods Mol. Biol. 1982, 17–36 (2019).
44.Cai, S., Batra, S., Shen, L., Wakamatsu, N. & Jeyaseelan, S. Both TRIF- and MyD88-dependent signaling contribute to host defense against pulmonary Klebsiella infection. J. Immunol. 183, 6629–6638 (2009).
45.Calvo-Garrido, J. et al. Autophagy in Dictyostelium: Genes and pathways, cell death and infection. Autophagy 6, 686–701 (2010).
46.Cano, V. et al. Klebsiella pneumoniae survives within macrophages by avoiding delivery to lysosomes. Cellular Microbiology 17, 1537–1560 (2015).
47.Cantalupo, G., Alifano, P., Roberti, V., Bruni, C. B. & Bucci, C. Rab-interacting lysosomal protein (RILP): the Rab7 effector required for transport to lysosomes. EMBO J. 20, 683–693 (2001).
48.Cardelli, J. A., Bush, J. M., Ebert, D. & Freeze, H. H. Sulfated N-linked oligosaccharides affect secretion but are not essential for the transport, proteolytic processing, and sorting of lysosomal enzymes in Dictyostelium discoideum. J. Biol. Chem. 265, 8847–8853 (1990).
49.Carnell, M. et al. Actin polymerization driven by WASH causes V-ATPase retrieval and vesicle neutralization before exocytosis. J Cell Biol 193, 831–839 (2011).
50.Castillo, B., Kim, S.-H., Sharief, M., Sun, T. & Kim, L. W. SodC modulates ras and PKB signaling in Dictyostelium. Eur. J. Cell Biol. 96, 1–12 (2017).
51.Cemma, M., Kim, P. K. & Brumell, J. H. The ubiquitin-binding adaptor proteins p62/SQSTM1 and NDP52 are recruited independently to bacteria-associated microdomains to target Salmonella to the autophagy pathway. Autophagy 7, 341–345 (2011).
52.Cen, X., Liu, S. & Cheng, K. The Role of Toll-Like Receptor in Inflammation and Tumor Immunity. Front Pharmacol 9, (2018).
53.Charette, S. J. & Cosson, P. Altered Composition and Secretion of Lysosome-Derived Compartments in Dictyostelium AP-3 Mutant Cells. Traffic 9, 588–596 (2008).

54.Chavrier, P., Parton, R. G., Hauri, H. P., Simons, K. & Zerial, M. Localization of low molecular weight GTP binding proteins to exocytic and endocytic compartments. Cell 62, 317–329 (1990).
55.Chen, G., Zhuchenko, O. & Kuspa, A. Immune-like Phagocyte Activity in the Social Amoeba. Science 317, 678–681 (2007).
56.Christoforidis, S. et al. Phosphatidylinositol-3-OH kinases are Rab5 effectors. Nat. Cell Biol. 1, 249–252 (1999).
57.Clarke, M. et al. Dynamics of the vacuolar H+-ATPase in the contractile vacuole complex and the endosomal pathway of Dictyostelium cells. Journal of Cell Science 115, 2893–2905 (2002).
58.Coadic, M. L. et al. Phg1/TM9 Proteins Control Intracellular Killing of Bacteria by Determining Cellular Levels of the Kil1 Sulfotransferase in Dictyostelium. PLOS ONE 8, e53259 (2013).
59.Coppolino, M. G. et al. Inhibition of phosphatidylinositol-4-phosphate 5-kinase Ialpha impairs localized actin remodeling and suppresses phagocytosis. J. Biol. Chem. 277, 43849–43857 (2002).
60.Cornillon, S. et al. Two members of the beige/CHS (BEACH) family are involved at different stages in the organization of the endocytic pathway in Dictyostelium. J. Cell. Sci. 115, 737–744 (2002).
61.Cornillon, S., Froquet, R. & Cosson, P. Involvement of Sib Proteins in the Regulation of Cellular Adhesion in Dictyostelium discoideum. Eukaryot Cell 7, 1600–1605 (2008).
62.Cornillon, S. et al. Phg1p Is a Nine-transmembrane Protein Superfamily Member Involved in Dictyostelium Adhesion and Phagocytosis. J. Biol. Chem. 275, 34287–34292 (2000).
63.Cortés, G. et al. Molecular analysis of the contribution of the capsular polysaccharide and the lipopolysaccharide O side chain to the virulence of Klebsiella pneumoniae in a murine model of pneumonia. Infect. Immun. 70, 2583–2590 (2002).
64.Cosgrove, K. et al. Catalase (KatA) and alkyl hydroperoxide reductase (AhpC) have compensatory roles in peroxide stress resistance and are required for survival, persistence, and nasal colonization in Staphylococcus aureus. J. Bacteriol. 189, 1025–1035 (2007).
65.Cosson, P. & Soldati, T. Eat, kill or die: when amoeba meets bacteria. Curr. Opin. Microbiol. 11, 271–276 (2008).
66.Cox, D., Tseng, C.-C., Bjekic, G. & Greenberg, S. A Requirement for Phosphatidylinositol 3-Kinase in Pseudopod Extension. J. Biol. Chem. 274, 1240–1247 (1999).
67.Cruz, C. M. et al. ATP Activates a Reactive Oxygen Species-dependent Oxidative Stress Response and Secretion of Proinflammatory Cytokines in Macrophages. J. Biol. Chem. 282, 2871–2879 (2007).
68.de Back, D. Z., Kostova, E. B., van Kraaij, M., van den Berg, T. K. & van Bruggen, R. Of macrophages and red blood cells; a complex love story. Front Physiol 5, 9 (2014).
69.De, M. et al. The Vps13p–Cdc31p complex is directly required for TGN late endosome transport and TGN homotypic fusion. J Cell Biol 216, 425–439 (2017).
70.Delbrück, R., Desel, C., von Figura, K. & Hille-Rehfeld, A. Proteolytic processing of cathepsin D in prelysosomal organelles. Eur. J. Cell Biol. 64, 7–14 (1994).
71.Depraitère, C. & Darmon, M. [Growth of 'Dictyostelium discoideum' on different species of bacteria (author's transl)]. Ann. Microbiol. (Paris) 129 B, 451–461 (1978).
72.Derivery, E. et al. The Arp2/3 Activator WASH Controls the Fission of Endosomes through a Large Multiprotein Complex. Developmental Cell 17, 712–723 (2009).
73.Desjardins, M. et al. Molecular characterization of phagosomes. J. Biol. Chem. 269, 32194–32200 (1994).
74.Desjardins, M., Nzala, N. N., Corsini, R. & Rondeau, C. Maturation of phagosomes is accompanied by changes in their fusion properties and size-selective acquisition of solute materials from endosomes. J. Cell. Sci. 110 (Pt 18), 2303–2314 (1997).
75.Desjardins, M., Houde, M. & Gagnon, E. Phagocytosis: the convoluted way from nutrition to adaptive immunity. Immunological Reviews 207, 158–165 (2005).
76.Dhakshinamoorthy, R., Bitzhenner, M., Cosson, P., Soldati, T. & Leippe, M. The Saposin-Like Protein AplD Displays Pore-Forming Activity and Participates in Defense Against Bacterial Infection During a Multicellular Stage of Dictyostelium discoideum. Front Cell Infect Microbiol 8, (2018).
77.Di, A. et al. CFTR regulates phagosome acidification in macrophages and alters bactericidal activity. Nat Cell Biol 8, 933–944 (2006).
78.Di, A., Kiya, T., Gong, H., Gao, X. & Malik, A. B. Role of the phagosomal redox-sensitive TRP channel TRPM2 in regulating bactericidal activity of macrophages. J Cell Sci 130, 735–744 (2017).
79.Dieckmann, R. et al. The balance in the delivery of ER components and the vacuolar proton pump to the phagosome depends on myosin IK in Dictyostelium. Mol. Cell Proteomics 11, 886–900 (2012).

80.Dikic, I. & Elazar, Z. Mechanism and medical implications of mammalian autophagy. Nat Rev Mol Cell Biol 19, 349–364 (2018).
81.Dinh, C., Farinholt, T., Hirose, S., Zhuchenko, O. & Kuspa, A. Lectins modulate the microbiota of social amoebae. Science 361, 402–406 (2018).
82.Domínguez-Martín, E. et al. Methods to Monitor and Quantify Autophagy in the Social Amoeba Dictyostelium discoideum. Cells 6, (2017).
83.Domínguez-Martín, E., Hernández-Elvira, M., Vincent, O., Coria, R. & Escalante, R. Unfolding the Endoplasmic Reticulum of a Social Amoeba: Dictyostelium discoideum as a New Model for the Study of Endoplasmic Reticulum Stress. Cells 7, (2018).
84.Dormann, D., Kim, J.-Y., Devreotes, P. N. & Weijer, C. J. cAMP receptor affinity controls wave dynamics, geometry and morphogenesis in Dictyostelium. Journal of Cell Science 114, 2513–2523 (2001).
85.Douda, D. N., Khan, M. A., Grasemann, H. & Palaniyar, N. SK3 channel and mitochondrial ROS mediate NADPH oxidase-independent NETosis induced by calcium influx. Proceedings of the National Academy of Science 112, 2817–2822 (2015).
86.Dowling, J. E. & Sidman, R. L. Inherited retinal dystrophy in the rat. J. Cell Biol. 14, 73–109 (1962).
87.Doyle, S. E. et al. Toll-like receptors induce a phagocytic gene program through p38. J. Exp. Med. 199, 81–90 (2004).
88.Duclos, S. et al. Rab5 regulates the kiss and run fusion between phagosomes and endosomes and the acquisition of phagosome leishmanicidal properties in RAW 264.7 macrophages. J. Cell. Sci. 113 Pt 19, 3531–3541 (2000).
89.Duedu, K. O. & French, C. E. Data for discriminating dead/live bacteria in homogenous cell suspensions and the effect of insoluble substrates on turbidimetric measurements. Data Brief 12, 169–174 (2017).
90.Dunn, J. D. et al. Eat Prey, Live: Dictyostelium discoideum As a Model for Cell-Autonomous Defenses. Front Immunol 8, 1906 (2017).
91.Dupuis, S. et al. Impairment of Mycobacterial But Not Viral Immunity by a Germline Human STAT1 Mutation. Science 293, 300–303 (2001).
92.Dupuy, A. G. & Caron, E. Integrin-dependent phagocytosis: spreading from microadhesion to new concepts. J. Cell. Sci. 121, 1773–1783 (2008).
93.Düring, K., Porsch, P., Mahn, A., Brinkmann, O. & Gieffers, W. The non-enzymatic microbicidal activity of lysozymes. FEBS Letters 449, 93–100 (1999).
94.Eichinger, L. et al. The genome of the social amoeba Dictyostelium discoideum. Nature 435, 43–57 (2005).
95.Eigenbrod, T. & Dalpke, A. H. Bacterial RNA: An Underestimated Stimulus for Innate Immune Responses. J. Immunol. 195, 411–418 (2015).
96.Eigenbrod, T. & Dalpke, A. H. Bacterial RNA: An Underestimated Stimulus for Innate Immune Responses. The Journal of Immunology 195, 411–418 (2015).
97.El Chemaly, A., Nunes, P., Jimaja, W., Castelbou, C. & Demaurex, N. Hv1 proton channels differentially regulate the pH of neutrophil and macrophage phagosomes by sustaining the production of phagosomal ROS that inhibit the delivery of vacuolar ATPases. Journal of Leukocyte Biology 95, 827–839 (2014).
98.Escoll, P., Rolando, M. & Buchrieser, C. Modulation of Host Autophagy during Bacterial Infection: Sabotaging Host Munitions for Pathogen Nutrition. Front Immunol 7, (2016).
99.Eskelinen, E.-L. Roles of LAMP-1 and LAMP-2 in lysosome biogenesis and autophagy. Molecular Aspects of Medicine 27, 495–502 (2006).
100.Fang, F. C. Antimicrobial Actions of Reactive Oxygen Species. mBio 2, (2011).
101.Fernandes-Alnemri, T. et al. The AIM2 inflammasome is critical for innate immunity to Francisella tularensis. Nat. Immunol. 11, 385–393 (2010).
102.Fernández-Arenas, E. et al. Candida albicans actively modulates intracellular membrane trafficking in mouse macrophage phagosomes. Cell. Microbiol. 11, 560–589 (2009).
103.Flannagan, R. S. & Heinrichs, D. E. A Fluorescence Based-Proliferation Assay for the Identification of Replicating Bacteria Within Host Cells. Front Microbiol 9, (2018).
104.Flannagan, R. S., Heit, B. & Heinrichs, D. E. Intracellular replication of Staphylococcus aureus in mature phagolysosomes in macrophages precedes host cell death, and bacterial escape and dissemination. Cellular Microbiology 18, 514–535 (2016).
105.Flannagan, R. S., Jaumouillé, V. & Grinstein, S. The cell biology of phagocytosis. Annu Rev Pathol 7, 61–98 (2012).

106.Fleming Alexander & Wright Almroth Edward. On a remarkable bacteriolytic element found in tissues and secretions. Proceedings of the Royal Society of London. Series B, Containing Papers of a Biological Character 93, 306–317 (1922).
107.Foote, J. R., Behe, P., Frampton, M., Levine, A. P. & Segal, A. W. An Exploration of Charge Compensating Ion Channels across the Phagocytic Vacuole of Neutrophils. Front Pharmacol 8, (2017).
108.Fratazzi, C. et al. Macrophage apoptosis in mycobacterial infections. Journal of Leukocyte Biology 66, 763–764 (1999).
109.Freeman, S. A. & Grinstein, S. Phagocytosis: receptors, signal integration, and the cytoskeleton. Immunol. Rev. 262, 193–215 (2014).
110.Freeze, H. H., Bush, J. M. & Cardelli, J. Biochemical and genetic analysis of an antigenic determinant found on N-linked oligosaccharides in Dictyostelium. Dev. Genet. 11, 463–472 (1990).
111.Friedlaender, C. Ueber die Schizomyceten bei der acuten fibrösen Pneumonie. Archiv f. pathol. Anat. 87, 319–324 (1882).
112.Fritzsche, M., Lewalle, A., Duke, T., Kruse, K. & Charras, G. Analysis of turnover dynamics of the submembranous actin cortex. Mol Biol Cell 24, 757–767 (2013).
113.Froquet, R. et al. TM9/Phg1 and SadA proteins control surface expression and stability of SibA adhesion molecules in Dictyostelium. Mol Biol Cell 23, 679–686 (2012).
114.Fujiwara, Y., Wada, K. & Kabuta, T. Lysosomal degradation of intracellular nucleic acids—multiple autophagic pathways. J Biochem 161, 145–154 (2017).
115.Gagnon, E. et al. Endoplasmic Reticulum-Mediated Phagocytosis Is a Mechanism of Entry into Macrophages. Cell 110, 119–131 (2002).
116.Gao, X. et al. PI3K/Akt signaling requires spatial compartmentalization in plasma membrane microdomains. Proc Natl Acad Sci U S A 108, 14509–14514 (2011).
117.Garrick, M. D. et al. DMT1: which metals does it transport? Biol. Res. 39, 79–85 (2006).
118.Gerstenmaier, L. et al. The autophagic machinery ensures nonlytic transmission of mycobacteria. PNAS 112, E687–E692 (2015).
119.Gold, B. et al. Identification of a Copper-Binding Metallothionein in Pathogenic Mycobacteria. Nat Chem Biol 4, 609–616 (2008).
120.Goley, E. D. & Welch, M. D. The ARP2/3 complex: an actin nucleator comes of age. Nat. Rev. Mol. Cell Biol. 7, 713–726 (2006).
121.Gopaldass, N. et al. Dynamin A, Myosin IB and Abp1 Couple Phagosome Maturation to F-Actin Binding. Traffic 13, 120–130 (2012).
122.Gordon, S. Phagocytosis: An Immunobiologic Process. Immunity 44, 463–475 (2016).
123.Gotthardt, D. et al. High-Resolution Dissection of Phagosome Maturation Reveals Distinct Membrane Trafficking Phases. Mol Biol Cell 13, 3508–3520 (2002).
124.Grant, B. & Greenwald, I. The Caenorhabditis Elegans Sel-1 Gene, a Negative Regulator of Lin-12 and Glp-1, Encodes a Predicted Extracellular Protein. Genetics 143, 237–247 (1996).
125.Green, J. N., Kettle, A. J. & Winterbourn, C. C. Protein chlorination in neutrophil phagosomes and correlation with bacterial killing. Free Radical Biology and Medicine 77, 49–56 (2014).
126.Greenwald, I. & Kovall, R. Notch signaling: genetics and structure. (WormBook, 2018).
127.Griffin, F. M., Griffin, J. A., Leider, J. E. & Silverstein, S. C. Studies on the mechanism of phagocytosis. I. Requirements for circumferential attachment of particle-bound ligands to specific receptors on the macrophage plasma membrane. J. Exp. Med. 142, 1263–1282 (1975).
128.Gueho, A. et al. Dictyostelium EHD associates with Dynamin and participates in phagosome maturation. J Cell Sci 129, 2354–2367 (2016).
129.Gutierrez, M. G. Functional role(s) of phagosomal Rab GTPases. Small GTPases 4, 148–158 (2013).
130.Hagedorn, M. & Soldati, T. Flotillin and RacH modulate the intracellular immunity of Dictyostelium to Mycobacterium marinum infection. Cell. Microbiol. 9, 2716–2733 (2007).
131.Hagemann, N. et al. The serologically defined colon cancer antigen-3 interacts with the protein tyrosine phosphatase PTPN13 and is involved in the regulation of cytokinesis. Oncogene 32, 4602–4613 (2013).
132.Haldar, A. K. et al. IRG and GBP Host Resistance Factors Target Aberrant, "Non-self" Vacuoles Characterized by the Missing of "Self" IRGM Proteins. PLoS Pathog 9, (2013).
133.Hanawa-Suetsugu, K. et al. Phagocytosis is mediated by two-dimensional assemblies of the F-BAR protein GAS7. Nat Commun 10, 1–13 (2019).

134.Hao, X. et al. A role for copper in protozoan grazing - two billion years selecting for bacterial copper resistance. Mol. Microbiol. 102, 628–641 (2016).
135.Harris, E. & Cardelli, J. RabD, a Dictyostelium Rab14-related GTPase, regulates phagocytosis and homotypic phagosome and lysosome fusion. J. Cell. Sci. 115, 3703–3713 (2002).
136.Harrison, R. E., Bucci, C., Vieira, O. V., Schroer, T. A. & Grinstein, S. Phagosomes Fuse with Late Endosomes and/or Lysosomes by Extension of Membrane Protrusions along Microtubules: Role of Rab7 and RILP. Mol Cell Biol 23, 6494–6506 (2003).
137.Hatakeyama, S. TRIM Family Proteins: Roles in Autophagy, Immunity, and Carcinogenesis. Trends in Biochemical Sciences 42, 297–311 (2017).
138.Haud, N. et al. rnaset2 mutant zebrafish model familial cystic leukoencephalopathy and reveal a role for RNase T2 in degrading ribosomal RNA. Proc Natl Acad Sci U S A 108, 1099–1103 (2011).
139.Hennigar, S. R. & McClung, J. P. Nutritional Immunity: Starving Pathogens of Trace Minerals. American Journal of Lifestyle Medicine 10, 170–173 (2016).
140.Hentze, M. W., Muckenthaler, M. U., Galy, B. & Camaschella, C. Two to tango: regulation of Mammalian iron metabolism. Cell 142, 24–38 (2010).
141.Hilty, J., Smulian, A. G. & Newman, S. L. The Histoplasma capsulatum vacuolar ATPase is required for iron homeostasis, intracellular replication in macrophages and virulence in a murine model of histoplasmosis: V-ATPase and virulence in Histoplasma capsulatum. Molecular Microbiology 70, 127–139 (2008).
142.Hirose, S., Chen, G., Kuspa, A. & Shaulsky, G. The polymorphic proteins TgrB1 and TgrC1 function as a ligand–receptor pair in Dictyostelium allorecognition. J Cell Sci 130, 4002–4012 (2017).
143.Hodgkinson, V. & Petris, M. J. Copper homeostasis at the host-pathogen interface. J. Biol. Chem. 287, 13549–13555 (2012).
144.Holt, K. E. et al. Genomic analysis of diversity, population structure, virulence, and antimicrobial resistance in Klebsiella pneumoniae, an urgent threat to public health. Proc Natl Acad Sci U S A 112, E3574–E3581 (2015).
145.Horiuchi, H. et al. A novel Rab5 GDP/GTP exchange factor complexed to Rabaptin-5 links nucleotide exchange to effector recruitment and function. Cell 90, 1149–1159 (1997).
146.Hsieh, P.-F., Lu, Y.-R., Lin, T.-L., Lai, L.-Y. & Wang, J.-T. Klebsiella pneumoniae Type VI Secretion System Contributes to Bacterial Competition, Cell Invasion, Type-1 Fimbriae Expression, and In Vivo Colonization. J Infect Dis 219, 637–647 (2019).
147.Hsu, C.-R. et al. A Novel Role for the Klebsiella pneumoniae Sap (Sensitivity to Antimicrobial Peptides) Transporter in Intestinal Cell Interactions, Innate Immune Responses, Liver Abscess, and Virulence. J Infect Dis 219, 1294–1306 (2019).
148.Huang, J. et al. Activation of antibacterial autophagy by NADPH oxidases. Proc Natl Acad Sci U S A 106, 6226–6231 (2009).
149.Huckins, C. Spermatogonial intercellular bridges in whole-mounted seminiferous tubules from normal and irradiated rodent testes. American Journal of Anatomy 153, 97–121 (1978).
150.Hume, D. A. et al. The mononuclear phagocyte system revisited. J. Leukoc. Biol. 72, 621–627 (2002).
151.Huynh, K. K. et al. LAMP proteins are required for fusion of lysosomes with phagosomes. EMBO J. 26, 313–324 (2007).
152.Imlay, J. A. Iron-sulphur clusters and the problem with oxygen. Molecular Microbiology 59, 1073–1082 (2006).
153.Imlay, J. A. Cellular defenses against superoxide and hydrogen peroxide. Annu Rev Biochem 77, 755–776 (2008).
154.Imlay, J. A. Where in the world do bacteria experience oxidative stress? Environmental Microbiology 21, 521–530 (2019).
155.Iwasaki, A. & Medzhitov, R. Control of adaptive immunity by the innate immune system. Nat. Immunol. 16, 343–353 (2015).
156.Jabado, N. et al. Natural Resistance to Intracellular Infections. J Exp Med 192, 1237–1248 (2000).
157.Jankowski, A., Scott, C. C. & Grinstein, S. Determinants of the Phagosomal pH in Neutrophils. J. Biol. Chem. 277, 6059–6066 (2002).
158.Jeschke, A. & Haas, A. Sequential actions of phosphatidylinositol phosphates regulate phagosome-lysosome fusion. MBoC 29, 452–465 (2018).
159.Jia, K. et al. Autophagy genes protect against Salmonella typhimurium infection and mediate insulin signaling-regulated pathogen resistance. Proc. Natl. Acad. Sci. U.S.A. 106, 14564–14569 (2009).

160.Jiang, M.-X. et al. Expression profiling of TRIM protein family in THP1-derived macrophages following TLR stimulation. Sci Rep 7, (2017).
161.Jin, T. et al. Staphylococcus aureus Resists Human Defensins by Production of Staphylokinase, a Novel Bacterial Evasion Mechanism. The Journal of Immunology 172, 1169–1176 (2004).
162.Joo, H.-S., Fu, C.-I. & Otto, M. Bacterial strategies of resistance to antimicrobial peptides. Philos Trans R Soc Lond B Biol Sci 371, (2016).
163.Journet, A. et al. Characterization of Dictyostelium discoideum cathepsin D. J. Cell. Sci. 112 (Pt 21), 3833–3843 (1999).
164.Jubrail, J. et al. Inability to sustain intraphagolysosomal killing of Staphylococcus aureus predisposes to bacterial persistence in macrophages. Cellular Microbiology 18, 80–96 (2016).
165.Juttukonda, L. J. & Skaar, E. P. Chapter 31 - Manganese and Nutritional Immunity. in Molecular, Genetic, and Nutritional Aspects of Major and Trace Minerals (ed. Collins, J. F.) 377–387 (Academic Press, 2017). doi:10.1016/B978-0-12-802168-2.00031-2.
166.Kambe, T., Tsuji, T., Hashimoto, A. & Itsumura, N. The Physiological, Biochemical, and Molecular Roles of Zinc Transporters in Zinc Homeostasis and Metabolism. Physiol. Rev. 95, 749–784 (2015).
167.Kaminska, J. et al. Phosphatidylinositol-3-phosphate regulates response of cells to proteotoxic stress. Int. J. Biochem. Cell Biol. 79, 494–504 (2016).
168.Katoch, B. & Begum, R. Biochemical basis of the high resistance to oxidative stress in Dictyostelium discoideum. J. Biosci. 28, 581–588 (2003).
169.Katoch, B. & Begum, R. Biochemical basis of the high resistance to oxidative stress inDictyostelium discoideum. J. Biosci. 28, 581–588 (2003).
170.Katz, E. R. Dictyostelium: Evolution, Cell Biology, and the Development of Multicellularity. By Richard H Kessin. The Quarterly Review of Biology 77, 453–454 (2002).
171.Kawane, K. et al. Requirement of DNase II for definitive erythropoiesis in the mouse fetal liver. Science 292, 1546–1549 (2001).
172.Kawata, T. STAT signaling in Dictyostelium development. Development, Growth & Differentiation 53, 548–557 (2011).
173.Kay, R. R. & Williams, J. G. The Dictyostelium genome project an invitation to species hopping. Trends in Genetics 15, 294–297 (1999).
174.Kayath, C. A. et al. Escape of intracellular Shigella from autophagy requires binding to cholesterol through the type III effector, IcsB. Microbes Infect. 12, 956–966 (2010).
175.Khandelwal, S. & Saxena, R. K. Age-dependent increase in green autofluorescence of blood erythrocytes. J. Biosci. 32, 1139–1145 (2007).
176.Kim, B.-H. et al. IFN-induced Guanylate Binding Proteins in Inflammasome Activation and Host Defense. Nat Immunol 17, 481–489 (2016).
177.Kim, B.-H. et al. A family of IFN-γ-inducible 65-kD GTPases protects against bacterial infection. Science 332, 717–721 (2011).
178.Kim, Y. K., Shin, J.-S. & Nahm, M. H. NOD-Like Receptors in Infection, Immunity, and Diseases. Yonsei Med J 57, 5–14 (2016).
179.Kimura, T., Mandell, M. & Deretic, V. Precision autophagy directed by receptor regulators - emerging examples within the TRIM family. J. Cell. Sci. 129, 881–891 (2016).
180.Kinchen, J. M. et al. A pathway for phagosome maturation during engulfment of apoptotic cells. Nat. Cell Biol. 10, 556–566 (2008).
181.King, J. S. et al. WASH is required for lysosomal recycling and efficient autophagic and phagocytic digestion. Mol Biol Cell 24, 2714–2726 (2013).
182.Klionsky, D. J. & Emr, S. D. Membrane protein sorting: biosynthesis, transport and processing of yeast vacuolar alkaline phosphatase. EMBO J 8, 2241–2250 (1989).
183.Knaus, U. G., Heyworth, P. G., Evans, T., Curnutte, J. T. & Bokoch, G. M. Regulation of phagocyte oxygen radical production by the GTP-binding protein Rac 2. Science 254, 1512–1515 (1991).
184.Koller, B. et al. Dictyostelium discoideum as a Novel Host System to Study the Interaction between Phagocytes and Yeasts. Front Microbiol 7, (2016).
185.Kornmann, B. et al. An ER-Mitochondria Tethering Complex Revealed by a Synthetic Biology Screen. Science 325, 477–481 (2009).
186.Kosikowska, P. & Lesner, A. Antimicrobial peptides (AMPs) as drug candidates: a patent review (2003-2015). Expert Opin Ther Pat 26, 689–702 (2016).

187.Kovács, I., Horváth, M., Lányi, Á., Petheő, G. L. & Geiszt, M. Reactive oxygen species-mediated bacterial killing by B lymphocytes. Journal of Leukocyte Biology 97, 1133–1137 (2015).
188.Kumar, N. et al. VPS13A and VPS13C are lipid transport proteins differentially localized at ER contact sites. J Cell Biol 217, 3625–3639 (2018).
189.Kypri, E., Falkenstein, K. & De Lozanne, A. Antagonistic control of lysosomal fusion by Rab14 and the Lyst-related protein LvsB. Traffic 14, 599–609 (2013).
190.Lampe, E. O. et al. Dissection of Francisella-Host Cell Interactions in Dictyostelium discoideum. Appl. Environ. Microbiol. 82, 1586–1598 (2016).
191.Lamrabet, O., Jauslin, T., Lima, W. C., Leippe, M. & Cosson, P. The multifarious lysozyme arsenal of Dictyostelium discoideum. Dev. Comp. Immunol. 107, 103645 (2020).
192.Lardy, B. et al. NADPH oxidase homologs are required for normal cell differentiation and morphogenesis in Dictyostelium discoideum. Biochim. Biophys. Acta 1744, 199–212 (2005).
193.Lawrence, R. E. & Zoncu, R. The lysosome as a cellular centre for signalling, metabolism and quality control. Nat Cell Biol 21, 133–142 (2019).
194.Le Roux, D. et al. Antigen stored in dendritic cells after macropinocytosis is released unprocessed from late endosomes to target B cells. Blood 119, 95–105 (2012).
195.Leiba, J. et al. Vps13F links bacterial recognition and intracellular killing in Dictyostelium. Cell Microbiol 19, (2017).
196.Leippe, M. Pore-forming toxins from pathogenic amoebae. Appl. Microbiol. Biotechnol. 98, 4347–4353 (2014).
197.Lelong, E. et al. Role of magnesium and a phagosomal P-type ATPase in intracellular bacterial killing. Cellular Microbiology 13, 246–258 (2011).
198.Lemansky, P. & Hasilik, A. Chondroitin sulfate is involved in lysosomal transport of lysozyme in U937 cells. Journal of cell science 114, 345–352 (2001).
199.Lesage, S. et al. Loss of VPS13C Function in Autosomal-Recessive Parkinsonism Causes Mitochondrial Dysfunction and Increases PINK1/Parkin-Dependent Mitophagy. Am. J. Hum. Genet. 98, 500–513 (2016).
200.Levine, A. P. & Segal, A. W. The NADPH Oxidase and Microbial Killing by Neutrophils, With a Particular Emphasis on the Proposed Antimicrobial Role of Myeloperoxidase within the Phagocytic Vacuole. Microbiol Spectr 4, (2016).
201.Levine, A. P. & Segal, A. W. The NADPH Oxidase and Microbial Killing by Neutrophils, With a Particular Emphasis on the Proposed Antimicrobial Role of Myeloperoxidase within the Phagocytic Vacuole. Microbiology Spectrum 4, (2016).
202.Li, X. et al. A Molecular Mechanism to Regulate Lysosome Motility for Lysosome Positioning and Tubulation. Nat Cell Biol 18, 404–417 (2016).
203.Lima, W. C., Balestrino, D., Forestier, C. & Cosson, P. Two distinct sensing pathways allow recognition of Klebsiella pneumoniae by Dictyostelium amoebae. Cell Microbiol 16, 311–323 (2013).
204.Lima, W. C., Leuba, F., Soldati, T. & Cosson, P. Mucolipin controls lysosome exocytosis in Dictyostelium. J Cell Sci 125, 2315–2322 (2012).
205.Lima, W. C. et al. Genome sequencing and functional characterization of the non-pathogenic Klebsiella pneumoniae KpGe bacteria. Microbes Infect. 20, 293–301 (2018).
206.Litman, G. W., Rast, J. P. & Fugmann, S. D. The origins of vertebrate adaptive immunity. Nat. Rev. Immunol. 10, 543–553 (2010).
207.Liu, B. & Newburg, D. S. Human Milk Glycoproteins Protect Infants Against Human Pathogens. Breastfeed Med 8, 354–362 (2013).
208.Liu, W. et al. The involvement of NADPH oxidase-mediated ROS in cytokine secretion from macrophages induced by Mycobacterium tuberculosis ESAT-6. Inflammation 37, 880–892 (2014).
209.Llobet, E., March, C., Giménez, P. & Bengoechea, J. A. Klebsiella pneumoniae OmpA Confers Resistance to Antimicrobial Peptides. Antimicrobial Agents and Chemotherapy 53, 298–302 (2009).
210.Lodoen, M. B. & Lanier, L. L. Natural killer cells as an initial defense against pathogens. Curr. Opin. Immunol. 18, 391–398 (2006).
211.Lomakin, A. J. et al. Competition of two distinct actin networks for actin defines a bistable switch for cell polarization. Nat Cell Biol 17, 1435–1445 (2015).
212.Lööv, C., Mitchell, C. H., Simonsson, M. & Erlandsson, A. Slow degradation in phagocytic astrocytes can be enhanced by lysosomal acidification. Glia 63, 1997–2009 (2015).

213.Loovers, H. M. et al. Regulation of Phagocytosis in Dictyostelium by the Inositol 5-Phosphatase OCRL Homolog Dd5P4. Traffic 8, 618–628 (2007).
214.Lübke, T., Lobel, P. & Sleat, D. Proteomics of the Lysosome. Biochim Biophys Acta 1793, 625–635 (2009).
215.Lucas, M. et al. Structural Mechanism for Cargo Recognition by the Retromer Complex. Cell 167, 1623-1635.e14 (2016).
216.Lukacs, G. L., Rotstein, O. D. & Grinstein, S. Phagosomal acidification is mediated by a vacuolar-type H(+)-ATPase in murine macrophages. J. Biol. Chem. 265, 21099–21107 (1990).
217.Luzio, J. P., Hackmann, Y., Dieckmann, N. M. G. & Griffiths, G. M. The Biogenesis of Lysosomes and Lysosome-Related Organelles. Cold Spring Harb Perspect Biol 6, a016840 (2014).
218.Machado, D. et al. Ion Channel Blockers as Antimicrobial Agents, Efflux Inhibitors, and Enhancers of Macrophage Killing Activity against Drug Resistant Mycobacterium tuberculosis. PLoS One 11, (2016).
219.Maganto-Garcia, E., Punzon, C., Terhorst, C. & Fresno, M. Rab5 activation by Toll-like receptor 2 is required for Trypanosoma cruzi internalization and replication in macrophages. Traffic 9, 1299–1315 (2008).
220.Mahlapuu, M., Håkansson, J., Ringstad, L. & Björn, C. Antimicrobial Peptides: An Emerging Category of Therapeutic Agents. Front Cell Infect Microbiol 6, (2016).
221.March, C. et al. Role of Bacterial Surface Structures on the Interaction of Klebsiella pneumoniae with Phagocytes. PLoS One 8, (2013).
222.Maringer, K. et al. Dictyostelium discoideum RabS and Rab2 colocalize with the Golgi and contractile vacuole system and regulate osmoregulation. J. Biosci. 41, 205–217 (2016).
223.Martin, R. M. & Bachman, M. A. Colonization, Infection, and the Accessory Genome of Klebsiella pneumoniae. Front Cell Infect Microbiol 8, (2018).
224.Martinez, J. et al. Molecular characterization of LC3-associated phagocytosis (LAP) reveals distinct roles for Rubicon, NOX2, and autophagy proteins. Nat Cell Biol 17, 893–906 (2015).
225.Martins, M., Viveiros, M. & Amaral, L. Inhibitors of Ca2+ and K+ transport enhance intracellular killing of M. tuberculosis by non-killing macrophages. In Vivo 22, 69–75 (2008).
226.Mas, L., Cieren, A., Delphin, C., Journet, A. & Aubry, L. Calcium influx mediates the chemoattractant-induced translocation of the arrestin-related protein AdcC in Dictyostelium. J. Cell. Sci. 131, (2018).
227.Maxfield, F. R. & McGraw, T. E. Endocytic recycling. Nat. Rev. Mol. Cell Biol. 5, 121–132 (2004).
228.Maxson, M. E. et al. Integrin-based diffusion barrier separates membrane domains enabling the formation of microbiostatic frustrated phagosomes. eLife 7, e34798 (2018).
229.McCord, J. M., Keele, B. B. & Fridovich, I. An enzyme-based theory of obligate anaerobiosis: the physiological function of superoxide dismutase. Proc. Natl. Acad. Sci. U.S.A. 68, 1024–1027 (1971).
230.McGough, I. J. et al. Retromer binding to FAM21 and the WASH complex is perturbed by the Parkinson disease-linked VPS35(D620N) mutation. Curr. Biol. 24, 1670–1676 (2014).
231.Mercanti, V. et al. Selective membrane exclusion in phagocytic and macropinocytic cups. Journal of Cell Science 119, 4079–4087 (2006).
232.Mesquita, A. et al. Autophagy in Dictyostelium: Mechanisms, regulation and disease in a simple biomedical model. Autophagy 13, 24–40 (2016).
233.Meunier, E. & Broz, P. Interferon-inducible GTPases in cell autonomous and innate immunity. Cellular Microbiology 18, 168–180 (2016).
234.Miller, J. L., Velmurugan, K., Cowan, M. J. & Briken, V. The Type I NADH Dehydrogenase of Mycobacterium tuberculosis Counters Phagosomal NOX2 Activity to Inhibit TNF-α-Mediated Host Cell Apoptosis. PLOS Pathogens 6, e1000864 (2010).
235.Minegishi, Y. et al. Dominant-negative mutations in the DNA-binding domain of STAT3 cause hyper-IgE syndrome. Nature 448, 1058–1062 (2007).
236.Mittl, P. R. E. & Schneider-Brachert, W. Sel1-like repeat proteins in signal transduction. Cellular Signalling 19, 20–31 (2007).
237.Mogensen, T. H. IRF and STAT Transcription Factors - From Basic Biology to Roles in Infection, Protective Immunity, and Primary Immunodeficiencies. Front. Immunol. 9, (2019).
238.Monroe, K. M., McWhirter, S. M. & Vance, R. E. Identification of Host Cytosolic Sensors and Bacterial Factors Regulating the Type I Interferon Response to Legionella pneumophila. PLoS Pathog 5, (2009).
239.Moreau, K. et al. Autophagosomes can support Yersinia pseudotuberculosis replication in macrophages. Cell. Microbiol. 12, 1108–1123 (2010).

240.Morizawa, Y. M. et al. Reactive astrocytes function as phagocytes after brain ischemia via ABCA1-mediated pathway. Nat Commun 8, 1–15 (2017).
241.Mu, L. et al. A phosphatidylinositol 4,5-bisphosphate redistribution-based sensing mechanism initiates a phagocytosis programing. Nat Commun 9, 1–16 (2018).
242.Muller, F. L., Lustgarten, M. S., Jang, Y., Richardson, A. & Van Remmen, H. Trends in oxidative aging theories. Free Radical Biology and Medicine 43, 477–503 (2007).
243.Müller, I. et al. A Dictyostelium mutant with reduced lysozyme levels compensates by increased phagocytic activity. J. Biol. Chem. 280, 10435–10443 (2005).
244.Muñoz-Braceras, S., Calvo, R. & Escalante, R. TipC and the chorea-acanthocytosis protein VPS13A regulate autophagy in Dictyostelium and human HeLa cells. Autophagy 11, 918–927 (2015).
245.Muñoz-Braceras, S., Tornero-Écija, A. R., Vincent, O. & Escalante, R. VPS13A is closely associated with mitochondria and is required for efficient lysosomal degradation. Disease Models & Mechanisms 12, (2019).
246.Nakagawa, A., Shiratsuchi, A., Tsuda, K. & Nakanishi, Y. In vivo analysis of phagocytosis of apoptotic cells by testicular Sertoli cells. Mol. Reprod. Dev. 71, 166–177 (2005).
247.Nakaya, M., Kitano, M., Matsuda, M. & Nagata, S. Spatiotemporal activation of Rac1 for engulfment of apoptotic cells. PNAS 105, 9198–9203 (2008).
248.Nandrot, E. et al. Homozygous deletion in the coding sequence of the c-mer gene in RCS rats unravels general mechanisms of physiological cell adhesion and apoptosis. Neurobiol. Dis. 7, 586–599 (2000).
249.Nash, J. A., Ballard, T. N. S., Weaver, T. E. & Akinbi, H. T. The Peptidoglycan-Degrading Property of Lysozyme Is Not Required for Bactericidal Activity In Vivo. The Journal of Immunology 177, 519–526 (2006).
250.Nasser, W. et al. Bacterial discrimination by Dictyostelid amoebae reveals the complexity of ancient interspecies interactions. Curr Biol 23, 862–872 (2013).
251.Neuhaus, E. M. & Soldati, T. A myosin I is involved in membrane recycling from early endosomes. J. Cell Biol. 150, 1013–1026 (2000).
252.Newton, J. M., Schofield, D., Vlahopoulou, J. & Zhou, Y. Detecting cell lysis using viscosity monitoring in E. coli fermentation to prevent product loss. Biotechnology Progress 32, 1069–1076 (2016).
253.Neznanov, N., Neznanova, L., Angres, B. & Gudkov, A. V. Serologically defined colon cancer antigen 3 is necessary for the presentation of TNF receptor 1 on cell surface. DNA Cell Biol. 24, 777–785 (2005).
254.Nguyen, G. T., Green, E. R. & Mecsas, J. Neutrophils to the ROScue: Mechanisms of NADPH Oxidase Activation and Bacterial Resistance. Front Cell Infect Microbiol 7, (2017).
255.Nguyen, L. T., Haney, E. F. & Vogel, H. J. The expanding scope of antimicrobial peptide structures and their modes of action. Trends in Biotechnology 29, 464–472 (2011).
256.Niederweis, M., Wolschendorf, F., Mitra, A. & Neyrolles, O. Mycobacteria, Metals, and the Macrophage. Immunol Rev 264, 249–263 (2015).
257.Nordenfelt, P., Grinstein, S., Björck, L. & Tapper, H. V-ATPase-mediated phagosomal acidification is impaired by Streptococcus pyogenes through Mga-regulated surface proteins. Microbes Infect. 14, 1319–1329 (2012).
258.Nordmann, M. et al. The Mon1-Ccz1 complex is the GEF of the late endosomal Rab7 homolog Ypt7. Curr. Biol. 20, 1654–1659 (2010).
259.Núñez, G., Sakamoto, K. & Soares, M. P. Innate Nutritional Immunity. J Immunol 201, 11–18 (2018).
260.Ogawa, M. et al. Escape of intracellular Shigella from autophagy. Science 307, 727–731 (2005).
261.Oishi, Y. & Manabe, I. Macrophages in inflammation, repair and regeneration. Int. Immunol. 30, 511–528 (2018).
262.Osman, D. et al. Copper Homeostasis in Salmonella Is Atypical and Copper-CueP Is a Major Periplasmic Metal Complex. J Biol Chem 285, 25259–25268 (2010).
263.Ostrowski, P. P., Grinstein, S. & Freeman, S. A. Diffusion Barriers, Mechanical Forces, and the Biophysics of Phagocytosis. Dev. Cell 38, 135–146 (2016).
264.Ouertatani-Sakouhi, H. et al. Inhibitors of Mycobacterium marinum virulence identified in a Dictyostelium discoideum host model. PLOS ONE 12, e0181121 (2017).
265.Padh, H., Ha, J., Lavasa, M. & Steck, T. L. A post-lysosomal compartment in Dictyostelium discoideum. J. Biol. Chem. 268, 6742–6747 (1993).
266.Padilla, E. et al. Klebsiella pneumoniae AcrAB Efflux Pump Contributes to Antimicrobial Resistance and Virulence. Antimicrob Agents Chemother 54, 177–183 (2010).
267.Paganin, F. et al. Severe community-acquired pneumonia: assessment of microbial aetiology as mortality factor. European Respiratory Journal 24, 779–785 (2004).

268.Pan, M. et al. A G-protein-coupled chemoattractant receptor recognizes lipopolysaccharide for bacterial phagocytosis. PLOS Biology 16, e2005754 (2018).
269.Pan, M. et al. A G-protein-coupled chemoattractant receptor recognizes lipopolysaccharide for bacterial phagocytosis. PLoS Biol 16, (2018).
270.Pan, M., Xu, X., Chen, Y. & Jin, T. Identification of a Chemoattractant G-Protein-Coupled Receptor for Folic Acid that Controls Both Chemotaxis and Phagocytosis. Developmental Cell 36, 428–439 (2016).
271.Pan, P., Hall, E. M. & Bonner, J. T. Folic Acid as Second Chemotactic Substance in the Cellular Slime Moulds. Nature New Biology 237, 181–182 (1972).
272.Pape, K. A., Catron, D. M., Itano, A. A. & Jenkins, M. K. The humoral immune response is initiated in lymph nodes by B cells that acquire soluble antigen directly in the follicles. Immunity 26, 491–502 (2007).
273.Parisi, S. et al. Characterization of the most frequent ATP7B mutation causing Wilson disease in hepatocytes from patient induced pluripotent stem cells. Sci Rep 8, 1–11 (2018).
274.Park, H. H. Structure of TRAF Family: Current Understanding of Receptor Recognition. Front Immunol 9, (2018).
275.Park, J.-S. et al. Yeast Vps13 promotes mitochondrial function and is localized at membrane contact sites. Mol. Biol. Cell 27, 2435–2449 (2016).
276.Pauwels, A.-M., Trost, M., Beyaert, R. & Hoffmann, E. Patterns, Receptors, and Signals: Regulation of Phagosome Maturation. Trends Immunol. 38, 407–422 (2017).
277.Peracino, B. et al. Function and mechanism of action of Dictyostelium Nramp1 (Slc11a1) in bacterial infection. Traffic 7, 22–38 (2006).
278.Peracino, B. et al. Function and mechanism of action of Dictyostelium Nramp1 (Slc11a1) in bacterial infection. Traffic 7, 22–38 (2006).
279.Perdiguero, E. G. & Geissmann, F. The development and maintenance of resident macrophages. Nat. Immunol. 17, 2–8 (2016).
280.Perrin, J. et al. TM9 family proteins control surface targeting of glycine-rich transmembrane domains. J Cell Sci 128, 2269–2277 (2015).
281.Peschel, A. et al. Staphylococcus aureus Resistance to Human Defensins and Evasion of Neutrophil Killing via the Novel Virulence Factor Mprf Is Based on Modification of Membrane Lipids with l-Lysine. J Exp Med 193, 1067–1076 (2001).
282.Petanjek, Z. et al. Extraordinary neoteny of synaptic spines in the human prefrontal cortex. PNAS 108, 13281–13286 (2011).
283.Pflaum, K., Gerdes, K., Yovo, K., Callahan, J. & Snyder, M. L. D. Lipopolysaccharide induction of autophagy is associated with enhanced bactericidal activity in Dictyostelium discoideum. Biochem. Biophys. Res. Commun. 422, 417–422 (2012).
284.Piper, R. C. & Katzmann, D. J. Biogenesis and Function of Multivesicular Bodies. Annu Rev Cell Dev Biol 23, 519–547 (2007).
285.Pollitt, A. Y. & Insall, R. H. WASP and SCAR/WAVE proteins: the drivers of actin assembly. Journal of Cell Science 122, 2575–2578 (2009).
286.Pontel, L. B. et al. Xpf suppresses the mutagenic consequences of phagocytosis in Dictyostelium. J Cell Sci 129, 4449–4454 (2016).
287.Prashar, A., Schnettger, L., Bernard, E. M. & Gutierrez, M. G. Rab GTPases in Immunity and Inflammation. Front. Cell. Infect. Microbiol. 7, (2017).
288.Press, B., Feng, Y., Hoflack, B. & Wandinger-Ness, A. Mutant Rab7 causes the accumulation of cathepsin D and cation-independent mannose 6-phosphate receptor in an early endocytic compartment. J. Cell Biol. 140, 1075–1089 (1998).
289.Pujol, C. et al. Yersinia pestis can reside in autophagosomes and avoid xenophagy in murine macrophages by preventing vacuole acidification. Infect. Immun. 77, 2251–2261 (2009).
290.Rabinovitch, M. Professional and non-professional phagocytes: an introduction. Trends Cell Biol. 5, 85–87 (1995).
291.Rajnovic, D., Muñoz-Berbel, X. & Mas, J. Fast phage detection and quantification: An optical density-based approach. PLoS ONE 14, e0216292 (2019).
292.Raper, K. B. DICTYOSTELIUM DISCOIDEUM, A NEW SPECIES OF SLIME MOLD FROM DECAYING FOREST LEAVES’. 17.

293.Rathore, S. S., Cheepurupalli, L., Gangwar, J., Raman, T. & Ramakrishnan, J. Biofilm of Klebsiella pneumoniae minimize phagocytosis and cytokine expression by macrophage cell line. bioRxiv 623546 (2019) doi:10.1101/623546.
294.Ratsimandresy, R. A., Dorfleutner, A. & Stehlik, C. An Update on PYRIN Domain-Containing Pattern Recognition Receptors: From Immunity to Pathology. Front Immunol 4, (2013).
295.Reed, C. F. Phospholipid exchange between plasma and erythrocytes in man and the dog. J Clin Invest 47, 749–760 (1968).
296.Rifkin, J. L. & Goldberg, R. R. Effects of chemoattractant pteridines upon speed of D. discoideum vegetative amoebae. Cell Motil. Cytoskeleton 63, 1–5 (2006).
297.Rink, J., Ghigo, E., Kalaidzidis, Y. & Zerial, M. Rab conversion as a mechanism of progression from early to late endosomes. Cell 122, 735–749 (2005).
298.Rivero, F. & Xiong, H. Chapter Two - Rho Signaling in Dictyostelium discoideum. in International Review of Cell and Molecular Biology (ed. Jeon, K. W.) vol. 322 61–181 (Academic Press, 2016).
299.Robinson, J. S., Klionsky, D. J., Banta, L. M. & Emr, S. D. Protein sorting in Saccharomyces cerevisiae: isolation of mutants defective in the delivery and processing of multiple vacuolar hydrolases. Mol Cell Biol 8, 4936–4948 (1988).
300.Rohatgi, R. et al. The interaction between N-WASP and the Arp2/3 complex links Cdc42-dependent signals to actin assembly. Cell 97, 221–231 (1999).
301.Rosengarten, R. D. et al. Leaps and lulls in the developmental transcriptome of Dictyostelium discoideum. BMC Genomics 16, 294 (2015).
302.Rothman, J. H., Howald, I. & Stevens, T. H. Characterization of genes required for protein sorting and vacuolar function in the yeast Saccharomyces cerevisiae. EMBO J 8, 2057–2065 (1989).
303.Rowland, J. L. & Niederweis, M. A multicopper oxidase is required for copper resistance in Mycobacterium tuberculosis. J. Bacteriol. 195, 3724–3733 (2013).
304.Royer-Pokora, B. et al. Cloning the gene for an inherited human disorder—chronic granulomatous disease—on the basis of its chromosomal location. Nature 322, 32–38 (1986).
305.Royer-Pokora, B. et al. Cloning the gene for an inherited human disorder—chronic granulomatous disease—on the basis of its chromosomal location. Nature 322, 32–38 (1986).
306.Rupper, A. & Cardelli, J. Regulation of phagocytosis and endo-phagosomal trafficking pathways in Dictyostelium discoideum. Biochimica et Biophysica Acta (BBA) - General Subjects 1525, 205–216 (2001).
307.Rupper, A., Grove, B. & Cardelli, J. Rab7 regulates phagosome maturation in Dictyostelium. Journal of Cell Science 114, 2449–2460 (2001).
308.Russell, D. G., Vanderven, B. C., Glennie, S., Mwandumba, H. & Heyderman, R. S. The macrophage marches on its phagosome: dynamic assays of phagosome function. Nat. Rev. Immunol. 9, 594–600 (2009).
309.Russo, T. A. et al. Aerobactin Mediates Virulence and Accounts for Increased Siderophore Production under Iron-Limiting Conditions by Hypervirulent (Hypermucoviscous) Klebsiella pneumoniae. Infect Immun 82, 2356–2367 (2014).
310.Saito, Y. et al. Characterization of endonuclease III (nth) and endonuclease VIII (nei) mutants of Escherichia coli K-12. J Bacteriol 179, 3783–3785 (1997).
311.Santambrogio, L. et al. Developmental plasticity of CNS microglia. Proc Natl Acad Sci U S A 98, 6295–6300 (2001).
312.Sattler, N., Monroy, R. & Soldati, T. Quantitative analysis of phagocytosis and phagosome maturation. Methods Mol. Biol. 983, 383–402 (2013).
313.Sekine, R., Kawata, T. & Muramoto, T. CRISPR/Cas9 mediated targeting of multiple genes in Dictyostelium. Sci Rep 8, 1–11 (2018).
314.Seong, E. et al. Mutations in VPS13D lead to a new recessive ataxia with spasticity and mitochondrial defects. Ann. Neurol. 83, 1075–1088 (2018).
315.Seto, S., Tsujimura, K. & Koide, Y. Rab GTPases Regulating Phagosome Maturation Are Differentially Recruited to Mycobacterial Phagosomes. Traffic 12, 407–420 (2011).
316.Seto, S., Tsujimura, K. & Koide, Y. Rab GTPases regulating phagosome maturation are differentially recruited to mycobacterial phagosomes. Traffic 12, 407–420 (2011).
317.Shaha Chandrima, Tripathi Rakshamani & Mishra Durga Prasad. Male germ cell apoptosis: regulation and biology. Philosophical Transactions of the Royal Society B: Biological Sciences 365, 1501–1515 (2010).
318.Shin, D.-M. et al. Mycobacterium tuberculosis Eis Regulates Autophagy, Inflammation, and Cell Death through Redox-dependent Signaling. PLoS Pathog 6, (2010).

319.Siemsen, D. W., Kirpotina, L. N., Jutila, M. A. & Quinn, M. T. Inhibition of the Human Neutrophil NADPH Oxidase by Coxiella burnetii. Microbes Infect 11, 671–679 (2009).
320.Silva, M. T. When two is better than one: macrophages and neutrophils work in concert in innate immunity as complementary and cooperative partners of a myeloid phagocyte system. J. Leukoc. Biol. 87, 93–106 (2010).
321.Simeone, R. et al. Cytosolic access of Mycobacterium tuberculosis: critical impact of phagosomal acidification control and demonstration of occurrence in vivo. PLoS Pathog. 11, e1004650 (2015).
322.Simonetti, B. & Cullen, P. J. Endosomal Sorting: Architecture of the Retromer Coat. Curr. Biol. 28, R1350–R1352 (2018).
323.Snyderman, R. & Pike, M. C. Macrophage migratory dysfunction in cancer. A mechanism for subversion of surveillance. Am. J. Pathol. 88, 727–739 (1977).
324.Soehnlein, O. et al. Neutrophil primary granule proteins HBP and HNP1-3 boost bacterial phagocytosis by human and murine macrophages. J. Clin. Invest. 118, 3491–3502 (2008).
325.Soldati, T. & Neyrolles, O. Mycobacteria and the intraphagosomal environment: take it with a pinch of salt(s)! Traffic 13, 1042–1052 (2012).
326.Solomon, J. M., Leung, G. S. & Isberg, R. R. Intracellular replication of Mycobacterium marinum within Dictyostelium discoideum: efficient replication in the absence of host coronin. Infect. Immun. 71, 3578–3586 (2003).
327.Souza, G. M. et al. Dictyostelium lysosomal proteins with different sugar modifications sort to functionally distinct compartments. J. Cell. Sci. 110 (Pt 18), 2239–2248 (1997).
328.Srinivas, U. S., Tan, B. W. Q., Vellayappan, B. A. & Jeyasekharan, A. D. ROS and the DNA damage response in cancer. Redox Biology 25, 101084 (2019).
329.Stamm, C. E., Collins, A. C. & Shiloh, M. U. Sensing of Mycobacterium tuberculosis and consequences to both host and bacillus. Immunol Rev 264, 204–219 (2015).
330.Stanley, A., Thompson, K., Hynes, A., Brakebusch, C. & Quondamatteo, F. NADPH oxidase complex-derived reactive oxygen species, the actin cytoskeleton, and Rho GTPases in cell migration. Antioxid. Redox Signal. 20, 2026–2042 (2014).
331.Stapels, D. A. C. et al. Staphylococcus aureus secretes a unique class of neutrophil serine protease inhibitors. Proc Natl Acad Sci U S A 111, 13187–13192 (2014).
332.Steinberg, B. E. et al. A cation counterflux supports lysosomal acidification. J. Cell Biol. 189, 1171–1186 (2010).
333.Stevenson, K., McVey, A. F., Clark, I. B. N., Swain, P. S. & Pilizota, T. General calibration of microbial growth in microplate readers. Scientific Reports 6, 1–7 (2016).
334.Strasser, J. E. et al. Regulation of the macrophage vacuolar ATPase and phagosome-lysosome fusion by Histoplasma capsulatum. J. Immunol. 162, 6148–6154 (1999).
335.Sturgill-Koszycki, S. et al. Lack of acidification in Mycobacterium phagosomes produced by exclusion of the vesicular proton-ATPase. Science 263, 678–681 (1994).
336.Sun, H.-M. et al. PALLD Regulates Phagocytosis by Enabling Timely Actin Polymerization and Depolymerization. J. Immunol. 199, 1817–1826 (2017).
337.Sun-Wada, G.-H., Tabata, H., Kawamura, N., Aoyama, M. & Wada, Y. Direct recruitment of H+-ATPase from lysosomes for phagosomal acidification. J Cell Sci 122, 2504–2513 (2009).
338.Sunaga, N., Monna, M., Shimada, N., Tsukamoto, M. & Kawata, T. Expression of zinc transporter family genes in Dictyostelium. Int. J. Dev. Biol. 52, 377–381 (2008).
339.Swanson, J. A. et al. A contractile activity that closes phagosomes in macrophages. J. Cell. Sci. 112 (Pt 3), 307–316 (1999).
340.Swearengen, J. R. Choosing the right animal model for infectious disease research. Animal Models and Experimental Medicine 1, 100–108 (2018).
341.Tang, D., Kang, R., Coyne, C. B., Zeh, H. J. & Lotze, M. T. PAMPs and DAMPs: signal 0s that spur autophagy and immunity. Immunological Reviews 249, 158–175 (2012).
342.Tattoli, I. et al. Amino acid starvation induced by invasive bacterial pathogens triggers an innate host defense program. Cell Host Microbe 11, 563–575 (2012).
343.Temesvari, L. A., Rodriguez-Paris, J. M., Bush, J. M., Zhang, L. & Cardelli, J. A. Involvement of the vacuolar proton-translocating ATPase in multiple steps of the endo-lysosomal system and in the contractile vacuole system of Dictyostelium discoideum. Journal of Cell Science 109, 1479–1495 (1996).

344.Theurl, I. et al. On-demand erythrocyte disposal and iron recycling requires transient macrophages in the liver. Nat. Med. 22, 945–951 (2016).
345.Thurston, T. L. M. et al. Growth inhibition of cytosolic Salmonella by caspase-1 and caspase-11 precedes host cell death. Nat Commun 7, 1–15 (2016).
346.Tosi, M. F. Innate immune responses to infection. J. Allergy Clin. Immunol. 116, 241–249; quiz 250 (2005).
347.Touret, N. et al. Quantitative and Dynamic Assessment of the Contribution of the ER to Phagosome Formation. Cell 123, 157–170 (2005).
348.Toyooka, K., Takai, S. & Kirikae, T. Rhodococcus equi can survive a phagolysosomal environment in macrophages by suppressing acidification of the phagolysosome. J. Med. Microbiol. 54, 1007–1015 (2005).
349.Tretina, K., Park, E.-S., Maminska, A. & MacMicking, J. D. Interferon-induced guanylate-binding proteins: Guardians of host defense in health and disease. J Exp Med 216, 482–500 (2019).
350.Trimble, W. S. & Grinstein, S. Barriers to the free diffusion of proteins and lipids in the plasma membrane. J Cell Biol 208, 259–271 (2015).
351.Tsai, W. C. et al. Nitric oxide is required for effective innate immunity against Klebsiella pneumoniae. Infect Immun 65, 1870–1875 (1997).
352.Tsuji, A., Kaneko, Y., Takahashi, K., Ogawa, M. & Goto, S. The Effects of Temperature and pH on the Growth of Eight Enteric and Nine Glucose Non‐Fermenting Species of Gram‐Negative Rods. Microbiology and Immunology 26, 15‐24 (1982).
353.Tsuji, A., Akaza, Y., Kodaira, K.-I. & Yasukawa, H. Copper/zinc superoxide dismutases in Dictyostelium discoideum: amino acid sequences and expression kinetics. J. Biochem. Mol. Biol. Biophys. 6, 215–220 (2002).
354.Tsujioka, M. et al. Actin-binding domains mediate the distinct distribution of two Dictyostelium Talins through different affinities to specific subsets of actin filaments during directed cell migration. PLoS One 14, (2019).
355.Turnbaugh, P. J. et al. The human microbiome project: exploring the microbial part of ourselves in a changing world. Nature 449, 804–810 (2007).
356.Uribe-Querol, E. & Rosales, C. Control of Phagocytosis by Microbial Pathogens. Front. Immunol. 8, (2017).
357.van Egmond, W. N. & van Haastert, P. J. M. Characterization of the Roco Protein Family in Dictyostelium discoideum. Eukaryot Cell 9, 751–761 (2010).
358.van Furth, R. et al. Cell kinetic analysis of a murine macrophage cell line. Eur. J. Cell Biol. 44, 93–96 (1987).
359.Vargas, P. et al. Innate control of actin nucleation determines two distinct migration behaviours in dendritic cells. Nat. Cell Biol. 18, 43–53 (2016).
360.Velayos-Baeza, A., Vettori, A., Copley, R. R., Dobson-Stone, C. & Monaco, A. P. Analysis of the human VPS13 gene family. Genomics 84, 536–549 (2004).
361.Vidal, S. et al. The Ity/Lsh/Bcg locus: natural resistance to infection with intracellular parasites is abrogated by disruption of the Nramp1 gene. J. Exp. Med. 182, 655–666 (1995).
362.Vieira, O. V. et al. Distinct roles of class I and class III phosphatidylinositol 3-kinases in phagosome formation and maturation. J Cell Biol 155, 19–26 (2001).
363.Vieira, O. V. et al. Acquisition of Hrs, an Essential Component of Phagosomal Maturation, Is Impaired by Mycobacteria. Mol Cell Biol 24, 4593–4604 (2004).
364.Vignesh, K. S. & Deepe, G. S. Immunological Orchestration of Zinc Homeostasis: The Battle between Host Mechanisms and Pathogen Defenses. Arch Biochem Biophys 611, 66–78 (2016).
365.Vines, J. H. & King, J. S. The endocytic pathways of Dictyostelium discoideum. Int. J. Dev. Biol. 63, 461–471 (2019).
366.Vono, M. et al. Neutrophils acquire the capacity for antigen presentation to memory CD4+ T cells in vitro and ex vivo. Blood 129, 1991–2001 (2017).
367.Watts, G. D. J. et al. Inclusion body myopathy associated with Paget disease of bone and frontotemporal dementia is caused by mutant valosin-containing protein. Nat. Genet. 36, 377–381 (2004).
368.Weinberg, E. D. Nutritional Immunity: Host's Attempt to Withhold Iron From Microbial Invaders. JAMA 231, 39–41 (1975).
369.Weiss, G. & Schaible, U. E. Macrophage defense mechanisms against intracellular bacteria. Immunol Rev 264, 182–203 (2015).

370.Welin, A., Weber, S. & Hilbi, H. Quantitative Imaging Flow Cytometry of Legionella-Infected Dictyostelium Amoebae Reveals the Impact of Retrograde Trafficking on Pathogen Vacuole Composition. Appl Environ Microbiol 84, (2018).
371.Wessling-Resnick, M. Nramp1 and Other Transporters Involved in Metal Withholding during Infection. J. Biol. Chem. 290, 18984–18990 (2015).
372.Wideman, J. G., Gawryluk, R. M. R., Gray, M. W. & Dacks, J. B. The Ancient and Widespread Nature of the ER–Mitochondria Encounter Structure. Mol Biol Evol 30, 2044–2049 (2013).
373.Winterbourn, C. C. & Kettle, A. J. Redox reactions and microbial killing in the neutrophil phagosome. Antioxid. Redox Signal. 18, 642–660 (2013).
374.Wolschendorf, F. et al. Copper resistance is essential for virulence of Mycobacterium tuberculosis. Proc Natl Acad Sci U S A 108, 1621–1626 (2011).
375.Wong, C.-O. et al. Lysosomal Degradation is Required for Sustained Phagocytosis of Bacteria by Macrophages. Cell Host Microbe 21, 719-730.e6 (2017).
376.Wong, D., Bach, H., Sun, J., Hmama, Z. & Av-Gay, Y. Mycobacterium tuberculosis protein tyrosine phosphatase (PtpA) excludes host vacuolar-H+-ATPase to inhibit phagosome acidification. Proceedings of the National Academy of Sciences 108, 19371–19376 (2011).
377.Xu, H. & Ren, D. Lysosomal Physiology. Annu Rev Physiol 77, 57–80 (2015).
378.Yang, C.-S. et al. TLR3-Triggered Reactive Oxygen Species Contribute to Inflammatory Responses by Activating Signal Transducer and Activator of Transcription-1. The Journal of Immunology 190, 6368–6377 (2013).
379.Yang, D. et al. Beta-defensins: linking innate and adaptive immunity through dendritic and T cell CCR6. Science 286, 525–528 (1999).
380.Yao, H., Qin, S., Chen, S., Shen, J. & Du, X.-D. Emergence of carbapenem-resistant hypervirulent Klebsiella pneumoniae. The Lancet Infectious Diseases 18, 25 (2018).
381.Yi, Y.-S. Folate Receptor-Targeted Diagnostics and Therapeutics for Inflammatory Diseases. Immune Netw 16, 337–343 (2016).
382.Yu, F., Sharma, S., Skowronek, A. & Erdmann, K. S. The serologically defined colon cancer antigen-3 (SDCCAG3) is involved in the regulation of ciliogenesis. Sci Rep 6, 1–12 (2016).
383.Zeya, H. I. & Spitznagel, J. K. Cationic Proteins of Polymorphonuclear Leukocyte Lysosomes I. Resolution of Antibacterial and Enzymatic Activities. J Bacteriol 91, 750–754 (1966).
384.Zhang, W., Xiao, S. & Ahn, D. U. Protein oxidation: basic principles and implications for meat quality. Crit Rev Food Sci Nutr 53, 1191–1201 (2013).
385.Zhang, X., Krause, K.-H., Xenarios, I., Soldati, T. & Boeckmann, B. Evolution of the ferric reductase domain (FRD) superfamily: modularity, functional diversification, and signature motifs. PLoS ONE 8, e58126 (2013).
386.Zhang, X. & Soldati, T. Detecting, visualizing and quantitating the generation of reactive oxygen species in an amoeba model system. J Vis Exp e50717 (2013) doi:10.3791/50717.
387.Zhang, X. & Soldati, T. Of Amoebae and Men: Extracellular DNA Traps as an Ancient Cell-Intrinsic Defense Mechanism. Front Immunol 7, (2016).
388.Zhang, X., Zhuchenko, O., Kuspa, A. & Soldati, T. Social amoebae trap and kill bacteria by casting DNA nets. Nat Commun 7, 1–9 (2016).
389.Zhou, K., Takegawa, K., Emr, S. D. & Firtel, R. A. A phosphatidylinositol (PI) kinase gene family in Dictyostelium discoideum: biological roles of putative mammalian p110 and yeast Vps34p PI 3-kinase homologs during growth and development. Mol Cell Biol 15, 5645–5656 (1995).
390.Zhu, H., Hart, C. A., Sales, D. & Roberts, N. B. Bacterial killing in gastric juice--effect of pH and pepsin on Escherichia coli and Helicobacter pylori. J. Med. Microbiol. 55, 1265–1270 (2006).
391.Zhu, Y. et al. NADPH oxidase 2 inhibitor diphenyleneiodonium enhances ROS-independent bacterial phagocytosis in murine macrophages via activation of the calcium-mediated p38 MAPK signaling pathway. Am J Transl Res 9, 3422–3432 (2017).
392.Zhukovskaya, N. V. et al. Dd-STATb, a Dictyostelium STAT protein with a highly aberrant SH2 domain, functions as a regulator of gene expression during growth and early development. Development 131, 447–458 (2004).

APPENDIXES

I. Manuscript: Role of SpdA in cell spreading and phagocytosis in Dictyostelium

Published: PLoS One. 2016 Aug 11;11(8): e0160376.

Marco Dias[1], Cristiana Brochetta[1], Anna Marchetti[1], **Romain Bodinier[1]**, Franz Brückert[2], Pierre Cosson[1*]

Affiliations:
[1] Department for Cell Physiology and Metabolism, Faculty of Medicine, Geneva University, 1 rue Michel Servet, CH1211 Geneva 4, Switzerland
[2] Laboratoire des Matériaux et du Génie Physique (LMGP), UMR CNRS-Grenoble INP5628 Université Grenoble Alpes, 3 parvis Louis Néel, BP 257, 38016 Grenoble cedex 1, France
*To whom correspondence should be addressed: Pierre.Cosson@unige.ch

Keywords: Dictyostelium discoideum; Phagocytosis; Cell spreading; Cell adhesion; SpdA; Quorum sensing
Short title: Role of SpdA in cell spreading and phagocytosis in *Dictyostelium*

Personal contribution:

Figure + legends:

Object:	Analysis	Quantification	Figure	Text	Revision
Fig5 B	**RB**	**RB**	**RB**	**RB**	**RB**/PC

Manuscript:
Materials & Methods:

Object:	Text	Revision
Cell Spreading	**RB**	**RB**/PC

Results:

Object:	Text	Revision
Fig5	**RB**/PC	**RB**/PC

RESEARCH ARTICLE

Role of SpdA in Cell Spreading and Phagocytosis in *Dictyostelium*

Marco Dias[1], Cristiana Brochetta[1], Anna Marchetti[1], Romain Bodinier[1], Franz Brückert[2], Pierre Cosson[1]*

1 Department for Cell Physiology and Metabolism, Faculty of Medicine, Geneva University, Geneva, Switzerland, **2** Laboratoire des Matériaux et du Génie Physique (LMGP), UMR CNRS-Grenoble INP5628 Université Grenoble Alpes, 3 parvis Louis Néel, BP 257, Grenoble cedex 1, France

* Pierre.Cosson@unige.ch

Citation: Dias M, Brochetta C, Marchetti A, Bodinier R, Brückert F, Cosson P (2016) Role of SpdA in Cell Spreading and Phagocytosis in *Dictyostelium*. PLoS ONE 11(8): e0160376. doi:10.1371/journal.pone.0160376

Editor: Gareth Bloomfield, MRC Laboratory of Molecular Biology, UNITED KINGDOM

Received: May 4, 2016

Accepted: July 18, 2016

Published: August 11, 2016

Data Availability Statement: All relevant data are within the paper and its Supporting Information files.

Funding: This work has been supported by the Swiss National Science Foundation (grant 31003A-153326, PC), the Doerenkamp-Zbinden Foundation, and the E. Naef Foundation (FENRIV). (Swiss National Science Foundation : http://www.snf.ch/; Doerenkamp-Zbinden Foundation : http://www.doerenkamp.ch; E. Naef Foundation : http://www.fondation-naef.com). MD was financed throughout his PhD by the Swiss National Science Foundation (grant 31003A-153326, PC). The funders had no role in

Abstract

Dictyostelium discoideum is a widely used model to study molecular mechanisms controlling cell adhesion, cell spreading on a surface, and phagocytosis. In this study we isolated and characterize a new mutant created by insertion of a mutagenic vector in the heretofore uncharacterized *spdA* gene. *SpdA-ins* mutant cells produce an altered, slightly shortened version of the SpdA protein. They spread more efficiently than WT cells when allowed to adhere to a glass substrate, and phagocytose particles more efficiently. On the contrary, a functional *spdA* knockout mutant where a large segment of the gene was deleted phagocytosed less efficiently and spread less efficiently on a substrate. These phenotypes were highly dependent on the cellular density, and were most visible at high cell densities, where secreted quorum-sensing factors inhibiting cell motility, spreading and phagocytosis are most active. These results identify the involvement of SpdA in the control of cell spreading and phagocytosis. The underlying molecular mechanisms, as well as the exact link between SpdA and cell spreading, remain to be established.

Introduction

Phagocytosis is the process by which eukaryotic cells ingest big particles (diameter typically >1μm) such as bacteria or cell debris. This process plays a key role in the defense of mammalian organisms against invading microorganisms [1], as well as in the clearance of dead cells continuously generated by cell division and apoptosis [2]. Phagocytosis is a complex process that is initiated by binding of a phagocytic cell to a particle. This initial binding triggers a local activation cascade, leading to a local reorganization of the actin cytoskeleton and a change in cell shape, ultimately allowing the engulfment of the particle into a closed phagosome [3]. Cellular adhesion, regulated dynamics of the actin cytoskeleton, membrane fusion and fission events are at play at multiple steps of the phagocytic process, and multiple molecular players are implicated in this process. In addition, many signaling pathways regulate this core adhesion machinery and control cellular adhesion and particle engulfment [3].

study design, data collection and analysis, decision to publish, or preparation of the manuscript.

Competing Interests: The authors have declared that no competing interests exist.

Dictyostelium discoideum is a widely used model to study phagocytosis. This social amoeba lives in the soil, where it feeds by continuously ingesting microorganisms. The molecular processes at play are similar to those characterized in mammalian cells, and implicate notably an adhesion molecule with integrin beta features, which interacts with talin and myosin VII to regulate actin dynamics [4]. Many other gene products participating in phagocytosis directly or indirectly (for example by controlling surface levels of adhesion molecules) have been characterized in this system. One of the key experimental advantages of *Dictyostelium discoideum* is its small haploid genome, allowing the relatively easy generation of random and targeted mutant cells. Typically, the role and relative importance of any given gene product in phagocytosis is determined in this organism by comparing the rate of phagocytosis of the corresponding KO strain with that of parental cells. Some mutations can reduce phagocytosis efficiency drastically [5], others show more modest defects [6], and a few were reported to increase phagocytosis [7–9]. Upon detailed analysis, each gene product can usually be classified as directly involved in adhesion to phagocytic particles or in engulfment, or as a regulator of the phagocytic process.

In this study we report the identification and characterization of a new gene product, named *spdA*, which is involved in cell spreading. Genetic alterations of *spdA* modify the ability of cells to spread on a substrate, and to phagocytose particles.

Materials and Methods

Isolation of *spdA-ins* mutant cells

All *Dictyostelium* strains used in this study were derived from the subclone DH1-10 [5] of the DH1 strain, referred to as wild-type (WT) for simplicity. Cells were grown at 21°C in HL5 medium (14.3 g/L peptone (Oxoid, Hampshire, England), 7.15 g/L yeast extract, 18 g/L maltose monohydrate, 0.641 g/L $Na_2HPO_4{\cdot}2H_2O$, 0.490 g/L KH_2PO_4) and subcultured twice a week to maintain a maximal density of 10^6 cells/ml. Unless otherwise specified, all experiments presented in this study were done with cells grown to a density of approximately 500'000 cells per mL.

Random mutants were generated by restriction enzyme-mediated integration (REMI) mutagenesis [10], subcloned individually, then tested for their ability to grow on a lawn of bacteria as described previously [11]. In this study, one mutant growing inefficiently on a laboratory strain of *Micrococcus luteus* (*Ml*) bacteria was selected for further analysis. The genomic DNA from these *spdA-ins* mutant cells was recovered, digested with ClaI and religated, and the mutagenic plasmid was recovered together with the flanking regions of its genomic insertion site (Fig 1). This plasmid was sequenced to identify the insertion site. It was also used after ClaI digestion to transfect WT cells and generate targeted *spdA-ins* mutant cells. Three independent *spdA-ins* mutant clones were generated, and used in parallel in this study, with indistinguishable results (Fig 1).

Phagocytosis and Fluid Phase Uptake

Phagocytosis and fluid phase uptake were determined as described previously [5] by incubating cells for 20 min in suspension in HL5 medium containing either 1-μm-diameter Fluoresbrite YG carboxylate microspheres (Polysciences, Warrington, PA) or Alexa647-dextran (Life Technologies, Eugene, OR). Cells were then washed twice with HL5 containing 0.2% NaN_3, and the internalized fluorescence was measured by flow cytometry [5]. Kinetics of phagocytosis were determined similarly after 0, 5, 10, 15, 20, 30, 40, 60, 90, 120 and 150 min of incubation. Since these experiments required a large number of cells, the cells were grown to a higher concentration than for all other experiments described in this study (1.5x10^6 cells per mL vs 500'000 cells

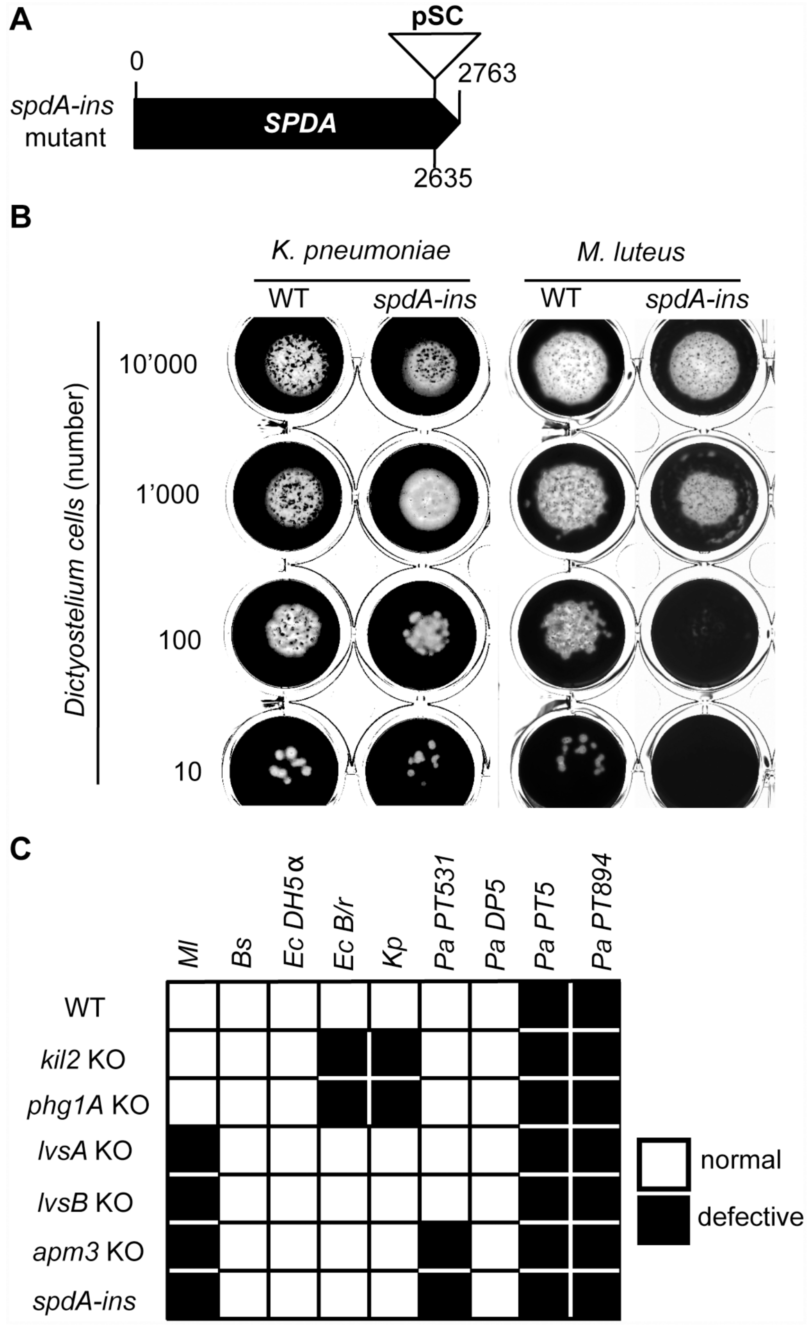

Fig 1. Characterization of *spdA-ins* mutant cells. (A) *SpdA-ins* mutant cells were originally created by the random insertion of a REMI mutagenic vector (pSC) in the coding sequence of gene DDB_G0287845 (position 2635). (B) To quantify growth of *Dictyostelium* on bacteria, we applied 10'000, 1'000, 100 or 10 *Dictyostelium* cells on a lawn of *K*. *pneumoniae* or *M*. *luteus* bacteria (black). WT cells created a phagocytic plaque (white). *SpdA* mutant cells grew as efficiently as WT cells on a lawn of *K*. *pneumoniae* but less efficiently in the presence of *M*. *luteus*. (C) Growth of *Dictyostelium* mutant strains in the presence of different bacterial species.

doi:10.1371/journal.pone.0160376.g001

per mL). This accounts for the fact that phagocytosis was less efficient for all strains in this set of experiments.

To determine if the elevated phagocytosis observed in *spdA-ins* mutant cells was a cell-autonomous phenotype, we mixed WT cells and *spdA-ins* mutant cells expressing GFP (ratio 1:1). After three days of co-culture in HL5, phagocytosis was analyzed as described above, but using latex beads fluorescent in the rhodamine channel (Polysciences, Inc). During flow cytometry, GFP fluorescence allowed to distinguish WT from *spdA-ins* mutant/GFP cells.

Cell spreading and motility

In order to visualize cell spreading on a substrate, 1.5×10^5 cells were allowed to adhere for 20 min on a glass surface in a FluoroDish (World Precision Instr., Sarasota, FL). To monitor the presence and spreading of *D. discoideum* cells we used an inverted microscope (Olympus IX71 or Zeiss Axiovert 100M) and imaged by phase contrast and Reflection Interference Contrast Microscopy (RICM) as previously described [12]. Images and movies (15 frames per second) were acquired with an Olympus DP30 CCD camera or a High resolution black/white CCD camera (Hamamatsu CCD cooled camera). RICM images were sub-sampled at 1 image per 1.2 s, the background was subtracted and flattened and the noise filtered. Dark cell-surface contact zones were defined by segmentation and quantified as described [13].

To measure cell motility, cells were observed for 60 min (picture every 30 sec) by phase contrast with a Plan-Neofluar 10x magnification. Pictures were taken with a Hamamatsu CCD cooled camera. We used Particle tracking from the Metamorph software to track individual cell trajectories.

Cell detachment assays

In these experiments, borosilicate glass plates were first cleaned with detergent in alkaline conditions, then briefly detached with a 14 M NaOH solution, thoroughly rinsed and dried. Radial flow experiments were performed essentially as described previously [14, 15]. Briefly, cells were resuspended in HL5 (10^6 cells/mL) and allowed to attach on the glass surface during 10 min, then a radial hydrodynamic flow was applied for 10 min and the density of the remaining attached cells was determined as a function of the distance to the center of the flow. The results were expressed as the percentage of detached cells as a function of the applied shear stress.

Microscopy

To visualize filamentous actin, cells were allowed to adhere on a glass coverslip for 10 min in HL5 and were fixed in PB containing 4% paraformaldehyde for 30 min. This fixation was sufficient to permeabilize the cells. The actin cytoskeleton was labeled by incubating the cells for 1h in phosphate-buffered saline (PBS) containing 0.2% bovine serum albumin and 1μg/ml tetramethylrhodamine B isothiocyanate (TRITC)-labeled phalloidin. The coverslips were then washed twice, mounted and observed by laser scanning confocal microscopy (Zeiss LSM 510). The pictures presented represent optical sections at the site of contact between the cells and the substrate.

For scanning electron microscopy, cells were incubated on glass coverslips overnight in HL5. Cells were then fixed with 2% glutaraldehyde in HL5 for 30 min followed by 2% glutaraldehyde in 100 mM PB (pH 7.14) for 30 min. Cells were rinsed and postfixed in 1% osmium tetroxide in 100 mM PB (pH 7.14) for 1 h. The fixative was removed, and cells were progressively dehydrated through a 25–100% ethanol series. After air-drying, cells were sputter-coated in gold and viewed on a JEOL-JSM-7001 FA Field Emission Scanning Electron Microscope.

Measuring cell size

To measure cell size based on electric current exclusion (CASY technology), cells were grown to a density of $50x10^4$ cells/mL, diluted to $1x10^4$ cells/mL, and 10 mL were analyzed using a CASY 1 cell counter (Roche; CASY Model TTC).

To determine packed cell volume, cells are grown to a density of $3x10^6$ cells/mL. Cells were counted under a Nikon eclipse TS100 microscope with a cell counting Neubauer chamber. $3x10^6$ cells in 1 mL were transferred in the packed cell volume (PCV) tube with calibrated capillary and volume graduation (5μL) (TPP Techno Plastic Products AG; Product no 87005). Cells were centrifuged 2 min at 1500 rpm, and the pellet volume measured in the calibrated capillary. The ratio μL of pellet/number of cells was calculated.

To measure the amount of protein per cell, 10^6 cells were collected by centrifugation, washed once in 1ml PBS, resuspended in 50 μL PBS containing triton X-100, 0.05% and transferred to a 96 well plate. To quantify protein content using a Lowry assay (DC Protein Assay, Bio-RAD) we added to each well 25 μL of reagent A and 200μL reagent B. After 15 min the absorbance at 750 nm was measured in a microplate reader, and compared to a set of calibrated serial dilutions.

Western blot analysis

To determine the cellular amounts of SibA, Phg1 and Talin, we resuspended cell pellets in sample buffer and separated the proteins on a polyacrylamide gel (7% for SibA and Talin and 10% for Phg1), after which they were transferred to a nitrocellulose membrane (Invitrogen, Carlsbad, CA). The membranes were incubated with a polyclonal anti-SibA antibody (SibA) [12], the YC1 rabbit antipeptide antiserum to a Phg1 peptide [5], or the anti-talin 169.477.5 [16], a kind gift from Prof. G. Gerisch (Martinsried, Germany). Binding of antibodies was revealed by ECL using a secondary HRP-coupled antibody (Amersham Biosciences). The signal intensity was evaluated using Quantity One software (Bio-Rad).

Results

Selection of *spdA-ins* mutant cells

Mutations affecting the organization or function of the endocytic/phagocytic pathway were previously shown to alter the ability of *Dictyostelium* cells to feed upon bacteria, while preserving their ability to feed upon HL5 medium. In order to identify new gene products potentially involved in phagocytosis, we created a library of random mutants by Restriction Enzyme Mediated Insertion, as described previously [11]. Briefly, a BamHI-digested pSC vector and the SauIIIA restriction enzyme were introduced in cells by electroporation. After selection of stably transfected cells in the presence of blasticidin, individual mutant cells were cloned by flow cytometry, and their ability to grow upon a variety of bacteria was tested. Previous results suggested that different gene products are essential for efficient growth on *K. pneumoniae*, *P. aeruginosa*, *M. luteus*, and *B. subtilis*, and that their common denominator is to be linked to one of the facets of the phagocytic process (adhesion, phagocytosis, intracellular killing. . .) [11]. The *spdA-ins* mutant was initially isolated as a mutant growing poorly on a lawn of *M. luteus*, a gram-positive bacterium. The mutagenic pSC plasmid was recovered from *spdA-ins* mutant cells, and the flanking genomic regions were sequenced. In *spdA-ins* mutant cells, the pSC plasmid is inserted on chromosome 5, 2636 nucleotides downstream of the start codon of DDB_G0287845 (Figs 1A and S1), hereafter called *spdA*. New *spdA-ins* mutant cells were generated by homologous recombination and three independent mutant lines were used in parallel for further characterization (S1 Fig). The predicted SpdA protein is composed of 920 amino acids, and the insertion of pSC in the coding sequence of *SPDA* results in the production of a truncated protein where the last 41 aminoacid residues are deleted. The SpdA protein exhibits no transmembrane domain or previously characterized domains. No clear ortholog could be identified in mammals or other species. A region extending from positions 3 to 450 shows homology with the N-terminal portion of many proteins from *D. discoideum*, *D. purpureum* and *D. lacteum* and may represent a novel undescribed domain. In *Dictyostelium discoideum*, the most conserved region encompassed the first 120 residues, and a Genome Blast search identified 18 gene products with homology to the N-terminal region of SpdA (S1 Table). Besides a conserved N-terminal region, none of these gene products exhibits a known functional domain. We are proposing to name the members of this putative new family SpdA to SpdS (S1 Table).

Growth of *spdA-ins* mutant cells in HL5 medium was unaffected compared to WT cells. To quantify growth of *Dictyostelium discoideum* strains on bacteria, 10'000, 1'000, 100 or 10 *Dictyostelium* cells were applied onto a bacterial lawn (Fig 1B). After 5 days in the presence of *K. pneumoniae* bacteria or of several other bacterial species, WT and *spdA*-ins mutant cells created phagocytic plaques cleared of bacteria with similar efficiencies (Fig 1B and 1C). On the contrary *spdA-ins* mutant cells grew less efficiently on a lawn of *M. luteus* and on the non-virulent PT531 *P. aeruginosa* strain (Fig 1B and 1C). Other mutant cells with poor growth on *M. luteus* characterized in our laboratory include *lvsA* KO cells [6], *lvsB* KO cells [6] and *apm3* KO cells [17] (Fig 1C). Since these three mutants have shown alterations in the organization and function of the endocytic and phagocytic pathway, we next tested the ability of *spdA-ins* mutant cells to perform phagocytosis and endocytosis.

SpdA-ins mutant cells phagocytose particles more efficiently than WT cells

To assess the function of the endocytic and phagocytic pathways, *spdA-ins* mutant cells and WT cells were incubated for 20 min in the presence of fluorescent dextran or fluorescent latex beads (1μm diameter). The internalized material was then measured by flow cytometry. Macropinocytosis of fluid phase was similar in WT cells and in *spdA-ins* mutant cells (Fig 2A). On the contrary, *spdA-ins* mutant cells phagocytosed latex beads more efficiently than WT cells (Fig 2B).

Analysis of phagocytosis kinetics further revealed that this difference was due to an increased rate of phagocytosis, evident at early phagocytosis times, while accumulation of ingested beads reached a similar plateau in WT and *spdA-ins* mutant cells after 120 min (Fig 2C). Phagocytosis and macropinocytosis both rely on similar rearrangements of the actin cytoskeleton, while phagocytosis requires in addition efficient adhesion of the cell to particles. Consequently several mutants defective in cell adhesion have been found to exhibit a decreased phagocytosis and no decrease in macropinocytosis [5, 12, 18].

To determine if the phenotype of *spdA-ins* mutant cells was cell-autonomous, we mixed *spdA-ins* mutant cells expressing GFP with WT cells. After three days of co-culture, we assessed the phagocytosis of rhodamine-labeled latex beads by flow cytometry. Expression of GFP allowed the identification of mutant cells (Fig 3A), and revealed that *spdA-ins* mutant cells co-cultured with WT cells still phagocytosed more efficiently than WT cells (Fig 3B).

SpdA-ins mutant cells adhere better than WT cells to their substrate

In order to assess the efficiency with which cells adhered to a substrate, cells were allowed to attach to a glass substrate, then subjected to a radial hydrodynamic flow for 10 min (Fig 4A) [19]. The shear stress applied to the cells depends on the velocity of the flux, which decreases

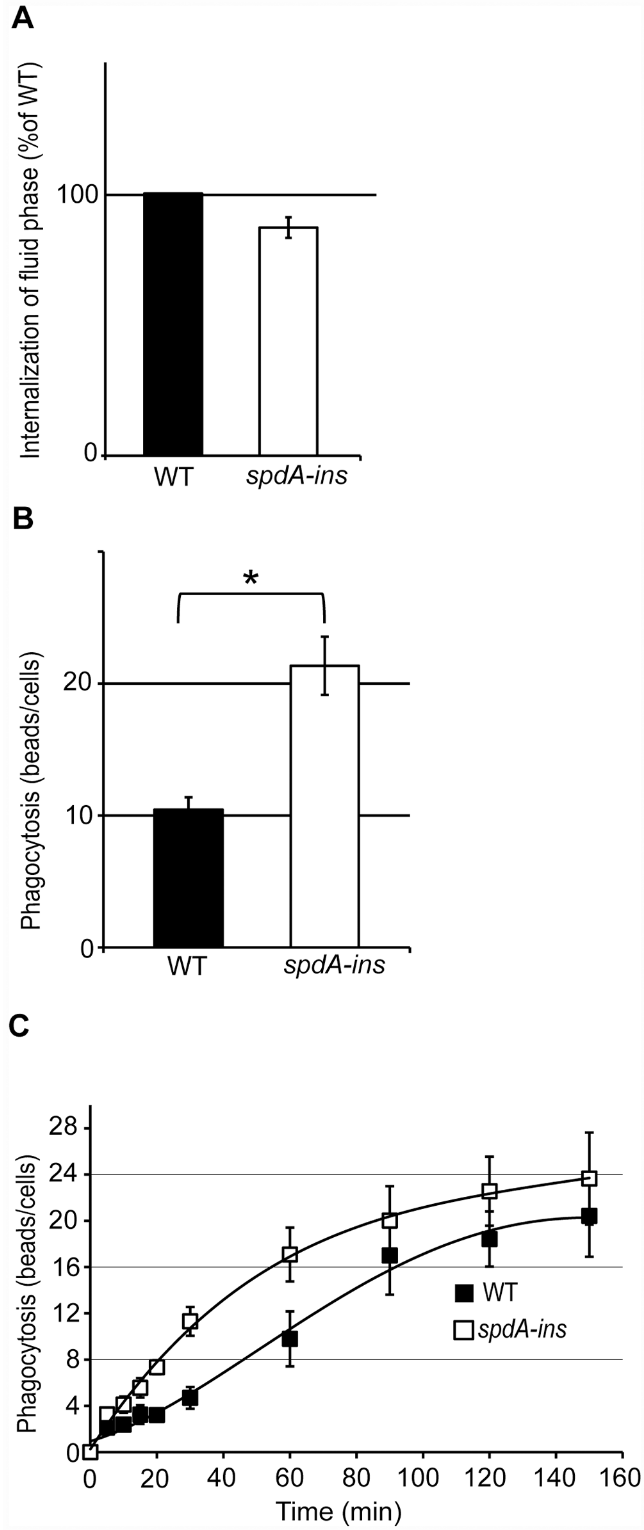

Fig 2. S*pdA-ins* mutant cells phagocytose particles faster than WT cells. Cells were incubated for 20 min in HL5 medium containing fluorescent dextran or fluorescent latex beads. Cells were then washed, and internalized fluorescence was measured by flow cytometry. (A) Uptake of fluorescent dextran was expressed as a percentage of the value obtained for the WT cells. (B) Phagocytosis of fluorescent beads was expressed as the average number of beads ingested per cell. The average and SEM of 6 independent samples are

presented. *: p<0.01 (Student t-test). (C) Cells were incubated for 0, 5, 10, 15, 20, 30, 60, 90, 120, or 150 min in HL5 medium containing fluorescent latex beads. The average and SEM of 4 independent experiments are presented. *SpdA-ins* mutant cells ingested particles faster than WT cells.

doi:10.1371/journal.pone.0160376.g002

when the distance to the center of the flow increases (Fig 4A). The percentage of cells detached by the flow was determined as a function of the distance to the center, and the results expressed as the percentage of detached cells as a function of the applied shear stress. At a low shear stress, between 0 and 0.5 Pa, *spdA-ins* mutant cells detached less readily than WT cells from

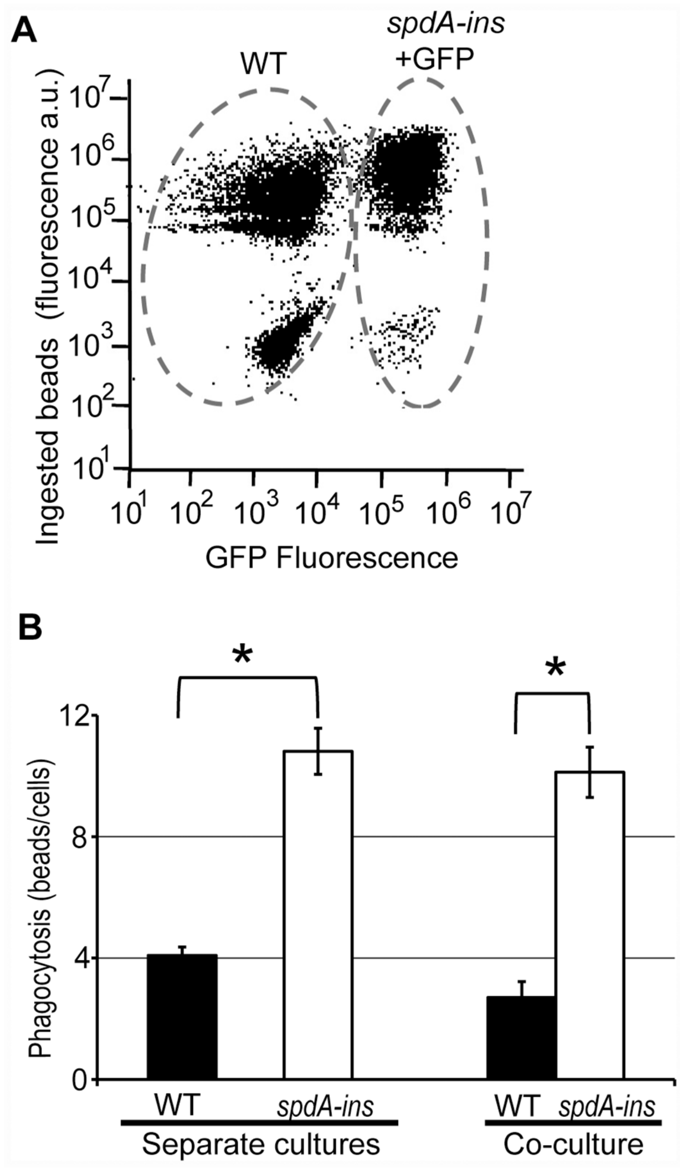

Fig 3. The phenotype of *spdA-ins* mutant cells is cell autonomous. (A) *SpdA* mutant cells expressing GFP were mixed with WT cells and cultured for three days. We then incubated the cells with rhodamine-labeled latex beads and assessed phagocytosis by flow cytometry. Expression of GFP allowed to distinguish WT cells from *spdA* mutant cells, and revealed that *spdA* mutant cells co-cultured with WT cells phagocytosed more efficiently than WT cells. (B) The phagocytosis of WT and *spdA-ins* cells cultured separately or co-cultured is indicated (mean±SEM; n = 6). *: p<0.01 (Student t-test).

doi:10.1371/journal.pone.0160376.g003

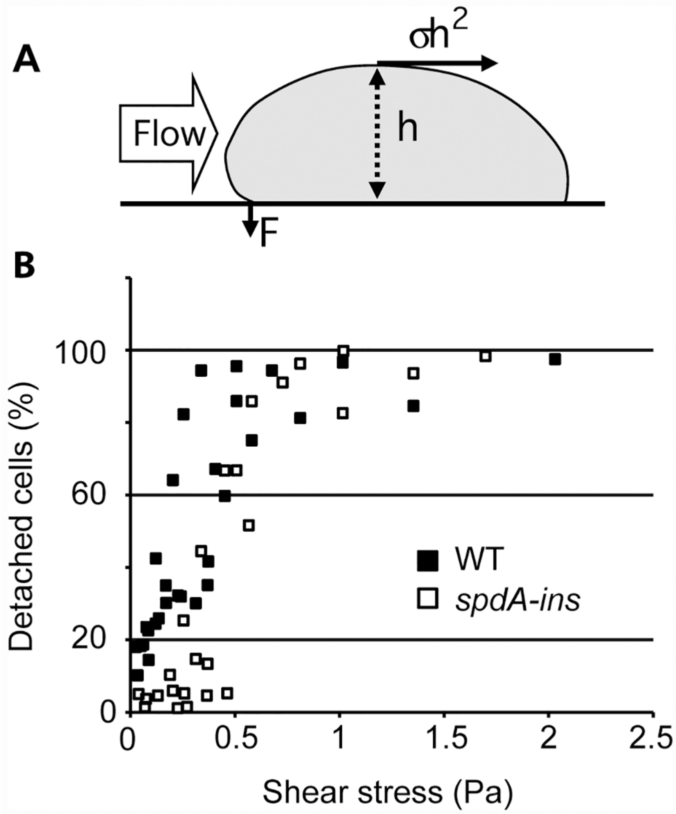

Fig 4. *SpdA-ins* cells adhere more efficiently than WT cells to their substrate. (A) Side view of a cell attached to its substrate and exposed to a flow of medium. The adhesion of the cell to its substrate can be assessed by determining the speed of a flow of medium that is necessary to detach the cells [19]. The strength applied by the flow of medium on the cell is σh^2, and its mechanical moment (σh^3) is balanced by the adhesive force (F). Inspired from [18]. (B) Percentage of detached cells as a function of the applied shear stress. At a low flow (between 0 and 0.5 Pa), *spdA-ins* cells detached less readily than WT cells from the substrate. At higher flow (>0.5 Pa) no significant difference can be seen between WT cells and *spdA-ins* cells. Data from three independent experiments is represented in this graph. A decrease in cell detachment can be the result of an increase in the adhesion force (F) or of a decrease in h (i.e. of a more efficient cell spreading).

doi:10.1371/journal.pone.0160376.g004

the substrate (Fig 4B). When the shear stress was higher than 0.5 Pa, almost 100% of both WT and *spdA-ins* mutant cells detached from the substrate (Fig 4B). These results indicate that *spdA-ins* mutant cells adhered more efficiently than WT cells to their substrate. An alternative interpretation is that mutant cells spread more readily on their substrate, which would decrease cell height (h in Fig 4A) and thus reduce the shear stress.

SpdA-ins mutant cells spread more efficiently than WT cells on a substrate

The spreading of cells on a substrate was first visualized by Scanning Electron Microscopy. WT cells appeared round and they did not spread much on their substrate. On the contrary, *spdA-ins* mutant cells formed extended contacts with the substrate, and their height may be reduced (Fig 5A). To quantify the difference between these two phenotypes, we visualized by Reflection Interference Contrast Microscopy (RICM) the size of the contact area between cells and their substrate. Cells were allowed to adhere to their substrate for 10 minutes, then they were observed by phase contrast and by RICM (Fig 5B). The average contact area between cells and

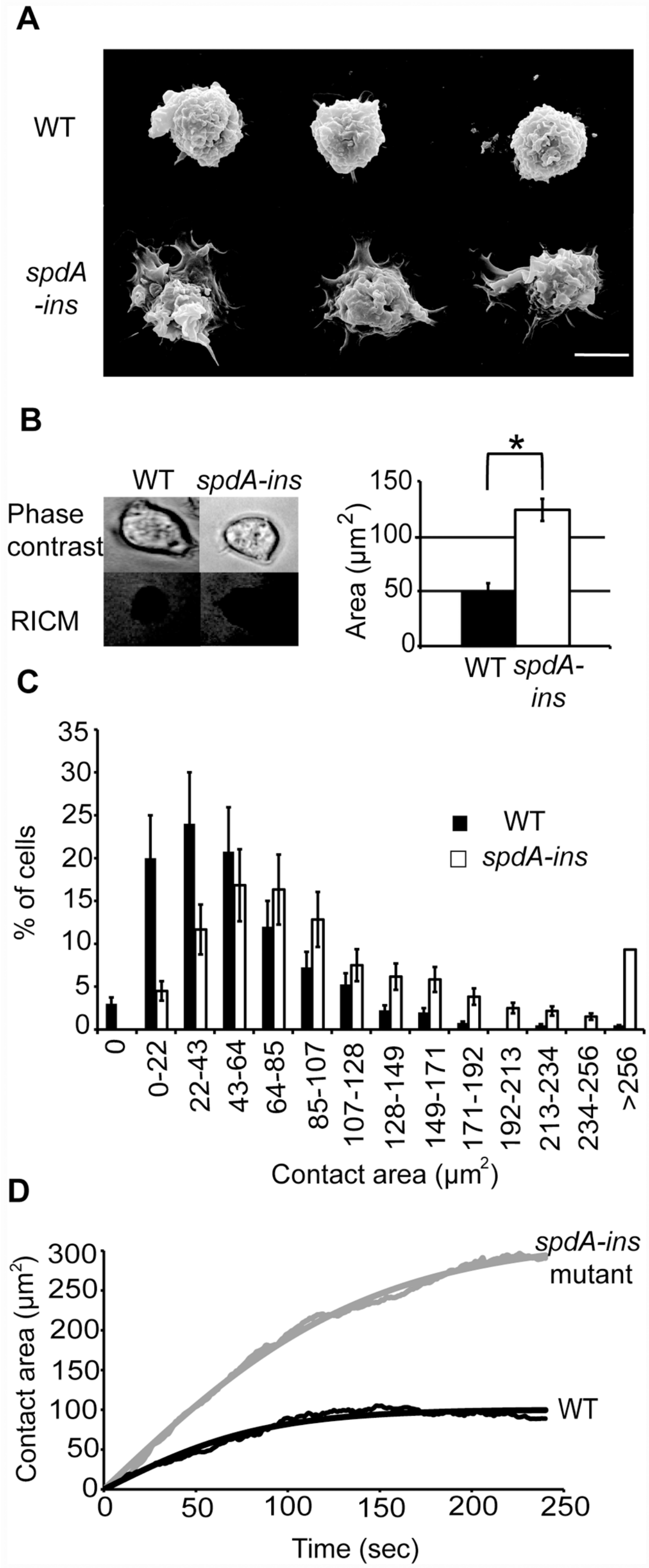

Fig 5. *SpdA-ins* cells spread more efficiently than WT cells. (A) WT and *spdA-ins* cells attached to a glass substrate were examined by scanning electron microscopy. Three representative pictures of each cell line are shown. *SpdA* cells spread more efficiently on their substrate than WT cells. Scalebar: 10µm. (B) To quantify cell spreading, cells were examined by phase contrast and RICM (Reflexion Interference Contrast

Microscopy). The contact area between cells and their substrate appears black and it was quantified for WT and *spdA-ins* cells (mean±SEM; n = 4 independent experiments. In each experiment 20 cells were analysed for each sample). *: p<0.01(Student t-test). (C) The contact area of individual cells is represented for the whole population of cells analyzed. (D) Kinetics of cell spreading was determined. S*pdA-ins* cells spread more and faster than WT cells. Thin lines: average spreading kinetics of cells (11 and 6 cells, respectively, representative of 3 independent experiments). Solid lines: fit with eq. 7 in ref 13, $A(t) = A_{max} \tanh(\alpha t)$.

doi:10.1371/journal.pone.0160376.g005

their substrate (black in RICM) was quantified, and was significantly higher for *spdA-ins* mutant cells than for WT cells (Fig 5B). When the contact area of each cell was plotted (Fig 5C) the whole population of *spdA-ins* mutant cells presented an increased area of close contact with the glass substrate. Finally, we measured the kinetics of cell spreading by RICM, and observed that *Dictyostelium spdA-ins* mutant cells spread more and faster than WT cells (Fig 5D). These observations confirm the proposal that *spdA-ins* mutant cells spread more efficiently on their substratum.

An increased spreading could result from increased expression of cellular proteins involved in cell adhesion, such as Talin [20], SibA [12] or Phg1A [5]. In order to evaluate this possibility, we analyzed by Western blot the amount of these proteins in WT and *spdA-ins* mutant cells. The amounts of SibA, Talin and Phg1A appeared very similar in WT and *spdA-ins* mutant cells (Fig 6).

We also visualized the organization of the actin cytoskeleton in WT and *spdA-ins* cells by fluorescence microscopy. For this, cells were allowed to adhere to a glass coverslip, fixed and stained with fluorescent phalloidin and observed by confocal microscopy. Pictures were taken in the region where cells are in contact with the substratum. The organization of actin did not appear significantly different in WT cells and in *spdA-ins* mutant cells showing small actin foci and peripheral accumulation at sites where pseudopods emanate from the cell body (Fig 7). Incubation in phosphate buffer induces the formation of filopodia in WT *Dictyostelium* cells [21] and a similar phenotype was observed in *spdA-ins* mutant cells (Fig 7). Similarly, the random migration of cells, a phenomenon highly dependent on the dynamics of the actin cytoskeleton was similar in WT and *spdA-ins* mutant cells (1.5 μm/min) (S2 Fig). Thus, the increased ability of *spdA-ins* mutant cells to spread on a substratum was not associated with a gross alteration of the organization or dynamics of the actin cytoskeleton.

The size of WT and *spdA-ins* mutant cells is similar

An increase in phagocytosis or in the area of contact with the substrate could potentially result from an increase in cell size, all other parameters unchanged. We used three independent methods to measure the size of WT and mutant cells. First, we used flow cytometry associated with a measure of electric current exclusion (CASY technology). The diameter of WT and of *spdA-ins* mutant cells was very similar (respectively 8.4 μm and 8.95 μm) (Fig 8A). Second, the packed cell volume was measured using graded centrifugation tubes, and was highly similar for WT and *spdA-ins* mutant cells (Fig 8B). Third, the amount of protein per cell was similar in WT and *spdA-ins* mutant cells (Fig 8C). Together these experiments indicate that WT and *spdA-ins* mutant cells have similar sizes.

Phagocytosis and spreading are decreased in *spdA* KO cells

In *spdA-ins* mutant cells the mutagenic plasmid was inserted close to the 3' of the *spdA* coding sequence resulting in the production of a slightly shorter version of the SpdA protein (See Fig 1A). This aberrant protein may either be functionally inactive or unstable, or on the contrary exhibit an increased activity or stability. To distinguish between these two possibilities,

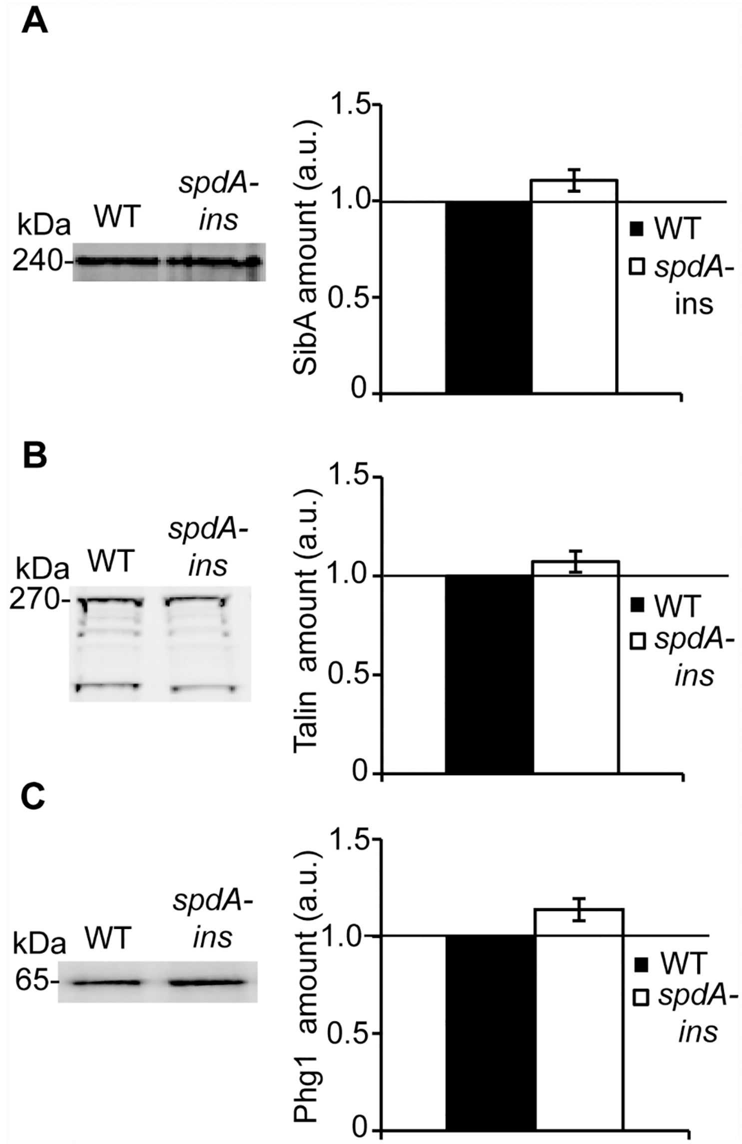

Fig 6. The cellular amounts of SibA, Phg1 and Talin are similar in WT cells and in *spdA-ins* cells. To determine the cellular amount of SibA, Pgh1A or Talin, cellular proteins were separated by electrophoresis and specific proteins revealed with antibodies against SibA (A), Talin (B) or Phg1A (C). The intensity of the signal was quantified and expressed in arbitrary units (a.u.). The average and SEM of four independent experiments are represented. The amounts of SibA, Phg1a and Talin were similar in WT cells and in *spdA-ins* cells.

doi:10.1371/journal.pone.0160376.g006

we generated by homologous recombination *spdA* KO cell lines where a large part of the *spdA* coding sequence was deleted (S3 Fig). In three independent clones of *spdA* KO cells, phagocytosis was found to be reduced compared to WT cells (51±4% of WT phagocytosis; mean±SEM; n = 6), while internalization of fluid phase was unchanged (103±2% of WT uptake; mean±SEM; n = 6). In addition, the spreading of *spdA* KO cells on a substrate was less efficient than that of WT cells (83±2% of WT spreading; mean±SEM; n = 7). This did not reflect a change in the size of the *spdA* KO cells, which was unchanged compared to WT cells (diameter WT 8.90±0.1μm; *spdA* KO 9.0±0.1μm; n = 6).

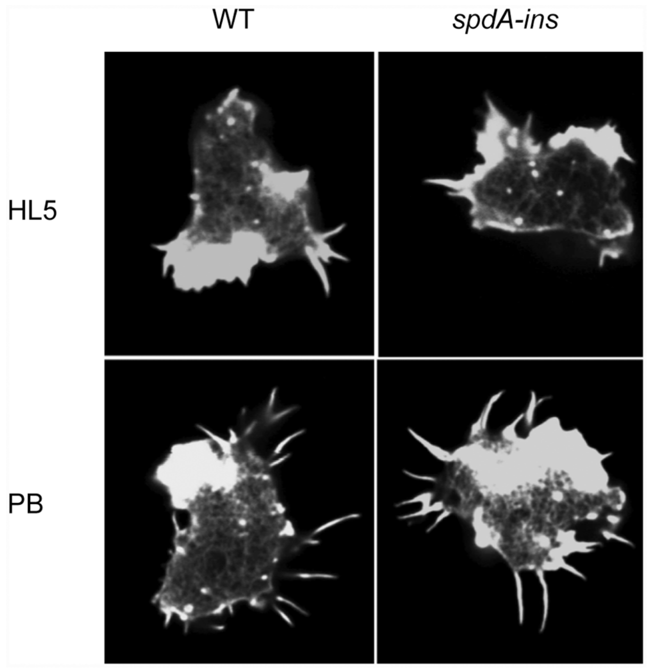

Fig 7. The actin organization is not significantly altered in *spdA-ins* cells. Cells were allowed to adhere to a glass coverslip for 10 min in HL5. After fixation filamentous actin was labeled with fluorescent phalloidin. The contact area between cells and their substrate was visualized by confocal microscopy, and did not reveal gross alterations of actin organization in *spdA-ins* cells. When cells were incubated in phosphate buffer (PB), formation of filopodia was induced in both WT and *spdA-ins* cells.

doi:10.1371/journal.pone.0160376.g007

The fact that the effect of a spdA genetic inactivation is to decrease phagocytosis and cell spreading confirms the implication of SpdA in these cellular functions. Moreover it indicates that SpdA either participates directly in cell spreading, or acts as an activator of these functions.

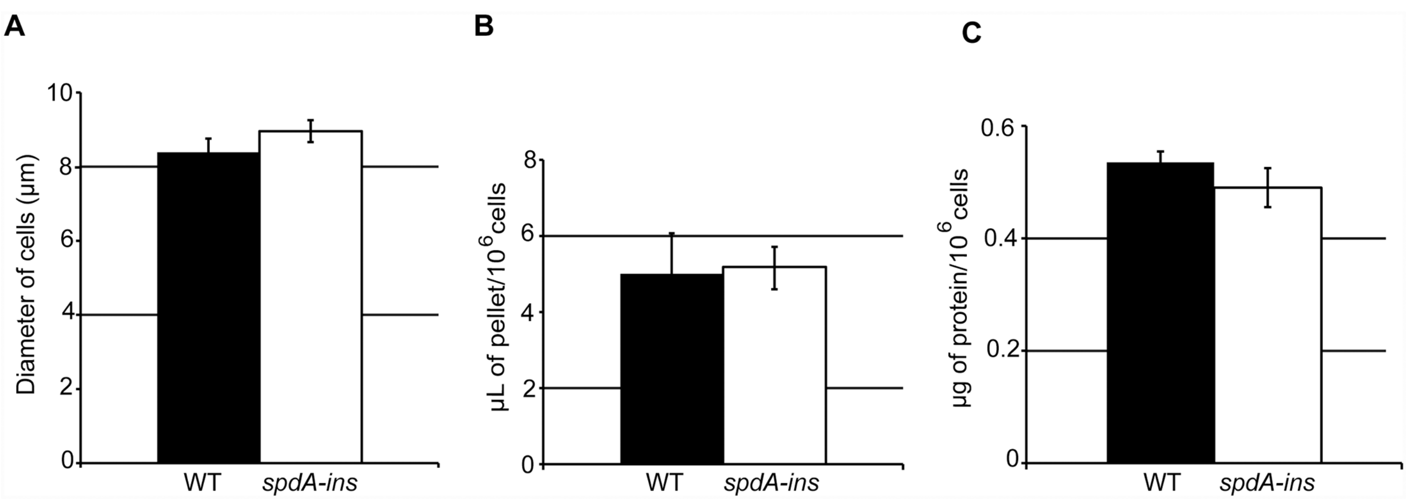

Fig 8. WT and *spdA-ins* cells have similar sizes. (A) Cell size was analyzed by electric current exclusion using a CASY 1 cell counter. (B) The packed cell volume of a known number of cells was determined in graded tubes. (C) The amount of protein per cell was determined using a Lowry assay. For each experiment, the average and SEM of three independent experiments is indicated. No significant differences were seen between WT and *spdA-ins* cells.

doi:10.1371/journal.pone.0160376.g008

Cell adhesion and phagocytosis are heavily regulated processes in Dictyostelium, and are in particular sensitive to cell density [22]. In order to evaluate if SpdA may participate in the regulation of cell spreading and phagocytosis, we grew cells at different densities, and assessed their ability to phagocytose latex beads. In WT *Dictyostelium* cells, phagocytosis strongly decreased when cellular density increased (Fig 9A). At very low cell density, phagocytosis was almost as

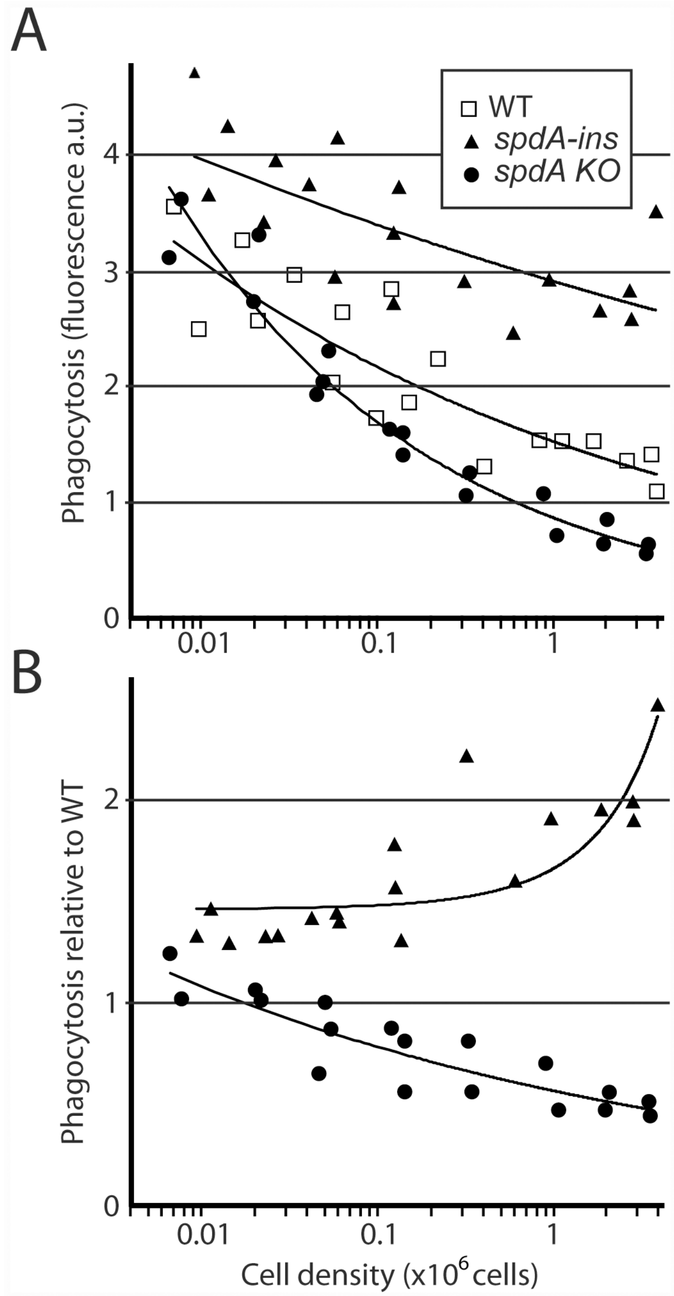

Fig 9. Role of SpdA in the regulation of phagocytosis by cell density. (A) Cells were grown to the indicated densities, and allowed to phagocytose fluorescent latex beads for 20 minutes. Phagocytosis was measured by flow cytometry. The results of three independent experiments were pooled in this figure. (B) In the experiment described in A, phagocytosis in mutant cells was directly compared to phagocytosis by WT cells grown at the same density. While both mutant cells phagocytosed like WT cells at low cell density, marked differences appeared when cellular density increased.

doi:10.1371/journal.pone.0160376.g009

efficient in WT, *spdA-ins* mutant cells, and *spdA KO* cells. On the contrary, as cell density increased, phagocytosis decreased less in *spdA-ins* mutant cells than in WT cells, and more in *spdA KO* cells than in WT cells (Fig 9).

Discussion

In this study we identified a new gene implicated in the control of cell adhesion and spreading, named *spdA*. *SpdA-ins* mutant cells spread faster and more efficiently than WT cells. They also phagocytose particles more efficiently than WT cells. These mutant cells were originally isolated based on the observation that they were defective for growth in the presence of *M. luteus* bacteria. It is likely that the inability of *spdA-ins* mutant cells to grow in the presence of *M. luteus* reflects the observed alterations in the function of the phagocytic pathway. This observation confirms that isolation of mutants defective for growth on certain bacteria does allow to identify new genes implicated in the organization and function of the endocytic and phagocytic pathways.

Previous studies have suggested that cell adhesion, phagocytosis and cell motility can be modulated negatively by secreted quorum-sensing factors in *Dictyostelium* [22, 23]. This allows cells to modulate their behavior as a function of cell density. Strikingly, at very low cell densities, both *spdA-ins* and *spdA KO* mutant cells phagocytosed as efficiently as WT cells. However, at increasing cell densities, *spdA KO* and *spdA-ins* mutant cells exhibited marked differences with WT cells: phagocytosis was inhibited more readily in *spdA KO* cells than in WT cells, and less in *spdA-ins* mutant cells than in WT cells. These results suggest that SpdA is involved in the pathway allowing cells to control their adhesion and phagocytosis as a response to cell density. SpdA may be directly involved in phagocytosis and cell spreading, and mobilized only when cells are growing at high densities and thus are exposed to high concentration of inhibitory quorum-sensing factors. Alternatively, SpdA may play a negative role in the quorum-sensing signaling pathway inhibiting cell adhesion and phagocytosis. Note that in *spdA* mutant cells, some phenomena implicating actin dynamics are affected (cell spreading, phagocytosis), while others are not (actin skeleton morphology, cell motility). It is thus possible that SpdA is involved specifically in certain facets of actin dynamics (cell spreading and phagocytosis) and not in others (e.g. cell motility).

As detailed above, *spdA-ins* and *spdA KO* mutations generate opposite phenotypes: phagocytosis and cell spreading are increased in *spdA-ins* cells and decreased in *spdA KO* cells compared to WT cells. In both cases three independent clones were analyzed, suggesting strongly that the phenotypes observed are truly generated by the mutations. This result suggests that in *spdA-ins* mutant cells, SpdA is either stabilized or hyperactive. We generated anti-SpdA recombinant antibodies (MRB19, 20 and 21). While they readily detected a full-length GFP-SpdA protein, they failed to detect endogenous SpdA, and this prevented us from testing whether the amount of SpdA was actually increased in *spdA-ins* mutant cells (data not shown). Very little is known on how *Dictyostelium* cells modulate phagocytosis, adhesion and cell motility in response to secreted quorum-sensing factors. SpdA is the first identified protein that may participate in these regulatory pathways. Further studies will be necessary to establish the precise molecular mechanisms linking SpdA to the regulation of cell spreading and phagocytosis.

Supporting Information

S1 Fig. Generation of *spdA-ins* mutant cells. Analysis of the genomic alteration of the original *SpdA-ins* mutant, design and usage of a mutagenic vector to create new *SpdA-ins* mutant cells. (TIF)

S2 Fig. Cell migration is unaffected in *spdA-ins* mutant cells. Analysis of random cell migration of a glass surface revealed no difference between WT and *SpdA-ins* mutant cells.
(TIF)

S3 Fig. Generation of *spdA-ins* mutant cells. Design of a vector to create *SpdA KO cells*, and selection of the mutant clones.
(TIF)

S1 Table. *Dictyostelium* gene products with significant homology to SpdA.
(DOCX)

Acknowledgments

The P.C. laboratory was supported by the Swiss National Science Foundation (grant 31003A-153326), the Doerenkamp-Zbinden Foundation, and the E. Naef Foundation (FENRIV).

Author Contributions

Conceived and designed the experiments: MD CB AM RB FB PC.

Performed the experiments: MD CB AM RB FB PC.

Analyzed the data: MD CB AM RB FB PC.

Wrote the paper: MD PC.

References

1. Pluddemann A, Mukhopadhyay S, Gordon S. Innate immunity to intracellular pathogens: macrophage receptors and responses to microbial entry. Immunological reviews. 2011; 240(1):11–24. doi: 10.1111/j.1600-065X.2010.00989.x PMID: 21349083.
2. Hochreiter-Hufford A, Ravichandran KS. Clearing the dead: apoptotic cell sensing, recognition, engulfment, and digestion. Cold Spring Harbor perspectives in biology. 2013; 5(1):a008748. doi: 10.1101/cshperspect.a008748 PMID: 23284042.
3. Cougoule C, Wiedemann A, Lim J, Caron E. Phagocytosis, an alternative model system for the study of cell adhesion. Seminars in cell & developmental biology. 2004; 15(6):679–89. doi: 10.1016/j.semcdb.2004.09.001 PMID: 15561587.
4. Cosson P, Soldati T. Eat, kill or die: when amoeba meets bacteria. Current opinion in microbiology. 2008; 11(3):271–6. doi: 10.1016/j.mib.2008.05.005 PMID: 18550419.
5. Cornillon S, Pech E, Benghezal M, Ravanel K, Gaynor E, Letourneur F, et al. Phg1p is a nine-transmembrane protein superfamily member involved in dictyostelium adhesion and phagocytosis. The Journal of biological chemistry. 2000; 275(44):34287–92. doi: 10.1074/jbc.M006725200 PMID: 10944536.
6. Cornillon S, Dubois A, Bruckert F, Lefkir Y, Marchetti A, Benghezal M, et al. Two members of the beige/CHS (BEACH) family are involved at different stages in the organization of the endocytic pathway in Dictyostelium. Journal of cell science. 2002; 115(Pt 4):737–44. PMID: 11865029.
7. Muller I, Subert N, Otto H, Herbst R, Ruhling H, Maniak M, et al. A Dictyostelium mutant with reduced lysozyme levels compensates by increased phagocytic activity. The Journal of biological chemistry. 2005; 280(11):10435–43. doi: 10.1074/jbc.M411445200 PMID: 15640146.
8. Annesley SJ, Bago R, Bosnar MH, Filic V, Marinovic M, Weber I, et al. Dictyostelium discoideum nucleoside diphosphate kinase C plays a negative regulatory role in phagocytosis, macropinocytosis and exocytosis. PloS one. 2011; 6(10):e26024. doi: 10.1371/journal.pone.0026024 PMID: 21991393; PubMed Central PMCID: PMC3186806.
9. Rosel D, Khurana T, Majithia A, Huang X, Bhandari R, Kimmel AR. TOR complex 2 (TORC2) in Dictyostelium suppresses phagocytic nutrient capture independently of TORC1-mediated nutrient sensing. Journal of cell science. 2012; 125(Pt 1):37–48. doi: 10.1242/jcs.077040 PMID: 22266904; PubMed Central PMCID: PMC3269021.

10. Kuspa A. Restriction enzyme-mediated integration (REMI) mutagenesis. Methods in molecular biology. 2006; 346:201–9. doi: 10.1385/1-59745-144-4:201 PMID: 16957292.
11. Lelong E, Marchetti A, Gueho A, Lima WC, Sattler N, Molmeret M, et al. Role of magnesium and a phagosomal P-type ATPase in intracellular bacterial killing. Cellular microbiology. 2011; 13(2):246–58. doi: 10.1111/j.1462-5822.2010.01532.x PMID: 21040356.
12. Cornillon S, Gebbie L, Benghezal M, Nair P, Keller S, Wehrle-Haller B, et al. An adhesion molecule in free-living Dictyostelium amoebae with integrin beta features. EMBO reports. 2006; 7(6):617–21. doi: 10.1038/sj.embor.7400701 PMID: 16699495; PubMed Central PMCID: PMC1479592.
13. Chamaraux F, Fache S, Bruckert F, Fourcade B. Kinetics of cell spreading. Physical review letters. 2005; 94(15):158102. PMID: 15904192.
14. Bruckert F, Decave E, Garrivier D, Cosson P, Brechet Y, Fourcade B, et al. Dictyostelium discoideum adhesion and motility under shear flow: experimental and theoretical approaches. Journal of muscle research and cell motility. 2002; 23(7–8):651–8. PMID: 12952064.
15. Decave E, Rieu D, Dalous J, Fache S, Brechet Y, Fourcade B, et al. Shear flow-induced motility of Dictyostelium discoideum cells on solid substrate. Journal of cell science. 2003; 116(Pt 21):4331–43. doi: 10.1242/jcs.00726 PMID: 12966168.
16. Kreitmeier M, Gerisch G, Heizer C, Muller-Taubenberger A. A talin homologue of Dictyostelium rapidly assembles at the leading edge of cells in response to chemoattractant. The Journal of cell biology. 1995; 129(1):179–88. PMID: 7698984; PubMed Central PMCID: PMC2120370.
17. de Chassey B, Dubois A, Lefkir Y, Letourneur F. Identification of clathrin-adaptor medium chains in Dictyostelium discoideum: differential expression during development. Gene. 2001; 262(1–2):115–22. PMID: 11179674.
18. Gebbie L, Benghezal M, Cornillon S, Froquet R, Cherix N, Malbouyres M, et al. Phg2, a kinase involved in adhesion and focal site modeling in Dictyostelium. Molecular biology of the cell. 2004; 15(8):3915–25. doi: 10.1091/mbc.E03-12-0908 PMID: 15194808; PubMed Central PMCID: PMC491846.
19. Decave E, Garrivier D, Brechet Y, Fourcade B, Bruckert F. Shear flow-induced detachment kinetics of Dictyostelium discoideum cells from solid substrate. Biophysical journal. 2002; 82(5):2383–95. doi: 10.1016/S0006-3495(02)75583-5 PMID: 11964228; PubMed Central PMCID: PMC1302030.
20. Niewohner J, Weber I, Maniak M, Muller-Taubenberger A, Gerisch G. Talin-null cells of Dictyostelium are strongly defective in adhesion to particle and substrate surfaces and slightly impaired in cytokinesis. The Journal of cell biology. 1997; 138(2):349–61. PMID: 9230077; PubMed Central PMCID: PMC2138202.
21. Dias M, Blanc C, Thazar-Poulot N, Ben Larbi S, Cosson P, Letourneur F. Dictyostelium ACAP-A is an ArfGAP involved in cytokinesis, cell migration and actin cytoskeleton dynamics. Journal of cell science. 2013; 126(Pt 3):756–66. doi: 10.1242/jcs.113951 PMID: 23264736.
22. Cornillon S, Froquet R, Cosson P. Involvement of Sib proteins in the regulation of cellular adhesion in Dictyostelium discoideum. Eukaryotic cell. 2008; 7(9):1600–5. doi: 10.1128/EC.00155-08 PMID: 18676957; PubMed Central PMCID: PMC2547077.
23. Gole L, Riviere C, Hayakawa Y, Rieu JP. A quorum-sensing factor in vegetative Dictyostelium discoideum cells revealed by quantitative migration analysis. PloS oneS. 2011; 6(11):e26901. doi: 10.1371/journal.pone.0026901 PMID: 22073217; PubMed Central PMCID: PMC3207821.

II. Manuscript: SpdA Supplementary data

Figure S1. Generation of spdA-ins mutant cells.
Analysis of the genomic alteration of the original SpdA-ins mutant, design and usage of a mutagenic vector to create new SpdA-ins mutant cells**.**

Figure S2. Cell migration is unaffected in spdA-ins mutant cells.
Analysis of random cell migration of a glass surface revealed no difference between WT and SpdA-ins mutant cells.

Figure S3. Generation of spdA-ins mutant cells.
Design of a vector to create SpdA KO cells, and selection of the mutant clones.

S1 Table. Dictyostelium gene products with significant homology to SpdA.

Figure S1:

A

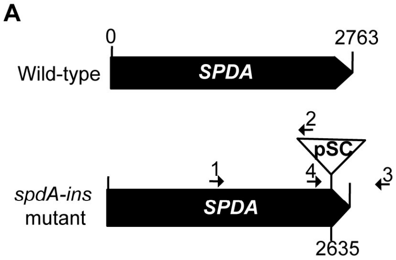

B

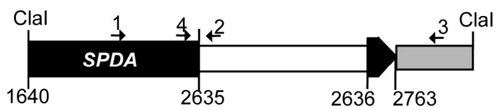

C

Oligo	Sequence
1	CTGATTATTTATTAACTCAAGCATTGG
2	AGAGACTTCCTGCCTCGTC
3	CCATTTTCGCACCATTTCTT
4	GAACATTTCTTCTCAATCATTGGTTCA

D

Oligo pair	WT (bp)	mutant (bp)
1+2	---	1089
3+4	756	---

E

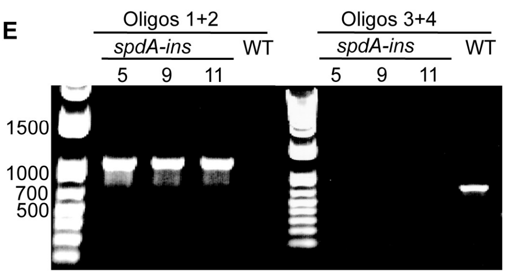

Figure S2:

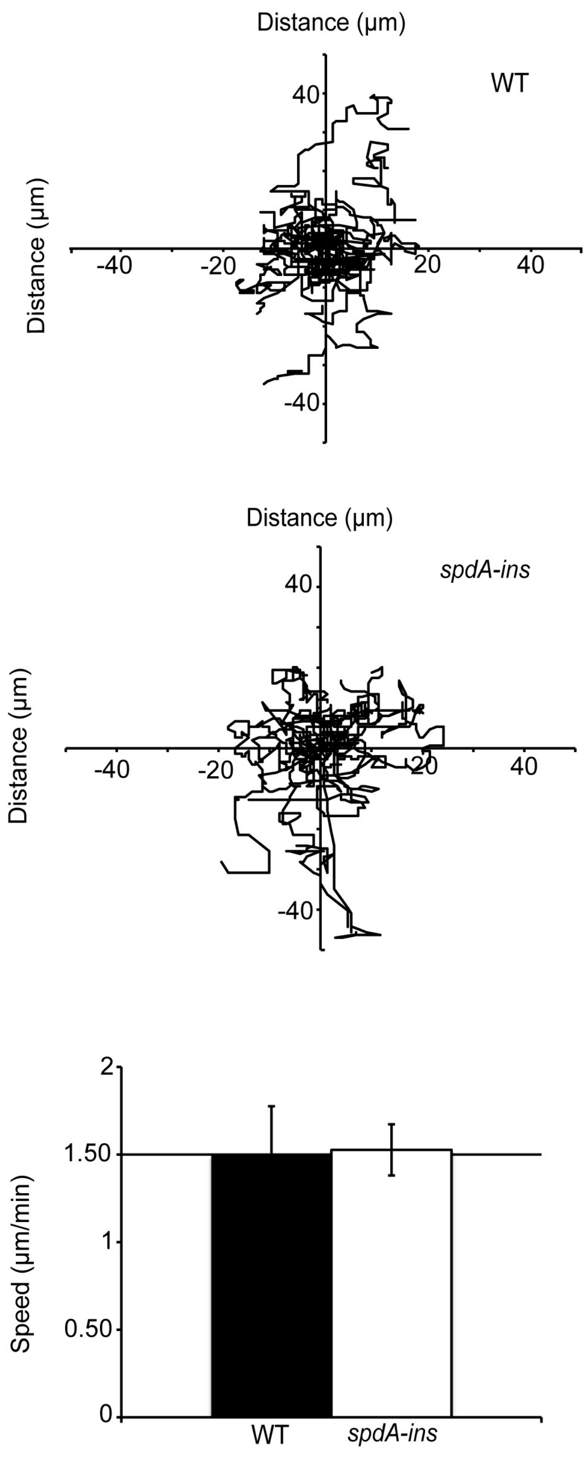
Distance (μm)
WT
Distance (μm)
40
-40
-20
20
40
-40
Distance (μm)
spdA-ins
Distance (μm)
40
-40
-20
20
40
-40
Speed (μm/min)
2
1.50
1
0.50
0
WT
spdA-ins

Figure S3:

A

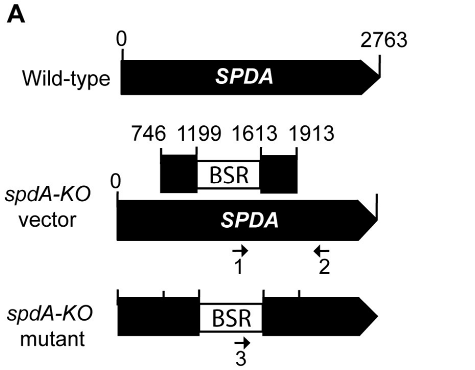

B

Oligo	Sequence
1	TGTCCATTACAATTCACAGATTCAACA
2	GAACCAATGATTGAGAAGAAATGTTCC
3	TTCAAATAATAATTAACCAACCCAAG

C

Oligo pair	WT (bp)	KO (bp)
1+2	901	---
3+2	---	797

D

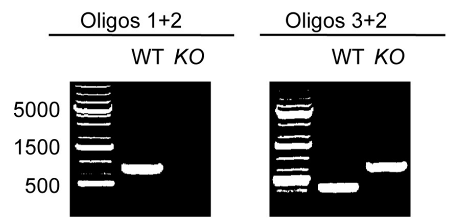

S1 Table:

Proposed Name	Gene ID (DDB_)	Size (AA)	chromosomal location	Id with SpdA
SpdA	G0287845	920	5(809663-812425)	
SpdB	G0293782	763	6 (3259115-3261522)	45/114
SpdC	G0293040	728	6 (2376674-2378860)	43/115
SpdD	G0273953	675	2(3594233-3596260)	43/117
SpdE	G0272903	675	2(2435526-2437553)	43/117
SpdF	G0279845	832	3(2628470-2630968)	41/122
SpdG	G0292932	768	6(2286339-2288645)	38/109
SpdH	G0293744	845	6(3261758-3264389)	44/148
SpdI	G0280509	884	3(3464216-3466870)	43/144
SpdJ	G0287615	782	5(470940-473288)	29/98
SpdK	G0272058	883	2(1124620-1127271)	29/56
SpdL	G0292950	774	6(2289490-2291814)	37/115
SpdM	G0278247	888	3(552139-554805)	27/55
SpdN	G0292952	908	6(2292229-2294955)	24/60
SpdO	G0292936	819	6(2298560-2301019)	38/117
SpdP	G0268692	325	1(1928290-1929267)	26/62
SpdQ	G0292934	780	6(2295609-2297951)	22/54
SpdR	G0292990	679	6(2303391-2305430)	26/59
SpdS	G0267746	535	1(774330-775937)	26/64